

**Pre-clinical Evaluation of Idoazomycin Arabinofuranoside (IAZA) and
Fluoroazomycin Arabinofuranoside (FAZA) as Hypoxia-targeting
Therapeutic Agents in a Head and Neck Cancer Model**

by
Faisal B Rashed

A thesis submitted in partial fulfillment of the requirements for the degree of

Doctor of Philosophy
in
Cancer Sciences

Department of Oncology
University of Alberta

© Faisal Bin Rashed, 2022

Abstract

Tumour hypoxia is a well-recognized clinical problem that promotes resistance to anti-cancer treatment (chemotherapy, radiotherapy, and immunotherapy), increases rates of recurrent disease, and ultimately leads to poor patient outcome. Eradication of hypoxic tumours is, therefore, essential for effective management of solid malignancies. Targeting hypoxic tumours requires a precision approach using compounds, such as nitroimidazoles (NIs), that are structurally equipped to reach and become activated within diffusion-limited tumour niches. NIs undergo bioreductive metabolism only under hypoxia and subsequently bind to cellular constituents, trapping the drug inside hypoxic cells. The selective accumulation of NIs has been successfully exploited for hypoxia diagnosis (either by radiological imaging or through immunological detection). However, their efficacy as anti-cancer agents is limited. Except for nimorazole, most NIs failed to provide definitive clinical advantage. Unfortunately, considerable gaps still remain in our understanding of their mechanism of action at the cellular level, which makes it challenging to further improve upon these compounds. The present study aimed to characterize the molecular phenotype induced by two 2-NI compounds, iodoazomycin arabinofuranoside (IAZA) and fluoroazomycin arabinofuranoside (FAZA), which are clinically validated hypoxia-selective radiotracers with promising therapeutic potentials. A major focus of this study was to identify and analyze the molecular targets of 2-NIs in order to elucidate their potential mechanism(s) of action.

Chapter 2 describes the synthesis and applications of azidoazomycin arabinofuranoside (N_3 -AZA), a novel click-chemistry compatible analogue of IAZA and FAZA, designed to facilitate (a) proteomic analysis of 2-NI targeted proteins in FaDu head and neck cancer cells, and (b) rapid and efficient labelling of hypoxic cells and tissues. A total of 62 target proteins were

identified; bioinformatic analysis revealed that many of them participate in key canonical pathways including glycolysis and hypoxia-inducible factor 1 α (HIF1A) signaling that play important roles in the cellular response to hypoxia. Proteins such as the glycolytic enzyme glyceraldehyde-3-phosphate dehydrogenase (GAPDH) and the detoxification enzyme glutathione S-transferase P (GSTP1) appeared as top hits, and N₃-AZA adduct formation significantly reduced their enzymatic activity selectively under hypoxia. Fluorescent staining of N₃-AZA-adducts also supported cell and tissue imaging for mapping tumour hypoxia, with comparable results to the current gold standard reagent, pimonidazole. However, because our approach uses click chemistry rather than immune-detection, the process is considerably less time-consuming and more cost-effective.

Chapter 3 provides a detailed analysis of the cellular phenotype induced by IAZA and FAZA under hypoxia. Hypoxic cells displayed higher sensitivity to IAZA and FAZA treatment, where the drugs induced cytostasis by compromising DNA replication, slowing down cell cycle progression and inducing replication stress. Effects of IAZA and FAZA on target cellular macromolecules (DNA, proteins and glutathione) were characterized. Covalent binding of NIs was only observed to cellular proteins, but not to DNA. While protein levels remained unaffected, catalytic activities of 2-NI target proteins, such as GAPDH and GSTP1 were significantly curtailed in response to IAZA/FAZA treatment under hypoxia. Single intraperitoneal (i.p.) injection of IAZA was well tolerated in mice (up to 600 mg/kg body weight), slowed down initial tumour growth, and reduced hypoxia levels in subcutaneous FaDu tumours.

Hypoxia selective radiosensitization capacities of IAZA and FAZA were explored in **Chapter 4**. Low dose radiation treatment with these 2-NI compounds mostly generated additive effects

under hypoxia. However, synergy was observed when hypoxic cells were treated with radiation doses >12 Gy (for IAZA) or >18 Gy (for FAZA). Combination treatment enhanced radiation induced DNA damage under hypoxia, observed through γ -H2AX immunocytochemistry and alkaline comet assay. No additional therapeutic benefit was observed when mice bearing subcutaneous FaDu tumours were injected i.p. with IAZA (400 mg/kg body weight) and irradiated with a single 10 Gy radiation dose. Given that chemotherapeutic agents are usually administered as multiple doses, it is worth exploring the effects of multi-dose treatment of IAZA on radiation response.

An overall discussion of the results and suggestions for future research is included in **Chapter 5**. Also, since ^{131}I -IAZA has potential for systemic radiotherapy, a preliminary toxicity analysis of non-radioactive IAZA administered in mice via an intravenous (i.v.) mode is provided, which indicates i.v. administration of IAZA is non-toxic. Established clinical efficacy of IAZA as a hypoxia imaging agent together with these data will support future *in vivo* experiments exploring IAZA as a potential theranostic agent.

Preface

This thesis is an original work by Faisal B Rashed. Portions of this thesis have been previously published as indicated below:

Chapter 2 has been published as Rashed FB, Stoica AC, Macdonald D, El-Saidi H, Ricardo C, Bhatt B, Moore J, Diaz-Dussan D, Ramamonjisoa N, Mowery Y, Damaraju S, Fahlman R, Wiebe LI, Kumar P, and Weinfeld W. “Identification of proteins and cellular pathways targeted by 2-nitroimidazole hypoxic cytotoxins.” *Redox biology*, vol. 41, 101905 (2021). Rashed FB, Kumar P and Weinfeld M designed the experiments. El-Saidi H and Ricardo C synthesized the compound. Rashed FB and Stoica AC performed *in vitro* validation experiments; Rashed FB, Macdonald D, Diaz-Dussan D and Ramamonjisoa N performed animal experiments and hypoxic fraction estimation analysis; Mowery Y provided mouse tumour samples; Rashed FB, Moore J, Bhatt B and Fahlman R performed mass spectrometry experiments and bioinformatic analysis. Rashed FB and Weinfeld M wrote the manuscript. All figures and tables have been re-numbered. All animal experiments were approved by the Animal Care Committee at the Cross Cancer Institute under protocol (#AC14208), and the Duke University Institutional Animal Care and Use Committee (IACUC, protocol #A032-19-02).

Chapter 3 has been submitted as Rashed FB, Diaz-Dussan D, Mashayekhi F, Macdonald D, Nation PN, Yang X, Sokhi S, Stoica AC, Narain R, Ismail IH, Wiebe LI, Kumar P, and Weinfeld W. “Cellular mechanism of action of 2-nitroimidzoles as hypoxia-selective therapeutic agents.” to the journal *Redox Biology*. Rashed FB, Kumar P and Weinfeld M designed the experiments. Rashed FB and Mashayekhi F performed *in vitro* experiments; Rashed FB, Diaz-Dussan D, Macdonald D and Nation PN carried out the animal experiments; Rashed FB and Weinfeld M wrote the manuscript. Ismail IH, Wiebe LI and Kumar P edited the manuscript. All figures and tables have been re-numbered. Animal experiments were approved by the Animal Care Committee at the Cross Cancer Institute under protocol (#AC18239)

Acknowledgements

This dissertation represents almost 7½ years of work, none of which would have been possible without direct and indirect help from a lot of people. First of all, I am thankful for being blessed with good health (even during a global pandemic) and with amazing mentors, Dr. Piyush Kumar and Dr. Michael Weinfeld, who masterfully guided me through this long, tedious journey. Both Piyush and Michael have been very supportive, patient and kind, and allowed me complete freedom (with a lot of guidance) to design and execute my research. A big thanks to my supervisory committee member, Dr. Lynne-Marie Postovit, for her insightful suggestions and feedback that helped me keep the project focused.

Over these years, I have had the opportunity to work with many excellent collaborators, namely, Dr. Richard Fahlman and team, Dr. Ismail Ismail and team, Dr. Sambasivarao Damaraju and team, and Dr. Yvonne Mowery, whose assistance and guidance was critical for the completion of this project. I thank Dr. Gordon Chan, Dr. Michael Hendzel, Dr. Armin Gamper and Dr. Roseline Godbout for always being available for discussions.

I feel fortunate to have worked with many wonderful people, both at the Weinfeld lab and the CRIO group, who taught me a lot about cancer research and hypoxia biology. My sincere gratitude to Dr. Leonard Wiebe for his encyclopedic knowledge about hypoxia targeting agents, and for editing my manuscripts. Many thanks to Dr. Alexandru Stoica for taking me under his wings and teaching me all the basic laboratory protocols, to Dr. Dawn Macdonald, Dr. Diana Diaz-Dussan, Xiao-Hong Yang and Dr. Nirilanto Ramamonjisoa for their help with the animal studies, and to Dr. Hassan El-Saidi and Dr. Carolynne Ricardo for synthesizing the test compounds. I extend my gratitude to Mesfin Fanta, Xiao-Yan Yang, Dr. Aghdass Rasouli-Nia and Dr. Feridoun Karimi-Busheri for being so friendly and supportive.

A big shout out to Sindhuja Raman, Dr. Zahra Shire, Dr. Bingcheng (Ted) Jiang and Wisdom Kate for their friendship, Dr. Amirali Bukhari, Dr. Cody Lewis, Bhumi Bhatt, Fatemeh Mashayekhi, Andrew Locke and Dr. Deepak Dinakaran for helping me out with cell-studies, bioinformatic analysis and mouse irradiation protocols, and to Sargun Sokhi, Aanchel Gupta and Stanley Woo for being amazing summer students.

I would like to thank Dr. Xuejun Sun and Geraldine Barron for their help with the cell and tissue imaging studies, Dan McGinn, Cheryl Santos, Daming Li, and Liping Jiang for their assistance in the vivarium, Dr. Anne Galloway for helping us order the gas cylinders, and April Scott and Jolanta Paul for autoclaving my glass petri-dishes in hundreds.

This study was made possible by the generous funding from Alberta Innovates through the CRIO program and CRIO Project Cancer, and with scholarships from Alberta Cancer Foundation, Terry Fox Foundation (STARS21 program), Yau Family Foundation and University of Alberta.

Lastly, thanks to my family for their love and support, and their faith in me.

Peace.

Table of contents

Chapter 1 Introduction	1
1.1 Tumour hypoxia	2
1.1.1 Chronic hypoxia	3
1.1.2 Acute hypoxia	3
1.1.3 Prevalence of hypoxia in human malignancies	6
1.2 Cellular adaptations to tumour hypoxia	8
1.2.1 Altered chromatin organization and gene transcription	8
1.2.2 Hypoxia inducible factor (HIF) transcription factor	9
1.2.3 Hypoxia-induced metabolic reprogramming	12
1.2.4 Angiogenesis	12
1.2.5 Global repression of protein synthesis and initiation of the unfolded protein response	13
1.2.6 Replication stress, altered DNA damage response and genetic instability	14
1.3 Clinical significance of tumour hypoxia.....	16
1.3.1 Resistance to radiation therapy	17
1.3.2 Resistance to chemotherapy	19
1.3.3 Resistance to immunotherapy	21
1.4 Hypoxia detection strategies.....	22
1.4.1 O ₂ electrode probe.....	22
1.4.2 Exogenous hypoxia reporters	22
1.4.3 Endogenous markers of tumour hypoxia	23
1.5 Hypoxia-targeted therapy	25
1.5.1 Increasing tumour oxygenation.....	25
1.5.2 Augmentation of RT delivery	26
1.5.3 Hypoxia-activated prodrugs	27
1.5.3.1 Nitroimidazoles as hypoxia-directed therapeutics	27
1.5.3.1.1 IAZA and FAZA	35
1.6 Research objectives	37
1.6.1 Specific aims	38

Chapter 2 Identification of Proteins and Cellular Pathways Targeted by 2-Nitroimidazole Hypoxia-selective Cytotoxins	39
2.1 Introduction	40
2.2 Materials and Methods	41
2.2.1 General synthesis methods	41
2.2.2 Cell culture	42
2.2.3 Drug stock preparation	43
2.2.4 Crystal violet staining assay	43
2.2.5 Click chemistry reaction cocktail preparation	43
2.2.6 Isolation of N ₃ -AZA-protein adducts	44
2.2.7 LC-MS/MS	44
2.2.8 Bioinformatics analysis	45
2.2.9 Western blot	45
2.2.10 Glyceraldehyde-3-phosphate dehydrogenase (GAPDH) activity assay	46
2.2.11 Glutathione S-transferase (GST) assay	46
2.2.12 N ₃ -AZA click staining of fixed cells	47
2.2.13 Immunocytochemistry:	47
2.2.14 Tumour generation and drug treatments	48
2.2.15 Tissue staining	49
2.2.16 Hypoxia fraction calculation	49
2.2.17 Data processing and statistics	49
2.3 Results	50
2.3.1 Synthesis of N ₃ -AZA	50
2.3.2 N ₃ -AZA is selectively cytotoxic to hypoxic cells	50
2.3.3 Identification of proteins that interact with 2-NI under hypoxia	53
2.3.4 N ₃ -AZA treatment did not affect the levels and localization of target proteins, but reduced GAPDH and GSTP1 enzymatic activity under hypoxia	60
2.3.5 Sub-cellular localization of N ₃ -AZA	63
2.3.6 N ₃ -AZA click chemistry for hypoxia mapping in tumours	66
2.4 Discussion	68
2.5 Acknowledgements	74
2.6 Declaration of interest	74

2.7 References	75
2.8 Supplementary information	80
2.8.1 Synthesis of N ₃ -AZA from Ts-AZA precursor	80
Chapter 3 Cellular mechanism of action of 2-nitroimidzoles as hypoxia selective therapeutic agents.....	94
3.1 Introduction	95
3.2 Materials and methods	96
3.2.1 Cell culture	96
3.2.2 Drug stock preparation.....	96
3.2.3 Crystal violet staining (CVS) assay	97
3.2.4 Clonogenic survival assay.....	97
3.2.5 Apoptosis assay	97
3.2.6 Senescence assay.....	98
3.2.7 Cell counting assay	98
3.2.8 Cell cycle profile analysis	98
3.2.9 Click-iT EdU incorporation assay.....	99
3.2.10 DNA fibre assay	99
3.2.11 Trapped in agarose DNA click staining (TARDCS).....	100
3.2.12 Immunocytochemistry	101
3.2.13 Alkaline comet assay.....	101
3.2.14 Assessing hydrogen peroxide (H ₂ O ₂) levels	102
3.2.15 Immunoblotting.....	102
3.2.16 Glyceraldehyde-3-phosphate dehydrogenase (GAPDH) activity assay	103
3.2.17 Glutathione S-transferase (GST) assay	103
3.2.18 Total glutathione (GSH) quantification	103
3.2.19 <i>In vivo</i> toxicity assay.....	104
3.2.20 Tumour growth delay assay and tissue staining.....	104
3.2.21 Data processing and statistics.....	105
3.3 Results	106
3.3.1 IAZA and FAZA selectively affect viability and clonogenicity of O ₂ starved cells.	106

3.3.2 IAZA and FAZA treatment under hypoxia do not increase cell death or senescence, but affect cell proliferation.....	109
3.3.3 Hypoxic treatment with IAZA or FAZA slows down cell cycle progression, represses DNA synthesis, and induces replication stress.	113
3.3.4 IAZA- and FAZA-treated hypoxic cells show higher γ -H2AX signal, but not a corresponding increase in comet tail moment.....	117
3.3.5 IAZA and FAZA treatment do not affect target protein levels, but significantly reduce their enzymatic activity.....	121
3.3.6 IAZA-treated mice showed an initial delay in tumour growth and a decrease in endpoint hypoxia levels.....	123
3.4 Discussion.....	126
3.5 Acknowledgements.....	132
3.6 References.....	133
3.7 Supplementary information.....	139
Chapter 4 Assessment of the Hypoxic Radiosensitization Potential of 2-Nitroimidazole Compounds, IAZA and FAZA, in a Head and Neck Tumour Model.....	145
4.1 Introduction.....	146
4.2 Materials and methods.....	147
4.2.1 Cell culture.....	147
4.2.2 Drug stock preparation.....	147
4.2.3 Clonogenic survival assay.....	147
4.2.4 Immunofluorescence.....	148
4.2.5 Alkaline comet assay.....	148
4.2.6 Tumour growth delay assay.....	149
4.2.7 Data processing and statistics.....	149
4.3 Results.....	150
4.3.1 IAZA and FAZA sensitize hypoxic cells to ionizing radiation.....	150
4.3.2 IAZA and FAZA increase DNA damage in hypoxic irradiated cells.	152
4.3.3 A single dose i.p. administration of IAZA with a single irradiation of 10 Gy did not improve therapy outcome in FaDu tumour bearing mice.	154
4.4 Discussion.....	156

Chapter 5 Discussion and future directions	160
Chapter 6 Bibliography	177

List of Tables

Table 1.1 Oxygenation status of tumours and healthy tissue in different human malignancies	7
Table 1.2 List of anticancer drugs that show reduced efficacy under hypoxia.....	20
Table 2.1 Proteins identified in eluates from N ₃ -AZA treated hypoxic cells using LC-MS/MS	55
Table 2.2 Top 10 canonical pathways identified through IPA analysis.....	59
Table 5.5.1 Blood chemistry analysis of male mice receiving IAZA (or vehicle control) via oral administration for 4 weeks, and after 2 weeks of recovery.	171
Table 5.2 Blood chemistry analysis of female mice receiving IAZA (or vehicle control) via oral administration for 4 weeks, and after 2 weeks of recovery.....	172
Table 5.3 Blood chemistry analysis of mice administered i.v. with IAZA (or vehicle control) showed no significant changes.....	175
Supplementary Table 2.1 Proteins identified in eluates from DMSO treated normoxic cells using LC-MS/MS.....	81
Supplementary Table 2.2 Proteins identified in eluates from N ₃ -AZA treated normoxic cells using LC-MS/MS.....	81
Supplementary Table 2.3 Proteins identified in eluates from DMSO treated hypoxic cells using LC-MS/MS.....	81
Supplementary Table 3.1 Blood chemistry analysis of mice injected i.p. with IAZA (or vehicle control) showed no significant changes.	139

List of Figures

Figure 1.1 Tumour hypoxia occurs in solid tumours when cells are exposed to suboptimal levels of O ₂	5
Figure 1.2 O ₂ -dependent regulation of HIF.	11
Figure 1.3 Compromised efficacy of IR in hypoxic cells.	18
Figure 1.4 Hypoxia selective entrapment of NIs.	29
Figure 1.5 Chemical structure of IAZA and FAZA.	36
Figure 2.1 N ₃ -AZA synthesis, cytotoxicity and click chemistry principle to isolate 2-NI target proteins.	52
Figure 2.2 Mass spectrometric analysis of N ₃ -AZA target proteins.	58
Figure 2.3 Effects of N ₃ -AZA on GAPDH and GSTP1 protein levels, GAPDH localization and their enzymatic activity.	62
Figure 2.4 N ₃ -AZA click chemistry as a hypoxia marker.	65
Figure 2.5 Pimonidazole immunostaining is comparable to that of N ₃ -AZA.	67
Figure 3.1 Hypoxic cells show preferential sensitivity towards IAZA and FAZA treatment.	108
Figure 3.2 IAZA and FAZA treatment do not induce apoptosis, senescence or ferroptosis under hypoxia, but reduce proliferation in hypoxic/reoxygenated cells.	112
Figure 3.3 Hypoxic cells treated with IAZA and FAZA show slower S phase progression, increased chromatin-bound PCNA staining, reduced DNA synthesis, and replication stress.	116
Figure 3.4 Analysis of DNA-NI binding characteristics and NI effects on DNA integrity under hypoxia.	120
Figure 3.5 The effects of IAZA and FAZA treatment on target proteins and glutathione levels under hypoxia.	122
Figure 3.6 <i>In vivo</i> evaluation of IAZA toxicity and tumour growth delay properties.	125
Figure 4.1 IAZA and FAZA sensitize hypoxic FaDu cells to IR.	151
Figure 4.2 Co-treatment of IAZA or FAZA with 5 Gy IR increases DNA damage only under hypoxia.	153
Figure 4.3 <i>In vivo</i> evaluation of IAZA as a hypoxic radiosensitizer.	155

Figure 4.4 Monitoring individual mice for body weight, tumour growth and endpoint hypoxia.	158
Figure 5.1 Potential mechanism of action for IAZA and FAZA (and by extension, for other 2- NIs in general).....	166
Figure 5.2 Oral administration of IAZA is relatively non-toxic in a mouse model.....	170
Figure 5.3: Intravenous administration of IAZA is non-toxic in mice.	174
Supplementary Figure 2.1 Spectral analysis of N ₃ -AZA.....	82
Supplementary Figure 2.2 Functional characterization of N ₃ -AZA target proteins.	83
Supplementary Figure 2.3 Effects of N ₃ -AZA treatment on its target proteins.....	84
Supplementary Figure 2.4 Estimation of N ₃ -AZA bound GAPDH fraction.	85
Supplementary Figure 2.5 Estimation of N ₃ -AZA bound GSTP1 fraction.	86
Supplementary Figure 2.6 Intensity of hypoxic N ₃ -AZA click staining increases with incubation time, hypoxia levels and is concentrated in the nuclei.....	88
Supplementary Figure 2.7 N ₃ -AZA click staining following reoxygenation.	89
Supplementary Figure 2.8 Pimonidazole shows hypoxia selective cytotoxicity.	90
Supplementary Figure 2.9 Autofluorescence in N ₃ -AZA and pimonidazole channel is minimal.	90
Supplementary Figure 2.10 N ₃ -AZA click staining is preferentially detected in tumours and can be quantified to determine hypoxic fractions in tumour.	91
Supplementary Figure 3.1 Hypoxia selective sensitivity to IAZA and FAZA in additional human cancer cell lines.	140
Supplementary Figure 3.2 IAZA- and FAZA-treated hypoxic cells have higher cyclin E1 levels, compromised DNA replication capacity even after reoxygenation, and show increased RPA retention.....	141
Supplementary Figure 3.3 Analysis of ROS generation in response to IAZA and FAZA treatment under hypoxia.....	142
Supplementary Figure 3.4 Quantification of GAPDH and GST protein levels in IAZA and FAZA treated cells.	143
Supplementary Figure 3.5 Monitoring individual mice for body weight, tumour growth and endpoint hypoxia.....	144

List of Movies

Supplementary Movie 2.1 N ₃ -AZA click staining is concentrated in nucleoli.....	92
Supplementary Movie 2.2 Pimonidazole immunostaining is excluded from nucleoli.	93

Abbreviations

(Met)-tRNA	Methionine transfer RNA
2-OG	2-Oxoglutarate
4E-BP1	Eukaryotic translation initiation factor 4E-binding protein 1
ACAD9	Acyl-CoA dehydrogenase family member 9
AKT	Protein kinase B
AMPK	AMP-activated protein kinase
ANGPT2	Angiopoietin 2
ANOVA	Analysis of variance
AQ4N	(1,4-bis([2-(dimethylamino-N-oxide)ethyl]amino)5,8-dihydroxy-anthracene-9,10-dione)
ARCON	Accelerated radiotherapy with carbogen and nicotinamide
ARNT	Aryl hydrocarbon nuclear translocator
ASK1	Apoptosis signal-regulating kinase
ATM	Ataxia telangiectasia mutated
ATP	Adenosine tri-phosphate
ATR	Ataxia telangiectasia and Rad3 related kinase
BNIP	Bcl-2 homology 3 domain-containing protein
BPG	1,3-bisphosphoglycerate
BRCA1	Breast cancer type 1 susceptibility protein
BSA	Bovine serum albumin
CAIX	Carbonic anhydrase IXCAS
CAST	Calpastatin
CBCT	Cone Beam Computed Tomography
CBP/p300	CREB-binding protein/E1A-binding protein p300
CD31	Cluster of differentiation 31
CD47	Cluster of differentiation 47
CDK4	Cyclin-dependent kinase 4
CDNB	1-chloro-2,4-dinitrobenzene
CHK1	Checkpoint kinase 1
CldU	5-chloro-2'-deoxyuridine
CPT	(S)-(+)-Camptothecin
CSC	Cancer stem cells
CT	Computed tomography
CTLA-4	Cytotoxic T lymphocyte associated protein 4
CVS	Crustal violet staining
CXCR4	C-X-C chemokine receptor type 4
Cys	Cysteine
DAHANCA	Danish Head and Neck Cancer
DAPI	4',6-diamidino-2-phenylindole
DFS	Disease-free survival

DHFR	Dihydrofolate reductase
DiOC7	Diheptyloxacarbocyanine iodide
DMEM	Dulbecco's Modified Eagle Medium
DMF	Dimethylformamide
DMM	Desmethyl-misonidazole
DMSO	Dimethylsulfoxide
DNA	Deoxyribonucleic acid
DNA-PKcs	DNA-dependent protein kinase, catalytic subunit
dNTP	Deoxynucleotide triphosphates
DSBs	Double strand breaks
DSM	Disease-specific mortality
DSS	Disease specific survival
DTNB	5,5'-dithio- <i>bis</i> -2-(nitrobenzoic acid)
DTT	Dithiothreitol
E2F1	E2F Transcription Factor 1
EDTA	Ethylenediamine tetraacetic acid
EdU	5-ethynyl-2'-deoxyuridine
EF5	2-(2-nitro-1H-imidazol-1-yl)-N-(2,2,3,3,3-pentafluoropropyl)-acetamide
eIF2	Eukaryotic Initiation Factor 2
ELISA	Enzyme-linked immunosorbent assay
ENOL	Enolase
ER	Endoplasmic reticulum
ERCC1	ERCC Excision Repair 1, Endonuclease Non-Catalytic Subunit
ERK1/2	Extracellular signal-regulated protein kinase
ESI-MS	Electrospray ionization mass spectrometry
FAZA	Fluoroazomycin arabinofuranoside
FDA	Food and Drug Administration
FIH-1	Factor inhibiting HIF1
FMISO	Fluoromisonidazole
FoxP3	Forkhead box P3
GAP	Glyceraldehyde-3-phosphate
GAPDH	Glyceraldehyde-3-phosphate dehydrogenase
GLUT1	Glucose transporter-1
GSH	Glutathione
GST	Glutathione-S-transferase
GSTP	Glutathione S-transferase P
GTP	Guanosine triphosphate
Gy	Gray
H ₂ O ₂	Hydrogen peroxide
H3K27me3	Histone 3 lysine 27 trimethylation
H3K4me3	Histone 3 lysine 4 trimethylation

H3K9me3	Histone 3 lysine 9 trimethylation
HAP	Hypoxia activated prodrug
HBO	Hyperbaric oxygen
HBOT	Hyperbaric oxygen therapy
hCNT	Human concentrative nucleoside transporters
HF	Hypoxic fraction
HIF1A	Hypoxia-inducible factor 1 α
HIF1B	Hypoxia-inducible factor 1 β
HNC	Head and neck cancer
HPLC	High-performance liquid chromatography
HPV	Human papillomavirus
HR	Homologous recombination
HRE	Hypoxia response elements
HRP	Horseradish peroxidase
HSF1	Heat shock factor 1
HSP70	Heat shock 70 kDa protein
HU	Hydroxyurea
i.p.	Intraperitoneal
i.v.	Intravenous
IACUC	Institutional Animal Care and Use Committee
IAZA	Iodoazomycin arabinofuranoside
IC ₅₀	Half-maximal inhibitory concentration
IdU	5-iodo-2'-deoxyuridine
IgG	Immunoglobulin G
IGRT	Image guided radiotherapy
IL8	Interleukin 8
IMRT	Intensity modulated RT
IPA	Ingenuity pathway analysis
IR	Ionizing radiation
IR-800	Infrared-800
IU/L	International units per liter
JNK	c-Jun N-terminal kinase
JNK1	Stress-activated protein kinase JNK
LC-MS/MS	Liquid chromatography–mass spectrometry
LD	Lethal dose
LDHA	Lactate dehydrogenase A
LOX	Lysyl oxidase
LRC	Local-regional control
LRF	Locoregional failure
m/z	Mass-to-charge ratio
MAP	Mitogen-activated protein
MBq	Megabecquerel

MCM7	Minichromosome maintenance complex component 7
MDR1	Multidrug resistance protein 1
MDSC	Myeloid derived suppressor cells
mGy	Milligray
MHC	Major histocompatibility complex
MHz	Megahertz
MICA	Major histocompatibility complex class I polypeptide-related sequence A
MLH1	MutL Homolog 1
mM	Millimolar
mm ³	Cubic millimetre
mmHg	Millimetre of mercury
MMR	Mismatch repair
MR	Magnetic resonance
MRI	Magnetic resonance imaging
MRN	Mre11-Rad50-Nbs1
mRNA	Messenger RNA
MRT	Molecular radiotherapy
MS	Mass spectrometry
MSH2	MutS homolog 2
MSH6	MutS homolog 6
mTOR	Mammalian target of rapamycin
mTORC1	Mammalian target of rapamycin complex 1
mTORC2	Mammalian target of rapamycin complex 2
MTX	Methotrexate
MW	Molecular weight
N ₃ -AZA	Azidoazomycin arabinofuranoside
NAC	N-Acetyl-L-cysteine
NADH	Nicotinamide adenine dinucleotide
NADPH	Nicotinamide adenine dinucleotide phosphate
NBS1	Nibrin
NER	Nucleotide excision repair
NfsA	Oxygen-insensitive NADPH nitroreductase
NfsB	Dihydropteridine reductase
NHEJ	Non-homologous end joining
NI	Nitroimidazole
NIH	National Institutes of Health
NK	Natural killer cells
NMR	Nuclear magnetic resonance
O.C.T.	optimal cutting temperature compound
OD	Optical density
ODD	O ₂ dependent domain

OPN	Osteopontin
OS	Overall survival
P	Partition coefficient
P402	Proline 402
p53	Tumor protein P53
P564	Proline 564
PBS	Phosphate buffered saline
PCNA	Proliferating cell nuclear antigen
PDGFB	Platelet-derived growth factor B
PDI	Protein disulfide-isomerase
PDK1	Pyruvate dehydrogenase kinase 1
PD-L1	Programmed death-ligand 1
PERK	Protein kinase R-like endoplasmic reticulum kinase
PET	Positron emission tomography
PFA	Paraformaldehyde
PFKL	Phosphofructokinase-liver type
PFS	Progression free survival
PGF	Placental growth factor
PGKI	Phosphoglycerate kinase
PHD	Prolyl hydroxylase
PI	Propidium iodide
PI3K	Phosphoinositide 3 kinase
PKM	Pyruvate kinase
PML	Loss of the promyelocytic leukaemia protein
pO ₂	Partial pressure of oxygen
PPIB	Peptidyl-prolyl cis-trans isomerase B
PPM	Parts per million
Prdx-1	Peroxiredoxin-1
Pro	Proline
PSM	Peptide-spectrum match
PTEN	Phosphatase and tensin homolog
RAD17	RAD17 Checkpoint Clamp Loader Component
RAD51	RAD51 Recombinase
Rdx4	Peroxiredoxin 4
RHEB	Ras homolog enriched in brain
RNA	Ribonucleic acid
ROS	Reactive oxygen species
RPA	Replication protein A
RS	Replication stress
RT	Radiation therapy
S.D.	Standard deviation
S.E.M	Standard error of the mean

S139	Serine-139
S317	Serine-317
S343	Serine-343
S345	Serine-345
S645	Serine-645
SARRP	Small Animal Radiation Research Platform
SA- β -gal	Senescence-associated beta-galactosidase
SBRT	Stereotactic body radiotherapy
SCF	Stem cell factor
SDF1	Stromal derived factor 1
SDS	Sodium dodecyl sulphate
SDS-PAGE	Sodium dodecyl sulphate–polyacrylamide gel electrophoresis
SER	Sensitizer enhancement ratio
SPECT	Single-photon emission computerized tomography
ssDNA	Single strand DNA
STAT3	Signal transducer and activator of transcription 3
STED	Stimulated emission depletion
T/B	Tumour/blood
TAMs	Tumour associated macrophages
TARDCS	Trapped in agarose click staining
TARDIS	Trapped in agarose DNA immunostaining
TCD ₅₀	50% local tumor control probability
TLC	Thin-layer chromatography
TNB	5-thio-2-nitrobenzoic acid
TPI1	Triosephosphate isomerase
TPM3	Tropomyosin alpha-3 chain
T-reg	Regulatory T cells
TrxR	Thioredoxin reductase
Ts-AZA	1- α -D-(5-O-tosyl-arabinofuranosyl)-2-nitroimidazole
TSC1/2	Tuberous sclerosis protein complex 1/2
UPR	Unfolded protein response
UV	Ultraviolet
V	Volt
v/v	Volume/volume
VEGF	Vascular endothelial growth factor
VEGFA	Vascular endothelial growth factor A
VHL	Von Hippel Lindau
VISTA	V-domain immunoglobulin suppressor of T-cell activation
XPC	Xeroderma pigmentosum, complementation group C
XPB	Xeroderma Pigmentosum Group D
γ -H2AX	Gamma H2A histone family member X

Chapter 1

Introduction

1.1 Tumour hypoxia

Cancer is a complex genetic disease that arises through accumulation of harmful mutations, often resulting from genetic predisposition, environmental exposure, and/or lifestyle factors (Anand, Kunnumakara et al. 2008, Wishart 2015). The disease manifests itself via disruption of normal cellular homeostatic mechanisms, leading to uncontrolled cell division and/or resistance to regular cell death stimuli (Fernald and Kurokawa 2013, Feitelson, Arzumanyan et al. 2015). These transformed cells routinely display high proliferative capacities and can quickly outgrow the vasculature, compromising the delivery of blood (and consequently nutrients and oxygen) to the growing tumour mass (Weidner 1999). The situation is further aggravated by the various structural deformities (in the form of leaky vessels, blind ends, and shunts) present in the tumour vascular network, which makes them prone to frequent collapse and failure (Siemann 2011). The resultant disparity between oxygen (O_2) supply and consumption means that cells within a solid tumour are regularly exposed to suboptimal levels of O_2 . In contrast to partial O_2 pressure (pO_2) in normal tissue that ranges from 40-60 mmHg ($\sim 5\% O_2$), O_2 levels in tumours are significantly lower (2-32 mmHg; $\sim 2\% O_2$) with most values falling well below 10 mmHg ($\leq 1\% O_2$) (Brown 1999, McKeown 2014). This pathophysiological condition, characterized by tumour regions with low O_2 tension, is clinically termed “tumour hypoxia” (Bertout, Patel et al. 2008). The presence of hypoxia has been reported in a wide range of human malignancies, making it a hallmark of solid tumours (McKeown 2014).

Hypoxia has long been recognized as a major clinical attribute that promotes resistance to therapy. Very often, hypoxic tumour cells persist after treatment, and give rise to recurrent disease. Tumour cells that can survive hypoxic stress are also likely to be a significant source of metastasis. There is substantial clinical evidence indicating a strong association between the presence of hypoxia in tumours and poor prognosis for patient outcome [reviewed in (Brown 1979, McKeown 2014, Walsh, Lebedev et al. 2014)]. Regrettably, very few strategies showed promise at efficiently targeting hypoxic tumours, and presently almost none are in use in routine clinical practice. This underscores the importance of developing novel hypoxia selective therapies. Indeed, tumour hypoxia may very well be the best-validated therapeutic target in cancer biology that is yet to be exploited to its full potential (Wilson and Hay 2011).

1.1.1 Chronic hypoxia

Much of our understanding about variable O₂ levels in solid tumours comes from the seminal works of Thomlinson and Gray published in 1955 (Thomlinson and Gray 1955). In studying clinical bronchial carcinoma, they made the critical observations that growth of tumour cells was restricted to ~150 µm from blood vessels, beyond which the onset of necrosis commences. In histological sections, these growing tumour cells would resemble a cord like structure, with tumour cells growing radially outwards from perfused blood vessels. Termed “tumour cord”, these structures were later identified in other tumour types, with cord diameter ranging from 70-200 µm (Olive, Vikse et al. 1992, Torres Filho, Leunig et al. 1994, Lanzen, Braun et al. 2006). This growth limiting distance coincides with the diffusion limit of O₂ in respiring tissue, indicating that dividing cells receive a progressively lower O₂ share as they move away from capillaries, until they receive none and become necrotic (Harris 2002). Further validation for such O₂ dependent growth limit came from mouse studies demonstrating that the tumour cord width can be decreased by gassing mice with low O₂ (10%) or increased by exposing them to high O₂ (100%) (Hirst, Hirst et al. 1991). Hypoxic cells reside at the edge of these tumour cords (lining the necrotic borders) where low O₂ levels can support these quiescent yet viable cells, but are not low enough for them to become necrotic. Hypoxia induced by the diffusion restrictions of tissue O₂ is therefore termed “chronic” or diffusion limited hypoxia (**Fig. 1.1A and B**).

1.1.2 Acute hypoxia

The vascular network (composed of arteries, arterioles, capillaries, venules, and veins) in normal healthy tissue is organized in a strict hierarchical fashion (Traore and George 2017). In contrast, tumour vasculature is tortuous, underdeveloped, and lacks structural resolution and maturity. Vessel membranes in tumours are also sparsely distributed, which makes them prone to leakage (Baluk, Morikawa et al. 2003). Combined with the poor lymphatic drainage (Guo and Fu 2012), this leads to build up of fluid in the interstitial space (Leu, Berk et al. 2000, Padera, Kadambi et al. 2002). The resulting high interstitial fluid pressure constricts the disorganized tumour vessels and generates poor pressure gradients for blood flow. Consequently, this causes intermittent vascular collapse within tumours, creating local regions

of hypoxia in the surrounding cells. This phenomenon, where hypoxia is induced by perfusion failure, was first characterized by Brown and colleagues in 1979, and was termed “acute” or perfusion limited hypoxia (Brown 1979). Interestingly, these acutely hypoxic cells would readily be reoxygenated when the vascular network is re-established. Duration of such hypoxia can vary greatly; studies with animal tumours reported the duration to be somewhere between 20 mins to several hours (Chaplin, Peters et al. 1991, Dewhirst 2009). Because of this dynamic nature, acute hypoxia is also referred to as intermittent or cyclic hypoxia (**Fig. 1.1A and C**).

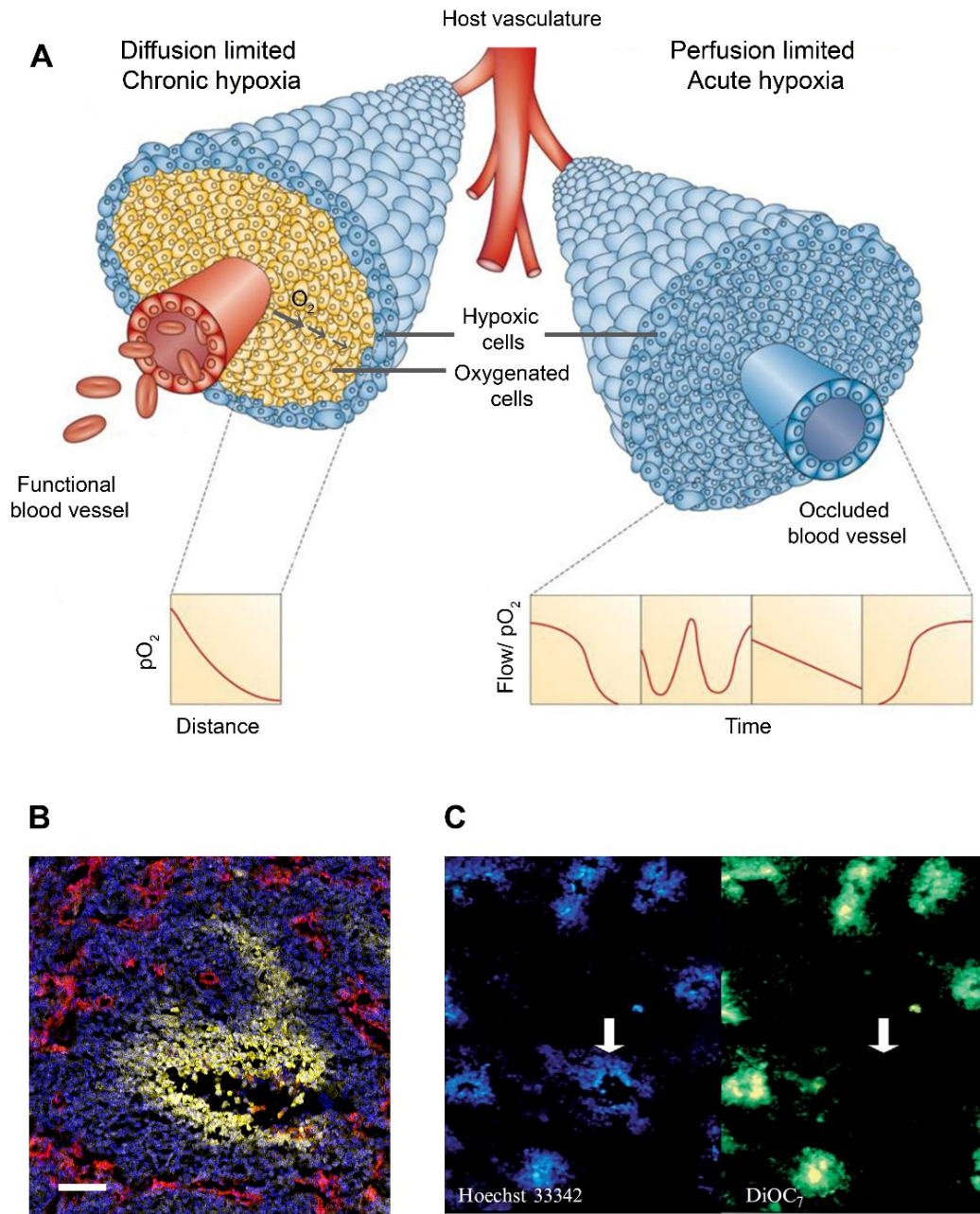


Figure 1.1 Tumour hypoxia occurs in solid tumours when cells are exposed to suboptimal levels of O_2 .

(A) Tumour hypoxia may arise either due to rapid cell growth beyond the diffusion limit of O_2 in respiring tissue (left), or as a result of heterogenous blood flow in the tumour mass (right) [adapted from (Horsman, Mortensen et al. 2012)]. (B) Immunofluorescence staining showing tumour vasculature in red (CD31), distal chronic hypoxic cells in yellow (pimonidazole immunostaining), and cell nucleus in blue (Hoechst); scale bar=200 μm [modified from (Rashed, Stoica et al. 2021)]. (C) Difference in perfusion geometry in tumours is demonstrated by injecting mice with two different perfusion markers Hoechst (blue) and DiOC₇ (green) with a 20 min lag between two injections; arrow shows functional blood vessel present with the first dye, but not with the second dye, indicating the vessel has closed down in the 20 min interval (Brown 2007).

1.1.3 Prevalence of hypoxia in human malignancies

Poor oxygenation in solid tumours has been known since the 1950s, albeit through indirect observations. In 1991, Vaupel and colleagues provided the first explicit evidence of hypoxia in human cervical cancer by directly measuring O₂ levels using polarographic electrodes (discussed further in section 1.4.1) (Höckel, Schlenger et al. 1991). The group later went on to document O₂ measurements for squamous head and neck tumours and breast cancers (Vaupel, Höckel et al. 2007). Additionally, the presence of hypoxic regions has also been confirmed in cancers of the prostate (Zhong, Semenza et al. 2004), rectum (Kuwai, Kitadai et al. 2003), pancreas (Duffy, Eibl et al. 2003), gliomas (Wei, Wu et al. 2011), soft tissue sarcomas (Nordsmark, Alsner et al. 2001), malignant melanomas (Hartmann, Kunz et al. 1999) and many more. Due to its wide distribution in different human malignancies, hypoxia is now considered a characteristic feature of solid tumours. **Table 1.1** lists comparative pO₂ values in different tumours and the tissue they originate from (McKeown 2014).

Table 1.1 Oxygenation status of tumours and healthy tissue in different human malignancies (McKeown 2014)

Tumour type	<i>n</i>	Median tumour pO₂	Median % O₂	<i>n</i>	Median normal tissue pO₂	Median % O₂
Brain	104	13	1.7	104	26	3.4
Head and neck cancer	592	10	1.3		ND	5.9
	30	12.2	1.6	14	40	5.3
	23	14.7	1.9	30	43.8	5.8
	65	14.6	1.9	65	51.2	6.7
Lung cancer	6	14.3	1.9		ND	5.6
	20	16.6	2.2		42.8	5.6
Breast cancer	212	10	1.3	212	52	6.8
Cervical cancer	730	9	1.2			
				48	42	5.5
Liver	4	6	0.8	4	30	3.9
Pancreatic cancer	7	2.7	0.4	7	51.6	6.8
	1	20.3				
Prostate cancer	59	2.4	0.3	59	30	3.9
	55	4.5	0.6		ND	
	10	9.4	1.2	2	26.2	3.4
Vulval cancer	29	11	1.4		ND	
	15	13	1.7		ND	
	19	11	1.4		ND	
	20	10	1.3		ND	
Melanoma	18	11.6	1.5	20	40.5	5.3
Renal cell carcinoma	3	10	1.3	3	37.6	4.9
Rectal carcinoma	14	32	4.2		52	4.8
	15	19	2.5		52	6.8
Sarcoma	283	14	1.8	28.3	51	6.7
Averages or total	2257	10.27	1.4	685	45.8	6
Ranges of medians		2-32	0.3-4.2		26-51.6	3.4-6.8

Table represents data from a meta-analysis by Vaupel et al. (Vaupel, Höckel et al. 2007), summarized by McKeown (McKeown 2014). n, number of patients; ND, not determined.

1.2 Cellular adaptations to tumour hypoxia

Cells exposed to low levels of O₂ utilize various hypoxia sensing mechanisms to coordinate their responses. Whether cells will withstand the low O₂ stress and become a resistant subpopulation, or succumb to the pressure and die depends on several factors, such as O₂ levels, duration of hypoxia and cell type. It should be mentioned here that our understanding of these complex (and often overlapping) cellular responses is compromised by the lack of a universal hypoxia model. Very often (including in this study), “normoxia” (referring to 20-21% O₂) is used as a non-hypoxia control. This is, however, not a true representation of normal tissue O₂ levels, which ranges from 3-7% (termed physoxia). Even when tissue O₂ levels fall below this range (i.e., hypoxic), cells display variable responses depending on the severity of hypoxia. “Physiological hypoxia” refers to transient drops in O₂ levels (2-6%) at which cells can activate O₂ homeostasis mechanisms (either by physiological means, such as vasodilation, increasing blood flow, and/or upregulation of hypoxia response genes) to maintain their preferred oxygenation status. When such mechanisms fail to reverse the phenotype, cells enter a state of persistently low O₂ levels; this can be referred to as “pathophysiological hypoxia” [reviewed in (McKeown 2014)]. Even with this understanding, the choice of a non-hypoxic control is still not straightforward because most cell lines used in biological research were generated by culturing them at 20-21% O₂, and over time have adjusted to this condition. Hence, simply exposing these cells to physoxic O₂ levels may not be a true representation of physiologically relevant non-hypoxic tissue. Again, another compromising factor is the use of 2D monolayer cell cultures in hypoxia research, which fails to emulate O₂ gradients seen in tumour microenvironments (Hompland, Fjeldbo et al. 2021). Despite these limitations, it is still possible to identify certain hypoxia selective responses in a cellular context. This section will briefly discuss a few of these hypoxia dependent cellular adaptations.

1.2.1 Altered chromatin organization and gene transcription

Mammalian DNA is wrapped around histone proteins to form nucleosomes, which then organize themselves into higher order structures called chromatin. Mature chromatin is dynamic in nature and may exist either in a highly compact (heterochromatin) or a relatively relaxed (euchromatin) state, through which it regulates the access of transcriptional machinery to DNA.

Additionally, post-translational modifications on histones (such as methylation, acetylation etc.) provide further regulation of transcriptional activities. For example, the tri-methylated version of histone 3 lysine 4 (H3K4me3) is found around active genes, whereas H3K9me3 and H3K27me3 are broadly considered to be repressive marks (Annunziato 2008). Interestingly, changes in chromatin conformation have been reported in response to hypoxic exposure (Batie and Rocha 2020). Using squamous cell carcinoma cells (A431), Dutta et al. showed that chromatin displays reduced sensitivity to mononuclease digestion under hypoxia, which is indicative of an increased heterochromatin signature (Dutta, Yan et al. 2014). Additionally, a global increase in histone methylation was observed in macrophages exposed to hypoxia (Tausendschön, Dehne et al. 2011). Similar observations were reported in hypoxic human bronchial epithelial cells (Beas-2B) and human lung carcinoma cells (A549) (Zhou, Sun et al. 2010). Such modifications have been attributed to inhibition of lysine demethylase activities. These enzymes, responsible for removing methyl groups from lysine residues, are dioxygenases and require O₂ for their function (Hompland, Fjeldbo et al. 2021). Hypoxic cells also display an increase in chromatin compaction, which is rapidly reversible upon reoxygenation (Dutta, Yan et al. 2014). While the full impact of chromatin modification under hypoxia is still poorly understood, it is presumed that such alterations may regulate access to DNA and selectively activate transcription of genes that provide survival advantage to hypoxic cells.

1.2.2 Hypoxia inducible factor (HIF) transcription factor

One of the best understood cellular responses to hypoxic stress is mediated by the transcription factor, hypoxia inducible factor (HIF). HIF belongs to the basic helix-loop-helix family of proteins, and consists of the O₂ sensitive subunit HIF-1 alpha (HIF1A) and the constitutively expressed aryl hydrocarbon nuclear translocator (ARNT) (also called HIF-1 beta, HIF1B). HIF1A contains an O₂ dependent domain (ODD) with two proline residues (P402 and P564 in humans) that are hydroxylated by the enzyme prolyl hydroxylase (PHD) under normal O₂ levels; iron, O₂ and 2-oxoglutarate (2-OG) are required for this step. The hydroxylated prolines on HIF1A are recognized by the Von Hippel Lindau (VHL) protein, which then recruits elongin B, C and cullin to form the E3 ubiquitin ligase complex, leading to polyubiquitination and subsequent proteasomal degradation of HIF1A. Under hypoxia, however, hydroxylation of HIF1A is inhibited due to substrate limitation (low O₂). This results in stabilization of HIF1A,

which then translocates to the nucleus and interacts with HIF1B to form the HIF1 heterodimer complex. HIF1A is also regulated through the factor inhibiting HIF1 (FIH-1) protein, which hydroxylates an asparagine on HIF1A in an O₂-dependent manner, and thereby prevents its dimerization with HIF1B (Mahon, Hirota et al. 2001, Sim, Cowburn et al. 2018). When active, the HIF complex binds to enhancer regions (called hypoxia response elements, HRE) on DNA, recruits co-activator CREB-binding protein/E1A-binding protein p300 (CBP/p300), and initiates the transcription of downstream genes. Altogether, transactivation of over 1500 genes has been linked to HIF1A, many of which promote growth and resistance in hypoxic cells (Prabhakar and Semenza 2015) (**Fig. 1.2**). Due to its overarching implications in hypoxia biology, HIF1A is often called the master regulator of hypoxia.

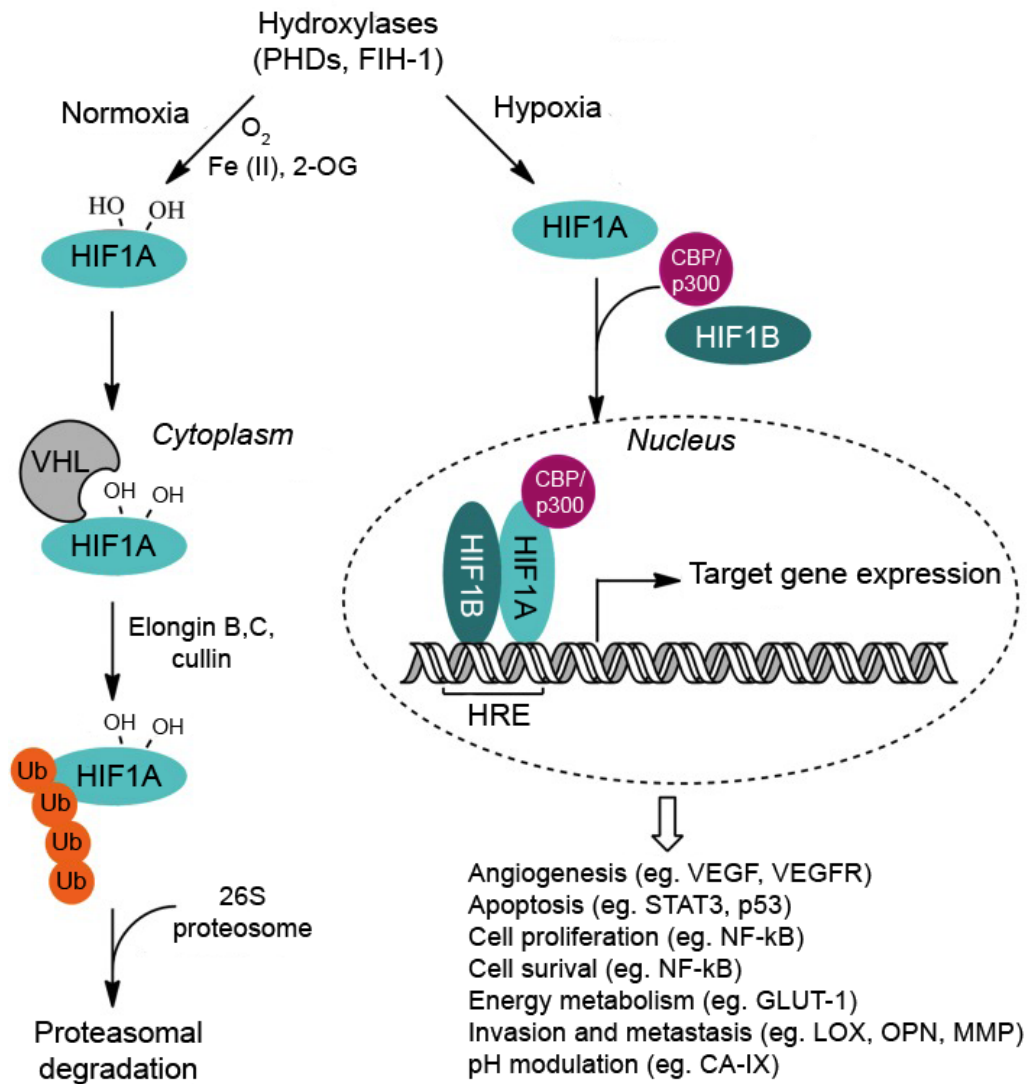


Figure 1.2 O₂-dependent regulation of HIF.

In normal O₂ levels, HIF1A is hydroxylated by PHD, which is recognized by pVHL leading to subsequent proteasomal degradation of HIF1A. FIH-1 can also hydroxylate HIF1A, which prevents its binding to the constitutively expressed HIF1B. Under hypoxia, low O₂ leads to HIF1A stabilization, which translocates to the nucleus, and together with HIF1B, forms the functional HIF transcription complex. Active HIF complex binds to HRE elements on target genes and drives their transcription [adapted from (Walsh, Lebedev et al. 2014)].

1.2.3 Hypoxia-induced metabolic reprogramming

Despite being less efficient at generating energy in the form of ATP, tumour cells generally favor glycolysis (followed by lactic acid fermentation) over oxidative phosphorylation for energy production, even in the presence of abundant O₂. This phenomenon, termed the Warburg effect, is thought to enable tumour cells to generate additional metabolites for sustaining their high proliferation rates (Liberti and Locasale 2016). Upregulation of proteins involved in this metabolic reprogramming has been observed under hypoxia, which is strictly regulated in a HIF-dependent manner. Hypoxia-induced stabilization of HIF1A directly increases expression of glucose transporter-1 (GLUT1), enhancing cellular capacity for glucose uptake (Chen, Pore et al. 2001). Additionally, HIF binding sites have been identified in the enhancer regions of genes encoding various glycolytic enzymes, such as glyceraldehyde-3-phosphate dehydrogenase (GAPDH), phosphofructokinase-liver type (PFKL), aldolase A (ALDOA), phosphoglycerate kinase (PGKI), enolase (ENOL) and lactate dehydrogenase A (LDHA) (Semenza, Roth et al. 1994, Higashimura, Nakajima et al. 2011). By selectively activating transcription of these enzymes, HIF ensures a high rate of glycolytic ATP production under hypoxia. Moreover, through induction of pyruvate dehydrogenase kinase 1 (PDK1) and LDHA, HIF1A also shuttles pyruvate (the end product of glycolysis) away from the tricarboxylic acid (TCA) cycle to lactic acid fermentation, further dampening oxidative phosphorylation. The resultant increase in glycolytic activity appears to provide hypoxic cells resistance to apoptosis, and can facilitate cellular proliferation even under low O₂ (Gwak, Yoon et al. 2005, Fulda and Debatin 2007).

1.2.4 Angiogenesis

Angiogenesis is the process through which new capillaries are formed from existing blood vessels. It is not surprising that angiogenesis is often stimulated under hypoxia to increase blood flow to O₂ starved regions (Rey and Semenza 2010). Many of the key regulators of this process, including vascular endothelial growth factor (VEGF), stromal derived factor 1 (SDF1), angiopoietin 2 (ANGPT2), placental growth factor (PGF), platelet-derived growth factor B (PDGFB) and stem cell factor (SCF) are either directly or indirectly regulated by HIF (Rey and Semenza 2010). HIFs play an essential role in embryonic development of the circulatory

system; HIF1A homozygous knockout mice show cardiac malformations, vascular regression, impaired hematopoiesis, and die *in utero* (Ryan, Lo et al. 1998). In addition to the secreted factors mentioned above, HIF also regulates expression of many cell surface receptors that allow endothelial cells to respond to angiogenic cytokines (Manalo, Rowan et al. 2005). Moreover, a recent study suggests that expression of the anti-angiogenic protein thrombospondin-2 is repressed in response to HIF1A stabilization (MacLauchlan, Calabro et al. 2018). High HIF1A expression has been associated with aggressive, highly vascularized tumour phenotypes, while loss of function of HIF1A decreases tumour growth and vascularization (Rey and Semenza 2010). Although the aim of HIF-mediated pro-angiogenic response in tumours is to provide relief by restoring O₂ homeostasis, the resultant tumour vasculature is mostly chaotic and poorly organized.

1.2.5 Global repression of protein synthesis and initiation of the unfolded protein response

Low O₂ levels (and associated energy crisis) pose a significant challenge for cell survival, and tumour cells often counteract it by slowing down or suppressing energy-consuming processes, such as protein translation. The mammalian target of rapamycin (mTOR) pathway plays a central role in cell growth, connecting cellular protein synthesis to the availability of growth factors, nutrients and energy, and is inactivated in response to O₂ deprivation (Wouters and Koritzinsky 2008). mTOR is a serine/threonine protein kinase that exists in two distinct complexes (mTORC1 and mTORC2). Activation of mTORC1 is regulated by RHEB (Ras homology expressed in brain), which itself is regulated by the tuberous sclerosis protein complex (TSC1/2). Active mTORC1 phosphorylates downstream targets, such as ribosomal protein S6 kinase and eukaryotic initiation factor 4E binding protein 1 (4E-BP1), which are regulators of protein synthesis. S6 kinase phosphorylates the ribosomal protein S6, whereas phosphorylation of 4E-BP1 prevents its interaction to the eukaryotic translation initiation factor 4E (eIF4E), leading to activation of cap-dependent translation. Under hypoxia, mTORC1 is repressed through activation of the TSC1/2 complex (and hence inhibition of mTORC1-RHEB interaction) by AMP-activated protein kinase (AMPK) (Arsham, Howell et al. 2003), which itself is triggered by hypoxia-induced reactive oxygen species (ROS) (Mungai, Waypa et al. 2011). Additional mechanisms for disrupting mTOR-RHEB association under hypoxia include competitive binding of mTOR to PML (loss of the promyelocytic leukaemia protein) (Bernardi,

Guernah et al. 2006), or of RHEB to BNIP (Bcl-2 homology 3 domain-containing protein) (Li, Wang et al. 2007). This leads to an overall repression of cap-dependent mRNA translation, and may aid in selective translation of hypoxia response genes that undergo cap-independent translation. Indeed, studies show that 4E-BP1 hypophosphorylation supports translation of genes implicated in hypoxic response, such as HIF1A and vascular endothelial growth factor A (VEGFA) (Richter and Sonenberg 2005).

Hypoxia also affects post-translational protein folding as formation of disulfide bonds is O₂-dependent (Koritzinsky, Levitin et al. 2013). Consequently, unfolded or misfolded proteins accumulate at the endoplasmic reticulum (ER) lumen, triggering the unfolded protein response (UPR) pathway. UPR activates ER stress sensor protein kinase R-like endoplasmic reticulum kinase (PERK) that phosphorylates its downstream target eukaryotic translation initiation factor 2 subunit 1 (eIF2 α) (Fels and Koumenis 2006, Koumenis and Wouters 2006). eIF2 α is a component of eIF2 protein complex, which is an early regulator of protein synthesis. Together with GTP and the initiator (Met)-tRNA, eIF2 forms a ternary complex, recruits the 40S ribosomal subunit, and scans the 5' ends of mRNA for AUG initiation codons. Formation of this ternary complex is regulated by eIF2 α , phosphorylation of which inhibits translation. While PERK-mediated phosphorylation of eIF2 α under hypoxia inhibits global protein synthesis, there is evidence that it simultaneously induces selective translation of mRNAs responsible for restoring ER homeostasis and promoting hypoxia tolerance (Koumenis and Wouters 2006).

1.2.6 Replication stress, altered DNA damage response and genetic instability

DNA replication is sensitive to low O₂ levels. Several enzymes involved in the nucleotide biosynthesis pathway (such as dihydroorotate dehydrogenase and ribonucleotide reductase) require O₂ for their function and hence, are suppressed under hypoxia. The resultant reduction in dNTP levels compromises DNA synthesis, stalls replication forks, generates single-stranded DNA and induces replication stress (RS) (Scanlon and Glazer 2015). This activates ATR (ataxia telangiectasia and Rad3 related kinase), a key RS sensor, initiating phosphorylation of downstream targets CHK1 (S317/S345), H2AX (S139), RAD17 (S645), and NBS1 (S343) (Hammond, Denko et al. 2002, Hammond, Dorie et al. 2003, Hammond, Green et al. 2003). In addition to RS, hypoxia induced heterochromatin-like state can also activate ATM (ataxia

telangiectasia mutated) in an MRN (Mre11-Rad50-Nbs1) complex independent manner, and thereby contrasts from the canonical DNA damage induced ATM activation (Olcina, Foskolou et al. 2013). Activation of ATR and ATM under hypoxia appears to be important for replication fork protection, as loss of either results in DNA damage under hypoxia (Hammond, Dorie et al. 2004, Olcina, Foskolou et al. 2013). Additionally, Fallone et al. reported that hypoxia induced ATR kinase activity may also regulate HIF1A translation since loss of ATR results in a decrease of HIF1-DNA binding under hypoxia (Fallone, Britton et al. 2013).

Interestingly, activation of ATR-Chk1 and ATM-Chk2 pathways (traditionally implicated in DNA damage response) happens under hypoxia in the absence of detectable DNA damage (Olcina, Foskolou et al. 2013). However, whether there is no actual damage to DNA under hypoxia, or the damage is below the threshold of current experimental detection techniques remains to be answered (Tang, Bolderson et al. 2021). Regardless, effects of hypoxia on DNA repair pathways are well documented. Depending on the severity and duration of hypoxia, genes involved in the homologous recombination (HR), mismatch repair (MMR), and potentially nucleotide excision repair (NER) pathways may be downregulated either in a HIF-dependent or HIF-independent manner. For example, prolonged severe hypoxia leads to epigenetic alterations in chromatin structure that downregulate *MLH1* and *MSH6* genes in the MMR pathway (Rodríguez-Jiménez, Moreno-Manzano et al. 2008), while short-term moderate hypoxia can inhibit *MSH2* and *MSH6* through HIF1A (Koshiji, To et al. 2005). Hypoxia-induced global repression of protein synthesis also downregulates many key HR enzymes (such as BRCA1 and RAD51) and consequently, hypoxic cells display ~3-8 fold decrease in HR capacity (Bindra, Schaffer et al. 2004, Bindra, Gibson et al. 2005). NER capacity also seems to be affected by low O₂ exposure, as evident from a reduction in cellular capacity to repair UV-damaged plasmid DNA under hypoxia (Yuan, Narayanan et al. 2000). Dudás et al. reported a downregulation of the NER gene, *ERCC1*, both at mRNA and protein levels in hypoxic pharyngeal carcinoma cells (Dudás, Schartinger et al. 2014). Again, NER factor *XPC* mRNA levels increase in response to downregulation or phosphorylation of HIF1A in human keratinocytes; however, a positive regulation was also reported between HIF1A and XPD protein levels (Rezvani, Mahfouf et al. 2010). In contrast, effects of hypoxia on non-homologous end joining (NHEJ) are less certain, and reports are often contradictory (Meng, Jalali et al. 2005, Ren, Hao et al. 2013). Nonetheless, the current consensus in the field seems

to be that NHEJ proteins (Ku70, Ku80 and DNA-PKcs) as well as NHEJ efficiency increase in response to hypoxic exposure (Madan, Gogna et al. 2012, Ren, Hao et al. 2013). Such alterations in DNA damage response machinery have direct implications for hypoxic cells. Attenuated HR and MMR response may likely contribute to elevated mutation frequency and generate genomic instability (Tang, Bolderson et al. 2021). Moreover, since the NHEJ pathway is an error-prone pathway, upregulation of NHEJ proteins can also drive increased mutagenesis under hypoxia/reoxygenation (Scanlon and Glazer 2015). Indeed, cells exposed to hypoxia often show chromosomal aberrations, DNA over-replication, gene amplification and fragile-site induction (Reynolds, Rockwell et al. 1996, Tang, Bolderson et al. 2021).

1.3 Clinical significance of tumour hypoxia

Hypoxic tumour cells are surprisingly well equipped to survive, remain viable and even expand in their persistently O₂-depleted microenvironment. The genetic and metabolic adaptations that enable them to withstand hypoxic insults can also favor clonal expansion of stress-resistant, more aggressive phenotypes. Intratumoural O₂ gradients also support plasticity and heterogeneity, and thereby promote metastasis. More importantly, hypoxic tumours can evade conventional cancer treatments (irrespective of their mode of action), and thus contribute to treatment failure and disease relapse [reviewed in (Walsh, Lebedev et al. 2014)]. Therefore, patients who present in clinics with highly hypoxic tumours usually fare poorly compared to those with well-oxygenated tumours. The presence of hypoxia has been associated with adverse clinical outcomes in multiple tumour types. For example, in a study carried out by Brizel et al., when head and neck cancer (HNC) patients were divided into less hypoxic (pO₂ >10 mmHg) and more hypoxic (pO₂ <10 mmHg) groups, the latter showed worse rates of 2-year local-regional control (LRC; 30 versus 73%), disease-free survival (DFS; 26 versus 73%) and overall survival (OS; 35 versus 83%) (Brizel, Dodge et al. 1999). Similarly, Rudat et al. reported that hypoxic fraction (HF_{2.5}) was predictive of poor OS in stage IV HNC patients treated with radiation (with or without chemotherapy) (Rudat, Vanselow et al. 2000). In both primary and recurrent cancers of the uterine cervix, hypoxia was associated with significantly worse DFS and OS (Höckel, Schlenger et al. 1996, Höckel, Schlenger et al. 1998). In line with these observations, hypoxia has been validated as a negative prognostic marker in many tumour types, such as gliomas (Huang, Michalek et al. 2021), soft tissue sarcoma (Brizel, Scully et al.

1996), as well as in cancers of the lung (Le, Chen et al. 2006, Hung, Yang et al. 2009) and prostate (Turaka, Buyyounouski et al. 2012). This section will highlight some of the key mechanisms through which hypoxic tumour cells can acquire therapy resistance.

1.3.1 Resistance to radiation therapy

Radiation therapy (RT) constitutes one of the major modalities of cancer treatment, both as a curative intervention and for palliative management of the disease (Baskar, Lee et al. 2012, Salminen, Clemens et al. 2012). Almost 50% of all cancer patients receive RT at some point during the course of their treatment (Barnett, West et al. 2009, Baskar, Lee et al. 2012). RT is also a highly cost effective single modality treatment, accounting for only ~5% of total cost of cancer care (Ringborg, Bergqvist et al. 2003). Therefore, reduced sensitivity of hypoxic cells to RT poses a significant challenge for treating cancer patients.

In clinics, RT is mostly delivered through an external beam of high energy ionizing rays (photons, protons or particle radiation), or sometimes using radioactive seeds, ribbons, or capsules for localized tumours (such as gynecological and prostate cancers) (Dietrich, Koi et al. 2015). DNA is the primary target of RT, and ionizing radiation (IR) works by damaging the DNA double helix structure. It can either directly disrupt the DNA sugar-phosphate backbone, or act through generation of hydroxyl free radicals by ionizing cellular water molecules; both processes ultimately produce DNA free radicals. Under normal O₂ levels, these DNA free radicals are oxidized and thereby fixed (i.e., made permanent). If cells accumulate high enough levels of DNA damage such as double strand breaks (DSBs), they undergo cell death or irreversible growth arrest (Brown and Wilson 2004, Baskar, Lee et al. 2012). In the absence of O₂, IR-induced DNA free radicals are more likely to be resolved (and subsequently quenched) through hydrogen donation from thiol-containing cellular macromolecules; this is known as “chemical restitution” [Fig. 1.3; reviewed in (Brown and Wilson 2004)]. Consequently, less net DNA damage is generated for a given radiation dose under hypoxia compared to well oxygenated conditions. In fact, hypoxic cells can demonstrate up to three times more resistance to RT compared to their well oxygenated counterparts (Rockwell, Dobrucki et al. 2009).

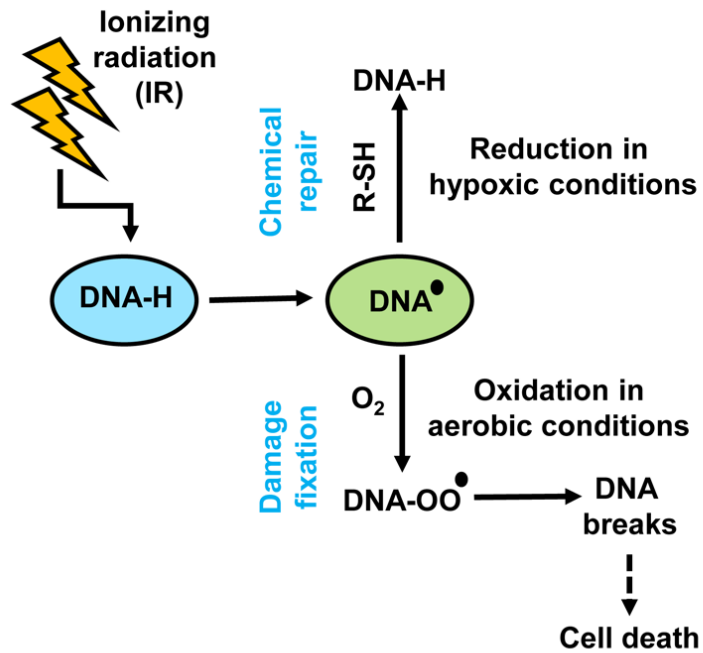


Figure 1.3 Compromised efficacy of IR in hypoxic cells.

IR induces DNA free radicals, which are stabilized by reaction with molecular O₂ under normoxia; cells accumulating high DSBs undergo cell death. In hypoxic cells, IR-induced DNA free radicals are chemically resolved by thiol-containing cellular macromolecules, through a process known as “chemical restitution” [adapted from (Brown 2007)].

1.3.2 Resistance to chemotherapy

Hypoxic cells have been reported to display reduced sensitivity to many anti-cancer drugs (listed in **Table 1.2**) (Graham and Unger 2018). Hypoxia-induced resistance to chemotherapy can be attributed to both physiological and genetic factors. Firstly, viable hypoxic cells can reside as far as 200 μm from nearby blood vessels (Olive, Vikse et al. 1992), creating a diffusion barrier that chemotherapeutic agents must overcome in order to reach the hypoxic tumour core. Drugs can often be metabolized by cells adjacent to the blood vessels before they can reach the distant hypoxic cells (Janssen, Haustermans et al. 2005). Chaotic tumour vasculature also promotes heterogeneous blood flow that affects physical delivery of the drug. Secondly, certain chemotherapeutic agents (e.g., bleomycin) require O_2 to impart their full cytotoxic potential, and thereby are less effective against hypoxic cells (Batchelder, Wilson et al. 1996). Thirdly, most anti-cancer drugs have been designed to target and destroy rapidly proliferating cells, and thus are less damaging to hypoxic cells because of their quiescent nature (Li, Wu et al. 2017). Hypoxia induces G1-arrest in cells in a HIF dependent manner (Goda, Ryan et al. 2003), which can lead to resistance to antifolates (such as methotrexate, MTX) (Raz, Sheban et al. 2014). MTX functions by compromising DNA/RNA synthesis through inhibition of folate-dependent enzyme dihydrofolate reductase (DHFR) activity (Raimondi, Randazzo et al. 2019). Hypoxic exposure causes *DHFR* gene amplification in Chinese hamster ovary cells, providing additional mechanisms to resist the drug (Rice, Ling et al. 1987). Similarly, hypoxic cells can also upregulate expression of additional proteins involved in drug resistance. For example, a significant increase in the expression of metallothionein was reported in hypoxic human squamous carcinoma cells, which promotes resistance to cisplatin by sequestering it (Murphy, Laderoute et al. 1994). Additionally, a HIF binding domain was identified in the promoter region of the *MDR1* gene, which expresses MDR1/P-glycoprotein (P-gp), a drug efflux pump responsible for transporting drugs out of cells and thereby reducing intracellular drug concentrations (Comerford, Wallace et al. 2002). Hypoxia-induced HIF1A stabilization can stimulate expression of metastasis related genes (such as osteopontin, lysyl oxidase, CXCR4, IL8, VEGF etc.), which can contribute to therapy resistance and malignant progression (McKeown 2014). Further complications arise from the fact that hypoxic stress can trigger selection of clones with mutated p53 proteins and reduced apoptotic potentials, counteracting the effects of drugs that depend on this pathway (Goda, Ryan et al. 2003). Finally, recent

observations also suggest that hypoxic regions may support growth and maintenance of therapy resistant cancer stem cells (CSCs) by modulating various signalling pathways (Keith and Simon 2007, Nejad, Najafgholian et al. 2021). Due to the presence of such multi-faceted resistance mechanisms in hypoxic cells, standard chemotherapeutic agents often fail to eliminate them, resulting in recurrent disease. Therefore, it is crucial to develop compounds that can overcome the hypoxia-mediated diffusion barrier and chemoresistance for proper management of solid malignancies.

Table 1.2 List of anticancer drugs that show reduced efficacy under hypoxia (Graham and Unger 2018)

Drug	Type of compound
5-Fluorouracil	Antimetabolite
Actinomycin D	Antitumour antibiotic
Bleomycin	Antitumour antibiotic
Carboplatin	Alkylating agent
Cisplatin	Alkylating agent
Docetaxel	Plant alkaloid, mitosis inhibitor, taxane
Doxorubicin	Anthracycline antibiotic
Etoposide	Plant alkaloid, topoisomerase II inhibitor
Gemcitabine	Antimetabolite
Irinotecan	Plant alkaloid, topoisomerase I inhibitor
Melphalan	Alkylating mustard analog
Methotrexate	Antimetabolite
Oxaliplatin	Alkylating agent
Procarbazine	Alkylating agent
Sorafenib	Multikinase inhibitor, antiangiogenic
Streptonigrin	Antitumour antibiotic
Temozolomide	Alkylating agent
Thiotepa	Alkylating agent
Vincristine	Plant alkaloid, vinca alkaloid
VP-16	Plant alkaloid, topoisomerase II inhibitor

1.3.3 Resistance to immunotherapy

In recent years, modulation of the immune system to potentiate anti-tumour immunity has emerged as a novel strategy to eliminate tumour cells. Of particular promise are agents that can block immune checkpoints, and thereby alleviate inhibitory signals on immunologic stimuli. Monoclonal antibodies targeting the cytotoxic T lymphocyte associated protein 4 (CTLA-4) and programmed cell death protein 1 (PD-1) have shown clinical benefits, paving the way for their approval by the FDA (Noman, Hasmim et al. 2019). However, early preclinical and clinical data indicate that the presence of hypoxia may compromise efficacy of anticancer immunotherapy (Chouaib, Messai et al. 2012, Lequeux, Noman et al. 2019). Hypoxia-induced inhibitory effects on immunotherapy can be broadly classified into two categories. Firstly, a hypoxic microenvironment can regulate the access of immune cells to the tumour. It has been observed that hypoxic tumour areas are poorly infiltrated by anti-tumour immune cells, while simultaneously they can attract large numbers of immune suppressive cells [such as myeloid derived suppressor cells (MDSCs), tumour associated macrophages (TAMs) and T-regulatory (T-reg) cells]. These cells can induce T-cell anergy, and dampen cell mediated killing by T-cells and natural killer (NK) cells. Secondly, hypoxia-induced stabilization of HIF1A can upregulate expression of inhibitory signals, such as programmed death-ligand 1 (PD-L1) (Noman, Desantis et al. 2014), V-domain immunoglobulin suppressor of T-cell activation (VISTA) (Deng, Li et al. 2019), and cluster of differentiation 47 (CD47) (Zhang, Lu et al. 2015). High expression of PD-L1 and VISTA can negatively impact T-cell proliferation and activity, whereas tumour cells expressing CD47 resist phagocytosis by macrophages and dendritic cells (Noman, Hasmim et al. 2019). HIF1A has been reported to activate transcription factor FoxP3, favoring differentiation of T-reg cells, which are responsible for effector T-cell suppression (Clambey, McNamee et al. 2012). Hypoxia can also stimulate tumour cells to shed their major histocompatibility complex (MHC) class I polypeptide-related sequence A (MICA) marks, which prevents their recognition by NK cells (Siemens, Hu et al. 2008).

1.4 Hypoxia detection strategies

Given the numerous treatment complications that arise due to tumour hypoxia, it is imperative to properly estimate tumour oxygenation status both for identifying patients likely to develop resistance, and to monitor their response to therapy. Over the years, various strategies have been devised to clinically detect tumour hypoxia. However, only a few of them can directly measure O₂ levels, while most utilize labelling of hypoxic cells with exogenous compounds or detection of hypoxic specific proteins or gene markers as a readout of hypoxia. This section will briefly discuss some of the more widely used hypoxia detection techniques.

1.4.1 O₂ electrode probe

Polarographic O₂ electrode probes provide direct measurement of pO₂ within the tumour, and therefore is recognized as the gold standard for hypoxia quantification (Collingridge, Young et al. 1997, Walsh, Lebedev et al. 2014). O₂ electrodes utilize the electrochemical reduction of O₂ at the probe (cathode) surface that produces OH⁻ ions and requires electron (e⁻) supply from an anode ($O_2 + 4e^- + 2H_2O \Rightarrow 4OH^-$). The resultant current is proportional to the pO₂ at the electrode tip (Collingridge, Young et al. 1997). While polarographic electrode probe readings have provided conclusive evidence for lower O₂ tension in tumours compared to healthy tissue (Vaupel, Höckel et al. 2007, McKeown 2014), their utility is compromised by several factors (Walsh, Lebedev et al. 2014). For example, due to their highly invasive nature, use of these probes requires skilled personnel, and inter-operator variability can be an issue. Additionally, this method is only applicable for tumour sites that are easily accessible (such as cancers of head and neck, breast, and cervix), but not for deeply seated tumours. These probes also need a definitive pO₂ threshold to distinguish between well oxygenated and hypoxic subgroups. Moreover, O₂ electrode probes cannot distinguish between viable and necrotic cells, which may lead to overestimation of hypoxia if necrotic areas are sampled (Vaupel, Höckel et al. 2007).

1.4.2 Exogenous hypoxia reporters

Exogenous hypoxia markers rely on hypoxia selective accumulation of agents to label and detect O₂ deprived cells. Nitroimidazoles (NIs), such as pimonidazole and EF5, have proven to be particularly useful for this purpose. NIs undergo enzymatic activation and subsequent

binding to cellular constituents in hypoxic cells, which traps them inside (discussed further in section 1.5.3.1). Detection of these drug-adducts can act as a surrogate marker for tissue hypoxia. Studies found that the rate of NI-adduct formation increases incrementally as O₂ levels decrease from 5% to 0.5% (Koch, Evans et al. 1995, Koch 2002). Since functional enzymes are required for NI activation, this approach therefore only labels viable cells (and not necrotic populations) (Walsh, Lebedev et al. 2014). Various methods have been developed to identify hypoxia selective formation of NI-adducts. The most common (and invasive) technique utilizes immunochemical detection of NI-adducts by microscopy, ELISA or flow cytometry (Koch, Evans et al. 1995, Azuma, Raleigh et al. 1997, Varia, Calkins-Adams et al. 1998). Immunohistochemical analysis of pimonidazole- and EF-5-adducts have been successfully incorporated in clinical studies, and were predictive of treatment outcome and metastasis (Kaanders, Wijffels et al. 2002, Evans, Fraker et al. 2006). Additionally, a highly desirable trait of NI based agents is that when radiolabelled, they facilitate non-invasive hypoxia tracking using PET/SPECT imaging. This allows for seamless incorporation of hypoxia detection within the existing treatment module, enables repeated monitoring of tumour oxygenation during the treatment duration, and can be applied without the need for biopsies. Examples of some clinically validated NI-based hypoxic radiotracers include ¹⁸F-FMISO, ¹⁸F-EF5, ¹⁸F-FAZA etc. Use of these radiotracers to (a) identify patients with tumours containing high hypoxic fractions, and (b) monitor dynamic changes in tumour O₂ levels following treatment, proved to be useful in clinical settings (particularly for HNC patients) and was predictive of patient outcome (Komar, Lehtiö et al. 2014, Servagi-Vernat, Differding et al. 2014, Saksø, Mortensen et al. 2020, Carles, Fechter et al. 2021).

1.4.3 Endogenous markers of tumour hypoxia

Molecular markers (such as proteins and genes) that are upregulated under hypoxia have been extensively studied as potential hypoxia diagnostics. Immunochemical detection of proteins, such as HIF1A [and its downstream targets carbonic anhydrase IX (CA-IX), GLUT-1, VEGF etc.], for hypoxia diagnosis does not require administration of an external agent, and hence can be applied to study archival tissue samples. However, clinical application of these endogenous markers showed mixed results. While some studies identified these proteins as prognostic factors for patient response in HNC, cervical cancer, breast cancer and small cell lung

carcinoma, others found no association with patient outcome in the same cancer model [reviewed in (Le and Courter 2008, Walsh, Lebedev et al. 2014)]. Overall, combined staining for multiple endogenous markers usually provides a higher predictive power of OS than a single marker alone. Hui et al. reported that combining HIF1A staining with CA-IX or VEGF staining could predict significantly worse progression free survival (PFS) in patients with nasopharyngeal carcinoma, while single markers could not (Hui, Chan et al. 2002). Similarly, a “hypoxic score” generated from combining staining information of lysyl oxidase (LOX), ephrin A1, galectin-1, and CA-IX proved to be prognostic for cancer-free survival and OS in HNC patients (Le, Kong et al. 2007). Nevertheless, use of endogenous proteins for hypoxia diagnosis suffers from certain inherent limitations. Firstly, HIF1A expression can be detected at O₂ levels as high as 2%, whereas the O₂ levels at which hypoxia affects prognosis are significantly lower (Brizel, Dodge et al. 1999, Rudat, Vanselow et al. 2000, Vordermark and Horsman 2016). HIF1A and CA-IX staining usually appears more diffuse and closer to the blood vessels than that of NI-stained regions, suggesting these proteins are upregulated at higher O₂ levels than is required to activate nitroimidazoles (Hoskin, Sibtain et al. 2003, Hutchison, Valentine et al. 2004). Additionally, expression of many of these proteins are linked to both hypoxic and non-hypoxic conditions. For example, apart from low O₂ stress, HIF1A can also be upregulated in response to other non-hypoxic stimuli, such as mutations in phosphatase and tensin homolog (PTEN), VHL, succinate dehydrogenase, or fumarate hydratase (Zhong, Chiles et al. 2000). Activation of the phosphoinositide 3 kinase (PI3K)/Akt/mTOR apoptosis pathway and the formation of mitochondrial ROS can also increase HIF1A expression or accumulation (Hudson, Liu et al. 2002, Semenza 2011). Finally, many of the endogenous protein markers showed poor correlation with polarographic electrode based pO₂ values (Mayer, Wree et al. 2004, Mayer, Höckel et al. 2005). Encouragingly, recent studies focusing on metagene analysis identified a few hypoxia gene signatures with prognostic value across multiple cancer types. Eustace et al. reported a 26-gene signature in laryngeal cancer that predicted benefit from hypoxia-modifying treatment (Eustace, Mani et al. 2013), whereas a 28-gene hypoxia signature showed a strong and independent prognostic value for prostate cancer patients (Yang, Roberts et al. 2018). Similar hypoxia specific gene signatures were reported in hepatocellular carcinoma (7 genes) (Bai, Qi et al. 2021), pancreatic cancer (8 genes) (Abou Khouzam, Rao et al. 2021)

and non-small-cell lung cancer (17 genes) (Chen, Zhang et al. 2019). Further studies would be required to assess their broader applicability in a clinical context.

1.5 Hypoxia-targeted therapy

Targeting tumour hypoxia is a difficult but necessary step to improve patient response to treatment. Despite many attempts in the last six decades, hypoxia has remained an elusive therapeutic target. Consequently, an effective hypoxia-directed therapy is still absent in standard cancer treatment regimens. Clinical efforts to address tumour hypoxia can be broadly categorized into three groups: (a) increasing tumour O₂ levels, (b) augmentation of RT delivery, and (c) using compounds that are selectively activated under hypoxia. A brief description of these methods is provided below.

1.5.1 Increasing tumour oxygenation

As early as the 1960s, attempts were undertaken to improve tumour oxygenation (and thereby enhance RT effects) by allowing patients to breathe high pressure O₂ (1.5-3 atm) during RT (Dische 1978). Termed hyperbaric oxygen therapy (HBOT), it works by increasing O₂ carrying capacity of plasma (Brizel, Lin et al. 1995, Jain 2017). In clinical studies, significantly improved rates of local control and survival were reported in advanced HNC and cervical cancer patients breathing HBO, but not in cases of lung and bladder cancer (Dische 1978, Watson, Hainan et al. 1978, Henk 1986). However, simultaneous delivery of HBO and RT proved to be technically challenging, cost inhibitory, and at times can increase risks of late tissue toxicities, radiation necrosis and seizures in patients (Kohshi, Kinoshita et al. 1996, Tharmalingham and Hoskin 2018). Subsequent studies identified carbogen (95% O₂, 5% CO₂) as a more reliable alternative, which was then combined with oral nicotinamide (a vitamin B3 analogue) and accelerated radiotherapy to avail the combined benefits of all three components. In murine mammary tumours, accelerated radiotherapy in combination with carbogen breathing and oral nicotinamide (ARCON) generated an enhancement ratio of 1.9 compared to conventional radiation alone, suggesting that ARCON use can generate similar effects to standard RT with almost a 50% lower radiation dose (Rojas, Hirst et al. 1996). In a phase III clinical trial, use of ARCON improved local control (81 versus 76%) and overall survival (59 versus 46%) over the radiotherapy alone arm in locally advanced bladder cancer patients (Hoskin, Rojas et al. 2010).

Additionally, Janssens et al. reported a phase III clinical trial with laryngeal cancer patients comparing the efficacy of ARCON against accelerated RT alone (Janssens, Rademakers et al. 2012). Although no improvement in local control was observed at 5 years, regional control was significantly improved by ARCON (by 13%; $p=0.04$) with strong response in patients with hypoxic tumours. More importantly, no additional toxicity was recorded in patients in the ARCON arm, unlike the responses seen with HBOT. One potential drawback of ARCON is that it can reduce the radiation tolerance of the spinal cord by almost 20%, which should be taken into account during RT planning with ARCON (Haustermans, Van der Kogel et al. 1994).

1.5.2 Augmentation of RT delivery

Since hypoxic cells display two to three times more resistance to RT, delivering a higher radiation dose could, at least in theory, eliminate these resistant subpopulations. The limiting factor for such an approach is normal tissue toxicity. Interestingly, it has been proposed that this issue can be circumvented by modulating RT dosage in such a way that only hypoxic tumour fractions would receive the elevated radiation. This strategy, termed dose painting, would spare the non-hypoxic cells from unnecessary higher radiation doses, and thereby promises to alleviate associated toxic side effects (Bentzen and Gregoire 2011, Grégoire, Guckenberger et al. 2020). Current advanced RT delivery technology, such as image guided RT (IGRT) and intensity modulated RT (IMRT), utilizes MRI or CT-scan based information to deliver radiation to contoured tumour volumes, sparing nearby non-malignant tissues. Incorporation of functional imaging (such as PET/MRI hypoxia imaging) to these techniques can enable dose-escalation specifically to hypoxic tumour regions, which is currently being tested in clinical settings. The feasibility of this approach was first described in a cohort of HNC patients, where hypoxic tumour regions (identified through ^{18}F -FMISO-PET) received a 20% dose-escalation to 84 Gy (and in case of one patient, as high as 105 Gy) while maintaining nontarget tissue doses below normal tolerance levels (70 Gy) (Lee, Mechalakos et al. 2008). Hendrickson et al. reported a 17% increase in tumour control probability when hypoxia specific dose-escalations were applied using combined ^{18}F -FMISO-PET imaging and IMRT on HNC patients, without increasing complications (Hendrickson, Phillips et al. 2011). An interim analysis from a stage II clinical study assessing patients with locally advanced HNC found better LRC rates (70%) in patients who had hypoxic tumours and received dose-escalation in

comparison to patients with hypoxic tumours only receiving standard radio-chemotherapy (44.4%). Similar levels of treatment compliance, acute and late toxicity were seen in both arms (Welz, Mönnich et al. 2017). Although these results are very promising, dose-escalation RT is still in its early days, and additional research would be necessary to assess its clinical applicability and to test the effects of hypoxia redistribution during ongoing treatment schedules. The latest RT devices that combine MR imaging and linear accelerators (MR-linacs) should aid in further development of this technique (Grégoire, Guckenberger et al. 2020).

1.5.3 Hypoxia-activated prodrugs

Hypoxia-activated prodrugs (HAPs) are select compounds with special chemical moieties (nitro groups, quinones, aromatic *N*-oxides, aliphatic *N*-oxides and transitional metals) that allow them to undergo preferential enzymatic reduction when O₂ levels are low, leading to their subsequent entrapment or activation in hypoxic cells (Wilson and Hay 2011). Due to their higher affinity for O₂-starved cells, many of these compounds were pursued as potential hypoxia-directed therapeutics, either as hypoxic cytotoxins (e.g., aromatic *N*-oxides such as tirapazamine and its analogue SN30000, and aliphatic *N*-oxides such as AQ4N and its deuterated analogue OCT1002) or as hypoxic radiosensitizers (nitroimidazoles, NIs). While the compounds showed promising results in pre-clinical models, in most cases these observations did not translate into improved outcome in clinical studies [reviewed in (Brown 2007, McKeown 2014, Walsh, Lebedev et al. 2014, McKenna, Errington et al. 2018)]. It is now well-accepted that failure of these trials can be attributed, at least in part, to poor study design that did not take into consideration the tumour oxygenation status of patients. With subsequent analysis where patients were stratified based on a hypoxia cut-off, the outcome looked more favourable (Overgaard, Eriksen et al. 2005, Toustrup, Sørensen et al. 2012). An in-depth review of the extensive field of HAP research is beyond the scope of this report, which will only focus on the NI family of HAP compounds.

1.5.3.1 Nitroimidazoles as hypoxia-directed therapeutics

Nitroimidazoles (NIs) are a class of organic heterocyclic compounds with a nitro group substituted at position 2, 4 or 5 on the imidazole ring. These highly electron-affinic molecules are reduced by flavoprotein nitroreductases (such as xanthine oxidase, NADPH cytochrome

P450 reductase, NADPH cytochrome C reductase etc.) as they enter cells, generating nitroradical anions ($R\text{-NO}_2^{\bullet-}$). This step is reversible in the presence of O_2 , which converts the anion free radical back to its parental form ($R\text{-NO}_2$) that can freely diffuse out of cells. This O_2 -directed futile cycle ensures that little to no drug is retained in well oxygenated cells. However, when the O_2 level is low (i.e., hypoxic), the initial free radical anion cannot revert to the parent molecule and instead undergoes radical decay, producing nitroso ($R\text{-NO}$) and finally the reactive hydroxylamine ($R\text{-NHOH}$) derivative. $R\text{-NHOH}$ is electrophilic in nature and can covalently bind to cellular macromolecules, which subsequently trap the drug inside hypoxic cells (Edwards 1986, Kedderis, Argenbright et al. 1989, Kizaka-Kondoh and Konse-Nagasawa 2009). Therefore, unlike O_2 (and other standard drugs), NI compounds can overcome the diffusion barrier to reach cells in hypoxic regions and not get metabolized by the well-oxygenated cells (**Fig. 1.4**). An O_2 independent reduction of NIs involving O_2 insensitive nitroreductases (such as NfsA, NfsB, RdxA etc.) has also been reported, but only in microbial systems (Thomas and Gwenin 2021).

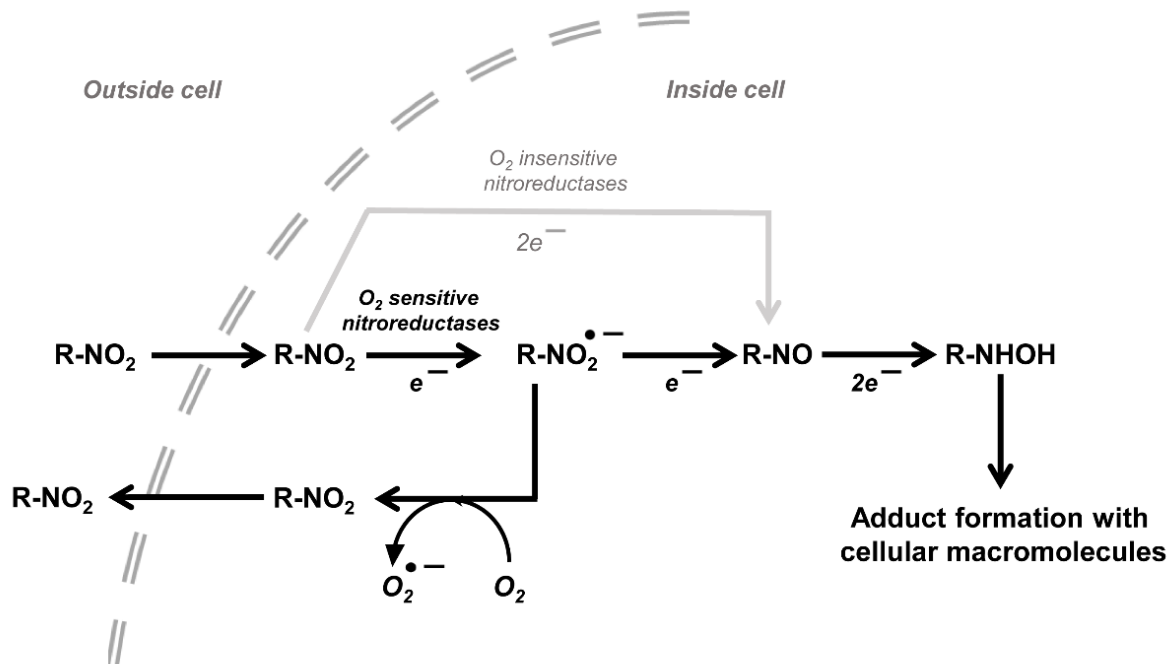


Figure 1.4 Hypoxia selective entrapment of NIs.

After entering cells through passive diffusion, NIs ($R-NO_2$) are reduced by cellular nitroreductases and generate a nitroradical anion ($R-NO_2^{\bullet-}$). $R-NO_2^{\bullet-}$ reacts with O_2 in well-oxygenated cells to revert to the parent molecule that can freely diffuse out of the cell. Under hypoxia, $R-NO_2^{\bullet-}$ undergoes further reduction to generate reactive hydroxylamine ($R-NHOH$) that binds to cellular macromolecules, leading to entrapment of the drug [adapted from (Kizaka-Kondoh and Konse-Nagasawa 2009, Thomas and Gwenin 2021)].

NIs have been used as antibiotics to treat infections caused by anaerobic bacteria and protozoans since the 1960s. Some well-known examples still used today include 5-NI based antibiotics, such as metronidazole (flagyl) and tinidazole (Gardner and Hill 2001). In 1973, Chapman and colleagues first reported that metronidazole can also sensitize hypoxic cells to radiation (Chapman, Reuvers et al. 1973). This sparked a global interest in NIs as potential hypoxia-targeted anti-cancer agents. In subsequent *in vitro* studies, 2-NI based compounds (such as misonidazole, initially referred to as Ro-07-0582) consistently outperformed 5-NIs including metronidazole (Asquith, Watts et al. 1974, Adams, Flockhart et al. 1976). Similar observations were reported by Denekamp et al. when comparing the hypoxic radiosensitization efficacies of 5-NI metronidazole and 2-NI misonidazole in albino mice using an epidermal cell survival assay. An enhancement ratio of ~1.5 was achieved with around half mean lethal dose (LD) of metronidazole and one fifth of mean LD of misonidazole. At 50% of its mean LD, misonidazole gave an enhancement ratio of ~2.2 (Denekamp, Michael et al. 1974). This difference in efficacy has been attributed to the reduction potential of the 2-NI moiety (-0.39 V), which is higher than both 4-NI (-0.56 V) and 5-NI (-0.47 V), but lower than that of O₂ (around -0.15 V) (Kizaka-Kondoh and Konse-Nagasawa 2009). Hence, later studies mostly concentrated on 2-NI derivatives for therapeutic targeting of hypoxic tumours.

One of the early 2-NI candidates that was heavily pursued as a hypoxia-directed therapeutic agent was misonidazole, which underwent extensive preclinical and clinical evaluations. Mammalian cell-based assays demonstrated encouraging results where the drug showed preferential cytotoxicity and radiosensitization under hypoxia (Sridhar, Koch et al. 1976, Michaels, Peterson et al. 1981, Palcic and Skarsgard 1984). In tumour bearing mice, administration of misonidazole before single dose RT showed improved outcome; the radiation dose required to control 50% of the tumours (TCD₅₀) dropped from 43.8 Gy to 24.1 Gy (enhancement ratio: 1.82) (Sheldon, Foster et al. 1974). Fractionated RT in murine tumours also showed more potency when misonidazole was added to the treatment (Sheldon and Fowler 1978). In initial single dose clinical testing, appreciable tumour uptake was reported, with some gastrointestinal side-effects at the highest doses (Gray, Dische et al. 1976). However, multiple dose administration resulted in encephalopathy, forcing researchers to reduce the total dose, and to co-administer dexamethasone and phenytoin sodium to alleviate the symptoms. Regardless, peripheral neuropathy still persisted in about 30-49% of the patients (Dische,

Saunders et al. 1977, Phillips, Wasserman et al. 1981). Subsequent clinical studies aimed to address this issue by testing different treatment plans with misonidazole administration and RT combinations. The results from these trials, however, were largely disappointing. No benefits were observed in the majority of randomized trials in bronchial cancer, cervical cancer, HNC, gliomas and bladder cancer, although a subset of patients with HNC and bladder cancer did show improved response [reviewed in (Dische 1985)]. The dose-limiting toxicity along with the underwhelming clinical outcome deflated scientific enthusiasm in misonidazole. Consequently, attention shifted to other NI compounds, such as 2-NIs desmethyl-misonidazole (DMM), etanidazole, and 5-NI ornidazole etc., which were perceived as less toxic alternatives to misonidazole. In tumour bearing rats, significantly lower levels of DMM (compared to misonidazole) were detected in brains (Akel, Canal et al. 1983), but neurotoxicity was still present at chronic drug dosages (Edwards, Gordon et al. 1984). Lee et al. observed no global benefit of adding etanidazole with conventional RT in patients with advanced HNC (Lee, Cosmatos et al. 1995), and similar results were reported in prostate cancer patients (Lawton, Coleman et al. 1996). Although ornidazole generated no neurotoxic side effects (Okkan, Yazici et al. 1986), it too did not significantly improve OS and DFS rates in patients with locally advanced cervical cancer (Okkan, Atkovar et al. 1996). Interestingly, when stratified based on staging, patients with stage IIIB cancer in the ornidazole treated group did show improved LRC and DFS rates, but the analysis was statistically compromised due to small sample size.

Amidst these unsuccessful NIs reports, one notable exception is the clinical trial by the Danish Head and Neck Cancer (DAHANCA) group that assessed the effects of combining nimorazole (a 5-NI) with standard fractionated RT in advanced HNC patients. In a double-blind phase III study with 414 patients, a significantly improved rate of loco-regional control was observed in the nimorazole group over the placebo group (49 versus 33%, $p=0.002$). Similarly, OS was also higher in patients who received nimorazole, but to a lesser, non-significant extent (26 versus 16%, 10-year actuarial values, $p=0.32$). Unlike misonidazole, nimorazole was well tolerated, and it was possible to administer the planned dose to 98% of the participants (Overgaard, Hansen et al. 1998). It was evident from this study that not all patients with HNC benefited from hypoxia modification, which led to three subsequent retrospective analyses to identify patients most likely to respond to nimorazole. The feasibility of using hypoxia markers, such as osteopontin (OPN), CA-IX and a 15-gene hypoxia signifier were analyzed to separate

responders from non-responders. While CA-IX failed to show any prognostic value (Eriksen and Overgaard 2007), both OPN and the hypoxia gene classifier demonstrated the necessity of stratifying patients to appreciate the full therapeutic effects of nimorazole (Overgaard, Eriksen et al. 2005, Toustrup, Sørensen et al. 2012). In the placebo arm, high OPN levels (indicative of a more hypoxic state) dictated poorer 5-year outcomes, increased locoregional failure (LRF), and higher disease-specific mortality (DSM) when compared to patients with moderate-to-low OPN levels. Importantly, reduced LRF and DSM rates (i.e. better therapy response) were observed in patients with high OPN levels who received nimorazole (Overgaard, Eriksen et al. 2005). Similarly, the hypoxia responsive gene set analysis could also identify more hypoxic (and hence more radioresistant) patients from the less hypoxic, less radioresistant population (LRC 18 versus 44%; disease specific survival, DSS 30 versus 51%). Patients in the “more hypoxic” group fared better when treated with nimorazole and RT, than RT alone (LRC 49 versus 18%, DSS 48 versus 30%). No significant improvement was seen with nimorazole in patients with “less hypoxic” tumours (Toustrup, Sørensen et al. 2012). Clinical trials are currently ongoing to test the effects of adding nimorazole to a combined accelerated RT with cisplatin treatment regimen (Bentzen, Toustrup et al. 2015).

Although the successful results with nimorazole from the DAHANCA studies have led to its incorporation into routine clinical management of HNC in Denmark, it has not yet been adopted by the wider clinical community (Metwally, Frederiksen et al. 2014). Unfortunately, NIs are often viewed in a negative light due to prior failed clinical trials, leading to diminished scientific interest in NI based anti-cancer therapeutics. Instead, research with NIs shifted focus to repurposing these compounds as hypoxia diagnostics, which proved to be highly successful (discussed in section 1.4.2). More recently, several NI-based compounds were described that utilize the NI moiety only to guide the therapeutic effector molecule (inhibitors of DNA repair enzyme DNA-PK) to hypoxic cells (Lindquist 2009, Hay, Liew et al. 2020). Nevertheless, while analyzing the data from failed clinical trials with NIs, it should be considered that these studies were being operated on the assumption that all tumours would display uniform levels of hypoxia, which as we know now is incorrect. Therefore, none of these studies evaluated patients for their tumour oxygenation status. This glaring omission might have compromised (or even masked) the expected gains with hypoxia modifications. Indeed, retrospective analysis of the DAHANCA study conclusively showed that therapeutic gains with nimorazole were only

prominent in patients who had “more hypoxic” tumours (Overgaard, Eriksen et al. 2005, Toustrup, Sørensen et al. 2012). Even with this limitation, a meta-analysis of 50 randomized NI clinical trials identified an overall improvement in patient outcome with NIs [3.9% increase in local control ($p = 0.004$)]; the highest response was seen in HNC, and to a lesser extent in bladder cancer (Overgaard 1994). This brings us to the second factor that must be considered: it is very likely that not all tumour types will respond to NIs, and certain malignancies (such as HNC) appear to benefit the most from hypoxia-targeted therapy. Regardless of the mode of hypoxia modification, HNC patients consistently showed at least some degree of response, be it ARCON (Janssens, Rademakers et al. 2012), dose-escalated RT (Welz, Mönnich et al. 2017), misonidazole (Dische 1985), and of course nimorazole (Overgaard, Hansen et al. 1998). It is important to note that the 5 year survival rate of HNC patients receiving standard treatment is only about 40 to 50%, with locoregional recurrence occurring in up to 30% of patients (Curry, Sprandio et al. 2014). Hypoxia has been identified as a major driver for therapy resistance and poor outcome in HNC patients (Nordsmark, Overgaard et al. 1996, Nordsmark, Bentzen et al. 2005). Given the promising effects NIs have in HNC, it is worthwhile to pursue NI-based therapeutics, at least to improve outcome in HNC patients with hypoxic tumours.

The lack of a detailed mechanism of action for NI compounds has hindered further development of NI-based anti-cancer therapeutics. Despite being available for more than 60 years, considerable gaps still remain in our understanding of how these drugs sensitize cells under hypoxia. From a mechanistic perspective, the mode of action of NIs can be roughly divided into three stages: (a) their hypoxia selective uptake, (b) binding to cellular macromolecules and the subsequent effects, and (c) capability to induce damage to DNA and/or to potentiate IR-induced DNA damage. Out of all these, only the mechanism behind their hypoxia selective accumulation is relatively well understood. However, the effector component of the metabolized/active drugs demands more investigation, particularly in a cellular context and at physiologically relevant concentrations. Using ^{14}C -labelled radioactive NIs, early studies confirmed that activated (reduced) NIs bind to DNA and proteins; conflicting reports exist regarding their ability to bind to RNA (Ings, McFadzean et al. 1974, LaRusso, Tomasz et al. 1977, Varghese and Whitmore 1980, Kedderis, Argenbright et al. 1989). For DNA, binding happened preferentially to guanine/cytosine rich polynucleotides, and was suggested to be mostly covalent in nature on the basis of the stability of drug-DNA adducts (LaRusso, Tomasz

et al. 1977). In addition to binding, activated NIs have also been reported to induce DNA damage. Rowley et al. observed a decrease in DNA viscosity, with an increase in the single strand content and migration distance of DNA, when NIs were electrolytically reduced in the presence of *E. coli* DNA (Rowley, Knight et al. 1979). DNA with more A+T content showed higher vulnerability to NI-induced damage (Rowley, Knight et al. 1980). It is worth mentioning here that very high drug concentrations were used in these cell-free “*in vitro*” experiments, and the relevance of these observations in hypoxic tumour cells at biologically achievable concentrations should be carefully tested. NIs also showed capacity to inhibit DNA synthesis in *Clostridia* and *Bacteroides*, but no effects were seen on the activity of DNA polymerase (Plant and Edwards 1976, Sigeti, Guiney Jr et al. 1983). Furthermore, the ability of NIs to increase IR-induced DNA damage under hypoxia has been demonstrated in cancer cell lines (Koike, Kota et al. 2020), which is attributed to the capacity of NIs to act as O₂ mimetics to “fix” IR-induced DNA free radicals. Interestingly, a recent study employing imaging mass spectrometry described binding of NIs to glutathione (GSH), since glutathione conjugates of amino-pimonidazole were detected in hypoxic regions (Masaki, Shimizu et al. 2016). This might offer an additional explanation for the observed phenomenon, where NIs may trap GSH and thereby, directly inhibit thiol-catalyzed “chemical restitution” of DNA damage induced by RT.

Early studies with NIs mostly focused on DNA, and consequently their protein targets remained relatively unexplored. LaRusso et al. reported that on a weight basis, binding of chemically reduced 5-NI metronidazole to DNA is almost 3-fold higher than to bovine serum albumin (BSA) protein (LaRusso, Tomasz et al. 1977). However, caution should be taken when interpreting these (mostly) cell-free data in a cellular context, where protein content per cell (~221 pg; average from 4 human cancer cell lines) is >30 fold that of DNA content (6-7 pg) (Wiśniewski, Hein et al. 2014, Gillooly, Hein et al. 2015, Bäumer, Fisch et al. 2018). Therefore, it is highly possible that in hypoxic cells, protein-NI adduct formation rates may surpass that of DNA-NI adducts, which may have direct biological implications. Several studies have demonstrated that NI-protein adducts are stable, and can be detected in tumours days after injection (Azuma, Raleigh et al. 1997, Ljungkvist, Bussink et al. 2005). This raises questions about the consequences of such stable adduction on target protein stability and function. However, the protein targets for NIs have rarely been investigated in human cancer models; the

existing handful of proteomic studies mostly concentrated on reaction of 5-NIs in protozoans (Leitsch, Kolarich et al. 2007, Leitsch, Kolarich et al. 2009, Leitsch, Schlosser et al. 2012). Interestingly, in microbial systems, NIs have been reported to inhibit activities of certain crucial enzymes, such as GAPDH (Marcus, Tal et al. 2016), glutathione-S-transferase (GST) (Kumar and Weiss 1986, O'Dwyer, LaCreta et al. 1993) and thioredoxin reductase (TrxR) (Leitsch, Kolarich et al. 2007). These observations underscore the importance of studying NI-protein adducts in cancer cells to elucidate their contribution to NI-mediated sensitization of hypoxic cells.

1.5.3.1.1 IAZA and FAZA

Iodoazomycin arabinofuranoside (IAZA) and fluoroazomycin arabinofuranoside (FAZA) are 2-NI (azomycin) based hypoxia selective radiopharmaceuticals that were developed at the University of Alberta (Mannan, Somayaji et al. 1991, Kumar, Stypinski et al. 1999). Built upon a common scaffold, both compounds contain an azomycin moiety for hypoxia targeting, a pentose sugar to facilitate cell uptake, and a halogen moiety for radiolabelling (**Fig. 1.5**). Synthesis of radiolabeled IAZA was first reported by Mannan et al. in 1991; the compound showed a 3-fold higher rate of binding to hypoxic cells when compared to misonidazole (Mannan, Somayaji et al. 1991). Clinical efficacy of ¹²³I-IAZA as a non-invasive hypoxic radiotracer was validated in HNC, small cell lung carcinoma, glioblastoma and soft tissue sarcoma (Urtasun, Parliament et al. 1996). In 1999, Kumar et al. described the synthesis of FAZA, which is a less lipophilic analogue of IAZA (partition coefficient, P=1.10 for FAZA versus 4.98 for IAZA) (Kumar, Stypinski et al. 1999). Radiolabelled FAZA (¹⁸F-FAZA) is an excellent PET imaging agent for hypoxia diagnosis, with a relatively faster clearance rate in comparison to ¹⁸F-FMISO, and demonstrates high tumour-to-background ratios (Reischl, Dorow et al. 2007). The diagnostic value of FAZA has been demonstrated in malignancies of the head and neck (Souvatzoglou, Grosu et al. 2007), lung (Verwer, Bahce et al. 2014), malignant lymphoma and high grade glioma (Postema, McEwan et al. 2009). ¹⁸F-FAZA PET/CT has been applied to stratify patients based on their tumour oxygenation status, and has proven to be a strong prognostic tool for predicting the outcome of RT (Mortensen, Johansen et al. 2012) and hypoxia modification therapy (Beck, Röper et al. 2007, Bol, Labar et al. 2015). ¹⁸F-FAZA PET has also been successfully used to observe patient response (Trinkauss, Blum et

al. 2013), and to monitor fluctuations in hypoxia during treatment (Chapman, Jans et al. 2014, Servagi-Vernat, Differding et al. 2014).

Efficient labelling of hypoxic tumour cells by radioactive IAZA and FAZA proves that these compounds can overcome the diffusion barrier to reach O₂-starved therapy-resistant cells, even when used at trace amounts. Therefore, it is tempting to ponder the effects IAZA and FAZA might have if large enough dosage (i.e., therapeutically effective) can be successfully delivered to hypoxic tumour niches. Early cell-based assays with these compounds offer clues, where both compounds showed some degree of therapeutic potentials. For example, IAZA has been described as a hypoxic cytotoxin in a murine breast cancer model, *in vitro* (Mannan, Somayaji et al. 1991). Both free and encapsulated IAZA sensitized hypoxic human hepatocellular carcinoma cells to IR (Quan, Wang et al. 2015). FAZA has been reported as a hypoxic radiosensitizer in human colorectal cancer cells (Kumar, Emami et al. 2009). However, no report exploring the therapeutic efficacy of IAZA and FAZA exists to date in a HNC model.

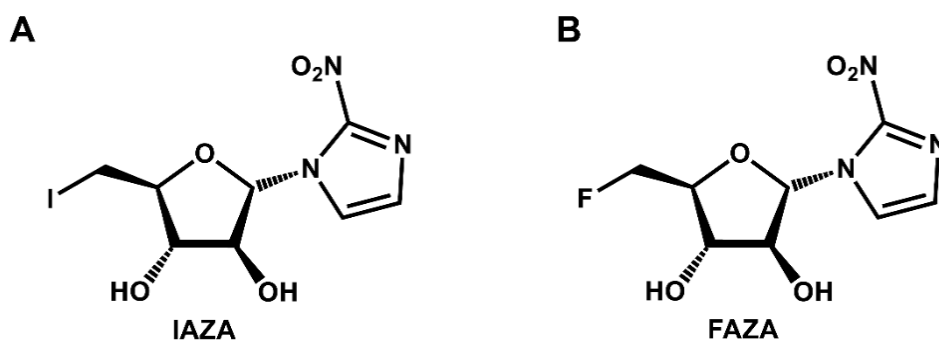


Figure 1.5 Chemical structure of IAZA and FAZA.

IAZA (A) and FAZA (B) share a common backbone; an azomycin moiety for hypoxia-selective activation, a pentose sugar to facilitate cell uptake, and a halogen moiety that, when replaced by the corresponding radioactive isotope, impart diagnostic (^{123/124/131}I-IAZA and ¹⁸F-FAZA) and radiotherapeutic (¹³¹I-IAZA) properties.

IAZA is a particularly interesting therapeutic candidate to pursue because of its iodine moiety. The presence of iodine in NIs has been reported to increase their hypoxic cytotoxicity (Krause, Jordan et al. 2005). More importantly, it makes IAZA a bi-functional “theranostic” molecule that can be labelled with different iodine radioisotopes suited for imaging (¹²³I, ¹²⁴I), or for molecular radiotherapy, MRT (¹³¹I). I-131 is a beta emitting radionuclide, which has the

capacity to destroy cells that it penetrates. While iodine-131 radioactive isotope has been widely used in treating patients with hyperthyroidism and well-differentiated thyroid cancer, its use in the context of targeting hypoxic tumours has rarely been explored (Mumtaz, Lin et al. 2009, Van Nostrand 2009). By taking advantage of the NI moiety to direct the radioactivity to the otherwise radioresistant hypoxic tumour cells, ^{131}I -IAZA may provide a unique approach to irradiating the tumour from within (*in situ*), and synergise with external beam RT, chemotherapy or immunotherapy. Radiolabelling of ^{131}I -IAZA has been described before; the compound showed high stability for at least 2 weeks, with minimal degradation in its specific activity over the storage time (Kumar, McQuarrie et al. 2005). Biodistribution studies in a murine EMT-6 tumour model reported high tumour radiation dose of 7.4 mGy/MBq, with the highest tumor/blood radioactivity ratio (T/B; 4.8) at 24 h after dosing. Given the mutagenic property of ^{131}I isotope, thyroid blocking must be accompanied with this kind of treatment. Also, IAZA shows delayed clearance from the body due to its lipophilicity, which can present a challenge for its use as MRT. Interestingly, Mercer et al. described a wash-out technique with cold IAZA that accelerated clearance in mouse tumours (Mercer, McEwan et al. 2013).

1.6 Research objectives

For decades, tumour hypoxia has remained an unresolved clinical problem. Despite several limitations, NIs still possess considerable promise as hypoxia-targeted anti-cancer agents. However, a lack of mechanistic studies has made it challenging to develop next generation NI based therapeutics. Under these circumstances, the present study aims to assess the sensitization capacity of NI compounds (IAZA and FAZA) in hypoxic HNC cells, and to characterize the cellular fate in response to NIs treatment. We chose a HNC model since clinical studies with HNC patients showed the strongest response to different hypoxia modification treatments. Based on previous cell data, we predict that IAZA and FAZA will sensitize hypoxic HNC cells, and may even enhance the damaging effects of radiation under hypoxia. A particular focus of this study is to identify the protein targets of NIs, and to assess how NI adduction might affect their stability and function. Therefore, the overarching hypothesis of the project is that ***“Bioreductive activation of IAZA and FAZA will compromise hypoxic HNC cell viability through binding to critical cellular proteins, and by potentiating IR induced DNA damage”***.

1.6.1 Specific aims

- I. To identify the protein targets of NIs and to characterize the effects of NI-adduction on their stability, turnover and activities.
- II. To evaluate the cellular phenotype induced by NIs (IAZA and FAZA) under hypoxia, and the role that NI-targeted adduction plays in the observed phenotype.
- III. To investigate the hypoxia-targeted radiosensitization potentials of IAZA and FAZA in regard to their ability to reduce tumour hypoxia and to delay tumour growth in HNC animal models.

Chapter 2

Identification of Proteins and Cellular Pathways Targeted by 2-Nitroimidazole Hypoxia-selective Cytotoxins.

2.1 Introduction

Rapid growth of cancer cells, coupled with chaotic tumour vasculature, creates regions within the tumour where cells are deprived of nutrients and oxygen (Bertout, Patel et al. 2008). This phenomenon, clinically termed “tumour hypoxia”, has been reported in almost all solid malignancies. Cells residing in these hypoxic niches up-regulate a myriad of pro-survival adaptive responses including impaired drug delivery (Janssen, Haustermans et al. 2005), oncogene activation (Zeng, Kikuchi et al. 2010), abnormal cellular metabolism (House, Warburg et al. 1956) and deregulated DNA damage checkpoint signalling (Kumareswaran, Ludkovski et al. 2012). Furthermore, low O₂ tension stimulates metastasis, invasion and relapse (Teicher 1995), and sustains growth and maintenance of tumour initiating cells (Keith and Simon 2007). Most importantly, these adaptations make hypoxic cancer cells resistant to radiation, chemotherapy and immunotherapy, resulting in poor patient prognosis (Walsh, Lebedev et al. 2014, Ai, Budhani et al. 2015). While this rationalizes the need for hypoxia directed therapy, it has yet to become a part of routine clinical practice.

Nitroimidazoles (NIs) are a class of hypoxia-activated prodrugs that are bioreductively activated in an inverse O₂-dependent manner. The process involves reduction by nitroreductases that generates nitroradical anions; this intermediate is re-oxidized in the presence of O₂, allowing the drug to freely diffuse out of well-oxygenated cells. Under hypoxia, the nitroradical anion undergoes reductive decay producing a reactive hydroxylamine, which covalently binds to cellular macromolecules, leading to hypoxia-selective accumulation of the drug (Kizaka - Kondoh and Konse - Nagasawa 2009). This unique property makes NIs ideal for targeting hypoxic tumour cells, both as cytotoxins and radiosensitizers. However, despite showing early promise, several NIs failed in clinical trials as hypoxia-directed cancer therapeutics (Overgaard, Hansen et al. 1989, Lee, Cosmatos et al. 1995). These disappointing outcomes can be attributed, in part, to our limited understanding of the precise molecular mechanism of NIs. Indeed, the protein targets of NIs in a human cancer context have never been explored, making it difficult to comprehend their effects on target proteins. Here, we outline a strategy to label and isolate NI target proteins using a novel click chemistry compatible 2-NI agent, azidoazomycin arabinofuranoside (N₃-AZA). The proteins were then characterized using

liquid chromatography coupled mass spectrometry (LC-MS/MS). Bioinformatics analysis revealed that many of these proteins play critical roles in the cellular response to hypoxia.

The modular nature of N₃-AZA click reaction also supported its use as an excellent hypoxia marker. 2-NIs are widely used as hypoxia diagnostics, both in radiologic imaging and in immune-based detection. Positron emission tomography (PET) scans using radiolabelled 2-NIs, such as ¹⁸F-fluoromisonidazole (¹⁸F-FMISO) or ¹⁸F-fluoroazomycin arabinoside (¹⁸F-FAZA), allow for non-invasive functional imaging of tumour hypoxia (Rajendran, Wilson et al. 2003, Mortensen, Johansen et al. 2012). The current histological test for examining and evaluating tumour hypoxia involves the administration of 2-NI compounds, such as pimonidazole (Hypoxyprobe™) and EF5 [2-(2-nitro-1*H*-imidazol-1-yl)-*N*-(2,2,3,3,3-pentafluoropropyl)acetamide], and immunochemical detection of drug-protein adducts on tissue biopsies (Varia, Calkins-Adams et al. 1998, Evans, Hahn et al. 2000). In contrast, N₃-AZA click chemistry offers an antibody-independent alternative by using fluorescently tagged alkynes to visualize histological hypoxia. The result is a hypoxia-selective histochemical reagent that is simple, precise and time efficient.

2.2 Materials and Methods

2.2.1 General synthesis methods

Solvents used in reactions were purified before use by successive passage through columns of alumina and copper under an argon atmosphere. All reagents were purchased from commercial sources and were used without further purification unless noted otherwise. All reactions were carried out under a positive pressure argon atmosphere and monitored by thin-layer chromatography (TLC) on Silica Gel G-25 UV254 (0.25 mm) unless stated otherwise. TLC spots were detected under UV light and/or by charring with a solution of anisaldehyde in EtOH, acetic acid and H₂SO₄. Column chromatography was performed on Silica Gel 60 (40–60 mm). Organic solutions were concentrated under vacuum at <50 °C. ¹H and ¹³C NMR spectra were recorded at 400 and 101 MHz, respectively. ¹H and ¹³C NMR chemical shifts are referenced to CD₃OD (δ=3.35 and 4.78 for ¹H, 48.9 for ¹³C). ¹H NMR data are reported as though they are first order, and the peak assignments were made on the basis of 2D-NMR (¹H–¹H COSY and

HMQC) experiments. ESI-MS spectra were obtained on samples suspended in CH₃OH with added NaCl.

Synthesis of N₃-AZA (**Fig. 2.1A**) was explored from two precursors, namely 1- α -D-(5-*O*-tosyl-arabinofuranosyl)-2-nitroimidazole (Ts-AZA) (Kumar, Wiebe et al. 2002) [See section **2.8.1**] and 1- α -D-(5-deoxy-5-iodo-arabinofuranosyl)-2-nitroimidazole (IAZA) (Mannan, Somayaji et al. 1991). The IAZA route described here showed better yield and accommodated the increase in the reaction temperature to 100 °C without producing detectable side products. Briefly, NaN₃ (0.33 g, 10.2 mmol) was added to a solution of IAZA (1.8 g, 5.1 mmol) in DMF (15 mL) and the reaction mixture was heated at 100 °C for 2 h. After cooling to room temperature, the reaction mixture was concentrated under vacuum and quenched with H₂O (20 mL). The product was extracted into EtOAc (3 x 10 ml) and the organic layer was dried over anhydrous Na₂SO₄, filtered and the solvent was removed under reduced pressure. The crude product was purified using a short column chromatography (10:1, v/v, CH₂Cl₂/CH₃OH) to give N₃-AZA (1.4 g, 93%) as an amorphous pale yellow solid: *R*_f, 0.39 (10:1 CH₂Cl₂/CH₃OH); ¹H NMR (400 MHz, CD₃OD): δ 7.65 (d, *J* = 1.3 Hz, 1H, H-5Im), 7.12 (d, *J* = 1.3 Hz, 1H, H-4Im), 6.46 (d, *J* = 1.5 Hz, 1H, H-1), 4.54 (ddd, *J* = 7.5, 5.0, 2.5 Hz, 1H, H-2), 4.28 (t, *J* = 1.8 Hz, 1H, H-3), 4.06 (t, *J* = 2.3 Hz, 1H, H-4), 3.63 (dd, *J* = 12.9, 7.4 Hz, 1H, H-5), 3.47 (dd, *J* = 12.9, 5.0 Hz, 1H, H-5); ¹³C NMR (101 MHz, CD₃OD) δ 140.02 (C-2Im), 126.76 (C-4Im), 123.83 (C-5Im), 95.56 (C-1), 88.48 (C-2), 82.38 (C-3), 77.12 (C-4), 52.29 (C-5); HRMS (ESI) calcd for [M+Na]⁺ C₈H₁₀N₆O₅Na: 293.0605, found: 293.0604.

2.2.2 Cell culture

Human head and neck squamous cell carcinoma cell line, FaDu, was purchased directly from American Type Culture Collection (ATCC HTB-43, Manassas VA). Additional cell lines used include A549 (human lung epithelial carcinoma), PC3 (human prostate carcinoma) [both purchased directly from ATCC] and A172 (human glioblastoma) [kindly provided by Dr. Roseline Godbout, University of Alberta, Canada]. Cells were expanded and frozen at early passage in liquid nitrogen until used. Cells were grown as monolayer cultures in DMEM/F-12 media supplemented with 10% fetal bovine serum, 1% of 2 mM L-glutamine and 1% penicillin streptomycin. Prior to initiation of experiments, cells were tested for mycoplasma

contamination by Hoechst 33342 staining (Life Technologies) and confocal imaging. Cell cultures were maintained in a humidified incubator at 37 °C with 5% CO₂, for a maximum of 2 months (~25-30 passages). Hypoxic incubations were carried out in a humidified chamber under controlled O₂ flow (ProOx P110, BioSpherix, Parish, NY). O₂ levels below 0.1% were achieved using an in-house degassing/ regassing system (Koch, Howell et al. 1979).

2.2.3 Drug stock preparation

N₃-AZA and pimonidazole hydrochloride (hereafter referred to as pimonidazole; HypoxyprobeTM, Burlington, MA) were prepared as 500 μM and 656 μM solutions in DMSO respectively and stored at -20 °C.

2.2.4 Crystal violet staining assay

Cells seeded in 96-well plates (Cellstar®; 655180, Sigma-Aldrich, Oakville, ON) at densities ranging from 1500 to 5000 cells per well (depending on the cell line) were left overnight to attach and treated with increasing concentrations of N₃-AZA or pimonidazole (0 μM to 2000 μM). Drug treatment lasted for 72 h under normoxia (20% O₂) or hypoxia (0.1% O₂); 0.02% DMSO was used as vehicle control. Afterwards, media was discarded, attached cells were stained with 0.05% crystal violet (Sigma-Aldrich, C6158), washed and left to dry for 24 h. Crystal violet stained cells were resuspended in 150 μl of methanol and the optical density (OD) was measured at 584 nm using a FLUOstar OPTIMA microplate reader (BMG Labtech, Ortenberg, Germany). Percent cell survival was calculated by subtracting OD of blank wells and then normalizing DMSO controls to 100%. The first point on each curve represents 0 μM drug.

2.2.5 Click chemistry reaction cocktail preparation

The Click-IT reaction cocktail (Molecular Probes, Eugene, OR) was made up according to the manufacturer's directions using a 1:500 dilution of 10 mg/ml biotin-alkyne (Cat. # C37B0, Lumiprobe, Hallandale Beach, FL) for proteomic studies or with a 1:5000 dilution of the 2 mg/mL Alexafluor 488-, 555- or 594-conjugated alkyne stock (A10267, A20013, A10275, Molecular Probes) for imaging. Reaction cocktail was used within 10 min of preparation. All reactions were carried out at room temperature in the dark.

2.2.6 Isolation of N₃-AZA-protein adducts

FaDu cells treated with 100 μ M N₃-AZA (or vehicle control, 0.02% DMSO) for 24 h under normoxia or hypoxia (<0.1% O₂) were harvested directly in RIPA buffer supplemented with protease inhibitor. Click chemistry was performed on cell lysates at room temperature for 30 min using a biotin-labelled alkyne. Streptavidin-mutinin beads were resuspended and processed as per the manufacturer's guidelines (Cat. # Roche 03708152001, Sigma-Aldrich). Clicked lysates (without equilibration buffer) were loaded on 1% BSA blocked streptavidin-mutinin beads and put on a rocker overnight at 4 °C. Afterwards, the supernatant was removed, the beads were washed several times, and the bound biotinylated protein fraction was either eluted from the beads using free biotin (Sigma-Aldrich) or by boiling the beads in SDS-PAGE loading dye.

2.2.7 LC-MS/MS

Clicked crude extracts and eluates were run on SDS-PAGE, stained with Coomassie G-250 and processed for in-gel trypsin digestion. Briefly, excised gel bands were de-stained twice in 100 mM ammonium bicarbonate/acetonitrile (50:50 v/v). The samples were then reduced in 10 mM 2-mercaptoethanol in 100 mM sodium bicarbonate and alkylated by treatment with 55 mM iodoacetamide in 100 mM bicarbonate. After dehydration, enough trypsin (6 ng/ μ L, Promega sequencing grade, Madison, WI) was added to just cover the gel pieces and the digestion proceeded overnight (~16 h) at room temperature. Tryptic peptides were first extracted from the gel using 97% water/2% acetonitrile/1% formic acid, followed by a second extraction using 50% of the first extraction buffer with 50% acetonitrile. Fractions containing tryptic peptides were resolved and ionized using a nanoflow HPLC (Easy-nLC II, Thermo Scientific, Waltham, MA) coupled to an LTQ XL-Orbitrap hybrid mass spectrometer (Thermo Scientific). Nanoflow chromatography and electrospray ionization were accomplished using a Picofrit fused silica capillary column (ProteoPepII, C18) with 100 μ m inner diameter (300 \AA , 5 μ m, New Objective, Woburn, MA). Peptide mixtures were injected onto the column at a flow rate of 3000 nl/min and resolved at 500 nl/min using a 60 min linear gradient from 0 to 45% v/v aqueous acetonitrile in 0.2% v/v formic acid. The mass spectrometer was operated in data-dependent acquisition mode, recording high-accuracy and high-resolution survey Orbitrap spectra using external mass calibration, with a resolution of 30,000 and m/z range of 400–2000. The fourteen most intense

multiply charged ions were sequentially fragmented by using collision induced dissociation, and spectra of their fragments were recorded in the linear ion trap; after two fragmentations, all precursors selected for dissociation were dynamically excluded for 60 s. Data was processed using Proteome Discoverer 1.4 (Thermo Scientific) and a human proteome database (UniProt) was searched using SEQUEST (Thermo Scientific). Search parameters included a precursor mass tolerance of 10 ppm and a fragment mass tolerance of 0.8 Da. Peptides were searched with carbamidomethyl cysteine as a static modification, and oxidized methionine and deamidated glutamine and asparagine as dynamic modifications. Protein IDs were manually analyzed, and unreviewed UniProtKB/TrEMBL IDs were substituted with respective reviewed UniProtKB/Swiss-Prot IDs for downstream data analysis.

2.2.8 Bioinformatics analysis

Proteins identified through LC-MS/MS were plotted as a Venn diagram using the FunRich network analysis tool (Pathan, Keerthikumar et al. 2015). An enrichment profile was generated by comparing the relative ion intensities of individual proteins in lysates and eluates from N₃-AZA treated hypoxic cells, and plotted using GraphPad Prism V7. Canonical protein sequences of putative N₃-AZA target proteins were retrieved from the UniProt database and analyzed for cysteine (Cys) and proline (Pro) content. Functional categorization of target proteins was performed using gene ontology by PANTHER classification system (biological processes, molecular activity, and cellular components) (Mi, Muruganujan et al. 2019). The proteomic data set was submitted into Ingenuity Pathway Analysis (IPA) for core analysis (Kramer, Green et al. 2014). IPA calculates a distinct p-value (p-value of overlap calculated using Fisher's Exact Test) which depicts the association between the protein molecules in our dataset to the literature-reported molecules in IPA knowledgebase. The identified canonical pathways were ranked based on P value. Upstream regulatory analysis was performed to identify the N₃-AZA target proteins regulated by common regulators.

2.2.9 Western blot

N₃-AZA treated FaDu cells (0 μ M, 100 μ M and 250 μ M, 24 h) were harvested in RIPA buffer supplemented with protease inhibitor. Crude protein extracts were separated on a 10% polyacrylamide gel for 55-70 min at 180 V, transferred onto nitrocellulose membranes and

blocked for 1 h with 5% milk [in phosphate-buffered saline (PBS), 0.1% Triton-100]. Total protein was visualized using Revert™ 700 Total Protein Stain (926-11016, LI-COR, Lincoln, NE). Membranes were probed with the following primary antibodies: anti-hypoxia inducible factor 1 alpha (1:2000 dilution; NB100-449, Novus Biologicals), anti-beta tubulin (1:4000 dilution; ab6046, Abcam), anti-glyceraldehyde-3-phosphate dehydrogenase (1:1000 dilution, ab9482, Abcam), anti-glutathione S-transferase P (1:2000 dilution, ABS1650, Millipore), anti-beta actin (1:2000 dilution; sc1616/ sc47778, Santa Cruz Biotechnology) and anti-heat shock protein 90 (1:2000 dilution; ab13492, Abcam). Secondary antibodies used include goat anti-rabbit-HRP (1:2000 dilution; Jackson Immunoresearch, West Grove, PA), IR-800 goat conjugated anti-mouse (1:2000 dilution, 926-80010, LI-COR) and IR-800 conjugated goat anti-rabbit (1:2000 dilution; 926-32211, LI-COR). For clicked lysates and eluates, membranes were probed with Streptavidin-HRP (1:2000 dilution, RPN1231V; GE Healthcare Life Sciences, Mississauga, ON). Membranes were then processed with West Pico PLUS chemiluminescent substrate (Thermo Fisher Scientific, Edmonton, AB) and developed on film, or scanned with an Odyssey Fc imager (LI-COR).

2.2.10 Glyceraldehyde-3-phosphate dehydrogenase (GAPDH) activity assay

The activity of cellular GAPDH enzyme was quantified using a GAPDH activity assay kit (Abcam, ab204732). Briefly, FaDu cells grown on 60-mm glass petri dishes were treated with either N₃-AZA (100 μM or 250 μM) or vehicle control (0.02% DMSO) for 24 h under normoxia or hypoxia (<0.1% O₂). Afterwards, attached cells were harvested by trypsinization, counted, pelleted by centrifugation and dissolved in GAPDH assay buffer (1 x 10⁶ cells per 0.5 ml buffer); 25 μl cell lysate was used to measure GAPDH enzymatic activity using 96 well plates according to the manufacturer's protocol. Absorbance was measured at 450 nm in kinetic mode with a FLUOstar OPTIMA microplate reader; a total of 30 readings were recorded over 48.3 min. GAPDH activity was calculated according to the manufacturer's guidelines.

2.2.11 Glutathione S-transferase (GST) assay

A GST assay kit (Sigma, CS0410) was used to measure the enzymatic activity of total cellular GST. In short, FaDu cells treated similarly as described above (GAPDH assay) were scraped, resuspended in 10 ml PBS, counted, and pelleted by centrifugation. The cell pellet was

dissolved in PBS containing 2 mM EDTA (1 x 10⁶ cells per 0.1 ml PBS-EDTA) and sonicated. After centrifugation, 10 µl of supernatant was used to measure GST activity in a 96-well plate using the manufacturer's protocol. Absorbance was measured at 340 nm in kinetic mode using a FLUOstar OPTIMA microplate reader; a total of 15 readings were recorded over 20.3 min. GST activity was calculated according to the manufacturer's guidelines.

2.2.12 N₃-AZA click staining of fixed cells

Cells grown in 35-mm tissue culture plates containing sterilized 22 x 22 mm glass coverslips were incubated with vehicle control (0.02% DMSO) or different concentrations of N₃-AZA (1 µM, 10 µM or 100 µM) under normoxia (20% O₂) and hypoxia (1% O₂ or <0.1% O₂) for 6 h. Afterwards, cells were washed with PBS and fixed in 2% paraformaldehyde (PFA). Fixed cells were blocked and permeabilized with 1% bovine serum albumin (BSA) in PBS containing 0.1% Triton X-100 for 20 min, followed by incubation with click cocktail containing Alexafluor 488-/555-/594-conjugated alkyne for 30 min at room temperature. Cell nuclei were stained with Hoechst 33342 (1:10,000 dilution in PBS, Life Technologies) for 5 min, washed and mounted on glass slides (Fluoroshield Mounting Medium, Abcam, Cambridge, UK). Images were obtained with a Plan-Apochromat 40X/1.3 Oil DIC lens on a Zeiss 710 confocal microscope using Zen 2011 software (Carl Zeiss, Jena Germany).

2.2.13 Immunocytochemistry

Cells treated with N₃-AZA or pimonidazole or both (at indicated concentrations and duration) under normoxia and hypoxia (<0.1% O₂) were fixed with PFA and processed for immunocytochemistry. Pimonidazole treated cells (alone or in combination with N₃-AZA) were stained with a rabbit anti-pimonidazole antibody (1:100 dilution for 2 h; Pab2627, HypoxyprobeTM) and an Alexa Fluor 647 labelled goat-anti-rabbit secondary antibody (1:1000 dilution for 1 h; A21245, Molecular Probes). N₃-AZA treated cells were processed for the following primary antibodies: anti-nucleolin antibody (1:1000 dilution; ab22758, Abcam or 1:500 dilution; sc17826, Santa Cruz Biotechnology), anti-alpha-tubulin antibody (1:4000 dilution; T6158, Sigma-Aldrich) and anti-glyceraldehyde-3-phosphate dehydrogenase antibody (1:200 dilution; ab9482, Abcam). Alexa Fluor 488 conjugated anti-rabbit (1:1000 dilution; Molecular Probes) and Alexa Fluor 594 conjugated anti-mouse (1:250 dilution; Molecular

Probes) secondary antibodies were used for visualizing protein localization. N₃-AZA treated cells were also processed for actin polymerization using Phalloidin-iFluor 488 reagent (1:1000 dilution; ab176753, Abcam). Click chemistry using an Alexafluor 488-/594-/555-conjugated alkyne (1:5000 dilution; Molecular Probes) was performed only after finishing all antibody staining steps. Cell nuclei were counter-stained with Hoechst (1:10,000 dilution; Life Technologies). Cells stained for actin and tubulin were not processed for click staining. Mounted coverslips on glass slides were imaged as described earlier.

2.2.14 Tumour generation and drug treatments

Female BALB/c nude mice (Charles River Laboratories, Wilmington, MA) aged 6 weeks were used and cared for with protocols approved by the Cross Cancer Institute Animal Care Committee (protocol #AC14208) in accord with the Canadian Council on Animal Care guidelines. We subcutaneously injected 6×10^6 FaDu cells in 0.1 ml of sterile 0.9% NaCl into the upper right flank to form palpable tumours. The tumours were measured daily until they reached desired volume, when the mice were divided into 4 groups and injected intraperitoneally (i.p.) with 0.15 ml 0.9% NaCl containing (i) 80 mg/kg N₃-AZA, (ii) 80 mg/kg pimonidazole, (iii) total 80 mg/kg N₃-AZA: pimonidazole in a 1:1 ratio and (iv) 0.9% NaCl control. We also used a primary mouse model of HPV-negative squamous cell carcinoma of the oral cavity, developed by Dr. Yvonne Mowery (Mowery, Carpenter et al. 2018). These animal studies were performed in accordance with protocols approved by the Duke University Institutional Animal Care and Use Committee (IACUC, protocol #A032-19-02) and adhered to the NIH Guide for the Care and Use of Laboratory Animals. In brief, tumours were generated by breeding *KRT5-CreER^{T2}* mice (tamoxifen-inducible Cre in basal epithelial cells) with *Trp53^{fl/fl}*; *Rb^{fl/fl}* or *p53^{fl/fl}*; *Ink4a/Arf^{fl/fl}* mice, and applying 4-hydroxytamoxifen and the carcinogen, benzo[a]pyrene, topically to oral mucosa of these genetically engineered mice. Mice containing varying sizes of tumours were administered i.p. with 80 mg/kg N₃-AZA: pimonidazole in a 1:1 ratio. 2 h after injection, mice were euthanized, tumours and organs (brain, lung, liver, kidney and cervical lymph nodes) removed and frozen in optimal cutting temperature compound (O.C.T, Fisher Healthcare 4585). Serial sections (7-10 microns each) from tumours and organs were taken, dried and stored at -80 °C.

2.2.15 Tissue staining

Frozen sections were air dried for 25 min, fixed in acetone for 5 min precooled to -20 °C, air dried 25 min and blocked in PBS with 1% BSA for 20 min. Sections were incubated with primary antibodies for small vessel endothelium (rat anti-CD31, 1:50 dilution; 550274, BD Pharmingen) and hypoxia (rabbit anti-pimonidazole, 1:100 dilution; Hypoxyprobe) for 2 h at room temperature, followed by three 5-min washes in PBS. The secondary antibodies (Alexa Fluor 488 conjugated anti-rabbit and Alexa Fluor 647 conjugated anti-rat; 1:1000 dilution; Molecular Probes), with 4',6-diamidino-2-phenylindole (DAPI) to stain DNA, were incubated for 30 min at 37 °C in the dark, followed by three 5-min washes with PBS. The Click-iT reaction cocktail (containing Alexafluor 488-/594-/555-conjugated alkyne) was incubated with the sections for 30 min. Sections were washed 5 times with PBS for 5 min and mounted using Mowiol 4-88 (Millipore, Etobicoke, ON) mounting media. Slides were stored at 4 °C until imaged. Images were obtained by tile scan with a Leica SP8 STED microscope.

2.2.16 Hypoxia fraction calculation

An estimate of hypoxic tumour fraction was calculated with MATLAB R2018b (MATLAB and Image Processing Toolbox Release 2018b, The MathWorks, Inc., Natick, Massachusetts, United States) using a modified protocol described previously (Dubois, Lieuwes et al. 2011). To account for background staining on the click channel, a manual threshold was determined from a negative control (click staining performed on tumour section from saline injected mice) and was applied for the N₃-AZA-stained slides. The Otsu threshold was chosen for DAPI (Otsu 1979). Images were converted to binary according to their respective threshold and the hypoxic fraction estimate was calculated using following formula:

$$\text{Hypoxic fraction (HF)} = \frac{\text{Area of pixels stained with N}_3\text{-AZA}}{\text{Area of pixels stained with DAPI}} * 100$$

2.2.17 Data processing and statistics

Immunoblots and microscopic images were processed with Adobe Photoshop to adjust for brightness and contrast, to add scale bars, and for rearrangement and labelling. Gel scans were

quantified using Image Studio lite v5.2 (LI-COR) and normalized to vehicle treated normoxia controls. Microscopic images were processed with IMARIS software (Bitplane, Zürich, Switzerland) to quantify area and channel intensity of cell, nucleus and cytoplasm. GraphPad Prism V7 (GraphPad Software, La Jolla, CA) was used to generate graphs and to perform statistical analysis. Non-linear regression analysis was performed on crystal violet staining data to obtain IC₅₀ values. Graphs display the mean with standard error of the mean (S.E.M.). Statistical analysis was performed using 2-tailed unpaired t-test, with p<0.05 considered statistically significant. GAPDH activity was analyzed using Dunnett's 2-way ANOVA. Asterisks depict statistically significant differences: ns (not significant), * (P≤0.05), ** (P≤0.01), *** (P < 0.001), **** (P < 0.0001).

2.3 Results

2.3.1 Synthesis of N₃-AZA

Fig. 2.1A depicts the synthesis of the target compound N₃-AZA from two precursors namely Ts-AZA (Kumar, Wiebe et al. 2002) and IAZA (Mannan, Somayaji et al. 1991). Since the latter route provided better scalability and no detectable side products, the reaction was carried out on a multigram scale with a yield of 93%. Atomic numbering and NMR analysis of N₃-AZA is shown in **Suppl. Fig. 2.1**. N₃-AZA dissolves in DMSO and remains active, even in solution, for months when stored at -20 °C.

2.3.2 N₃-AZA is selectively cytotoxic to hypoxic cells

The hypoxia selectivity of N₃-AZA was first validated to determine doses that would limit the utility of the compound. A crystal violet staining (CVS) assay was used to determine the cytotoxicity of the drug under normoxia and hypoxia (Feoktistova, Geserick et al. 2016). In all four human cancer cell lines tested, N₃-AZA was more toxic under hypoxia than normoxia (**Fig. 2.1B-E**). Cytotoxicity of N₃-AZA in FaDu cells was directly compared to that of pimonidazole. For N₃-AZA, hypoxic FaDu cells had an IC₅₀ value >5 fold lower than under normoxia (normoxic and hypoxic IC₅₀ values for N₃-AZA were ~1463 μM and ~271 μM, respectively). Importantly, the compound showed almost no toxicity at concentrations ≤100 μM, even under

hypoxia (**Fig. 2.1B**). A similar toxicity profile was seen with pimonidazole, with an IC_{50} of $\sim 179 \mu\text{M}$ under hypoxia and $\sim 3035 \mu\text{M}$ under normoxia (**Suppl. Fig. 2.8**).

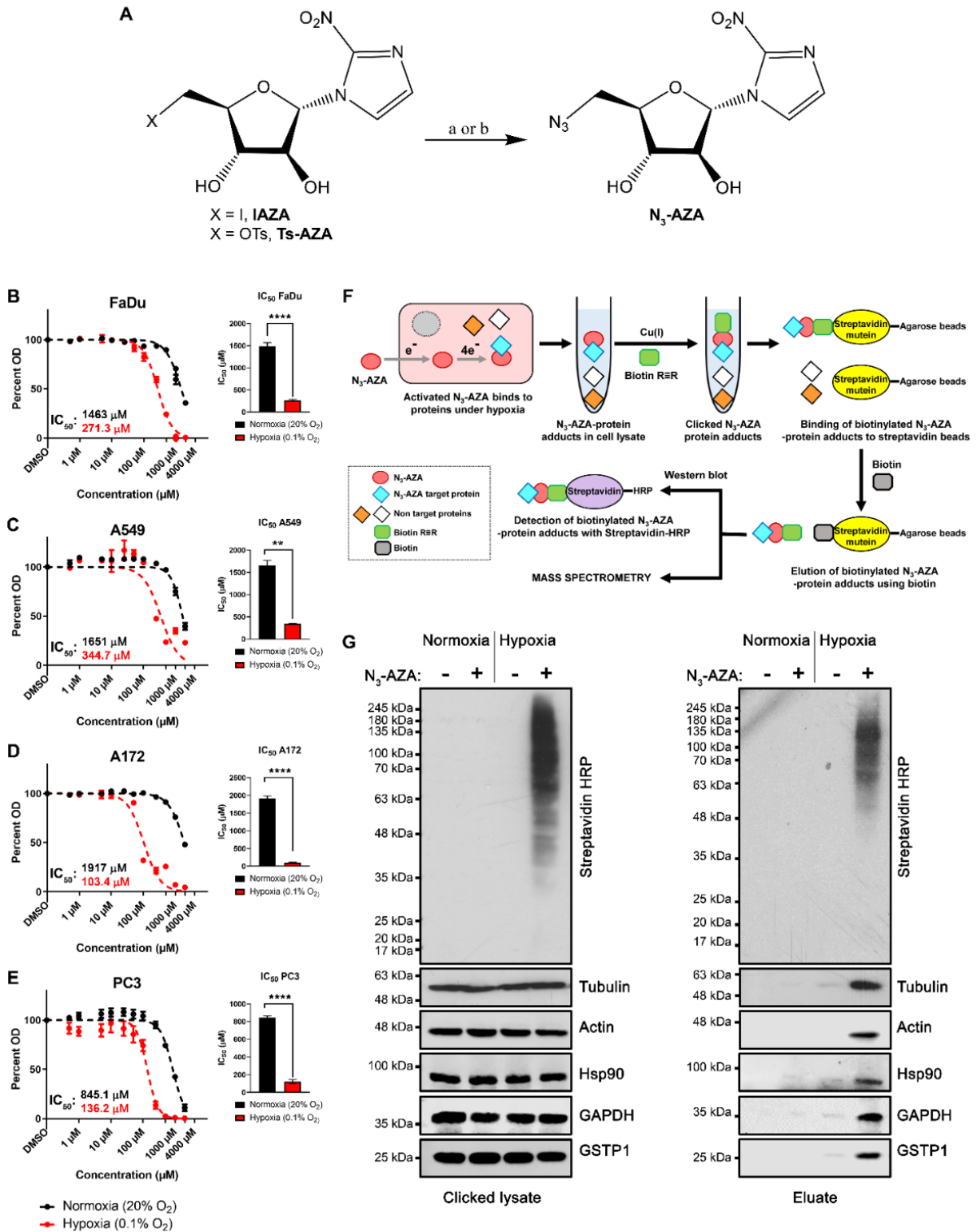


Figure 2.1 N₃-AZA synthesis, cytotoxicity and click chemistry principle to isolate 2-NI target proteins.

(A) Synthesis of N₃-AZA. Reagents and conditions: (a) Ts-AZA, NaN₃, DMSO, 50 °C, overnight, 69%; (b) IAZA, NaN₃, DMF, 100 °C, 2 h, 93%. N₃-AZA shows preferential cytotoxicity in hypoxic FaDu (B), A549 (C), A172 (D) and PC3 cells (E), with statistically significant differences between their normoxic and hypoxic IC₅₀ values. Data represents mean± S.E.M. from at least three independent experiments. (F) Experimental design for isolation and visualization of N₃-AZA bound proteins. (G) Click chemistry was performed on cell extracts collected from N₃-AZA (or DMSO) treated normoxic and hypoxic FaDu cells using a biotin alkyne. Western blotting showed that the signal for Streptavidin-HRP is only present in drug treated hypoxic samples. Drug bound proteins could successfully be isolated using streptavidin-mutinin beads, with no significant background binding. Representative immunoblots are displayed from three independent experiments.

2.3.3 Identification of proteins that interact with 2-NI under hypoxia

In hypoxic cells, activated (bio-reduced) 2-NIs bind to cellular proteins and form drug-protein adducts. To identify these protein targets, normoxic and hypoxic FaDu cells were treated with N₃-AZA (or 0.02% DMSO vehicle), lysed, and click chemistry was performed on protein lysates with a biotin labelled alkyne. “Clicked” lysates were processed for western blotting and probed using horse radish peroxidase-conjugated streptavidin (streptavidin-HRP), which showed that “clicked” proteins were present only in N₃-AZA treated hypoxic cells. These proteins were then successfully isolated with streptavidin-mutated beads (**Fig. 2.1F**). Immunoblotting confirmed low background binding of non-biotinylated proteins to the column matrix (**Fig. 2.1G**). The recovered proteins were identified by mass spectrometry, and bioinformatic analysis was carried out for functional characterization. From the combined proteomic dataset of eluates obtained from three independent experiments, a total of 65 proteins were identified with a peptide-spectrum match (PSM) score of ≥ 2 PSM, of which 5 were in “Normoxia+ DMSO” eluate (**Suppl. Table 2.1**), 13 were in “Normoxia+ N₃-AZA” eluate (**Suppl. Table 2.2**), 10 were in “Hypoxia+ DMSO” eluate (**Suppl. Table 2.3**) and 62 were in “Hypoxia+ N₃-AZA” eluate (**Table 2.1**). Overall, 48 proteins were exclusively identified in the “Hypoxia+ N₃-AZA” eluate (**Fig. 2.2A**). All proteins identified in the eluates of cells treated with N₃-AZA (normoxic and hypoxic) are shown with their average PSM scores (**Fig. 2.2B**). Enrichment analysis between crude extracts and eluates from N₃-AZA-treated hypoxic cells revealed that mostly high abundance proteins reacted with the drug. However, several highly abundant proteins also escaped labelling by N₃-AZA (e.g., acyl-CoA dehydrogenase family member 9, ACAD9). Likewise, several relatively low-abundant proteins, such as ferritin heavy chain, desmoplakin and calpastatin were readily modified by N₃-AZA (**Fig. 2.2C**). Activated 2-NI compounds are known to attack cellular nucleophiles to form adducts. Cysteine (Cys) has often been proposed as the site of attack on proteins (Wislocki, Bagan et al. 1984). Hence, N₃-AZA target protein sequences were analyzed to assess any association with their Cys content. Surprisingly, 5 of these proteins did not have any Cys residues whereas 34 proteins had 1-5 Cys, 17 had 6-10 Cys, 3 had 11-15 Cys, and only 3 proteins had >20 Cys residues (**Suppl. Fig. 2.2A**). This prompted analysis of the dataset for the next most nucleophilic amino acid, proline (Pro) (Brotzel and Mayr 2007). Interestingly, all but one (tropomyosin alpha-3 chain, TPM3) of the

N₃-AZA target proteins contained proline residues, with almost 60% of them containing >15 Pro residues (**Suppl. Fig. 2.2B**). TPM3, on the other hand, contains 1 Cys residue.

The 62 putative target proteins of N₃-AZA were categorized using PANTHER classification system (cellular component, molecular function and biological process) (**Suppl. Fig. 2.2C**). Cellular component analysis showed that N₃-AZA target proteins are mostly cytoplasmic (44 out of 62 proteins; ~71%), followed by 13 nuclear proteins (~21%), 4 plasma membrane proteins and 1 with an annotated extracellular matrix localization. According to molecular function, most of the proteins belong to the subcategories of binding (33), catalytic activity (24) and structural activity (12). Biological process-related proteins mainly belong to the subcategories of cellular process, metabolic process, localization, biological regulation and response to stimulus. IPA identified literature reported canonical pathways these proteins are involved in, and the top 10 pathways (based on the P value) are listed (**Table 2.2**). The dataset was also analyzed to assess if these target proteins are under the regulation of common upstream regulators. Two clusters, pertinent to hypoxic response, are reported here: (i) cluster 1 regulated by heat shock transcription factor 1, HSF1 (8 proteins) (**Fig. 2.2D**) and (ii) cluster 2 regulated by hypoxia inducible factor 1 subunit alpha, HIF1A (8 proteins) (**Fig. 2.2E**).

Table 2.1 Proteins identified in eluates from N₃-AZA treated hypoxic cells using LC-MS/MS

Gene	Protein name	Average PSM score	Size (amino acid)	#Cys	#Pro
GAPDH	Glyceraldehyde-3-phosphate dehydrogenase	18.33	335	3	12
HSP90AB1	Heat shock protein HSP 90-beta	12.67	724	6	23
ACTB	Actin, cytoplasmic 1	12.33	375	6	19
HSPA8 ^a	Heat shock cognate 71 kDa protein	11.00	646	4	25
CTTN	Src substrate cortactin	10.67	550	3	17
GSTP1 ^a	Glutathione S-transferase P	10.67	210	4	11
TUBB	Tubulin beta chain	10.00	444	8	20
HSP90AA1	Heat shock protein HSP 90-alpha	9.33	732	7	21
EEF1A1 ^a	Elongation factor 1-alpha 1	9.33	462	6	25
ALDOA ^a	Fructose-bisphosphate aldolase A	8.00	364	8	19
ANXA2 ^a	Annexin A2	7.67	339	4	7
TUBB4B ^a	Tubulin beta-4B chain	7.00	445	8	20
PKM ^a	Pyruvate kinase PKM	6.33	531	10	24
HSPD1	60 kDa heat shock protein, mitochondrial	6.00	573	3	19
TPM3 ^a	Tropomyosin alpha-3 chain	6.00	285	1	0
PRDX1	Peroxiredoxin-1	5.33	199	4	13
TUBA1C ^a	Tubulin alpha-1C chain	5.33	449	12	20
HSPA1A ^a	Heat shock 70 kDa protein 1A	4.67	641	5	24
LDHB	L-lactate dehydrogenase B chain	4.33	334	5	11
TPI1	Triosephosphate isomerase	4.00	286	5	10
TUBA1B ^a	Tubulin alpha-1B chain	3.00	451	12	20
FASN ^a	Fatty acid synthase	3.00	2511	46	149
YWHAZ	14-3-3 protein zeta/delta	2.67	245	3	4
LMNA ^a	Prelamin-A/C	2.50	664	5	15
ACTBL2 ^a	Beta-actin-like protein 2	2.33	376	6	21
HSPA5 ^a	Endoplasmic reticulum chaperone BiP	2.33	654	2	27
HNRNPK ^a	Heterogeneous nuclear ribonucleoprotein K	2.33	463	5	41
PCBP1 ^a	Poly(rC)-binding protein 1	2.00	356	9	19
LDHA ^a	L-lactate dehydrogenase A chain	2.00	332	5	11
RPL4 ^a	60S ribosomal protein L4	1.67	427	5	25
RPSA ^a	40S ribosomal protein SA	1.67	295	2	20
HIST1H1C	Histone H1.2	1.67	213	0	21
ENO1	Alpha-enolase	1.67	434	6	16
HSPA9 ^a	Stress-70 protein, mitochondrial	1.67	679	5	22
SERPINC1 ^a	Antithrombin-III	1.67	464	8	21
EIF4A2 ^a	Eukaryotic initiation factor 4A-II	1.33	407	4	12
RPS3 ^a	40S ribosomal protein S3	1.33	243	3	17
ANXA1 ^a	Annexin A1	1.33	346	4	8
PRMT1 ^a	Protein arginine N-methyltransferase 1	1.33	371	11	12
PPIB ^a	Peptidyl-prolyl cis-trans isomerase B	1.33	216	1	8
P4HB ^a	Protein disulfide-isomerase	1.33	508	7	21
SFN ^a	14-3-3 protein sigma	1.33	248	2	7
DLST ^a	Dihydropolyllysine-residue succinyltransferase component of 2-oxoglutarate dehydrogenase complex, mitochondrial	1.33	453	6	39
SUB1	Activated RNA polymerase II transcriptional coactivator p15	1.33	127	0	6
SLC25A5 ^a	ADP/ATP translocase 2	1.00	298	4	7

Table 2.1. Proteins identified in eluates from N₃-AZA treated hypoxic cells using LC-MS/MS (continued)

Gene	Protein name	Average PSM score	Size (amino acid)	#Cys	#Pro
DLAT ^a	Acetyltransferase component of pyruvate dehydrogenase complex	1.00	647	9	69
GOT2 ^a	Aspartate aminotransferase, mitochondrial	1.00	430	7	21
HNRNPA1 ^a	Heterogeneous nuclear ribonucleoprotein A1	1.00	372	2	10
CNBP ^a	Cellular nucleic acid-binding protein	1.00	177	22	4
DSP ^a	Desmoplakin	1.00	2871	43	55
NCL ^a	Nucleolin	1.00	710	1	31
EEF1B2 ^a	Elongation factor 1-beta	0.67	225	3	10
ATP5F1A ^a	ATP synthase subunit alpha, mitochondrial	0.67	553	2	18
PHB2 ^a	Prohibitin	0.67	299	0	10
RPL18 ^a	60S ribosomal protein L18	0.67	188	2	10
ATP5F1B ^a	ATP synthase subunit beta	0.67	529	0	32
H4C1 ^a	Histone H4	0.67	103	0	1
CAST ^a	Calpastatin	0.67	708	7	69
TAGLN2 ^a	Transgelin-2	0.67	199	3	9
DUT ^a	Deoxyuridine 5'-triphosphate nucleotidohydrolase, mitochondrial	0.67	252	5	21
FTH1 ^a	Ferritin heavy chain	0.67	183	3	3
NASP ^a	Nuclear autoantigenic sperm protein	0.67	788	5	33

[^a] Proteins identified exclusively in this group

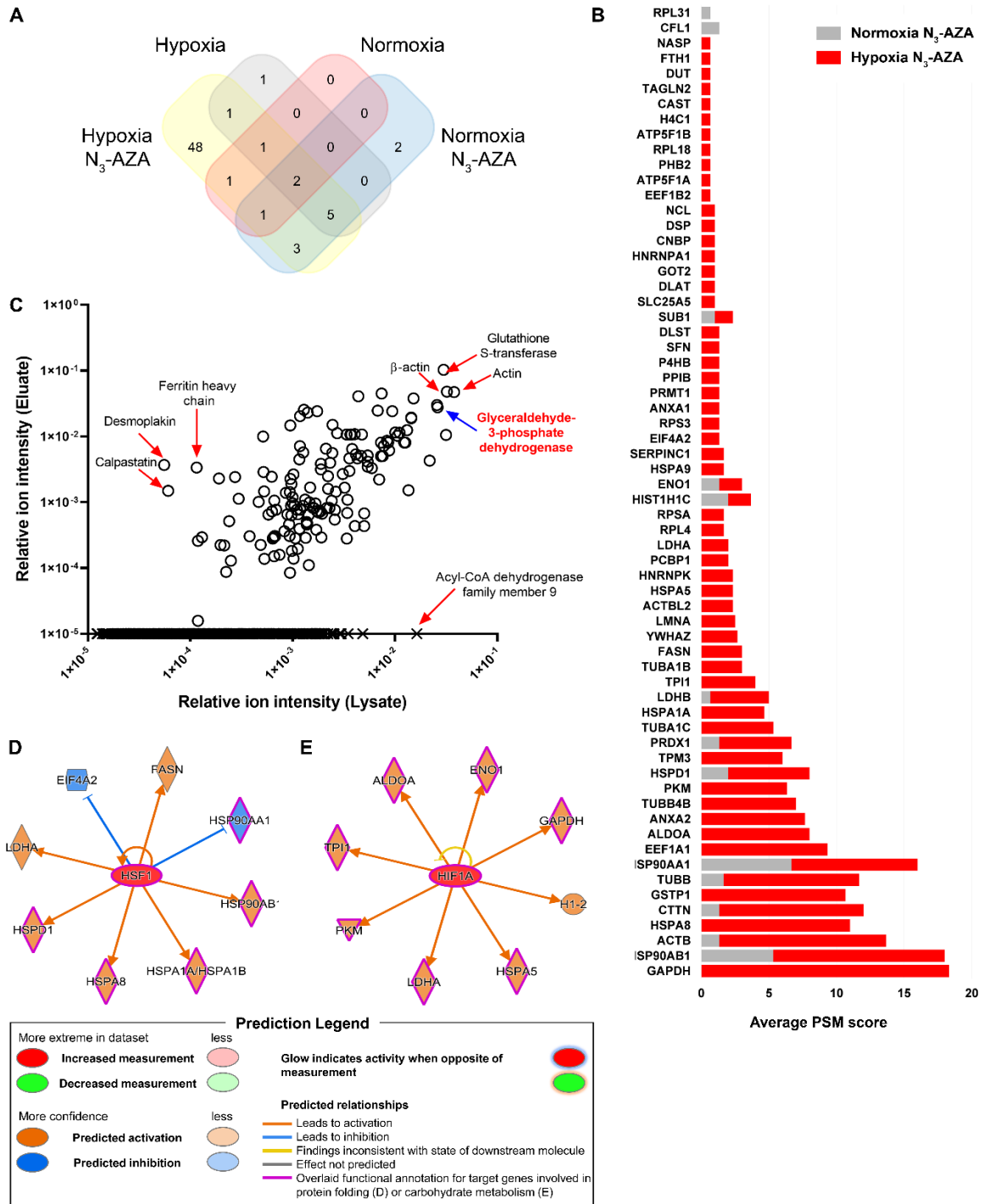


Figure 2.2 Mass spectrometric analysis of N₃-AZA target proteins.

(A) Venn diagram showing the distribution of proteins identified by mass spectroscopic analysis based on the different treatment conditions. (B) Comparison of PSM values for proteins identified in eluates from N₃-AZA treated normoxic and hypoxic cells. Data represent cumulative averages for each protein from three independent experiments. (C) Enrichment analysis demonstrated that the likelihood N₃-AZA labelling is generally dependent on the abundance of target proteins. (D and E) Upstream regulatory analysis by IPA identified 2 clusters of 8 proteins, each under the regulation of a common upstream regulator HSF1 (D) or HIF1A (E). 5 of HSF1 downstream targets are implicated in protein folding while 7 of HIF1A downstream targets are involved in carbohydrate metabolism.

Table 2.2 Top 10 canonical pathways identified through IPA analysis

Ingenuity Canonical Pathways	P-value ^a	% Overlap ^b	Molecules
BAG2 Signaling Pathway	1.81E-09	14.0% (6/43)	ANXA2, HSP90AA1, HSPA1A, HSPA5, HSPA8, HSPA9
Glycolysis I	8.05E-09	19.2% (5/26)	ALDOA, ENO1, GAPDH, PKM, TPI1
HIF1A Signaling	8.48E-08	3.9% (8/205)	HSP90AA1, HSPA1A, HSPA5, HSPA8, HSPA9, LDHA, LDHB, PKM
Sirtuin Signaling Pathway	9.12E-08	3.1% (9/291)	ATP5F1A, ATP5F1B, GOT2, H1-2, LDHA, LDHB, SLC25A5, TUBA1B, TUBA1C
EIF2 Signaling	1.68E-07	3.6% (8/224)	ACTB, EIF4A2, HNRNPA1, HSPA5, RPL18, RPL4, RPS3, RPSA
Aldosterone Signaling in Epithelial Cells	2.44E-07	4.4% (7/158)	HSP90AA1, HSP90AB1, HSPA1A, HSPA5, HSPA8, HSPA9, HSPD1
Unfolded protein response	4.39E-07	8.9% (5/56)	HSPA1A, HSPA5, HSPA8, HSPA9, P4HB
Role of PKR in Interferon Induction and Antiviral Response	7.93E-07	5.1% (6/117)	HSP90AA1, HSP90AB1, HSPA1A, HSPA5, HSPA8, HSPA9
Remodeling of Epithelial Adherens Junctions	1.17E-06	7.4% (5/68)	ACTB, TUBA1B, TUBA1C, TUBB, TUBB4B
14-3-3-mediated Signaling	1.28E-06	4.7% (6/127)	SFN, TUBA1B, TUBA1C, TUBB, TUBB4B, YWHAZ

[^a] P-value: p-value of overlap calculated using Fisher's Exact Test

[^b] % Overlap: number of proteins from our dataset overlapped with total proteins in a certain pathway in IPA knowledgebase

2.3.4 N₃-AZA treatment did not affect the levels and localization of target proteins, but reduced GAPDH and GSTP1 enzymatic activity under hypoxia

To assess the effects of N₃-AZA treatment on its target proteins, the following proteins were studied: actin, tubulin, heat shock protein 90 (Hsp-90), glyceraldehyde-3-phosphate dehydrogenase (GAPDH) and glutathione S-transferase P (GSTP1); HIF1A was used as an indicator of successful hypoxia induction. Hypoxic cells treated with 250 μM N₃-AZA appeared more compact, with fewer projections, however no significant difference was observed in target protein levels nor their cellular localization following N₃-AZA treatment (**Fig. 2.3A-B; Suppl. Fig. 2.3**). To examine if N₃-AZA treatment affects GAPDH enzymatic activity, we used an assay that measures NADH generation during GAPDH catalyzed oxidation of glyceraldehyde-3-phosphate (GAP) into 1,3-bisphosphoglycerate (BPG); the amount of NADH generated is proportional to the activity of GAPDH present during the reaction time. N₃-AZA, at a concentration close to its hypoxic IC₅₀ value (250 μM), significantly reduced GAPDH enzyme activity only under hypoxia (0.1254 nmol/min/μl vs 0.08511 nmol/min/μl in 0.02% DMSO and 250 μM N₃-AZA treated samples, respectively). No effect on GAPDH activity was seen under normoxia (~0.13 nmol/min/μl in all treatment groups) (**Fig. 2.3C**). Total GST activity was determined using an assay that measures the conjugation of 1-chloro-2,4-dinitrobenzene (CDNB) with reduced glutathione, resulting in an increase in absorbance at 340 nm. The rate of increase is directly proportional to the GST activity in the sample. While hypoxic exposure markedly increased GST activity in vehicle treated cells, in agreement with others (Millar, Phan et al. 2007), N₃-AZA treated hypoxic cells showed a significant dose-dependent reduction in GST activity (**Fig. 2.3D**). We estimate a minimum of 40±13% GAPDH and 57±5% GSTP1 protein was modified by cell exposure to 100 μM N₃-AZA (**Suppl. Fig. 2.4 and 2.5**).

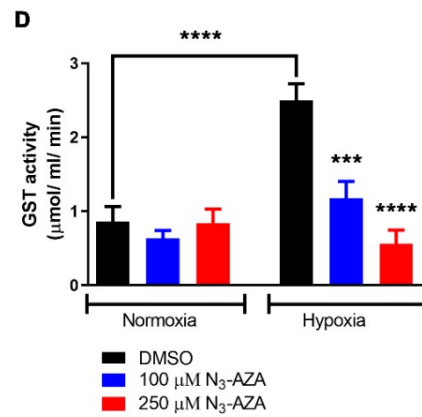
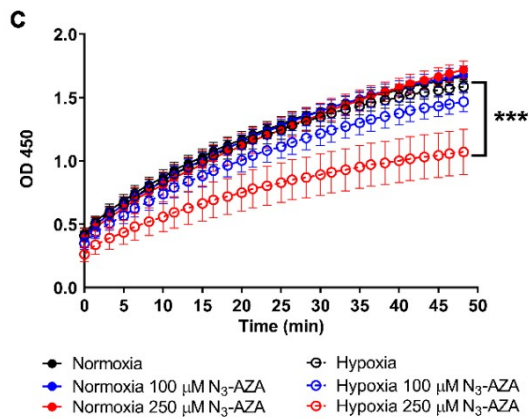
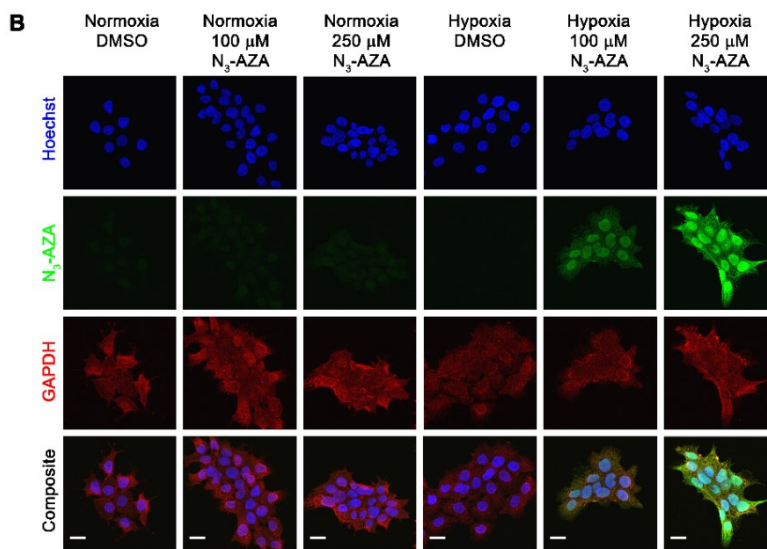
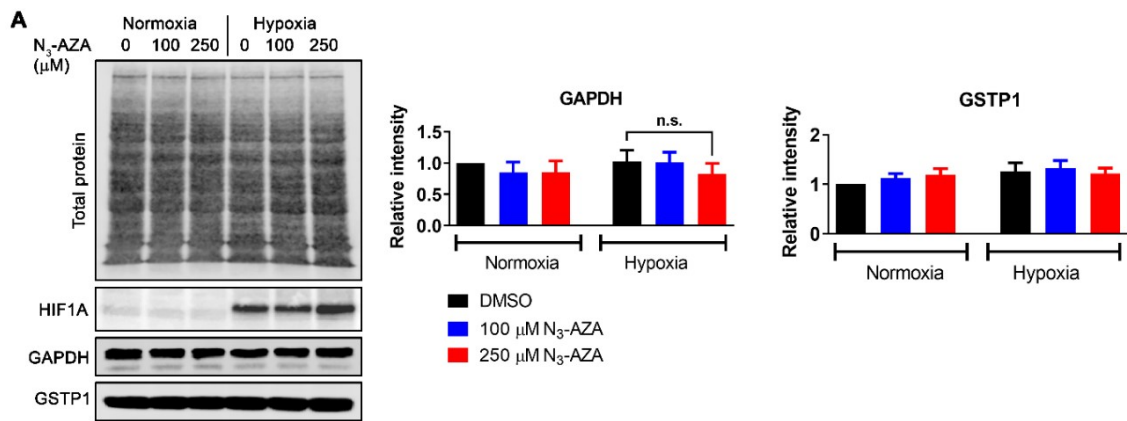


Figure 2.3 Effects of N₃-AZA on GAPDH and GSTP1 protein levels, GAPDH localization and their enzymatic activity.

(A) Lysates prepared from N₃-AZA (or 0.02% DMSO) treated normoxic and hypoxic cells were processed for western blotting. N₃-AZA treatment did not alter GAPDH and GSTP1 protein levels regardless of O₂ conditions. Representative immunoblots and quantitation [mean± S.E.M.] from three independent experiments are displayed. (B) Cells treated with N₃-AZA (or 0.02% DMSO) under normoxia and hypoxia were processed for immunocytochemistry to monitor GAPDH localization; no change in cellular localization of GAPDH was observed in response to N₃-AZA treatment. The micrographs are representative of at least three independent experiments; scale bar = 20 μm. (C and D) FaDu cells treated with N₃-AZA (or 0.02% DMSO) under normoxia and hypoxia were processed for GAPDH activity assay (C) or GST activity assay (D); the enzymatic activities of GAPDH and GST were significantly reduced only in N₃-AZA treated hypoxic cells. Data represent mean± S.E.M. from three independent experiments.

2.3.5 Sub-cellular localization of N₃-AZA

Click chemistry between the azido moiety of N₃-AZA and a fluorophore-conjugated alkyne enabled us to image the sub-cellular localization of N₃-AZA adducts formed under hypoxia using fluorescence microscopy. Fluorescent staining was observed only in O₂-starved cells when treated with N₃-AZA for 6 h (**Fig. 2.4A-D**); incubation duration was determined from a separate time course experiment (**Suppl. Fig. 2.6A**). Furthermore, the compound was entrapped in FaDu cells in an inverse oxygen-dependent manner, with the highest retention seen in cells cultured under <0.1% O₂. Normoxic cells showed minimal to almost no click staining. Staining of N₃-AZA under hypoxia increased in a dose dependent manner, with 100 μM concentration demonstrating the most vivid differences (**Fig. 2.4D**, **Suppl. Fig. 2.6B**). N₃-AZA-treated hypoxic cells showed strong nuclear staining (**Suppl. Fig. 2.6C**) with a nucleolar uptake pattern; the latter was confirmed by immunostaining for nucleolin (**Fig. 2.4E**, **Suppl. Movie 2.1**). A similar hypoxia selective N₃-AZA staining pattern was confirmed in additional cancer cell lines (**Suppl. Fig. 2.6D**).

To assess the metabolic stability of N₃-AZA-protein adducts upon reoxygenation, FaDu cells were treated with 100 μM N₃-AZA for 6 h under hypoxia and then reoxygenated, fixed at the indicated time points and processed for N₃-AZA click staining; N₃-AZA was present in the medium throughout the reoxygenation period. N₃-AZA click fluorescent signal could be detected up to 24 h following reoxygenation, suggesting that N₃-AZA modification is relatively stable. Although the intensity weakened by about 40%, the decrease in intensity appeared to be a consequence of cell doubling (data not shown). Minimal background was seen in their normoxic counterparts even after prolonged incubation with the compound (**Suppl. Fig. 2.7**).

To confirm the hypoxia selectivity of N₃-AZA click staining, cells treated simultaneously with pimonidazole and N₃-AZA were processed for pimonidazole immunostaining followed by N₃-AZA click chemistry. Both N₃-AZA click staining and pimonidazole immunostaining were detected only in drug treated hypoxic cells, with minimal signal in normoxic samples (**Fig. 2.5A**). Both staining strategies were equally efficient at differentiating between normoxic and hypoxic cells, however, N₃-AZA click staining proved to be simpler and faster compared to pimonidazole immunostaining and produced better signal to background ratio (**Fig 2.5B**).

Interestingly, although both compounds contain 2-NI moieties, they showed perceptibly different cellular staining patterns. N₃-AZA generated a strong nucleolar signal in hypoxic cells (**Suppl. Movie 2.1**), whereas pimonidazole staining remained excluded from nucleoli (**Suppl. Movie 2.2**).

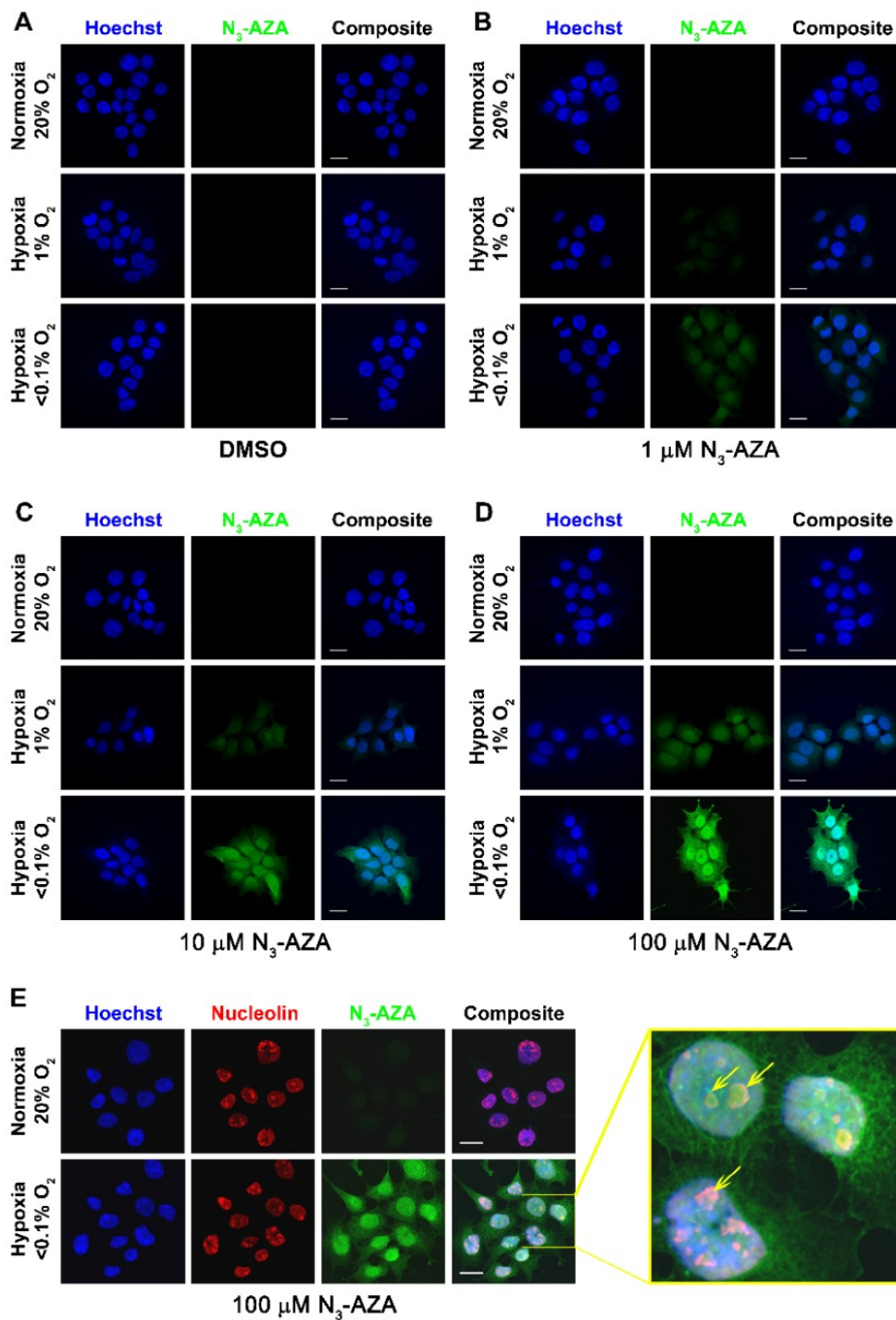


Figure 2.4 N₃-AZA click chemistry as a hypoxia marker.

(A-D) FaDu cells, treated with different concentration of N₃-AZA (or 0.02% DMSO vehicle control) were incubated under normoxia or hypoxia (0.1% O₂ or <0.1% O₂), and click chemistry was performed on paraformaldehyde fixed cells using a fluorescently tagged alkyne. N₃-AZA click staining was present only in drug treated hypoxic cells. Intensity of N₃-AZA click staining increased with drug concentration and decreased with O₂ levels. (E) N₃-AZA click staining is concentrated in nucleoli. Micrographs displayed are representative of at least three independent experiments; scale bar = 20 μm.

2.3.6 N₃-AZA click chemistry for hypoxia mapping in tumours

Since N₃-AZA click chemistry could efficiently stain hypoxic cells, its capacity to detect hypoxic regions in tumour tissue was examined in comparison to pimonidazole. Initially, a FaDu cell subcutaneous xenograft model was used, which has previously been shown to have a hypoxic fraction of 11-12% (Yaromina, Zips et al. 2006). Regions of tumour hypoxia defined by the click chemistry reaction were present in areas bordering necrosis and were independent of the vasculature (**Fig. 2.5C**). Pimonidazole immunostaining generated a similar staining pattern (**Fig. 2.5D**). Pimonidazole and N₃-AZA staining co-localized to areas bordering necrotic regions as expected (**Fig. 2.5E**). These findings were then validated in mouse primary head and neck tumours (**Fig. 2.5F**). For both tumour models, a low level of non-specific staining of tumour sections by the secondary antibodies used for pimonidazole and CD31 was observed; N₃-AZA click staining provided a clearer background. We further quantified the hypoxic fraction in tumours with different volumes to determine if there is a relationship between tumour size and hypoxia. Our data (**Suppl. Fig. 2.10A**) did not indicate a size dependence, which implies that small tumours may retain a hypoxic fraction that is resistant to therapy. Importantly, significant click staining was not seen in any of the harvested organs, which suggests that N₃-AZA preferentially accumulates in hypoxic tumour niches (**Suppl. Fig. 2.10B-G**).

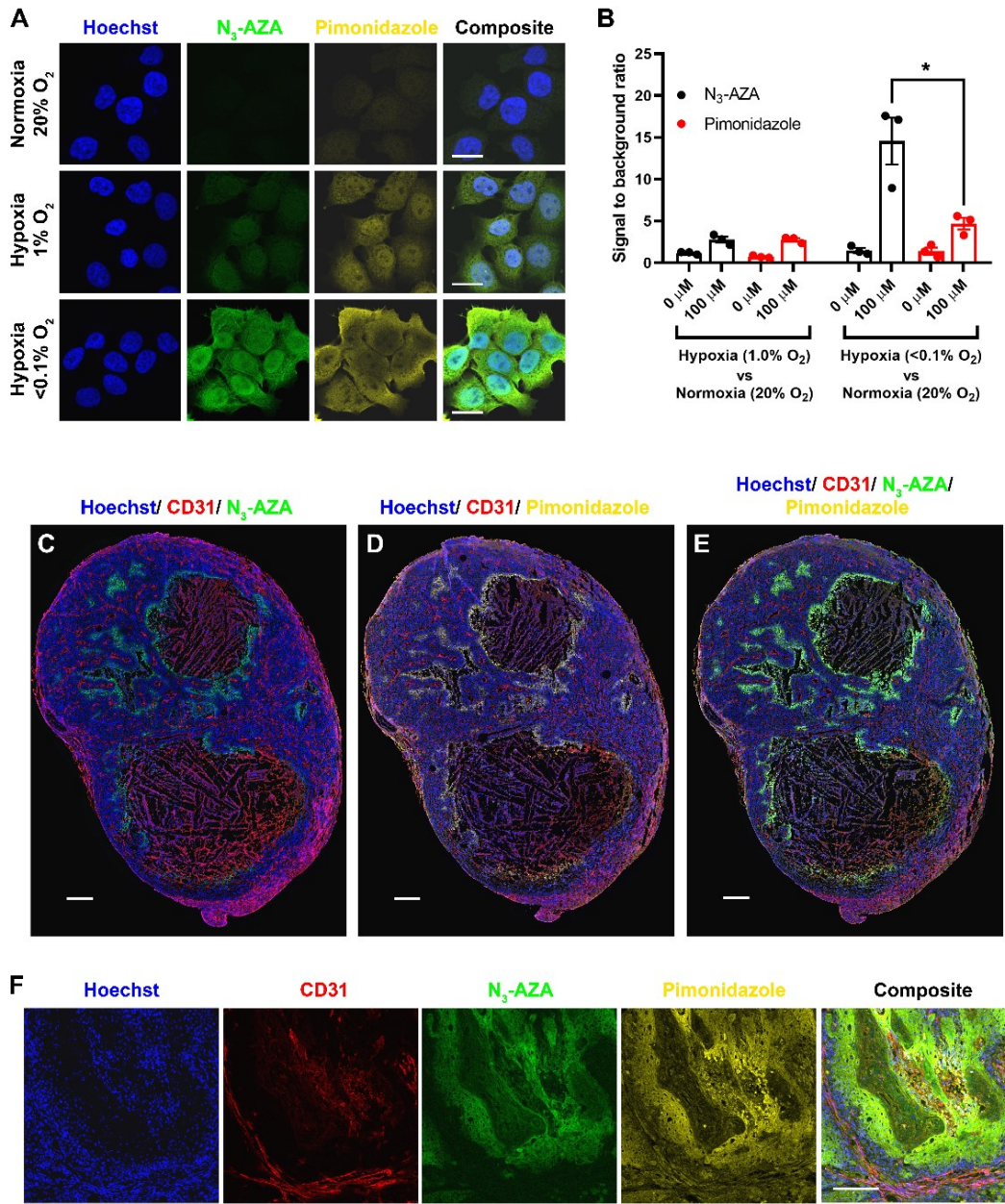


Figure 2.5 Pimonidazole immunostaining is comparable to that of N₃-AZA.

(A) Representative micrographs from three independent experiments showing that N₃-AZA click staining and pimonidazole immunostaining overlaps in hypoxic FaDu cells co-treated with both compounds. (B) The micrographs were processed with IMARIS software to quantify channel intensities from N₃-AZA click staining and pimonidazole immunostaining. The ratios of signal (hypoxia):background (normoxia) intensities for cells co-treated with N₃-AZA and pimonidazole [or vehicle control (0.02% DMSO), i.e. columns labeled 0 μM, see **Suppl. Fig. 2.9** for micrographs of cells not treated with N₃-AZA or pimonidazole] are shown (mean± S.E.M.). N₃-AZA click staining generated a higher signal to noise ratio compared to pimonidazole immunostaining. (C-F) *In vivo* comparison of N₃-AZA click staining with pimonidazole immunostaining. Both are concentrated in the same regions of a mouse subcutaneous tumour section (C-E) and of a primary mouse head and neck tumour section (F). Representative micrographs are displayed from at least three independent experiments; scale bar represents 20 μm (A), 1 mm (C-E) and 200 μm (F).

2.4 Discussion

The tumour microenvironment has garnered considerable attention in recent times for its role in therapy outcome (Hirata and Sahai 2017). Hypoxia, a key feature of the tumour microenvironment, offers both a challenge and a vulnerability that can be exploited for therapy. However, very few strategies have yielded successful results when it comes to targeting hypoxic tumours. Despite several setbacks, NIs still hold significant value as hypoxia-directed therapeutics. For example, nimorazole (a 5-NI), in combination with radiotherapy, showed promise in treating advanced head and neck cancer patients (Overgaard, Hansen et al. 1998). Interestingly, meta analysis of NI clinical trials showed an overall improvement in patient outcome, particularly when stratified depending on tumour oxygenation status (Overgaard 1994). Therefore, an in depth understanding of NI molecular mechanism is crucial to better guide future development of NI based cancer therapeutics.

NIs have long been known to bind to nucleic acids and proteins in hypoxic cells (Varghese and Whitmore 1980). While early NI studies almost exclusively concentrated on their potential to induce DNA damage (Zahoor, Lafleur et al. 1987, Jenner, Sapora et al. 1988, Edwards 2013), NI protein targets remained relatively unexplored. A handful of proteomic studies do exist, albeit mostly limited to reaction of 5-NIs in protozoans (Leitsch, Kolarich et al. 2007, Leitsch, Kolarich et al. 2009, Leitsch, Schlosser et al. 2012). Recently, a click chemistry based method to identify candidate 5-NI drug targets in *Giardia lamblia* using a modified metronidazole (metronidazole alkyne) and an azido-biotin was outlined (Lauwaet, Miyamoto et al. 2020). The current study shows that N₃-AZA click chemistry with a biotin-alkyne is compatible with mammalian cell-based assays to efficiently biotinylate proteins that interact with activated 2-NIs under hypoxia (**Fig. 2.1G**). These proteins were then isolated, identified by mass spectrometry and characterized for functional significance with respect to molecular targeting of hypoxia. We report a total of 62 protein targets of N₃-AZA, 48 of which were not present in our control samples (**Fig. 2.2A, Table 2.1**). For proteins that appeared ubiquitously across the panel, their abundance was generally multiple-fold higher in the N₃-AZA treated hypoxic sample (based on PSM scores, **Fig. 2.2B**). To assess if N₃-AZA is binding to a subset of proteins, a relative enrichment profile was generated by comparing crude extracts and eluates from N₃-AZA treated hypoxic cells (**Fig. 2.2C**). Overall, N₃-AZA-protein interaction appeared to be

dictated by the abundance of the protein, with a few exceptions; several highly abundant proteins (such as ACAD9) did not react with N₃-AZA, while proteins like desmoplakin and calpastatin, despite being relatively low in abundance, appeared as positive hits. This suggests that there might be some degree of selectivity for NI-protein interaction. In contrast to previous reports proposing thiol groups as a major site for NI attack (Wislocki, Bagan et al. 1984), no clear association was found between the Cys content of a protein and its likelihood of binding to N₃-AZA, which is consistent with the findings described by Lauwaet *et al* (2020). For example, despite having 11 Cys residues, ACAD9 escaped N₃-AZA binding while 5 of the N₃-AZA target proteins (histone H1.2, prohibitin, ATP synthase subunit beta, histone H4 and activated RNA polymerase II transcriptional coactivator p15) lack any Cys residues (**Suppl. Fig. 2.2A**). While this observation could be a result of Cys residues being buried within the protein structure or forming cysteine-cysteine disulfide bonds, it could also imply that other nucleophilic amino acids, such as Pro, may serve as the site of adduct formation for NI compounds. Indeed, the current analysis showed that most of the N₃-AZA target proteins are enriched for Pro residues (**Suppl. Fig. 2.2B**). Unfortunately, without the exact chemical formula of the N₃-AZA-amino acid derivatives, we were unable to identify potential conjugates by MS.

Analysis of the proteomic data was performed using several bioinformatics platforms. N₃-AZA target proteins appeared to be predominantly cytoplasmic (~71%) with only ~21% being nuclear proteins (**Suppl. Fig. 2.2C**). Upstream regulatory analysis with IPA identified two regulatory clusters with direct implications to hypoxic response. Cluster 1 (regulated by HSF1) has 8 downstream targets, 5 of which are molecular chaperones directly involved in adaptations to low O₂ levels and protect against reoxygenation-induced oxidative stress (HSP90AA1, HSP90AB1, HSPA1A, HSPA8 and HSPD1) (**Fig. 2.2D**) (Baird, Turnbull et al. 2006, Jain, Suryakumar et al. 2014). Of particular interest to us was cluster 2, consisting of 8 target proteins of N₃-AZA, which are under the regulation of HIF1A. HIF1A, known as the master regulator of hypoxia, plays a key role in cellular response to hypoxic insults (Nagao, Kobayashi et al. 2019). Hypoxia induced stabilization of HIF1A results in upregulation of pro-survival genes, including those involved in glucose metabolism. 7 out of the 8 N₃-AZA target proteins in cluster 2 are implicated in carbohydrate metabolism (**Fig. 2.2E**). Whether or not binding of N₃-AZA (and other 2-nitimidazole compounds) to these downstream targets can counteract the actions of HIF1A remains to be explored.

Interestingly, from our list of 62 target proteins (**Table 2.1**), canonical pathway analysis identified glycolysis I as one of the top hits with a P value of 8.05E-09; five of the N₃-AZA target proteins belong to this pathway (ALDOA, ENO1, GAPDH, PKM and TPI1) and are regulated by HIF1A (**Table 2.2, Fig. 2.2E**). It is important to note that reprogramming of glucose metabolism through upregulation of glycolysis is a crucial hallmark of tumorigenesis. Despite being less efficient than the mitochondrial respiration system, cancer cells readily utilize aerobic glycolysis for ATP production, mostly to counteract mitochondrial defects or to compensate for the defective mitochondrial oxidative phosphorylation under hypoxia. Increased glycolysis also provides an acidic microenvironment through elevated production of lactate, and thus facilitates malignant progression (Pelicano, Martin et al. 2006). GAPDH was identified as the top target for N₃-AZA with an average PSM score of 18.3. It is a Cys-directed glycolytic enzyme that catalyzes the reversible conversion of glyceraldehyde-3-phosphate (GAP) to 1,3-bisphosphoglycerate (BPG). GAPDH transcription has been reported to be upregulated in hypoxic cells in a HIF1A dependent manner (Yamaji, Fujita et al. 2003, Higashimura, Nakajima et al. 2011), however, such regulation appears to be cell-type specific (Said, Hagemann et al. 2007). In addition to its role in glycolysis, GAPDH has also been implicated in diverse physiological and pathophysiological processes (Pelicano, Martin et al. 2006, Tristan, Shahani et al. 2011, Ganapathy-Kanniappan and Geschwind 2013). This makes GAPDH an interesting target to follow-up on. Three aspects of N₃-AZA treatment on GAPDH were explored: total protein level, cellular distribution, and enzymatic activity. Total GAPDH protein levels remained unaffected in response to N₃-AZA treatment, both under normoxia and hypoxia. (**Fig. 2.3A**). NIs (such as PA-824) can induce nitrosative stress by acting as an NO donor, which can lead to oxidization/ S-nitrosylation of GAPDH and its translocation to the nucleus (Manjunatha, Boshoff et al. 2009). Immunocytochemical analysis showed that N₃-AZA treatment did not alter GAPDH cellular distribution (**Fig. 2.3B**). The highly conserved active site of GAPDH contains a Cys residue, which is readily acetylated during the reversible oxidative phosphorylation of GAP (Knight, Kofoed et al. 1996), is essential for its role in oxidative stress response (Nakajima, Amano et al. 2007, Hildebrandt, Knuesting et al. 2015, Kubo, Nakajima et al. 2016), and could potentially serve as a binding site to 2-NIs. Importantly, ornidazole (a 5-NI) has been reported to inhibit GAPDH activity in mouse spermatocytes (Bone and Cooper 2000), protozoa and anaerobic bacteria (Marcus, Tal et al. 2016), and depletion of

GAPDH has also been reported to induce cytostatic effects on human cancer cell lines (Phadke, Krynetskaia et al. 2009). This prompted us to explore the effects of N₃-AZA treatment on GAPDH enzymatic activity. GAPDH activity did not differ significantly between the normoxic-treatment groups, whereas upon hypoxic incubation, its enzymatic activity was reduced by >30% in cells treated with 250 μM N₃-AZA as compared to vehicle control (**Fig. 2.3C**).

Another key protein target identified in our analysis was GST family protein GSTP1 (**Table 2.1**), which is the predominant non-hepatic isozyme that eliminates toxic by-products of oxidative stress and xenobiotics by catalyzing their conjugation with glutathione (GSH) (Chatterjee and Gupta 2018). GSTP1 has also been implicated in the mitogen-activated protein (MAP) kinase pathway through protein: protein interactions with c-Jun N-terminal kinase 1 (JNK1) and ASK1 (apoptosis signal-regulating kinase), which are activated in response to cellular stress (Townsend and Tew 2003). While GSTs can prevent tumour formation by protecting cellular proteins and DNA from endogenous reactive compounds, their detoxification properties may aid in multi-drug resistance in tumour cells. Indeed, tumours often express high levels of GST (particularly GSTP1), and GSTs are frequently overexpressed in multidrug-resistant cells (Tew 1994). Additionally, hypoxic exposure is often accompanied by an increase in GST activity to cope with the altered intracellular redox potential and the generation of increased cellular reactive oxygen species (ROS) (Millar, Phan et al. 2007). Interestingly, inhibition of GSTP1 reduces cell viability and induces vulnerability to both intracellular oxidative stress and hypoxia/ reoxygenation stress (Fletcher, Boshier et al. 2015). Nitroimidazoles, such as etanidazole and misonidazole, have previously been reported to inhibit GST activity (Kumar and Weiss 1986, O'Dwyer, LaCreta et al. 1993). Our analysis is in agreement with these findings, and show a significant reduction in GST specific activity only in N₃-AZA treated hypoxic cells. Compared to vehicle treated cells, we observed >50% reduction in hypoxic cells treated with 100 μM N₃-AZA and >75% reduction in hypoxic cells treated with 250 μM N₃-AZA (**Fig. 2.3D**). The inhibitory effect of the drug does not seem to be due to proteolysis since no significant change in GSTP1 protein levels was observed in response to drug treatment or hypoxic exposure (**Fig. 2.3A**). While our data does not preclude toxicity arising from DNA damage (Edwards 2013), given the dynamic roles of GAPDH and

GSTP1 in the hypoxic tumour microenvironment, such an effect of N₃-AZA on their activity may partially explain the observed hypoxic cytotoxicity of the drug.

The list of NI-targeted proteins (**Table 2.1**) includes additional proteins that demand further attention, for example, peroxiredoxin-1 (Prdx1). Similar to other members of this protein family, Prdx1 active site contains two Cys residues that are essential for its catalytic function and could serve as potential binding sites for thiol-reacting NIs (Hanschmann, Godoy et al. 2013). It is therefore tempting to postulate that binding of N₃-AZA to Prdx1 through its catalytic Cys residues may exert a negative impact on its enzymatic activity. Prdx1 plays a key role in cellular detoxification, functions as a chaperone, has anti-apoptotic property, is upregulated in cancer and contributes to radioresistance (Kim, Ahn et al. 2007, Ding, Fan et al. 2017). Interestingly, Prdx1 is upregulated under hypoxia possibly to counteract the detrimental effects of hypoxia/reoxygenation mediated accumulation of reactive oxygen species and to provide aggressive survival advantage for malignant progression (Kim, Ahn et al. 2007, Zhang, Hou et al. 2014). Hence, N₃-AZA binding and subsequent reduction in enzymatic activity of Prdx1 could provide an additional mechanism for its hypoxic cytotoxicity. Further studies will be required to test this hypothesis. Interestingly, a related protein, thioredoxin reductase (TrxR), has previously been reported as a common target for 5-NIs across three microorganisms (Leitsch, Kolarich et al. 2007, Leitsch, Kolarich et al. 2009, Leitsch, Schlosser et al. 2012).

A unique feature of N₃-AZA click chemistry is its versatility since it can also be used as a hypoxia marker. N₃-AZA shares structural homology with ¹⁸F-FAZA, which itself has proven to be superior in comparison to other 2-NI hypoxia radiotracers (Reischl, Dorow et al. 2007). 2-NIs are widely used for immunohistological hypoxia diagnosis, aided by the development of antibodies against pimonidazole- and EF-5-protein adducts (Varia, Calkins-Adams et al. 1998, Evans, Hahn et al. 2000). N₃-AZA click chemistry offers a simpler alternative by exploiting the Cu(I) catalyzed click chemistry instead to visualize cellular hypoxia. While the 2-NI moiety of N₃-AZA ensures that it is selectively forming drug-protein adducts in hypoxic cells, the azido group can be exploited to fluorescently label these adducts using a fluorescently tagged alkyne molecule in the presence of a Cu(I) catalyst. A similar strategy for fluorescent labelling of hypoxic cells using an alkyne conjugated NI, SN33267, has previously been reported in a patent and a MSc. thesis (Tercel and Pruijn 2011, Hou 2016).

N₃-AZA click fluorescence is extremely selective for hypoxic cells, with minimal background staining in their normoxic counterparts. It significantly reduces the staining duration (30 min versus 2.5 h for pimonidazole) while still maintaining high fidelity. An inverse relationship between O₂ levels and N₃-AZA click staining intensity is reported (**Fig. 2.4A-D, Suppl. Fig. 2.6B**). N₃-AZA demonstrated preferential uptake by the nucleus (**Suppl. Fig. 2.6C**) and concentrated in nucleoli (**Fig. 4E, Suppl. Movie 2.1**). While this does not necessarily agree with the proteomic analysis (N₃-AZA target proteins being predominantly cytoplasmic, **Suppl. Fig. 2.2C**), some of the nuclear N₃-AZA click staining may be attributed to the formation of drug-nucleic acid adducts. N₃-AZA-nucleic acid binding was not investigated here, however, previous studies reported direct binding of activated NIs to DNA (Varghese and Whitmore 1980).

N₃-AZA and pimonidazole showed similar cytotoxicity patterns in FaDu cells (preferential toxicity under hypoxia) (**Fig. 2.1B and Suppl. Fig. 2.8**). Both pimonidazole immunostaining and N₃-AZA click chemistry efficiently labeled hypoxic cells, however, the latter was significantly faster and produced a clearer background (**Fig. 2.5A-B**). The efficiency of N₃-AZA and pimonidazole as hypoxia probes was also compared *in vivo*, using two mouse models of head and neck cancer; (i) FaDu cell based subcutaneous tumour model (**Fig. 2.5C-E**) and (ii) a Cre-LoxP-based primary mouse model of HPV-negative squamous cell carcinoma (**Fig. 2.5F**). In tumour sections, N₃-AZA- and pimonidazole-stained areas overlapped, suggesting that N₃-AZA click chemistry is staining the same regions that are considered hypoxic by pimonidazole immunostaining (**Fig. 2.5E**). As expected, both N₃-AZA and pimonidazole stained regions were mostly mutually exclusive with vasculature (CD31 positive regions). N₃-AZA click chemistry following pimonidazole immunostaining did not affect the latter (**Fig. 2.5D**). Also, no significant click staining was detected in organs (brain, lung, liver, kidney and cervical lymph nodes) harvested from tumour-bearing mice administered with N₃-AZA, indicating that N₃-AZA is preferentially accumulating in the hypoxic regions of tumours (**Suppl. Fig. 2.10B-G**). An important clinical question is to what degree does tumour size dictate hypoxia levels? Previous data obtained by computerized Eppendorf pO₂ histography indicated that hypoxia is independent of tumour size (Vaupel, Höckel et al. 2007). N₃-AZA click staining performed on tumours ranging in volume between ~150-350 mm³ also indicated no clear association between tumour size and hypoxia levels (**Suppl. Fig. 2.10A**).

In summary, N₃-AZA click chemistry provided a robust chemical strategy to identify potential protein targets of 2-NI compounds in a human head and neck tumour model. N₃-AZA binding to the glycolytic enzyme GAPDH and detoxification enzyme GSTP1 showed a profound effect on their enzymatic activities only under hypoxia, which creates an interesting avenue for not only further mechanistic exploration of NI compounds in general, but also suggests their potential role in targeted hypoxia therapy. In addition, the modularity of the N₃-AZA click reaction allowed for its application as an antibody independent histological hypoxia marker that offers a faster but equally efficient alternative to pimonidazole immunostaining.

2.5 Acknowledgements

The authors would like to thank Dr. Lynne-Marie Postovit, Dr. Ravin Narain and Dr. Hans-Sonke Jans for their guidance and advice, and Dr. Xuejun Sun, Geraldine Barron, Xiao-Hong Yang and Dan Mcginn for technical assistance. This work was supported through grants 201201164 and 20131051 from Alberta Innovates through the CRIO program and CRIO Project-Cancer (P.K.; M.W.), grant 2017-05792 from the Natural Sciences and Engineering Research Council of Canada (R. F.), the Canadian Institutes of Health Research and Canadian Breast Cancer Foundation-Prairies/NWT Chapter (S.D.) and P30 Cancer Centre Support Grant and Duke University Physician-Scientist Strong Start Award (Y.M.). FBR received scholarships from the Terry Fox Foundation, Strategic Training in Transdisciplinary Radiation Science for the 21st Century (STARS21) program, the Yau Family Foundation, Alberta Cancer Foundation (Antoine Noujaim Scholarship), and the University of Alberta.

2.6 Declaration of interest

The authors Michael Weinfeld, Piyush Kumar and Hassan El-Saidi are included in the following patent application: Markers, conjugates, compositions and methods for hypoxia imaging, mapping, and therapy. International PCT Patent, Application No. PCT/CA2018/051165. Other authors declare no competing interests.

2.7 References

- Ai, M., P. Budhani, J. Sheng, S. Balasubramanyam, T. Bartkowiak, A. R. Jaiswal, C. R. Ager, D. D. Haria and M. A. Curran (2015). "Tumor hypoxia drives immune suppression and immunotherapy resistance." *Journal for ImmunoTherapy of Cancer* 3(S2): P392.
- Baird, N. A., D. W. Turnbull and E. A. Johnson (2006). "Induction of the Heat Shock Pathway during Hypoxia Requires Regulation of Heat Shock Factor by Hypoxia-inducible Factor-1." *Journal of Biological Chemistry* 281(50): 38675-38681.
- Bertout, J. A., S. A. Patel and M. C. Simon (2008). "The impact of O₂ availability on human cancer." *Nature Reviews Cancer* 8(12): 967.
- Bone and Cooper (2000). "In vitro inhibition of rat cauda epididymal sperm glycolytic enzymes by ornidazole, α -chlorohydrin and 1-chloro-3-hydroxypropanone." *International Journal of Andrology* 23(5): 284-293.
- Brotzel, F. and H. Mayr (2007). "Nucleophilicities of amino acids and peptides." *Organic & Biomolecular Chemistry* 5(23): 3814-3820.
- Chatterjee, A. and S. Gupta (2018). "The multifaceted role of glutathione S-transferases in cancer." *Cancer Letters* 433: 33-42.
- Ding, C., X. Fan and G. Wu (2017). "Peroxiredoxin 1—an antioxidant enzyme in cancer." *Journal of Cellular and Molecular Medicine* 21(1): 193-202.
- Dubois, L. J., N. G. Lieuwes, M. H. Janssen, W. J. Peeters, A. D. Windhorst, J. C. Walsh, H. C. Kolb, M. C. Öllers, J. Bussink and G. A. van Dongen (2011). "Preclinical evaluation and validation of [18F] HX4, a promising hypoxia marker for PET imaging." *Proceedings of the National Academy of Sciences* 108(35): 14620-14625.
- Edwards, D. I. (2013). "Reduction of nitroimidazoles in vitro and DNA damage." *Bioreduction in the Activation of Drugs*; Alexander, P., Gielen, J., Sartorelli, AC, Eds: 53.
- Evans, S. M., S. Hahn, D. R. Pook, W. T. Jenkins, A. A. Chalian, P. Zhang, C. Stevens, R. Weber, G. Weinstein, I. Benjamin, N. Mirza, M. Morgan, S. Rubin, W. G. McKenna, E. M. Lord and C. J. Koch (2000). "Detection of hypoxia in human squamous cell carcinoma by EF5 binding." *Cancer Research* 60(7): 2018-2024.
- Feoktistova, M., P. Geserick and M. Leverkus (2016). "Crystal violet assay for determining viability of cultured cells." *Cold Spring Harbor Protocols* 2016(4): pdb. prot087379.
- Fletcher, M. E., P. R. Boshier, K. Wakabayashi, H. C. Keun, R. T. Smolenski, P. A. Kirkham, I. M. Adcock, P. J. Barton, M. Takata and N. Marczin (2015). "Influence of glutathione-S-transferase (GST) inhibition on lung epithelial cell injury: role of oxidative stress and metabolism." *American Journal of Physiology-Lung Cellular and Molecular Physiology* 308(12): L1274-L1285.
- Ganapathy-Kanniappan, S. and J.-F. H. Geschwind (2013). "Tumor glycolysis as a target for cancer therapy: progress and prospects." *Molecular Cancer* 12(1): 152.
- Hanschmann, E.-M., J. R. Godoy, C. Berndt, C. Hudemann and C. H. Lillig (2013). "Thioredoxins, glutaredoxins, and peroxiredoxins—molecular mechanisms and health significance: from cofactors to antioxidants to redox signaling." *Antioxidants & Redox Signaling* 19(13): 1539-1605.
- Higashimura, Y., Y. Nakajima, R. Yamaji, N. Harada, F. Shibasaki, Y. Nakano and H. Inui (2011). "Up-regulation of glyceraldehyde-3-phosphate dehydrogenase gene expression by HIF-1 activity depending on Sp1 in hypoxic breast cancer cells." *Archives of Biochemistry and Biophysics* 509(1): 1-8.

- Hildebrandt, T., J. Knuesting, C. Berndt, B. Morgan and R. Scheibe (2015). "Cytosolic thiol switches regulating basic cellular functions: GAPDH as an information hub?" *Biological Chemistry* 396(5): 523-537.
- Hirata, E. and E. Sahai (2017). "Tumor microenvironment and differential responses to therapy." *Cold Spring Harbor Perspectives in Medicine* 7(7): a026781.
- Hou, A. L. (2016). A Novel Click Chemistry-Based Method to Detect Hypoxic Tumour Cells and Characterise Their Gene Expression, *ResearchSpace@ Auckland*.
- House, S. W., O. Warburg, D. Burk and A. L. Schade (1956). "On respiratory impairment in cancer cells." *Science* 124(3215): 267-272.
- Jain, K., G. Suryakumar, L. Ganju and S. B. Singh (2014). "Differential hypoxic tolerance is mediated by activation of heat shock response and nitric oxide pathway." *Cell Stress and Chaperones* 19(6): 801-812.
- Janssen, H., K. Haustermans, A. Balm and A. Begg (2005). "Hypoxia in head and neck cancer: how much, how important?" *Head & Neck* 27(7): 622-638.
- Jenner, T. J., O. Saporá, P. O'Neill and E. M. Fielden (1988). "Enhancement of DNA damage in mammalian cells upon bioreduction of the nitroimidazole-aziridines RSU-1069 and RSU-1131." *Biochemical Pharmacology* 37(20): 3837-3842.
- Keith, B. and M. C. Simon (2007). "Hypoxia-inducible factors, stem cells, and cancer." *Cell* 129(3): 465-472.
- Kim, Y.-J., J.-Y. Ahn, P. Liang, C. Ip, Y. Zhang and Y.-M. Park (2007). "Human prx1 gene is a target of Nrf2 and is up-regulated by hypoxia/reoxygenation: implication to tumor biology." *Cancer Research* 67(2): 546-554.
- Kizaka-Kondoh, S. and H. Konse-Nagasawa (2009). "Significance of nitroimidazole compounds and hypoxia-inducible factor-1 for imaging tumor hypoxia." *Cancer Science* 100(8): 1366-1373.
- Knight, R. J., K. F. Kofoed, H. R. Schelbert and D. B. Buxton (1996). "Inhibition of glyceraldehyde-3-phosphate dehydrogenase in post-ischaemic myocardium." *Cardiovascular Research* 32(6): 1016-1023.
- Koch, C., R. Howell and J. Biaglow (1979). "Ascorbate anion potentiates cytotoxicity of nitroaromatic compounds under hypoxic and anoxic conditions." *British Journal of Cancer* 39(3): 321-329.
- Kramer, A., J. Green, J. Pollard, Jr. and S. Tugendreich (2014). "Causal analysis approaches in Ingenuity Pathway Analysis." *Bioinformatics* 30(4): 523-530.
- Kubo, T., H. Nakajima, M. Nakatsuji, M. Itakura, A. Kaneshige, Y.-T. Azuma, T. Inui and T. Takeuchi (2016). "Active site cysteine-null glyceraldehyde-3-phosphate dehydrogenase (GAPDH) rescues nitric oxide-induced cell death." *Nitric Oxide* 53: 13-21.
- Kumar, K. S. and J. F. Weiss (1986). "Inhibition of glutathione peroxidase and glutathione transferase in mouse liver by misonidazole." *Biochemical Pharmacology* 35(18): 3143-3146.
- Kumar, P., L. Wiebe, M. Asikoglu, M. Tandon and A. McEwan (2002). "Microwave-assisted (radio) halogenation of nitroimidazole-based hypoxia markers." *Applied Radiation and Isotopes* 57(5): 697-703.
- Kumareswaran, R., O. Ludkovski, A. Meng, J. Sykes, M. Pintilie and R. G. Bristow (2012). "Chronic hypoxia compromises repair of DNA double-strand breaks to drive genetic instability." *Journal of Cell Science* 125(1): 189-199.

- Lauwaet, T., Y. Miyamoto, S. Ihara, C. Le, J. Kalisiak, K. A. Korthals, M. Ghassemian, D. K. Smith, K. B. Sharpless and V. V. Fokin (2020). "Click chemistry-facilitated comprehensive identification of proteins adducted by antimicrobial 5-nitroimidazoles for discovery of alternative drug targets against giardiasis." *PLOS Neglected Tropical Diseases* 14(4): e0008224.
- Lee, D.-J., D. Cosmatos, V. A. Marcial, K. K. Fu, M. Rotman, J. S. Cooper, H. G. Ortiz, J. J. Beitler, R. A. Abrams and W. J. Curran (1995). "Results of an RTOG phase III trial (RTOG 85-27) comparing radiotherapy plus etanidazole with radiotherapy alone for locally advanced head and neck carcinomas." *International Journal of Radiation Oncology* Biology* Physics* 32(3): 567-576.
- Leitsch, D., D. Kolarich, M. Binder, J. Stadlmann, F. Altmann and M. Duchêne (2009). "Trichomonas vaginalis: metronidazole and other nitroimidazole drugs are reduced by the flavin enzyme thioredoxin reductase and disrupt the cellular redox system. Implications for nitroimidazole toxicity and resistance." *Molecular Microbiology* 72(2): 518-536.
- Leitsch, D., D. Kolarich, I. B. Wilson, F. Altmann and M. Duchêne (2007). "Nitroimidazole action in *Entamoeba histolytica*: a central role for thioredoxin reductase." *PLoS Biology* 5(8).
- Leitsch, D., S. Schlosser, A. Burgess and M. Duchêne (2012). "Nitroimidazole drugs vary in their mode of action in the human parasite *Giardia lamblia*." *International Journal for Parasitology: Drugs and Drug Resistance* 2: 166-170.
- Manjunatha, U., H. I. Boshoff and C. E. Barry (2009). "The mechanism of action of PA-824: novel insights from transcriptional profiling." *Communicative & Integrative Biology* 2(3): 215-218.
- Mannan, R. H., V. V. Somayaji, J. Lee, J. R. Mercer, J. D. Chapman and L. I. Wiebe (1991). "arabinofuranosyl)-2-thioimidazole." *Journal of Nuclear Medicine* 32: 1764-1770.
- Marcus, Y., N. Tal, M. Ronen, R. Carmieli and M. Gurevitz (2016). "The drug ornidazole inhibits photosynthesis in a different mechanism described for protozoa and anaerobic bacteria." *Biochemical Journal* 473(23): 4413-4426.
- Mi, H., A. Muruganujan, D. Ebert, X. Huang and P. D. Thomas (2019). "PANTHER version 14: more genomes, a new PANTHER GO-slim and improvements in enrichment analysis tools." *Nucleic Acids Research* 47(D1): D419-D426.
- Millar, T. M., V. Phan and L. A. Tibbles (2007). "ROS generation in endothelial hypoxia and reoxygenation stimulates MAP kinase signaling and kinase-dependent neutrophil recruitment." *Free Radical Biology and Medicine* 42(8): 1165-1177.
- Mortensen, L. S., J. Johansen, J. Kallehauge, H. Primdahl, M. Busk, P. Lassen, J. Alsner, B. S. Sørensen, K. Toustrup and S. Jakobsen (2012). "FAZA PET/CT hypoxia imaging in patients with squamous cell carcinoma of the head and neck treated with radiotherapy: results from the DAHANCA 24 trial." *Radiotherapy and Oncology* 105(1): 14-20.
- Mowery, Y. M., D. J. Carpenter, A. J. Wisdom, C. T. Badea, L. Luo, Y. Ma, A. Pendse and D. G. Kirsch (2018). Characterization of novel primary mouse models of HPV-negative squamous cell carcinoma of the oral cavity. Radiation Research Society Annual Meeting. Chicago, Illinois
- Nagao, A., M. Kobayashi, S. Koyasu, C. C. Chow and H. Harada (2019). "HIF-1-dependent reprogramming of glucose metabolic pathway of cancer cells and its therapeutic significance." *International Journal of Molecular Sciences* 20(2): 238.

- Nakajima, H., W. Amano, A. Fujita, A. Fukuhara, Y.-T. Azuma, F. Hata, T. Inui and T. Takeuchi (2007). "The active site cysteine of the proapoptotic protein glyceraldehyde-3-phosphate dehydrogenase is essential in oxidative stress-induced aggregation and cell death." *Journal of Biological Chemistry* 282(36): 26562-26574.
- O'Dwyer, P., F. LaCreta, J. Walczak, T. Cox, S. Litwin, J. Hoffman, M. Zimny and R. Comis (1993). "Phase I/pharmacokinetic/biochemical study of the nitroimidazole hypoxic cell sensitiser SR2508 (etanidazole) in combination with cyclophosphamide." *British Journal of Cancer* 68(4): 756-766.
- Otsu, N. (1979). "A threshold selection method from gray-level histograms." *IEEE transactions on systems, man, and cybernetics* 9(1): 62-66.
- Overgaard, J. (1994). "Clinical evaluation of nitroimidazoles as modifiers of hypoxia in solid tumors." *Oncology Research Featuring Preclinical and Clinical Cancer Therapeutics* 6(10-11): 509-518.
- Overgaard, J., H. S. Hansen, A. Andersen, M. Hjelm-Hansen, K. Jørgensen, E. Sandberg, A. Berthelsen, R. Hammer and M. Pedersen (1989). "Misonidazole combined with split-course radiotherapy in the treatment of invasive carcinoma of larynx and pharynx: report from the DAHANCA 2 study." *International Journal of Radiation Oncology• Biology• Physics* 16(4): 1065-1068.
- Overgaard, J., H. S. Hansen, M. Overgaard, L. Bastholt, A. Berthelsen, L. Specht, B. Lindeløv and K. Jørgensen (1998). "A randomized double-blind phase III study of nimorazole as a hypoxic radiosensitizer of primary radiotherapy in supraglottic larynx and pharynx carcinoma. Results of the Danish Head and Neck Cancer Study (DAHANCA) Protocol 5-85." *Radiotherapy and Oncology* 46(2): 135-146.
- Pathan, M., S. Keerthikumar, C. S. Ang, L. Gangoda, C. Y. Quek, N. A. Williamson, D. Mouradov, O. M. Sieber, R. J. Simpson and A. Salim (2015). "FunRich: An open access standalone functional enrichment and interaction network analysis tool." *Proteomics* 15(15): 2597-2601.
- Pelicano, H., D. Martin, R. Xu, and P. Huang (2006). "Glycolysis inhibition for anticancer treatment." *Oncogene* 25(34): 4633-4646.
- Phadke, M. S., N. F. Krynetskaia, A. K. Mishra and E. Krynetskiy (2009). "Glyceraldehyde 3-phosphate dehydrogenase depletion induces cell cycle arrest and resistance to antimetabolites in human carcinoma cell lines." *Journal of Pharmacology and Experimental Therapeutics* 331(1): 77-86.
- Rajendran, J., D. Wilson, E. Conrad, L. Peterson, J. Bruckner, J. Rasey, L. Chin, P. Hofstrand, J. Grierson and J. Eary (2003). "[18 F] FMISO and [18 F] FDG PET imaging in soft tissue sarcomas: correlation of hypoxia, metabolism and VEGF expression." *European Journal of Nuclear Medicine and Molecular Imaging* 30(5): 695-704.
- Reischl, G., D. S. Dorow, C. Cullinane, A. Katsifis, P. Roselt, D. Binns and R. J. Hicks (2007). "Imaging of tumor hypoxia with [124I] IAZA in comparison with [18F] FMISO and [18F] FAZA—first small animal PET results." *Journal of Pharmacy and Pharmaceutical Sciences* 10(2): 203-211.
- Said, H. M., C. Hagemann, J. Stojic, B. Schoemig, G. H. Vince, M. Flentje, K. Roosen and D. Vordermark (2007). "GAPDH is not regulated in human glioblastoma under hypoxic conditions." *BMC Molecular Biology* 8(1): 55.
- Teicher, B. A. (1995). "Angiogenesis and cancer metastases: therapeutic approaches." *Critical Reviews in Oncology/Hematology* 20(1): 9-39.

- Tercel, M. and F. B. Pruijn (2011). Agents and methods for detection and/or imaging of hypoxia, Google Patents.
- Tew, K. D. (1994). "Glutathione-associated enzymes in anticancer drug resistance." *Cancer Research* 54(16): 4313-4320.
- Townsend, D. M. and K. D. Tew (2003). "The role of glutathione-S-transferase in anti-cancer drug resistance." *Oncogene* 22(47): 7369-7375.
- Tristan, C., N. Shahani, T. W. Sedlak and A. Sawa (2011). "The diverse functions of GAPDH: views from different subcellular compartments." *Cellular Signalling* 23(2): 317-323.
- Varghese, A. and G. Whitmore (1980). "Binding to cellular macromolecules as a possible mechanism for the cytotoxicity of misonidazole." *Cancer Research* 40(7): 2165-2169.
- Varia, M. A., D. P. Calkins-Adams, L. H. Rinker, A. S. Kennedy, D. B. Novotny, W. C. Fowler Jr and J. A. Raleigh (1998). "Pimonidazole: a novel hypoxia marker for complementary study of tumor hypoxia and cell proliferation in cervical carcinoma." *Gynecologic Oncology* 71(2): 270-277.
- Vaupel, P., M. Höckel and A. Mayer (2007). "Detection and characterization of tumor hypoxia using pO₂ histography." *Antioxidants & Redox Signaling* 9(8): 1221-1236.
- Walsh, J. C., A. Lebedev, E. Aten, K. Madsen, L. Marciano and H. C. Kolb (2014). "The clinical importance of assessing tumor hypoxia: relationship of tumor hypoxia to prognosis and therapeutic opportunities." *Antioxidants & Redox Signaling* 21(10): 1516-1554.
- Wislocki, P. G., E. S. Bagan, W. J. Vandenheuvel, R. W. Walker, R. F. Alvaro, B. H. Arison, A. Y. Lu and F. J. Wolf (1984). "Drug residue formation from ronidazole, a 5-nitroimidazole. V. Cysteine adducts formed upon reduction of ronidazole by dithionite or rat liver enzymes in the presence of cysteine." *Chemico-Biological Interactions* 49(1-2): 13-25.
- Yamaji, R., K. Fujita, S. Takahashi, H. Yoneda, K. Nagao, W. Masuda, M. Naito, T. Tsuruo, K. Miyatake and H. Inui (2003). "Hypoxia up-regulates glyceraldehyde-3-phosphate dehydrogenase in mouse brain capillary endothelial cells: involvement of Na⁺/Ca²⁺ exchanger." *Biochimica et Biophysica Acta (BBA)-Molecular Cell Research* 1593(2-3): 269-276.
- Yaromina, A., D. Zips, H. D. Thames, W. Eicheler, M. Krause, A. Rosner, M. Haase, C. Petersen, J. A. Raleigh and V. Quennet (2006). "Pimonidazole labelling and response to fractionated irradiation of five human squamous cell carcinoma (hSCC) lines in nude mice: the need for a multivariate approach in biomarker studies." *Radiotherapy and Oncology* 81(2): 122-129.
- Zahoor, A., M. Lafleur, R. Knight, H. Loman and D. Edwards (1987). "DNA damage induced by reduced nitroimidazole drugs." *Biochemical Pharmacology* 36(19): 3299-3304.
- Zeng, M., H. Kikuchi, M. S. Pino and D. C. Chung (2010). "Hypoxia activates the K-ras proto-oncogene to stimulate angiogenesis and inhibit apoptosis in colon cancer cells." *PLoS One* 5(6): e10966.
- Zhang, M., M. Hou, L. Ge, C. Miao, J. Zhang, X. Jing, N. Shi, T. Chen and X. Tang (2014). "Induction of peroxiredoxin 1 by hypoxia regulates heme oxygenase-1 via NF- κ B in oral cancer." *PLoS One* 9(8).

2.8 Supplementary information

2.8.1 Synthesis of N₃-AZA from Ts-AZA precursor

1- α -D-(5-*O*-tosyl-arabinofuranosyl)-2-nitroimidazole (Ts-AZA) (0.028 g, 0.07 mmol) and NaN₃ (0.0455 g, 0.70 mmol) were dissolved in DMSO (5 mL) and stirred at 50 °C overnight (16 h). The reaction mixture was quenched with H₂O (10 ml), allowed to cool to room temperature and the product was extracted in EtOAc (3 x 5 ml). The combined organic extracts were dried over anhydrous Na₂SO₄, filtered and solvent was removed under reduced pressure. The crude product was purified using column chromatography (10:1, v/v, CH₂Cl₂/CH₃OH) to afford 13 mg (0.048 mmol, 69% yield) of N₃-AZA.

Supplementary Table 2.1 Proteins identified in eluates from DMSO treated normoxic cells using LC-MS/MS

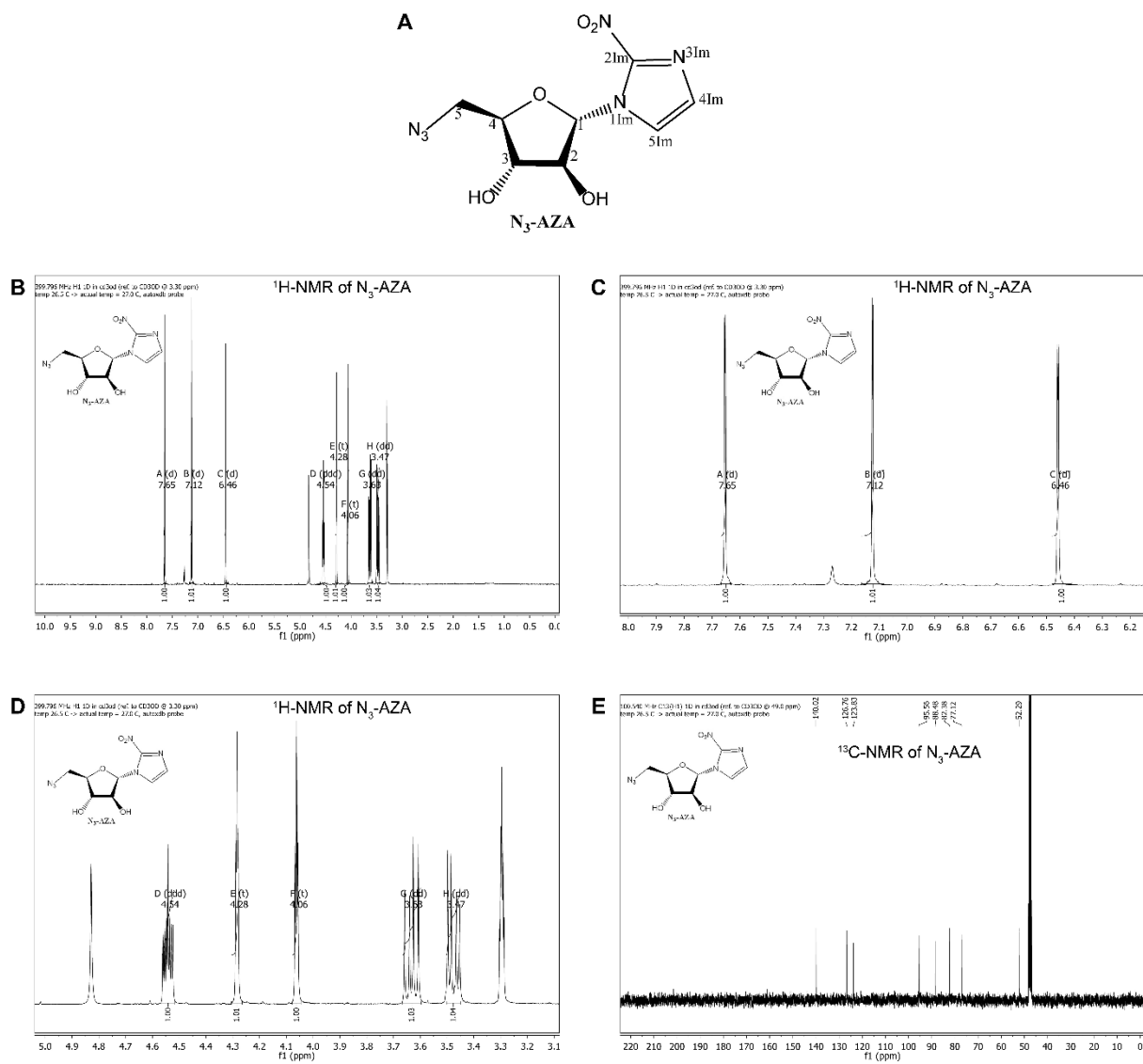
Gene	Protein name	PSM score	Size (amino acid)	#Cys	#Pro
HSP90AB1	Heat shock protein HSP 90-beta	9	724	6	23
GAPDH	Glyceraldehyde-3-phosphate dehydrogenase	5	335	3	12
CTTN	Src substrate cortactin	4	550	3	17
TPI1	Triosephosphate isomerase	2	286	5	11
HIST1H1C	Histone H1.2	2	213	0	21

Supplementary Table 2.2 Proteins identified in eluates from N₃-AZA treated normoxic cells using LC-MS/MS

Gene	Protein name	PSM score	Size (amino acid)	#Cys	#Pro
HSP90AA1	Heat shock protein HSP 90-alpha	6.67	732	7	21
HSP90AB1	Heat shock protein HSP 90-beta	5.33	724	6	23
HIST1H1C	Histone H1.2	2.00	213	0	21
HSPD1	60 kDa heat shock protein, mitochondrial	2.00	573	3	19
TUBB	Tubulin beta chain	1.67	444	8	20
CTTN	Src substrate cortactin	1.33	550	3	17
CFL1	Cofilin 1 (Non-muscle), isoform CRA_a	1.33	166	4	6
ENO1	Alpha-enolase	1.33	434	6	16
PRDX1	Peroxiredoxin-1 (Fragment)	1.33	199	4	13
ACTB	Actin, cytoplasmic 1	1.33	375	6	19
SUB1	Activated RNA polymerase II transcriptional coactivator p15	1.00	127	0	6
LDHB	L-lactate dehydrogenase (Fragment)	0.67	334	5	11
RPL31	60S ribosomal protein L31	0.67	125	0	6

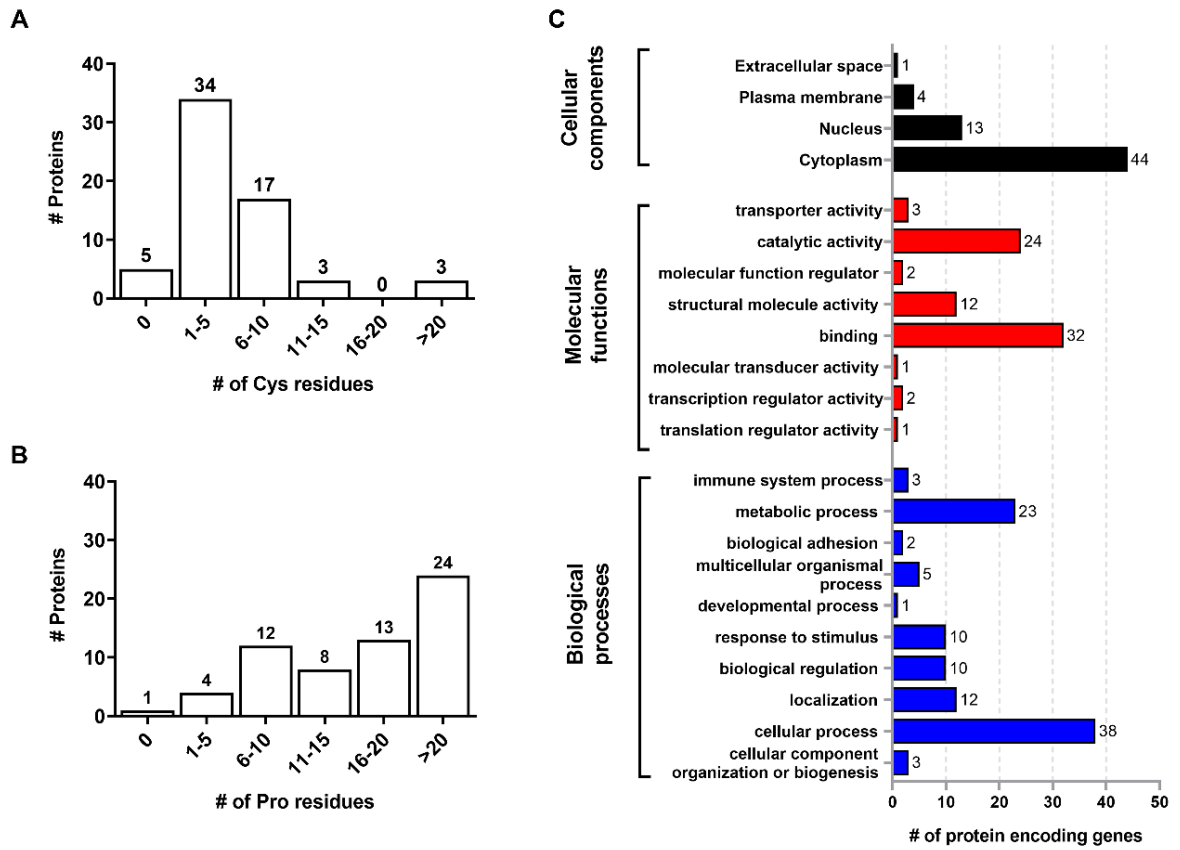
Supplementary Table 2.3 Proteins identified in eluates from DMSO treated hypoxic cells using LC-MS/MS

Gene	Protein name	PSM score	Size (amino acid)	#Cys	#Pro
HSP90AB1	Heat shock protein HSP 90-beta	10	724	6	23
ENO1	Alpha-enolase	10	434	6	16
GAPDH	Glyceraldehyde-3-phosphate dehydrogenase	7	335	3	12
TUBB	Tubulin beta chain	6	444	8	20
PRDX1	Peroxiredoxin-1 (Fragment)	5	199	4	13
YWHAZ	14-3-3 protein zeta/delta	3	245	3	4
ANXA2P2	Putative annexin A2-like protein	3	339	3	7
LDHB	L-lactate dehydrogenase (Fragment)	3	334	5	11
HIST1H1C	Histone H1.2	3	213	0	21
HSPD1	60 kDa heat shock protein, mitochondrial	3	573	3	19



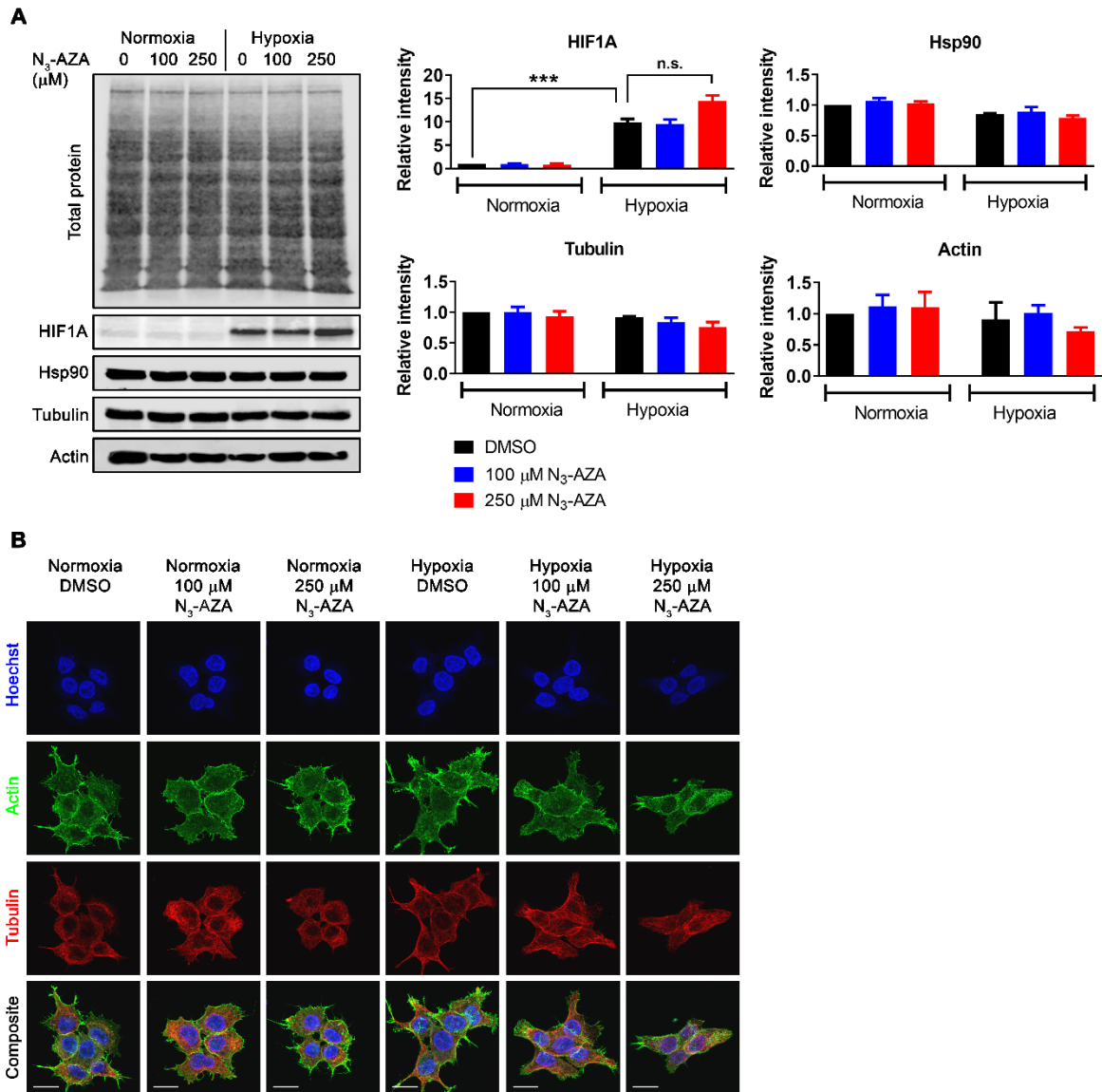
Supplementary Figure 2.1 Spectral analysis of N₃-AZA.

(A) Structure of N₃-AZA and atom assignments used in spectral analysis. (B-D) Proton NMR and (E) carbon-13 NMR of N₃-AZA.



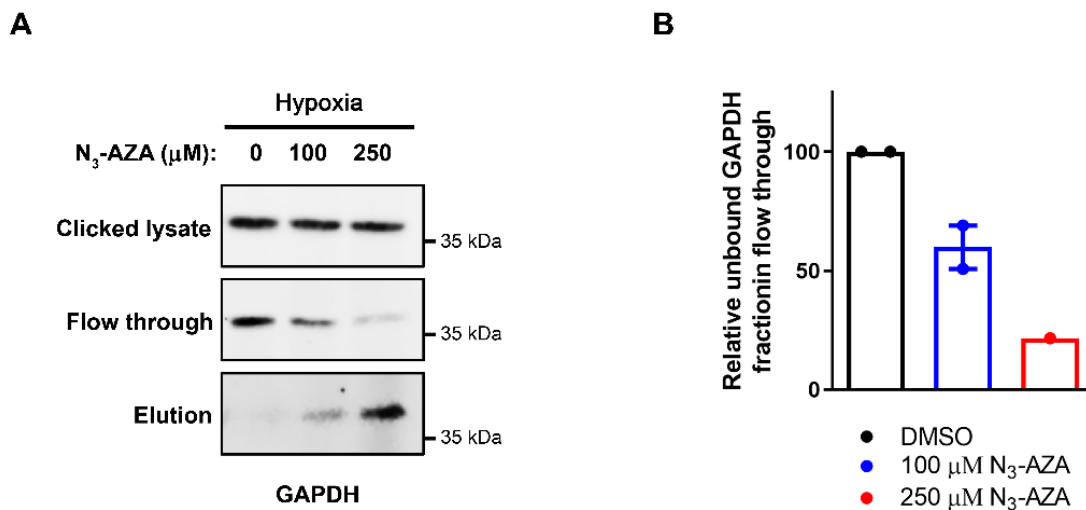
Supplementary Figure 2.2 Functional characterization of N₃-AZA target proteins.

(A and B) Distribution of N₃-AZA target proteins based on their cysteine and proline content, respectively. (C) Distribution of N₃-AZA target proteins based on cellular component, molecular function and biological process, generated by PANTHER classification system.



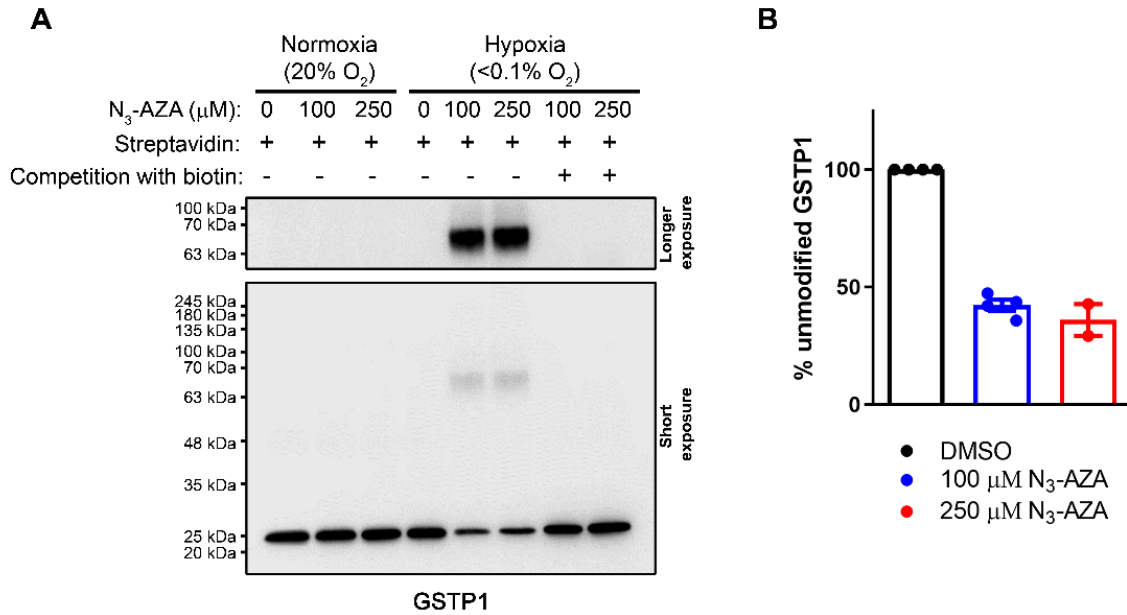
Supplementary Figure 2.3 Effects of N₃-AZA treatment on its target proteins.

(A) Extracts were prepared from FaDu cells treated with 0.02% DMSO or N₃-AZA (100 μM or 250 μM) and processed for HIF1A, Hsp90, tubulin, actin, and total protein by immunoblot. No statistically significant difference was found in target protein levels in response to N₃-AZA treatment. Representative immunoblots and quantification [mean± S.E.M.] from three independent replicates are displayed. (B) FaDu cells treated with 0.02% DMSO or N₃-AZA (100 μM or 250 μM) were processed for immunofluorescence imaging for actin (green) and tubulin (blue); nuclei were counter stained with Hoechst. N₃-AZA treatment did not alter the cellular distribution of these proteins, albeit hypoxic drug treated cells showed fewer cell projections and a condensed morphology. Micrographs presented are representative of at least three independent experiments; scale bar = 20 μm.



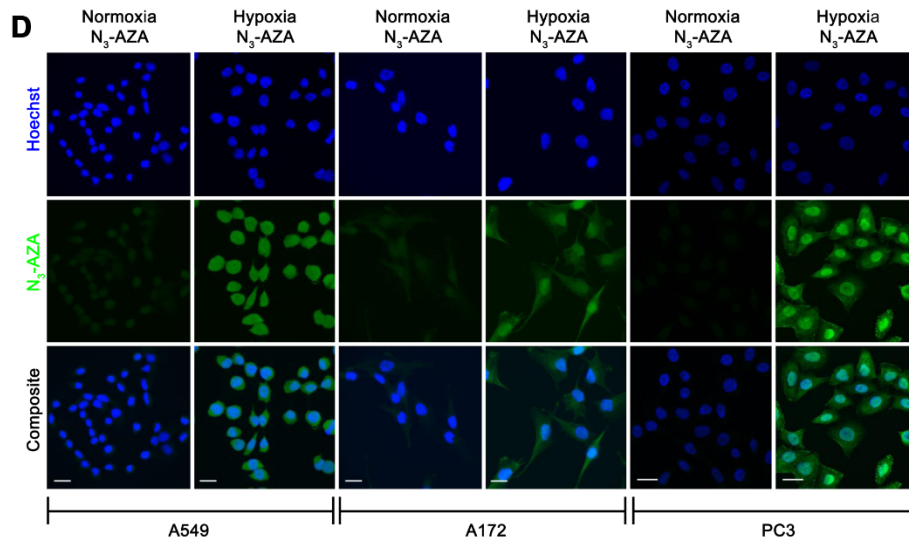
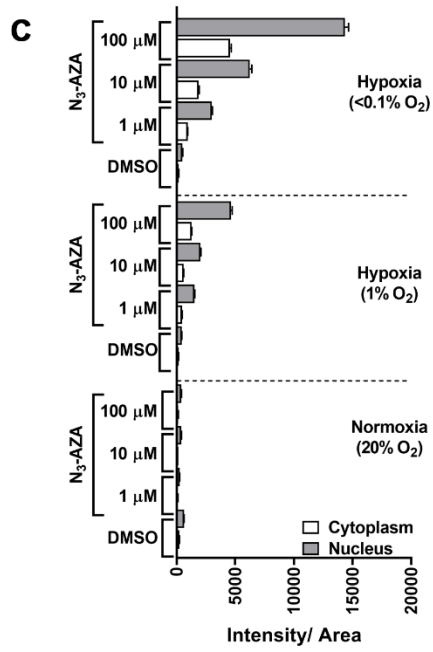
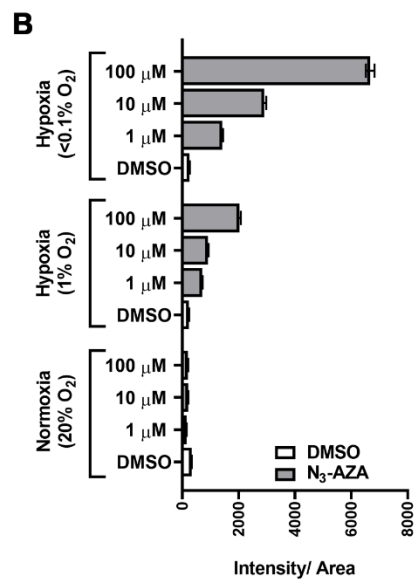
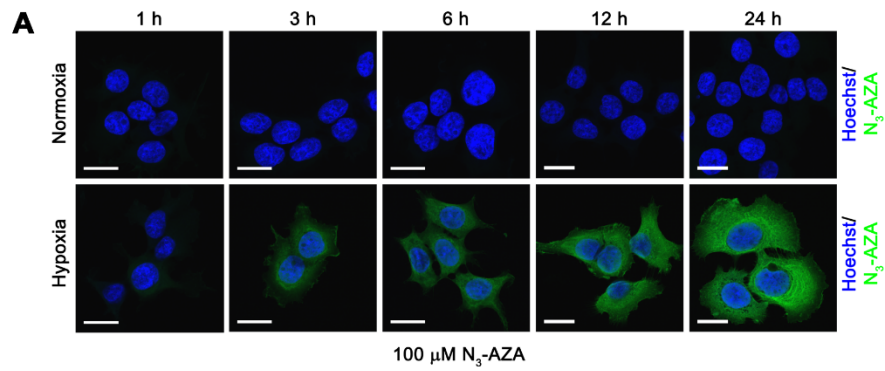
Supplementary Figure 2.4 Estimation of N_3 -AZA bound GAPDH fraction.

300 μ g of protein lysates (in 150 μ l of RIPA buffer) from hypoxic FaDu cells treated with N_3 -AZA (or vehicle control) were mixed with 150 μ l of reaction cocktail containing biotin alkyne for 1 h to allow for click reaction. Clicked lysates were loaded on BSA blocked streptavidin-mutinin beads, incubated overnight at 4 $^{\circ}$ C, followed by collection of the flowthrough fractions. Beads were resuspended in 300 μ l of 1:1 ratio of dH₂O: SDS loading dye and boiled for 10 min. An equal volume of clicked cell lysates (input), flowthrough fractions (unbound fractions i.e., non-biotinylated proteins) and resuspended beads (bound fractions i.e. biotinylated proteins) were run on SDS-PAGE. Proteins were transferred to nitrocellulose membrane and probed for GAPDH protein (A). GAPDH band intensities in the flowthrough were quantified and normalized to the vehicle treated lane. Relative unbound GAPDH fraction (non-biotinylated i.e. not reacting with N_3 -AZA) in flowthrough is shown in the graph (B). Lane 1 and 2 (DMSO and 100 μ M N_3 -AZA treatment) each show the mean \pm S.E.M. from two independent replicates.



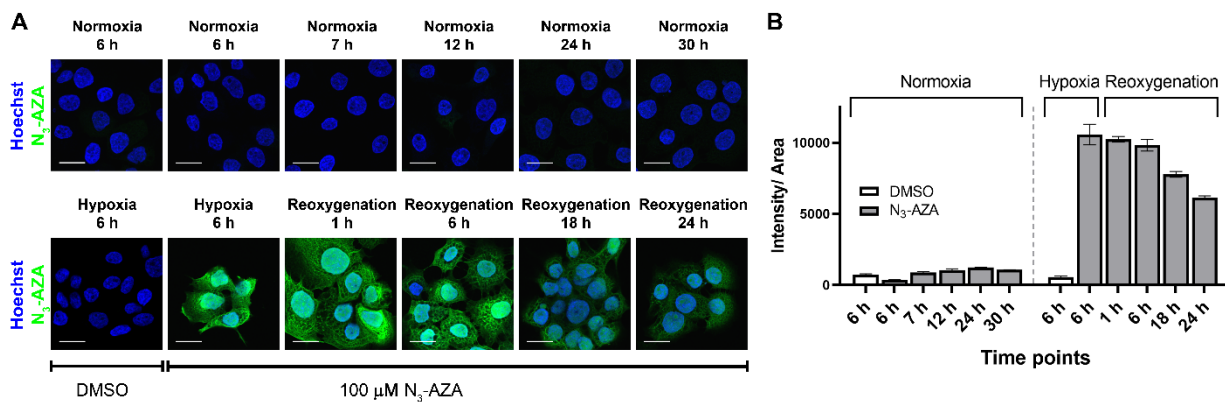
Supplementary Figure 2.5 Estimation of N₃-AZA bound GSTP1 fraction.

N₃-AZA (or vehicle control) treated FaDu cell extracts (normoxic/ hypoxic) underwent reaction with biotin conjugated alkyne for 1 h. Excess biotin from the clicked lysates was removed using microconcentrators (3K cut off, UFC500308, Millipore). Afterwards, the biotin-free clicked lysates (100 μg) were mixed with streptavidin (50 μg, Cat. # 85878, Sigma-Aldrich) and incubated overnight at 4 °C. For biotin competition samples, 20 μg of biotin was added. Samples were processed for immunoblotting and probed for GSTP1. A clear shift in GSTP1 band was seen in hypoxic N₃-AZA treated clicked samples containing streptavidin. Addition of extra biotin to these samples inhibited this supershift (A). Signal intensities of unmodified GSTP1 was calculated and normalized to the vehicle treated lane. Data show mean ± S.E.M. from at least two independent experiments (B).



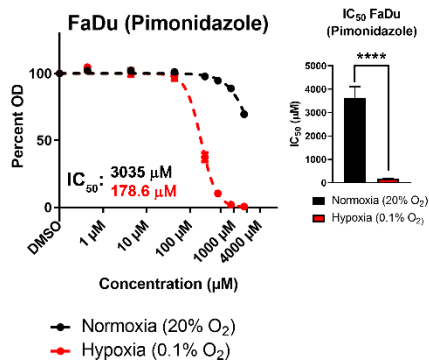
Supplementary Figure 2.6 Intensity of hypoxic N₃-AZA click staining increases with incubation time, hypoxia levels and is concentrated in the nuclei.

FaDu cells were treated with 100 μ M N₃-AZA for different durations under normoxia (20% O₂) and hypoxia (<0.1% O₂), and were fixed in 2% paraformaldehyde at indicated time points. Cells were processed for N₃-AZA click chemistry and nuclei were counterstained with Hoechst. **(A)** Confocal microscopy images show that intensity of hypoxia selective N₃-AZA click staining increased with longer drug incubation, although appreciable intensity was observed in the 6 h treatment group. Notably, no significant N₃-AZA click staining was observed in normoxic cells, even after prolonged drug incubation. Scale bar= 20 μ m. **(B)** FaDu cells treated with different concentrations of N₃-AZA (6 h) were processed for N₃-AZA click chemistry. Confocal microscopy images were processed using IMARIS software to quantify N₃-AZA click fluorescence staining intensity along with cell, nuclei and cytoplasm areas. N₃-AZA click staining is inversely dependent on the O₂ levels and is proportional to drug concentration. Quantification shows mean \pm S.E.M. from three independent replicates. **(C)** Cell compartment-based analysis identified N₃-AZA click intensity to be more concentrated in the nucleus. Error bar represents standard error of the mean. **(D)** A549 lung cancer, A172 glioblastoma and PC-3 prostate cancer cells were treated with 10 μ M of N₃-AZA for 6 h under normoxia (20% O₂) or hypoxia (<0.1% O₂), fixed with 2% paraformaldehyde and processed for N₃-AZA click chemistry and Hoechst staining. Across the panel, hypoxic cells stained positive for N₃-AZA click staining with minimal staining in their normoxic counterparts. Micrographs are representative of at least two independent experiments; scale bar = 20 μ m.



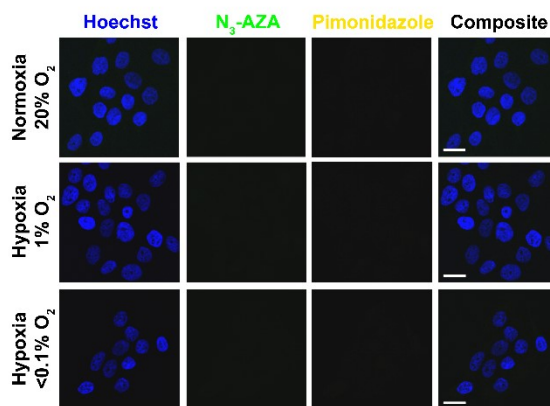
Supplementary Figure 2.7 N₃-AZA click staining following reoxygenation.

FaDu cells treated with 100 μM N₃-AZA (or 0.02% DMSO) were fixed with 2% paraformaldehyde at indicated time points. For hypoxia/ reoxygenation group, cells were fixed either after 6 h of hypoxic incubation or after 1, 6, 18 and 24 h of reoxygenation. Drug was present in the media throughout the reoxygenation period. Fixed cells, processed for N₃-AZA click chemistry and Hoechst staining, were imaged and quantified as described. N₃-AZA click staining can be detected in hypoxic reoxygenated cells even after 24 h of reoxygenation (A), however the intensity of the click signal intensity decreases over time (B). Micrographs are representative of at least two independent experiments; scale bar = 20 μm. Quantification shows mean ± S.E.M. from three independent replicates.



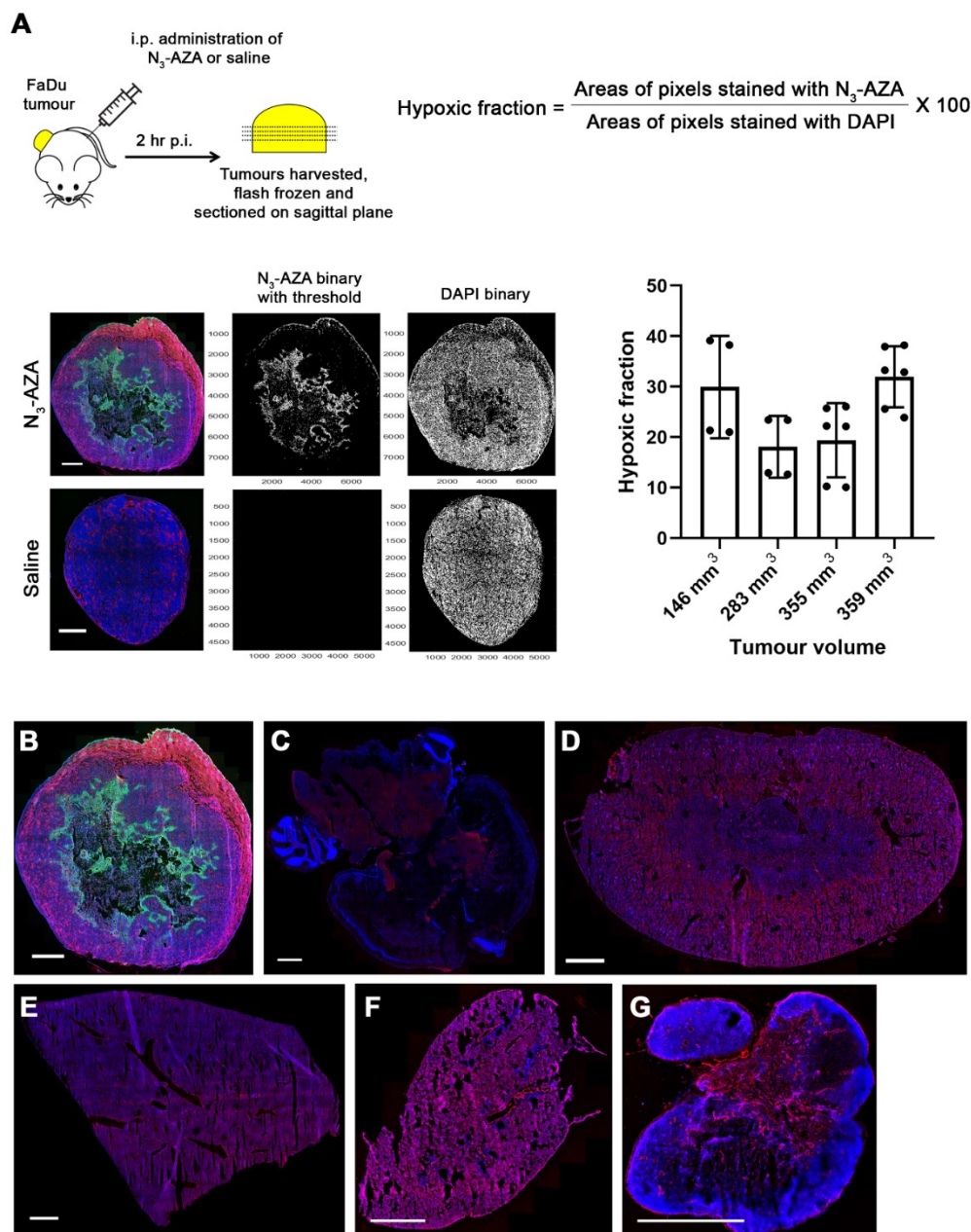
Supplementary Figure 2.8 Pimonidazole shows hypoxia selective cytotoxicity.

FaDu cells were treated with increasing concentrations of pimonidazole, incubated for 72 h under normoxia (20% O₂) and hypoxia (0.1% O₂), and crystal violet staining assay was performed. Pimonidazole shows preferential cytotoxicity in hypoxic FaDu cells, with statistically significant differences between their normoxic and hypoxic IC₅₀ values. Data represents mean \pm S.E.M. from at least three independent experiments.



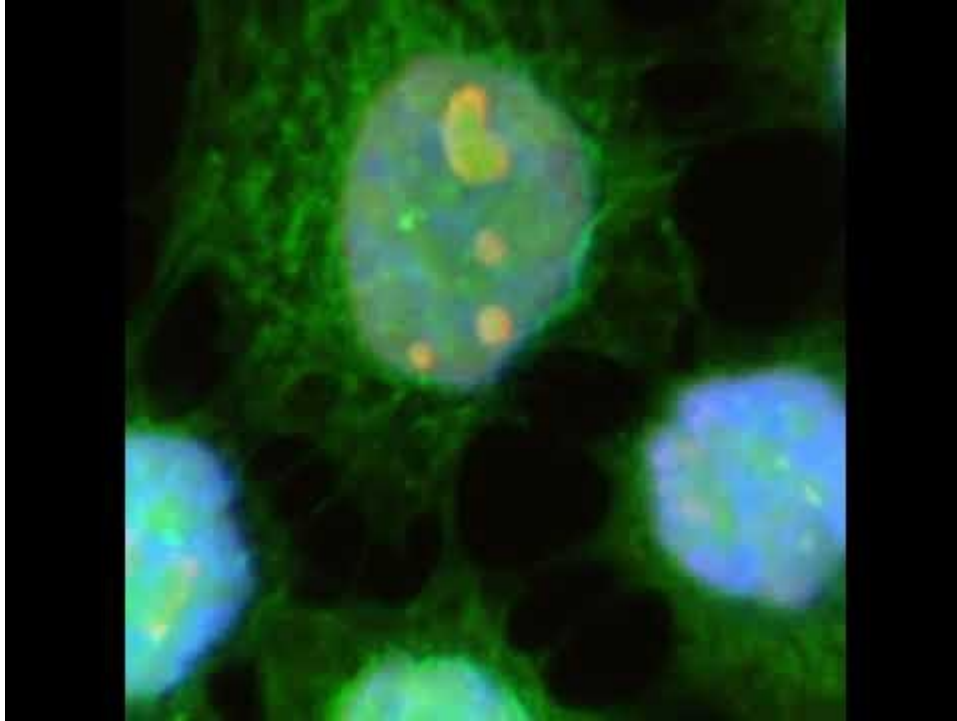
Supplementary Figure 2.9 Autofluorescence in N₃-AZA and pimonidazole channel is minimal.

FaDu cells treated with vehicle control (0.02% DMSO i.e. 0 μM N₃-AZA and 0 μM pimonidazole) were stained for N₃-AZA click chemistry and pimonidazole immunostaining. Images were obtained in parallel with cells treated and displayed in Fig. 2.5A. Minimal fluorescence from N₃-AZA and pimonidazole channels was seen in vehicle treated FaDu cells. Representative micrographs are shown from three independent experiments; scale bar = 20 μm .



Supplementary Figure 2.10 N_3 -AZA click staining is preferentially detected in tumours and can be quantified to determine hypoxic fractions in tumour.

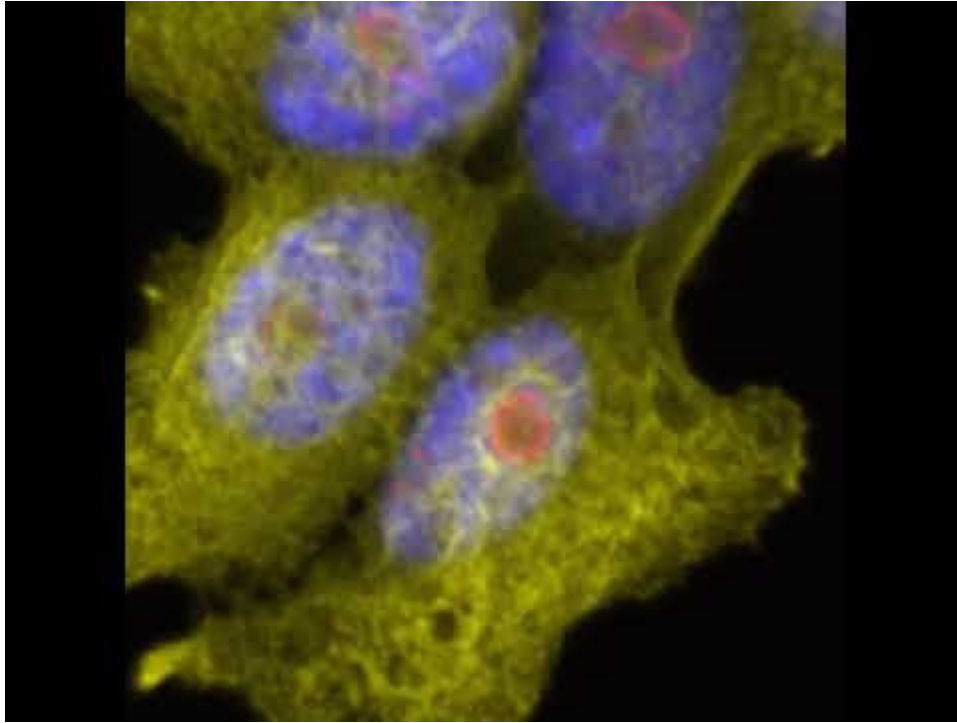
Mice containing subcutaneous FaDu tumors were injected i.p. with N_3 -AZA (or saline) and sacrificed 2 h after injection. Tumours and organs were harvested, and frozen sections were stained for N_3 -AZA click chemistry (hypoxia, green), blood vessels (CD31, red) and nuclei (DAPI, blue). (A) Images were converted to binary using MATLAB; a manual threshold was applied for the click channel and Otsu threshold for DAPI. Hypoxic fraction was quantified using the formula shown. The bar diagram depicts hypoxic fraction across different tumour sizes (means ± S.E.M.). At least 4 sections per tumour were stained and quantified independently by two different individuals. N_3 -AZA click staining was detected only in the tumour section (B) whereas different organs [brain (C), kidney (D), liver (E), lung (F) and cervical lymph node (G)] stained negative for N_3 -AZA click chemistry. This points to a preferential uptake of the drug by hypoxic tumour niches. Representative images are shown; scale bar = 1 mm.



Supplementary Movie 2.1 N₃-AZA click staining is concentrated in nucleoli.

FaDu cells, treated with 100 μ M N₃-AZA for 6 h under hypoxia (<0.1% O₂), were fixed and processed for nucleolin immunostaining (red) and N₃-AZA click chemistry (green); nuclei were counterstained with Hoechst (blue). Images were obtained in z-stacks with a Plan-Apochromat 40X/1.3 Oil DIC lens on a Zeiss 710 confocal microscope using Zen 2011 software and processed with IMARIS software to prepare a 3D movie. N₃-AZA click staining was higher in the nucleus, with the signal concentrated in nucleoli.

Link to video: (https://www.youtube.com/embed/uwd_1cXouEs?feature=oembed).



Supplementary Movie 2.2 Pimonidazole immunostaining is excluded from nucleoli.

FaDu cells, treated with 100 μ M pimonidazole for 6 h under hypoxia ($<0.1\%$ O_2), were fixed and processed for nucleolin immunostaining (red) and pimonidazole immunostaining (yellow); nuclei were counterstained with Hoechst (blue). Images were obtained in z-stacks with a Plan-Apochromat 40X/1.3 Oil DIC lens on a Zeiss 710 confocal microscope using Zen 2011 software and processed with IMARIS software to prepare a 3D movie. Pimonidazole immunostaining was excluded from nucleoli.

Link to video: (<https://www.youtube.com/embed/2rYupq4ZU04?feature=oembed>).

Chapter 3

Cellular mechanism of action of 2-nitroimidazoles as hypoxia selective therapeutic agents.

3.1 Introduction

Hypoxia or low oxygen tension is a characteristic feature of solid malignancies. It arises from an imbalance between O₂ consumption and supply, which is triggered by rapid proliferation of cancer cells and aberrant tumour vasculature (Brown 1999, McKeown 2014). Hypoxia-induced cellular adaptations confer resistance to radiation, chemotherapy and immunotherapy, leading to poor local control and overall survival (Walsh, Lebedev et al. 2014, Ai, Budhani et al. 2015). This underscores the importance of developing hypoxia-directed therapeutics for effective management of solid tumours.

Nitroimidazoles (NIs) are a class of electron-affinic molecules that are taken up by cells via diffusion and chemically reduced by various cellular nitroreductases, generating nitroradical anions. When cells are well-oxygenated, the nitroradical anions react with intra-cellular O₂ and revert to the parent molecule, which thereafter freely diffuse out of the cell. In the absence of O₂ (i.e. under hypoxia), the reduced NIs undergo further reduction to generate reactive hydroxylamine that binds to cellular macromolecules (such as DNA, proteins and glutathione), thereby trapping the drug inside hypoxic cells (Kizaka-Kondoh and Konse-Nagasawa 2009, Masaki, Shimizu et al. 2015). Due to their preferential accumulation in O₂ starved tissue, NIs have long been pursued as potential hypoxia-directed therapeutics. However, clinical trials with NIs have not been particularly successful. With the exception of nimorazole (Overgaard, Hansen et al. 1998), most NIs failed to provide therapeutic benefit in a clinical setting (Overgaard, Hansen et al. 1989, Lee, Cosmatos et al. 1995). Regardless, retrospective analysis of these studies found an improved outcome in patients with hypoxic tumours (Overgaard, Eriksen et al. 2005, Toustrup, Sørensen et al. 2012). This supports the notion that NIs can improve therapy outcome if patients are pre-selected based on their tumour oxygenation status. However, our poor understanding of the precise molecular mechanism of NIs makes it challenging to study them in a clinical setting.

Iodoazomycin arabinofuranoside (IAZA) and fluoroazomycin arabinofuranoside (FAZA) are 2-NI-based compounds that share a common backbone: an azomycin moiety for hypoxia targeting, a pentose sugar to facilitate cell uptake, and a halogen moiety suitable for radiolabelling to impart PET or SPECT imaging (and potential molecular radiotherapy for

IAZA) capacity (**Fig. 1A-B**). Originally developed as hypoxic radiotracers, radiolabeled IAZA and FAZA have been chemically characterized in the literature (Mannan, Somayaji et al. 1991, Kumar, Stypinski et al. 1999), and clinically validated as non-invasive hypoxia diagnostics (Souvatzoglou, Grosu et al. 2007, Postema, McEwan et al. 2009, Verwer, Bahce et al. 2014). Interestingly, both compounds displayed promising anti-tumour properties under hypoxia in early cell-based assays (Mannan, Somayaji et al. 1991, Kumar, Emami et al. 2009, Quan, Wang et al. 2015), necessitating a more in-depth study of their therapeutic potentials. Therefore, using IAZA and FAZA as representative compounds, this study aims at characterizing the anti-tumour effects of 2-NIs, with a particular emphasis on identifying the cellular phenotype induced by these drugs as well as analyzing their effects on target cellular macromolecules.

3.2 Materials and methods

3.2.1 Cell culture

All cell lines (FaDu, A549, PC3 and HCT116) were purchased directly from the American Type Culture Collection (Manassas, VA), and routinely tested for mycoplasma contamination. Cells were grown in DMEM/F-12 medium supplemented with 10% fetal bovine serum, 1% 2 mM L-glutamine and 1% penicillin streptomycin. Cells in culture were maintained for a maximum of 2 months (~25-30 passages) in a humidified incubator at 37 °C with 5% CO₂. A humidified chamber equipped with controlled O₂ flow was used for hypoxia levels up to 0.1% O₂ (ProOx P110, BioSpherix, Parish, NY). An in-house degassing/ regassing system, fitted with metal canisters, was used to achieve O₂ levels below 0.1% (Koch, Howell et al. 1979). Glass petri dishes were used to carry out hypoxic experiments in the canisters.

3.2.2 Drug stock preparation

Synthesis of IAZA (Mannan, Somayaji et al. 1991), FAZA (Kumar, Stypinski et al. 1999) and azidoazomycin arabinofuranoside (N₃-AZA) (Rashed, Stoica et al. 2021) have been described previously. IAZA, FAZA, N₃-AZA and Ferrostatin-1 (SML0583, Sigma-Aldrich, Oakville, ON) were prepared as 500 mM solutions in DMSO and stored at -20 °C. N-Acetyl-L-cysteine (NAC; A7250, Sigma-Aldrich) was dissolved in a 1:1 ratio of DMSO and distilled H₂O to prepare a fresh 250 mM stock solution for each experiment and added to medium to a final

concentration of 3 mM; medium was buffered to ~pH 7.4 before adding to cells. Stock solutions of 1 M hydroxyurea (HU; H8627, Sigma-Aldrich) and 10 mM (S)-(+)-Camptothecin (CPT; C9911, Sigma-Aldrich) were prepared in DMSO and kept at -20 °C.

3.2.3 Crystal violet staining (CVS) assay

Cells seeded in 96-well plates (Cellstar®; 655180, Sigma-Aldrich) were treated with increasing concentrations of IAZA or FAZA (up to 2000 μ M) for 72 h under normoxia (20% O₂) or hypoxia (1%, 0.5% and 0.1% O₂); 0.02% DMSO was used as vehicle control. Afterwards, medium was removed, and attached cells were stained with 0.05% crystal violet (C6158, Sigma-Aldrich), washed and air dried for 24 h. Modifications to this standard protocol include: (a) treatment with 100 μ M Ferrostatin-1 in addition to IAZA and FAZA for the ferroptosis inhibition assay, and (b) pre-incubation with 3 mM NAC for 2 h for reactive oxygen species (ROS) scavenger assay, after which medium was removed and treatment with IAZA or FAZA was carried out as described earlier. Stained cells were resuspended in 150 μ l of methanol and the optical density (OD) was measured at 584 nm using a FLUOstar OPTIMA microplate reader (BMG Labtech, Ortenberg, Germany). The percentage of attached cells was calculated by subtracting OD of blank wells and then normalizing DMSO controls (under respective O₂ levels) to 100%. The first point on each curve represents 0 μ M drug.

3.2.4 Clonogenic survival assay

FaDu cells seeded in 60 mm glass petri dishes (at densities ranging from 300 to 1500 cells per plate) were treated with different concentrations of IAZA or FAZA (up to 1000 μ M) for 24 h under normoxia or hypoxia (1% O₂, 0.1% O₂ and <0.1% O₂); 0.02% DMSO was used as vehicle control. After treatment, hypoxic cells were reoxygenated, medium was changed, and cells were allowed to grow in drug-free medium for 14 days. Colonies were stained with crystal violet and counted manually. Colony counts were converted to percentage of seeding densities, and then normalized to vehicle-treated controls under respective O₂ conditions.

3.2.5 Apoptosis assay

FaDu cells (8×10^5) were seeded on 60-mm glass petri dishes and allowed to attach overnight. Cells were then treated with either 0.02% DMSO or drug (100 μ M IAZA or 100 μ M FAZA)

and incubated under normoxia and hypoxia (<0.1% O₂) for 24 h, followed by incubation under normoxia for 48 h. Afterwards, cells were trypsinized, counted and 1x10⁶ cells per condition were stained with annexin V and propidium iodide (640914, BioLegend, San Diego, CA). Stained cells were analyzed using an Attune® NxT Acoustic Focusing Cytometer (Thermo Fisher Scientific, Waltham, MA); 100,000 events were recorded for each condition. CPT-treated cells (20 nM, 24 h) served as positive control for apoptosis.

3.2.6 Senescence assay

After treating FaDu cells with either 0.02% DMSO, 100 µM IAZA or 100 µM FAZA under normoxia and hypoxia (<0.1% O₂) for 24 h, drug containing medium was replaced with fresh medium, and cells were allowed to recover and grow for 4 days. To detect senescence, cells were stained with a beta-galactosidase staining kit following the manufacturer's protocol (9860, Cell Signalling Technology, Danvers, MA). Cells treated with 8 Gy ionizing radiation were used as positive control for senescence. Images were obtained with a ZEISS Axioscope colour microscope (Carl Zeiss, Jena, Germany).

3.2.7 Cell counting assay

FaDu cells (1x10⁵) seeded on 60-mm glass petri dishes were left overnight to attach, after which they were treated with either vehicle control (0.02% DMSO) or drug (100 µM IAZA or 100 µM FAZA) and incubated under normoxia and hypoxia (<0.1% O₂) for 24 h. Following treatment, cells were either immediately trypsinized and counted with a Beckman Coulter Z2 Particle Counter (Beckman Coulter, Brea, CA), or allowed to grow in drug free medium under normoxia. Subsequently, cells were trypsinized and counted every other day for up to 12 additional days.

3.2.8 Cell cycle profile analysis

FaDu cells treated with drug (IAZA or FAZA, 100 µM) or vehicle control (0.02% DMSO) under normoxia or hypoxia (<0.1% O₂) for 24 h were either immediately trypsinized after treatment, or allowed to recover in drug free medium under normoxia for up to 24 h. Trypsinized cells were counted and 1x10⁶ cells were fixed in 70% ethanol, washed with cold phosphate-buffered saline (PBS) and incubated with 100 µg/ml RNase A (1007885, QIAGEN,

Hilden, Germany) for 10 min at room temperature (~22 °C). Cells were then washed and mixed with propidium iodide (PI; P4170, Sigma-Aldrich) to a final concentration of 50 µg/ml to stain their DNA content. Processed samples were analyzed using a BD FACSCanto II flow cytometer (BD Biosciences, Franklin Lakes, NJ) to detect PI fluorescence upon gating for forward and side scatter; singlet population was chosen by gating for PI-width and PI-area.

3.2.9 Click-iT EdU incorporation assay

To assess the effects of IAZA and FAZA on DNA synthesis, FaDu cells grown on sterilized glass coverslips were incubated with drug (100 µM) or vehicle control (0.02% DMSO) in medium containing 10 µM 5-ethynyl-2'-deoxyuridine (EdU, C10339, Invitrogen, Waltham, MA) for 24 h under normoxia or hypoxia (<0.1% O₂), followed by fixation in 2% paraformaldehyde (PFA, P6148, Sigma-Aldrich). To assess the capacity of drug-treated cells to re-initiate DNA synthesis, FaDu cells treated with IAZA or FAZA (or 0.02% DMSO) for 24 h under normoxia and hypoxia (<0.1% O₂) were allowed to recover for 24 h in drug-free medium containing 10 µM EdU, and then fixed in 2% PFA. Fixed cells were processed for “click” staining according to the manufacturer’s protocol (C10339, Invitrogen); nuclei were counterstained with Hoechst (Life Technologies, Carlsbad, CA). Coverslips were mounted on glass slides (Fluoroshield Mounting Medium, Abcam, Cambridge, UK) and imaged with a Plan-Apochromat 40X/1.3 Oil DIC lens on a ZEISS 710 confocal microscope using Zen 2011 software (Carl Zeiss, Jena Germany).

3.2.10 DNA fibre assay

The effect of drugs on DNA replication was measured by a DNA fibre assay as previously described with some modifications (Locke, Hossain et al. 2021). Briefly, cells were incubated with 5-iodo-2'-deoxyuridine (33 µM; IdU; I7756, Sigma-Aldrich) for 30 min followed by several PBS washes. Afterwards, cells were incubated with 500 µM drug (or 0.02% DMSO) under normoxia or hypoxia (<0.1% O₂) for 3 h. When the incubation was over, drug containing medium was removed, cells were washed several times with PBS, and were allowed to recover for 30 min in fresh medium containing 5-chloro-2'-deoxyuridine (250 µM; CldU; C6891, Sigma-Aldrich). Following incubation with CldU, cells were trypsinized and harvested through centrifugation. The cell pellet was then resuspended in PBS at 100,000 cells/ml; 2 µL of the cell

suspension was spotted on a positive charged glass slide. The cell suspension drop was mixed with 10 μ l of DNA fiber lysis buffer (200 mM Tris-HCl pH 7.5, 50 mM EDTA, 0.5% SDS) and DNA strands were allowed to migrate down the slides by tilting the slides at a 15° angle. The resulting DNA spreads were then air dried for 40 min followed by a fixation in 3:1 methanol/acetic acid for 5 min. A 30 min incubation with 2.5 M hydrochloric acid was used to denature DNA fibers, then slides were washed with PBS and blocked for 1 h in 5% bovine serum albumin (BSA; A9647, Sigma-Aldrich) in PBS-0.1% Tween-20. DNA immunostaining was performed with a rat anti-BrdU/CldU antibody to detect CldU (1:200 dilution; 347580, BD Biosciences) and a mouse anti-BrdU/IdU antibody to detect IdU (1:200 dilution; ab6326, Abcam) in a humidified chamber for 1 h at room temperature. Secondary antibodies used include anti-rat-Alexa Fluor 488 (1:200 dilution; A-21470, Thermo Fisher Scientific) and goat anti-mouse-Alexa Fluor 546 (1:200 dilution; A-21123, Thermo Fisher Scientific). Slides were mounted in ProLong™ Gold Antifade Mountant (P10144, Thermo Fisher Scientific), and imaged with an upright fluorescence microscope (ZEISS AxioImager.Z1). More than 150 fibers were analyzed for each data set.

3.2.11 Trapped in agarose DNA click staining (TARDCS)

To assess direct drug-DNA binding, we modified a previously described trapped in agarose DNA immunostaining (TARDIS) assay (Cowell, Tilby et al. 2011). Instead of antibody based detection, our method utilizes click chemistry by using a click chemistry compatible 2-NI, N₃-AZA (**Fig. 1C**) (Rashed, Stoica et al. 2021). Briefly, FaDu cells treated with 100 μ M N₃-AZA (or 0.02% DMSO) under normoxia or hypoxia (<0.1% O₂) for 24 h were harvested by trypsinization and pelleted by centrifugation. The cell pellet was then mixed with 1% low melting point agarose and spread on glass slides pre-coated with 1% normal agarose. Slides were processed as described in reference (Cowell, Tilby et al. 2011) by placing them in lysis buffer for 30 min followed by a 30 min incubation in 1 M NaCl. Slides were then air dried, select slides were treated with either 1000 U DNase I (04536282001, Roche, Basel, Switzerland) or 0.2 mg proteinase K (19131, QIAGEN). Afterwards, slides were blocked in 1% BSA for 20 min and click staining was performed with an Alexa Fluor 594 alkyne (A10275, 1:5000 dilution, Molecular Probes, Eugene, OR) using a Click-iT™ Cell Reaction Buffer Kit (C10269, Thermo Fisher Scientific); DNA was counterstained with Hoechst. Slides were

imaged with a Plan-Apochromat 20X/ 0.8 M27 lens on a Zeiss 710 confocal microscope using Zen 2011 software.

3.2.12 Immunocytochemistry

FaDu cells grown on sterilized glass coverslips were treated with vehicle control or drug (100 μ M) for 24 h under normoxia or hypoxia (<0.1% O₂), after which cells were fixed in 2% PFA (or methanol), blocked in 1% BSA for 20 min, and probed with the following primary antibodies: anti-phospho-histone H2A.X (Ser139) (γ -H2AX; 1:5000 dilution, 05-636, Millipore Sigma, Burlington, MA), anti-replication protein A2 (RPA; 1:2500 dilution, ab2175, Abcam) or anti-proliferating cell nuclear antigen (PCNA; 1:250 dilution, ab29, Abcam). Secondary antibodies used include Alexa Fluor 488 conjugated anti-rabbit IgG (1:1000 dilution; Molecular Probes) and Alexa Fluor 594 conjugated anti-mouse IgG (1:250 to 1:1000 dilution; Molecular Probes). Cells processed for RPA were first incubated in extraction buffer (25 mM HEPES, 300 mM sucrose, 50 mM NaCl, 1 mM EDTA, 3 mM MgCl₂, 0.5% NP-40, pH 7.9) for 3 min prior to fixation in PFA. For chromatin bound PCNA detection, cells underwent a detergent extraction step in ice-cold hypotonic buffer (10 mM HEPES-KOH at pH 7.9, 10 mM KCl, 1.5 mM MgCl₂, 0.5 mM DTT, 0.1% Triton) for 10 min before they were fixed in cold methanol. Irradiated (5 Gy) cells and cells treated with 5 mM HU (24 h) served as positive controls for γ -H2AX and RPA staining, respectively. Nuclei were counterstained with Hoechst and coverslips were mounted on glass slides. Images were obtained with a Plan-Apochromat 40X/1.3 Oil DIC lens on a Zeiss 710 confocal microscope using Zen 2011 software.

3.2.13 Alkaline comet assay

FaDu cells were treated with drugs (100 μ M) or vehicle control for 24 h under normoxia and hypoxia (<0.1% O₂); cells exposed to 5 Gy ionizing radiation were used as positive controls. Immediately after irradiation, cells were harvested in PBS by scraping, mixed with low melting point agarose, and spread on comet slides. After the gel solidified, slides were put in lysis solution (4250-050-01, R&D Systems, Minneapolis, MN) for 1 h, and then in unwinding solution (200 mM NaOH, 2.5 mM EDTA) for 1 h at 4 °C. Slides were then placed in alkaline electrophoresis buffer (200 mM NaOH, 1 mM EDTA), and current was applied at 21 V for 45 min. Afterwards, slides were washed twice in distilled H₂O, fixed with 70% ethanol for 5 min,

and air dried before staining DNA with ethidium bromide (E7637, Sigma-Aldrich). Slides were imaged with an upright fluorescence microscope (ZEISS AxioImager.Z1), and comets were analyzed using CometScore™ software (TriTek Corp., Sumerduck, VA).

3.2.14 Assessing hydrogen peroxide (H₂O₂) levels

The ROS-Glo™ H₂O₂ assay kit (G8820, Promega, Madison, WI) was used to analyze the levels of H₂O₂ as a readout of the reactive oxygen species (ROS) generated in response to drug treatment. Briefly, FaDu cells seeded in 96-well plates were treated with IAZA (100 μM and 150 μM), FAZA (100 μM and 350 μM) or 0.02% DMSO for 72 h. Cells were then taken out of the hypoxia chamber and the H₂O₂ substrate was added, which generates a luciferin precursor upon reaction with H₂O₂. Cells were incubated with the substrate for 6 h, either under normal O₂ conditions (reoxygenation) or placed back in the hypoxia chamber. Afterwards, 50 μl of medium from each well was mixed with equal volume of ROS-Glo detection solution in a separate plate, incubated for 20 min, and the luciferin luminescence (which is directly proportional to the amount of H₂O₂ level present in the reaction well) was recorded using an OPTIMA microplate reader. Cells in the original sample plate were assayed for viability using crystal violet staining. Luminescence data were normalized by the cell viability results.

3.2.15 Immunoblotting

FaDu cells treated with 100 μM IAZA or FAZA (or 0.02% DMSO) for 24 h under normoxia and hypoxia (<0.1% O₂) were harvested in RIPA buffer supplemented with protease inhibitor. 50 μg of crude protein extracts were separated on a 10% polyacrylamide gel for 55-70 min at 180 V, transferred onto nitrocellulose membranes and blocked for 1 h with 5% milk (in PBS, 0.1% Triton-100). Total protein was visualized using Revert™ 700 Total Protein Stain (926-11016, LI-COR, Lincoln, NE). Membranes were probed with the following primary antibodies: anti-hypoxia inducible factor 1 alpha (1:2000 dilution; NB100-449, Novus Biologicals, Littleton, CO), anti-glyceraldehyde-3-phosphate dehydrogenase (1:1000 dilution, ab9482, Abcam), anti-glutathione S-transferase P (1:2000 dilution, ABS1650, Millipore Sigma), anti-cyclin E1 (1:1000 dilution, ab133266, Abcam) and anti-beta tubulin (1:4000 dilution; ab6046, Abcam). Secondary antibodies used include goat anti-rabbit-IgG-HRP (1:2000 dilution; Jackson ImmunoResearch, West Grove, PA), IR-800 conjugated goat anti-mouse IgG (1:2000

dilution, 926-80010, LI-COR) and IR-800 conjugated goat anti-rabbit IgG (1:2000 dilution; 926-32211, LI-COR). Membranes were then processed with West Pico PLUS chemiluminescent substrate (Thermo Fisher Scientific) and scanned with an Odyssey Fc imager (LI-COR).

3.2.16 Glyceraldehyde-3-phosphate dehydrogenase (GAPDH) activity assay

FaDu cells treated with IAZA (150 μ M), FAZA (350 μ M) or vehicle control (0.02% DMSO) for 24 h under normoxia or hypoxia (<0.1% O₂) were harvested by trypsinization and pelleted by centrifugation. Cellular GAPDH enzyme activity was quantified as described earlier using a GAPDH activity assay kit (ab204732, Abcam) (Rashed, Stoica et al. 2021).

3.2.17 Glutathione S-transferase (GST) assay

Total cellular GST enzymatic activity was measured using a GST assay kit (CS0410, Sigma-Aldrich). FaDu cells treated with IAZA (100 μ M and 150 μ M), FAZA (100 μ M and 350 μ M) or vehicle control (0.02% DMSO) for 24 h under normoxia or hypoxia (<0.1% O₂) were processed to quantify total GST activity as previously described (Rashed, Stoica et al. 2021).

3.2.18 Total glutathione (GSH) quantification

Total cellular GSH levels were measured with DTNB [5,5'-dithio-*bis*-2-(nitrobenzoic acid)] that reacts with GSH and produces yellow colored TNB (5-thio-2-nitrobenzoic acid); the rate of TNB production is directly proportional to the concentration of GSH in the sample (703002, Cayman Chemical, Ann Arbor, MI). Briefly, FaDu cells treated with IAZA and FAZA at indicated concentrations for 24 h under normoxia or hypoxia (<0.1%O₂) were harvested by scraping, counted, and pelleted by centrifugation. The cell pellet was dissolved in PBS containing 2 mM EDTA (1x10⁶ cells in 100 μ l), sonicated and centrifuged again. The supernatant was deproteinated using metaphosphoric acid (239275, Sigma-Aldrich) and mixed with 4 M triethanolamine (T58300, Sigma-Aldrich) as per the manufacturer's guidelines. The resultant samples were used to perform the total glutathione assay in a 96-well plate. A standard curve was generated using the GSH standard provided with the assay kit, and concentrations of GSH in samples were determined from the standard curve.

3.2.19 *In vivo* toxicity assay

Animal experiments were carried out according to the protocols approved by the Cross Cancer Institute Animal Care Committee (protocol # AC18239) in accord with the Canadian Council on Animal Care guidelines. To establish the toxicity profile of intraperitoneal (i.p.) administered IAZA, NOD/SCID/IL2R mice were injected with vehicle control (15% DMSO v/v in 150 µl sterile water) or with 3 different IAZA doses (200, 400 or 600 mg/kg body weight, b.w.). Mice were monitored for weight loss, responsiveness and body conditioning for 14 days, after which, animals were euthanized. During the post-mortem examination, blood was collected via heart puncture, and processed for blood chemistry (samples analyzed at IDEXX laboratory, Edmonton, AB). Additionally, a set of organs (brain, heart, kidney, liver and lung) was removed from each animal for pathological analysis. These were prepared by fixation in 10% neutral buffered formalin for a minimum of 24 h. Following fixation, tissues were trimmed with a scalpel to a thickness of 2-3 mm and a section of each organ was placed in a tissue cassette. Tissues in cassettes were processed into paraffin, embedded in a paraffin block, sectioned on a microtome to a thickness of 5 microns, placed on a microscope slide and stained with hematoxylin and eosin stain, all procedures following standard histology techniques. Slides were examined by a board-certified veterinary pathologist using a Nikon Eclipse 80i microscope and observations recorded for each section. Photomicrographs were taken using a Moticam 10 digital camera.

3.2.20 Tumour growth delay assay and tissue staining

For tumour growth control experiments, NU/NU nude mice were injected with $\sim 6 \times 10^6$ FaDu cells subcutaneously on the upper right flank. Tumours were measured with a Vernier caliper, and volume was determined by the formula: $(\pi/6)ab^2$, where a is the longest and b is the perpendicular shorter tumour axis. Once the tumours reached a volume between ~ 200 - 300 mm^3 , mice were injected i.p. with either vehicle control (up to 15% DMSO v/v in 150 µl sterile water) or IAZA (400 mg/kg b.w. in 150 µl DMSO: sterile water). Mice were monitored daily following treatment, and were sacrificed when tumours reached a volume of $\sim 1500 \text{ mm}^3$. 2 h prior to sacrifice, mice were injected i.p. with N₃-AZA (60 mg/kg b.w.). After euthanization, tumours were excised, flash frozen in optimal cutting temperature compound (O.C.T., 4585, Fisher

Scientific, Waltham, MA), and N₃-AZA click chemistry was performed on central sagittal tumour sections to determine endpoint hypoxia levels as described previously (Rashed, Stoica et al. 2021). Briefly, acetone-fixed frozen tumour sections were blocked in PBS with 1% BSA, incubated with primary antibody for small vessel endothelium (rat anti-CD31, 1:50 dilution; 550274, BD Pharmingen) for 2 h, followed by incubation with the secondary antibody (Alexa Fluor 647 goat anti-rat IgG, 1:1000 dilution; Molecular Probes) mixed with 4',6-diamidino-2-phenylindole (DAPI). Afterwards, tumour sections were incubated with the Click-IT reaction cocktail (Thermo Fisher Scientific) for 30 min, which was made up according to the manufacturer's directions using a 1:5000 dilution of the 2 mg/ml Alexafluor 555-conjugated alkyne stock (A20013, Molecular Probes). After washing, sections were mounted using Mowiol 4-88 mounting media (Millipore, Etobicoke, ON), and images were obtained by tile scan with a Leica SP8 STED microscope (Leica Microsystems GmbH, Wetzlar, Germany). An estimate of hypoxic tumour fraction was calculated with MATLAB R2018b (MATLAB and Image Processing Toolbox Release 2018b, The MathWorks, Inc., Natick, Massachusetts, United States) as described before (Rashed, Stoica et al. 2021). Images were converted to binary by applying a manual threshold (determined from the background tissue staining) to the N₃-AZA channel, while the Otsu threshold was applied to DAPI channel (Otsu 1979). The hypoxic fraction estimate was calculated using the following formula:

$$\text{Hypoxic fraction (HF)} = \frac{\text{Area of pixels stained with N}_3\text{-AZA}}{\text{Area of pixels stained with DAPI}} * 100$$

3.2.21 Data processing and statistics

Adobe Photoshop (Adobe Inc., San Jose, CA) was used to adjust for brightness and contrast, to add scale bars, and for rearrangement and labelling in immunoblots and microscopic images. Gel scans were quantified using Image Studio lite v5.2 (LI-COR Biosciences, Lincoln, NE); protein band values were divided by the total protein stain (or loading control) for respective lanes and normalized to vehicle-treated normoxia controls. EdU click staining, γ -H2AX, RPA and PCNA stained microscopic images were processed with IMARIS software (Bitplane, Zürich, Switzerland) to quantify click/antibody staining intensity within the nucleus using

Hoechst staining as a nuclear mask. Histograms were generated with intervals of staining intensity on the x axis and the percentage of cells with intensity levels that fall within that range on the y axis. For γ -H2AX data analysis, an arbitrary threshold was chosen such that the γ -H2AX staining intensity of ~95% of cells in the vehicle-treated normoxic sample fell below this threshold. The percentage of cells above this threshold was considered positive for γ -H2AX. To identify chromatin-bound PCNA positive cells, PCNA staining in mitotic cells was used as threshold for background staining. DNA fibre tract lengths were measured with MetaMorph software (Molecular Devices, San Jose, CA) to convert the pixel values to micrometers and plotted as scatterplots. Graph generation and statistical analysis were performed using GraphPad Prism V7 (GraphPad Software, La Jolla, CA). IC₅₀ values from the crystal violet staining and colony formation assays were generated using non-linear regression analysis. Graphs display the mean with standard error of the mean (S.E.M.). The 2-tailed unpaired t-test was used for statistical analysis, with $p < 0.05$ considered statistically significant. GAPDH activity was analyzed using Dunnett's 2-way ANOVA. Asterisks depict statistically significant differences: ns (not significant), * ($P \leq 0.05$), ** ($P \leq 0.01$), *** ($P < 0.001$), **** ($P < 0.0001$).

3.3 Results

3.3.1 IAZA and FAZA selectively affect viability and clonogenicity of O₂ starved cells.

Experiments were carried out primarily with a human head and neck squamous cell carcinoma cell line, FaDu. Additional cell lines used for validation purposes included A549 (human lung epithelial carcinoma), PC3 (human prostate carcinoma) and HCT116 (human colorectal carcinoma). Sensitivity of FaDu cells to IAZA and FAZA treatment under different O₂ levels was determined by crystal violet staining (**Fig. 3.1D** and **E**) and clonogenic survival assays (**Fig. 3.1G** and **H**); effects of O₂ levels on FaDu cell viability and clonogenicity are shown in **Fig. 3.1F** and **I**, respectively. Hypoxic cells displayed considerably greater sensitivity to both compounds than normoxic cells, with IAZA showing a more potent response than FAZA at the same concentrations. In the colony formation assay, IAZA and FAZA showed the strongest effects on cells cultured under $< 0.1\%$ O₂, with IC₅₀ values > 22 -fold (IAZA) or > 15 -fold (FAZA) lower than that obtained under normoxia (**Fig. 3.1F** and **G**). A similar trend was seen in other

cell lines used in this study as well, with hypoxic (0.1% O₂) cells displaying ~4-12 fold (IAZA) or ~7-12 fold (FAZA) more sensitivity to the drugs than their normoxic counterparts (**Suppl. Fig. 3.1**), regardless of their p53 status (FaDu and PC3 express mutated p53, while A549 and HCT116 have wild-type p53). In subsequent *in vitro* experiments assessing their therapeutic efficacy, a drug concentration of 100 μM was used, except for the DNA fibre assay (500 μM), ROS quantification (hypoxic IC₅₀ concentrations) and enzymatic assays (hypoxic IC₅₀ concentrations).

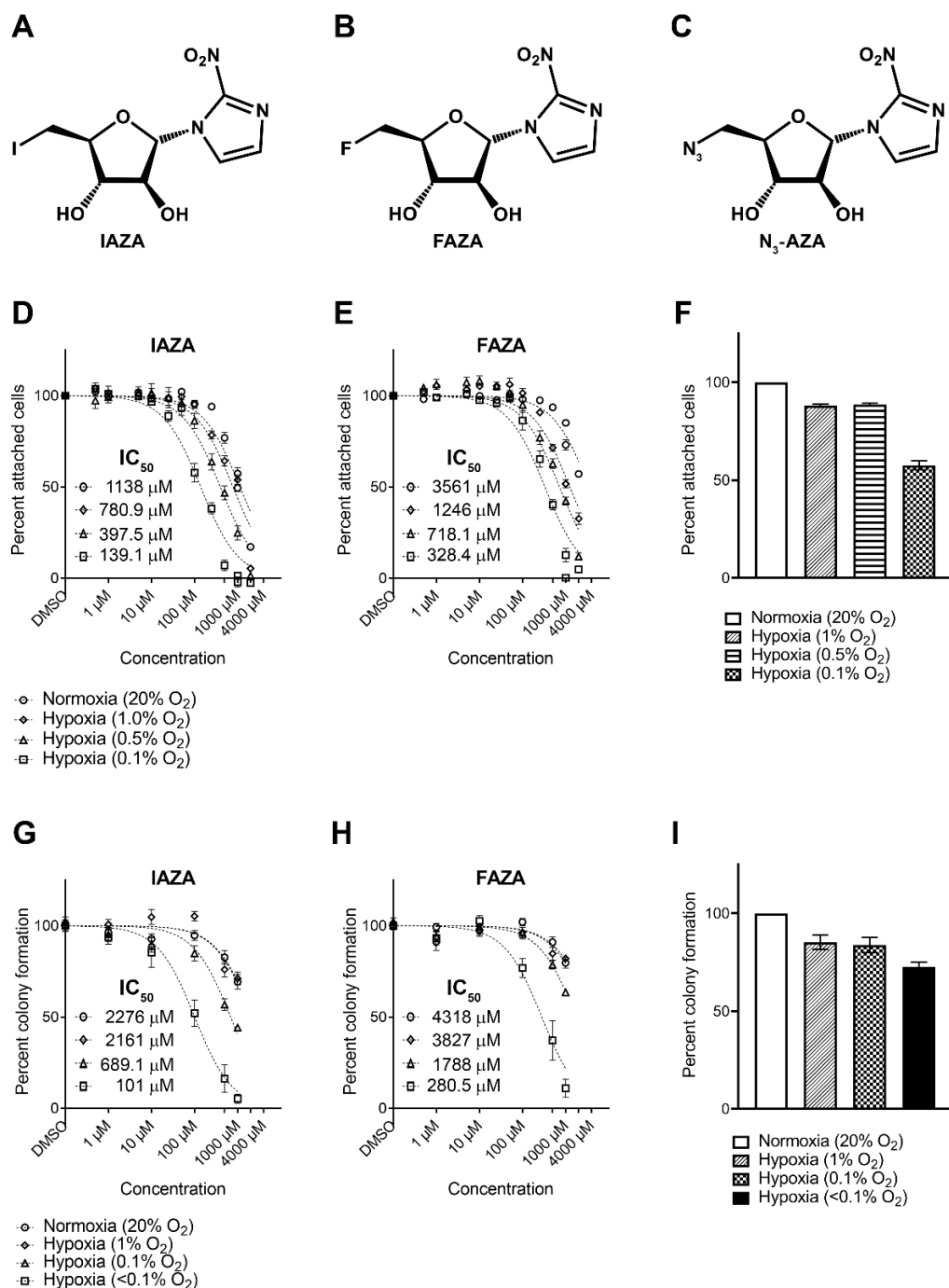


Figure 3.1 Hypoxic cells show preferential sensitivity towards IAZA and FAZA treatment.

Chemical formula for IAZA (A) FAZA (B) and N₃-AZA (C). Crystal violet staining assays were performed in FaDu cells under different O₂ levels (20%, 1%, 0.5% or 0.1% O₂). Cells were more sensitive to drug treatment under low O₂ levels (D and E). Colony formation assays with FaDu cells measured clonogenicity in response to drug treatment under normoxia (20% O₂) or different levels of hypoxia (1%, 0.1% or <0.1% O₂). Cells showed the most sensitivity to treatment when cultured under <0.1% O₂ (G and H). IAZA was more toxic than FAZA at the same concentrations. Effects of different levels of O₂ on cell viability (F) and clonogenicity (I) are shown. Data represent mean ± S.E.M. from at least three independent experiments.

3.3.2 IAZA and FAZA treatment under hypoxia do not increase cell death or senescence, but affect cell proliferation.

While standard cytotoxicity assays provide valuable insights into cells' sensitivity towards a particular treatment, they do not necessarily capture treatment-induced cellular fate (Damiani, Solorio et al. 2019). For example, the CVS assay measures relative attached (hence viable) cells; a decrease in which may result from either increased cell death or from induction of senescence or cytostasis (Feoktistova, Geserick et al. 2016). Similarly, recent observations with clonogenic survival assays identified certain dormant cell populations that can remain viable and metabolically active without forming macroscopic colonies (Mirzayans, Andrais et al. 2018). Hence, additional experiments are required to properly characterize cellular fate induced by a treatment. Morphologically, IAZA- and FAZA-treated hypoxic cells appeared more compact and stacked together (**Fig. 3.2A**). To determine if these 2-NI compounds induced cell death (apoptosis or necrosis) under hypoxia, FaDu cells treated with drugs (or vehicle control) were stained with annexin V and PI, and analyzed by flow cytometry. No significant increase in apoptotic or necrotic populations were observed in drug-treated hypoxic samples; most cells stained negative for annexin V and PI (alive) (**Fig. 3.2B-E**). Next, we checked if hypoxic cells underwent irreversible growth arrest (senescence) when treated with IAZA or FAZA. Senescent cells display increased lysosomal biogenesis, resulting in a characteristic beta-galactosidase (β -gal) activity detectable at pH 6.0 (termed senescence-associated beta-galactosidase' activity), which can be used to distinguish senescent cells within a population (Debacq-Chainiaux, Erusalimsky et al. 2009). Staining FaDu cells treated with IAZA and FAZA for beta-galactosidase activity revealed no difference between vehicle and drug-treated hypoxic cells, implying that these drugs do not induce senescence (**Fig. 3.2F**). Recently, 2-NIs (at millimolar range) were reported to induce ferroptosis in hypoxic glioma stem cells (Koike, Kota et al. 2020). Therefore, induction of ferroptosis was assessed by treating cells with IAZA/FAZA in the presence or absence of Ferrostatin-1 (a ferroptosis inhibitor), which protects cells from ferroptosis inducing agents. Interestingly, addition of Ferrostatin-1 did not improve viability of IAZA/FAZA-treated hypoxic cells, thus ruling out ferroptosis as a consequence of drug treatment (**Fig. 3.2G and H**). Since no induction of cell death or senescence was observed in IAZA- or FAZA-treated hypoxic cells, we next monitored changes in cell proliferation rates in response to drug treatment, and after fixed periods of recovery (and reoxygenation). Hypoxic

incubation with IAZA or FAZA (100 μM) decreased total cell counts when compared to vehicle-treated hypoxic cells; no effects were seen under normoxia (**Fig. 3.2I and J**). Drug-induced inhibitory effects on hypoxic/reoxygenated cell growth were not immediately alleviated by drug removal and reoxygenation, which was evident from the sustained slower proliferation rates during the recovery period. Since FAZA was used at a concentration ~ 3 times lower than its hypoxic IC_{50} value, it generated a milder response in comparison to IAZA.

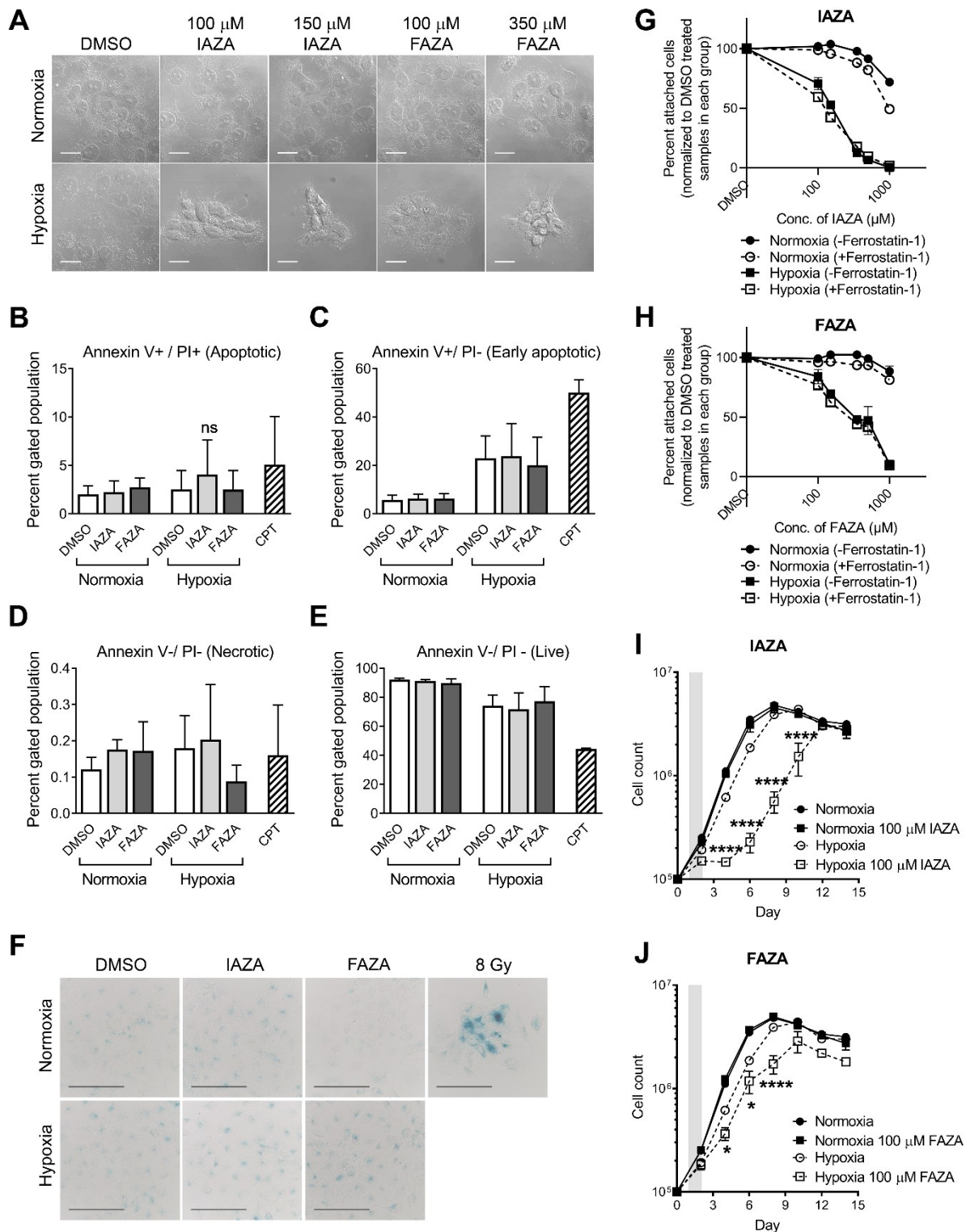


Figure 3.2 IAZA and FAZA treatment do not induce apoptosis, senescence or ferroptosis under hypoxia, but reduce proliferation in hypoxic/reoxygenated cells.

IAZA and FAZA treatment induced morphological changes in a dose dependent manner, but only under hypoxia (A). Compared to vehicle control, hypoxic/reoxygenated drug-treated cells did not show statistically significant change in apoptotic (B), early apoptotic (C), necrotic (D) or live population (E). IAZA- and FAZA-treated hypoxic/reoxygenated cells stained poorly for beta-galactosidase activity (F). Addition of Ferrostatin-1 did not change the toxicity profile of IAZA (G) or FAZA (H). IAZA- or FAZA-treated hypoxic/reoxygenated cells show slower proliferation rates (I and J); shaded regions show duration of drug exposure. Data represent mean \pm S.E.M; scale bar = 20 μ m (A) and 100 μ m (F).

3.3.3 Hypoxic treatment with IAZA or FAZA slows down cell cycle progression, represses DNA synthesis, and induces replication stress.

Given that IAZA and FAZA treatment negatively affected cell proliferation under hypoxia, their impacts on cell cycle distribution were analyzed using PI-flow cytometry. IAZA- and FAZA-treated hypoxic cells showed a significant increase in the S phase population. Time-course analysis of cell cycle progression revealed that drug-treated hypoxic cells progressed through S phase at a slower pace, even after treatment had ended (**Fig. 3.3A**). A significant increase in the chromatin bound PCNA-positive population (**Fig. 3.3B-C**) was seen in hypoxic cells treated with IAZA/FAZA, which is reflective of late G1 and early S phase cells (Sasaki, Kurose et al. 1993). Moreover, when compared to vehicle-treated hypoxic cells, IAZA- and FAZA-treated hypoxic cells showed higher cyclin E1 levels (**Suppl. Fig. 3.2A-B**), a cell cycle protein upregulated during G1/S transition (Ohtsubo, Theodoras et al. 1995). To identify why cells were stalling at S phase in response to 2-NI treatment under hypoxia, DNA replication efficiency was analyzed by monitoring the cellular uptake of EdU. EdU is a nucleoside analogue that gets incorporated into cellular DNA during replication; prolonged incubation with EdU can thereby be used to distinguish between replication proficient and replication deficient cells. Hypoxic cells treated with IAZA or FAZA (100 μ M) showed reduced EdU uptake, which is indicative of compromised DNA synthesis (**Fig. 3.3D**). Quantification of cellular EdU staining, presented as histograms (**Fig. 3.3E**), revealed that 24 h hypoxic exposure by itself affected EdU uptake in cells; addition of IAZA and FAZA under hypoxia further slowed down DNA replication rates (evident from a significant increase in cell fraction with low EdU). Moreover, replication was still compromised in hypoxic drug-treated cells that were allowed to reoxygenate and recover in drug-free medium (containing EdU) (**Suppl. Fig. 3.2C**).

Slower rates of DNA replication are known to cause replication stress, which can be determined by staining cells for replication protein A (RPA) (Zeman and Cimprich 2014). RPA binds to single-stranded DNA generated as an intermediate from stalled replication forks, or during recombination-mediated repair of DNA damage (Maréchal and Zou 2015). Chromatin-bound RPA resists detergent extraction that removes the nucleoplasmic and cytoplasmic proteins. Higher chromatin retention of RPA was seen in drug-treated hypoxic cells, which is suggestive of increased ssDNA. However, the effect was not as severe as seen in cells treated with

hydroxyurea (5 mM), a potent DNA replication inhibitor (**Suppl. Fig. 3.2D** and **E**). In response to replication stress, the replication fork also undergoes fork reversal for maintaining genome stability, which can be assessed through the DNA fibre assay (Qiu, Jiang et al. 2021). Nucleolytic degradation following replication fork stalling was monitored by pulse-labeling cells with two different thymidine analogs (IdU and CldU), with a 3 h drug treatment (under normoxia or hypoxia) in between the two labelling steps (**Fig. 3.3F**). Shortening of the first tract serves as a readout of nascent fork degradation, which in term reflects induction of replication stress (Qiu, Jiang et al. 2021). Only forks characterized by contiguous IdU-CldU signals (and not on forks that have only the IdU label) were analyzed to ensure that the shortening phenotype is indeed due to nucleolytic degradation of stalled replication forks, and not because of premature termination events (Vindigni and Lopes 2017). Quantification of DNA fibres revealed a significant decrease in IdU track lengths (**Fig. 3.3G**). CldU track lengths were also significantly shortened, which points towards an inability of drug-treated hypoxic cells to restart replication after reoxygenation (**Fig. 3.3H**). Taken together, these observations suggest that IAZA and FAZA, at concentrations used in these experiments, induced replication stress under hypoxia by compromising DNA synthesis and consequently slowed down cell cycle progression.

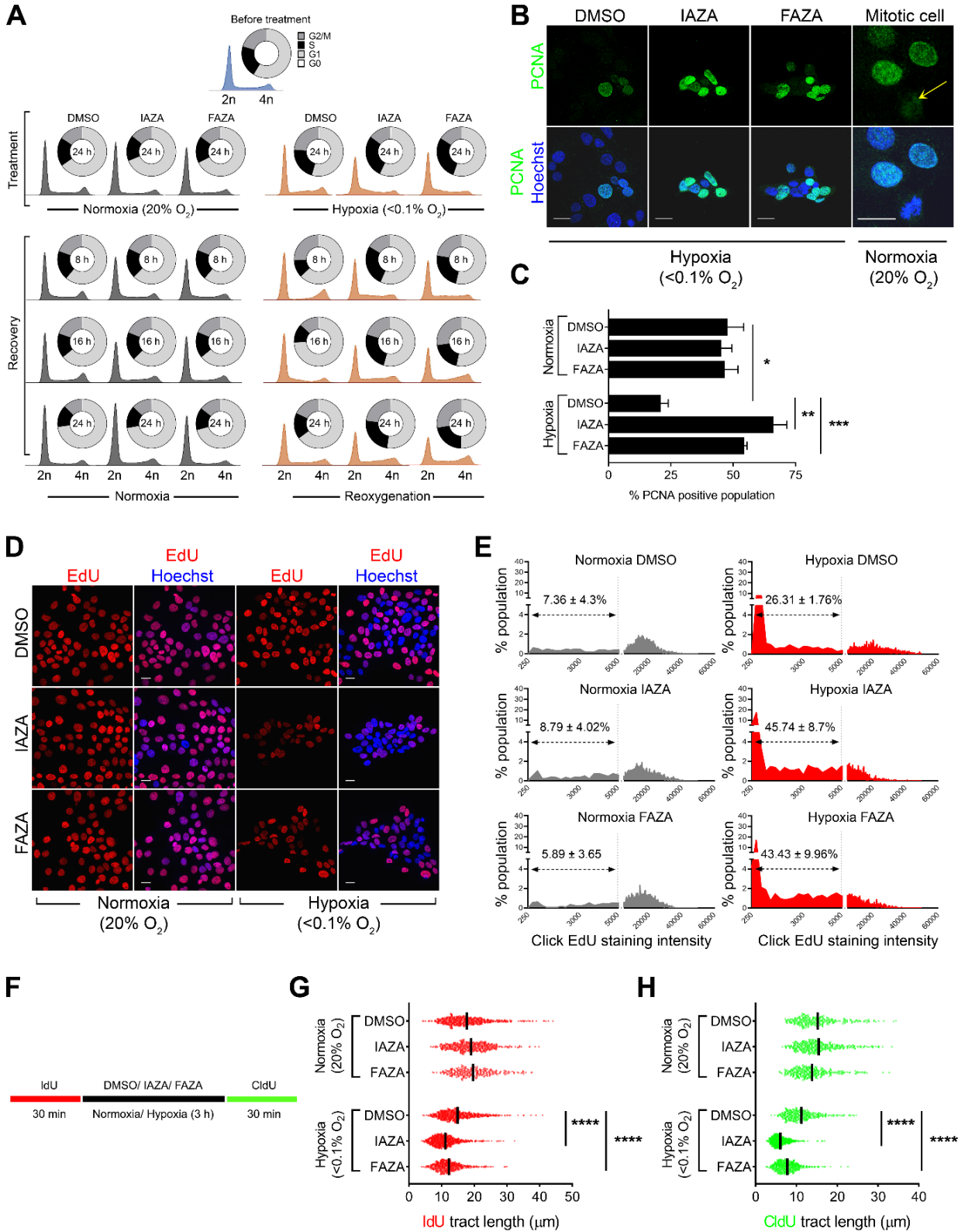


Figure 3.3 Hypoxic cells treated with IAZA and FAZA show slower S phase progression, increased chromatin-bound PCNA staining, reduced DNA synthesis, and replication stress.

Flow cytometric analysis for cell cycle phases showed an increase in S phase population in IAZA- and FAZA-treated hypoxic cells. These cells continuously showed slower S phase progression, even when drugs were removed, and hypoxic cells were allowed to reoxygenate (A). Hypoxic cells, when treated with IAZA and FAZA, showed increased chromatin bound PCNA staining, which is significantly higher than vehicle-treated hypoxic cells (B and C); yellow arrow shows mitotic cell (B). Hypoxic cells treated with IAZA and FAZA displayed reduced EdU incorporation (D). Intensity of EdU click stained micrographs was quantified and plotted as intensity versus %population histograms. Hypoxic exposure by itself increased cell population with low EdU staining; incubation with IAZA and FAZA under hypoxia further increased “low EdU stained” cell fractions (E). Experimental setup for DNA fibre assay (F). IAZA- and FAZA-treated cells showed nascent fork degradation (G) and diminished ability to restart replication (H) in the DNA fibre assay. Representative micrographs are shown; scale bar = 20 μ m (B and D). Quantification shows mean \pm S.E.M. from three independent experiments.

3.3.4 IAZA- and FAZA-treated hypoxic cells show higher γ -H2AX signal, but not a corresponding increase in comet tail moment.

DNA has often been cited as a major site of attack by activated NIs (Zahoor, Lafleur et al. 1987). It has long been argued that activated NIs can directly bind to DNA and induce strand breaks (Silver, O'Neill et al. 1985, Silver, Mcneil et al. 1986). To characterize the nature of DNA-NI interaction, we performed a modified TARDIS assay using N₃-AZA, which is an azido analogue of IAZA and FAZA (**Fig. 3.1C**). N₃-AZA allows for direct detection of NI-adducts with fluorescent alkynes in a Cu(I)-catalyzed click chemistry reaction (Rashed, Stoica et al. 2021). Similar to the standard TARDIS assay, the modified assay (hereafter referred to as TARDIS) involves high salt lysis of agarose-embedded unfixed cells, and thereby only preserves covalent DNA-drug or DNA-protein interactions (Cowell, Tilby et al. 2011). DNase I and proteinase K treatments were incorporated into the assay to characterize the molecular targets of activated NIs. Addition of DNase I did not affect N₃-AZA click staining, whereas cells treated with proteinase K lost all of their click signal (**Fig 3.34A and B**). This suggests that almost all covalent binding of NIs under hypoxia was to proteins, and interaction between DNA and activated NIs, if any, was likely not covalent in nature.

To assess effects of NIs on DNA integrity, immunofluorescence staining for γ -H2AX was performed as a read-out of DNA damage (**Fig 3.4C**). A significant increase in the percentage of cells with high γ -H2AX signal was seen in IAZA- and FAZA-treated hypoxic cells (**Fig 3.4D and E**). Interestingly, when DNA damage was measured directly by single cell gel electrophoresis (alkaline comet assay), a dampened response was observed (**Fig. 3.4F**). Although a less pronounced (but significant) increase was seen with IAZA under hypoxia, FAZA treatment did not generate any difference when compared to vehicle-treated hypoxic cells. The poor association between γ -H2AX staining and alkaline comet data likely indicates a non-canonical phosphorylation of H2AX under hypoxia in response to NI treatment, which appears to be independent of DNA damage and can potentially be attributed to replication stress induced γ -H2AX formation.

Accumulation of ROS has previously been reported in response to NI treatment in glioma stem cells (Koike, Kota et al. 2020). To check if IAZA/FAZA treatment can induce ROS generation,

CVS assays were performed where cells were pre-incubated for 2 h with 3 mM NAC, a ROS scavenger, before drug treatment. The NAC concentration, chosen based on previous reports (Halasi, Wang et al. 2013), was validated experimentally (**Suppl. Fig. 3.3F**). Pre-treating cells with NAC did not improve viability in IAZA- and FAZA-treated hypoxic cells (**Suppl. Fig. 3.3A-B**), which implies that these compounds do not generate toxic levels of ROS. Additionally, cellular ROS levels were also directly measured with a commercial kit. The kit uses a substrate that reacts with H₂O₂ to generate a luciferin precursor, which upon reaction with a detector reagent, is converted to luciferin and produces luminescence. Since the substrate must be added at the end of the hypoxic incubation, plates needed to be taken out of the hypoxia chamber, which inevitably led to reoxygenation. ROS generation was measured in cells that (after adding the H₂O₂ substrate) were either placed back in the hypoxia chamber, or were subjected to reoxygenation for the entire duration of substrate incubation (**Suppl. Fig. 3.3C**). While drug-treated hypoxic cells did show a dose dependent increase in ROS levels when they were put back under hypoxia, the changes were not statistically significant (**Suppl. Fig. 3.3D-E**). Also, due to the nature of the assay, the contribution of the brief reoxygenation on the ROS levels cannot be ruled out. A more potent and significant increase in ROS levels was observed in drug-treated hypoxic cells that were allowed to reoxygenate for 6 h (**Fig 3.4G and H**). This implies that hypoxic incubation with IAZA and FAZA can promote a compromised redox state that facilitates enhanced ROS generation upon reoxygenation.

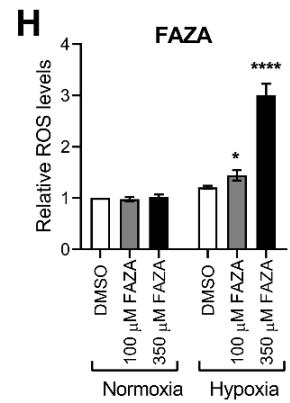
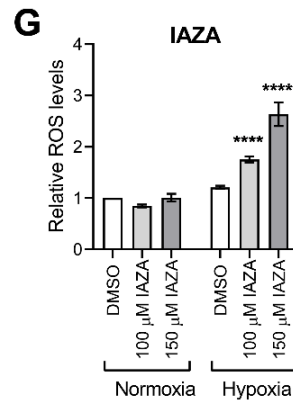
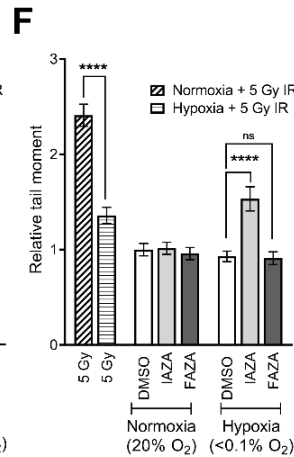
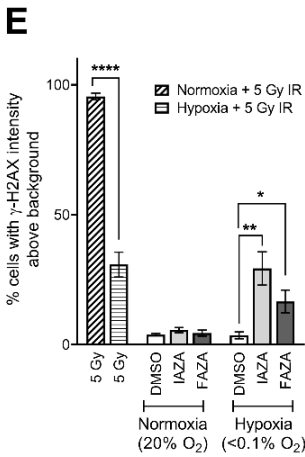
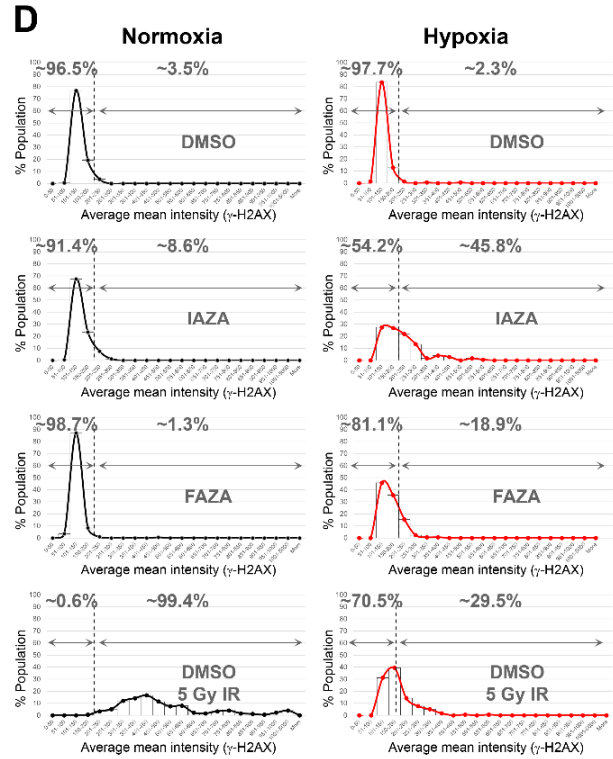
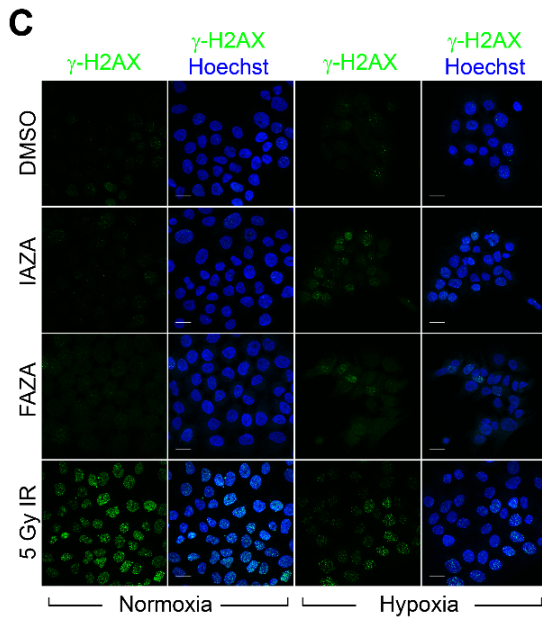
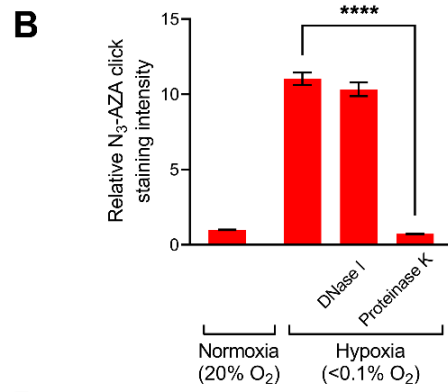
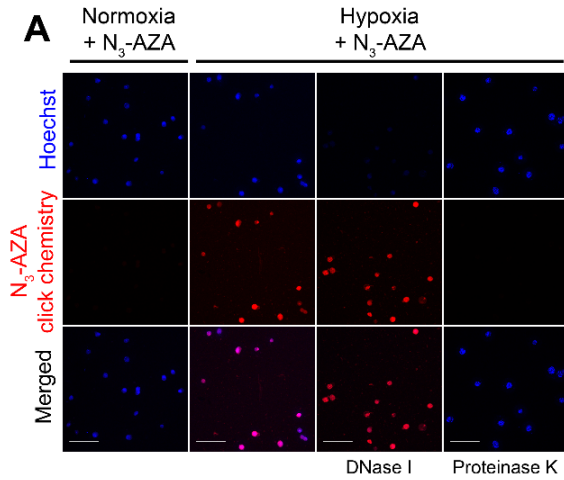


Figure 3.4 Analysis of DNA-NI binding characteristics and NI effects on DNA integrity under hypoxia.

Trapped in agarose DNA click staining (TARDCS) assay revealed proteins, rather than DNA, form covalent adducts with NIs (A). Quantification of N₃-AZA click staining in TARDCS assays (B). FaDu cells treated with DMSO, IAZA and FAZA under normoxia and hypoxia (<0.1% O₂) were processed for γ -H2AX immunostaining (C). Quantifications of γ -H2AX immunostaining data are represented as histograms (D). A statistically significant increase in percent population with γ -H2AX staining higher than background was seen in hypoxic drug-treated cells ©. Alkaline comet assay showed a significant increase in comet tail moment only in IAZA-treated hypoxic cells (F). A significant increase in H₂O₂ levels was found in IAZA (G) and FAZA (H) treated hypoxic cells upon reoxygenation. Representative micrographs are shown; scale bar = 100 μ m (A) and 20 μ m (C). Quantification shows mean \pm S.E.M. from at least three independent experiments.

3.3.5 IAZA and FAZA treatment do not affect target protein levels, but significantly reduce their enzymatic activity.

Activated NIs covalently bind to cellular proteins in hypoxic cells. Using N₃-AZA (a structural homolog of IAZA and FAZA), we have previously described a proteomic approach for identification of NI protein targets. A total of 62 proteins were reported to form adducts with NIs, including key enzymes in the glycolytic (GAPDH) and cellular detoxification (GST) pathways (Rashed, Stoica et al. 2021). The study also showed that N₃-AZA disrupted the catalytic activities of GAPDH and GST without affecting total protein levels. To check if IAZA- and FAZA-treated cells show similar trends, immunoblotting was performed with lysates harvested from IAZA or FAZA (and vehicle) treated normoxic and hypoxic cells. Successful induction of hypoxia was confirmed by probing for hypoxia inducible factor 1 alpha (HIF1A) protein. IAZA and FAZA treatment had no effect on GAPDH and GST protein levels, which is in agreement with our earlier findings (**Fig. 3.5A and B, Suppl. Fig. 3. 4**). The glycolytic enzyme GAPDH catalyzes the oxidation of glyceraldehyde-3-phosphate to 1, 3-bisphosphoglycerate, generating NADH, the amount of which serves as a direct readout of GAPDH activity. By assaying NADH generation in the reaction cocktail, we found that GAPDH activity was significantly reduced in IAZA- and FAZA-treated hypoxic cells (**Fig. 3.5C and D**). Total GST activity was measured using 1-chloro-2,4-dinitrobenzene (CDNB) that reacts with reduced glutathione and results in an increase in absorbance, which is directly proportional to the GST activity in the sample. IAZA and FAZA treatment dramatically reduced GST activity, but only under hypoxia. In comparison to the vehicle-treated hypoxic group, IAZA- and FAZA-treated hypoxic cells displayed ~90% and ~60% reduction in GST activity, respectively. GST appears to be more susceptible to IAZA/FAZA treatment than that of GAPDH, since a lower concentration of drug (100 μ M) was enough to severely inhibit its catalytic activity (**Fig. 3.5E and F**). This phenomenon cannot be attributed to exhaustion in the cellular glutathione pool [another potential cellular target of NIs (Masaki, Shimizu et al. 2016)] since total glutathione levels remained unaffected regardless of treatment (**Fig. 3.5G and H**).

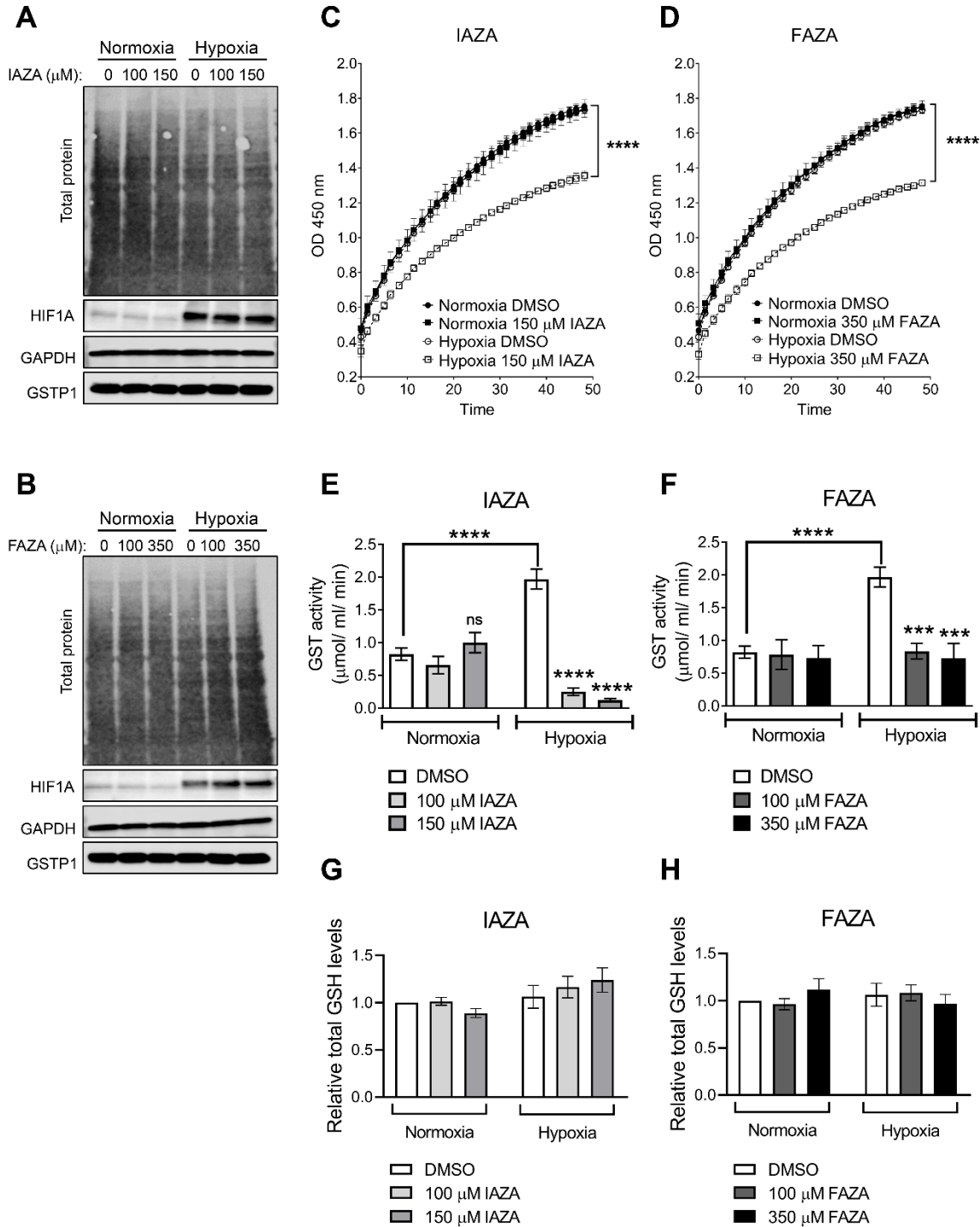


Figure 3.5 The effects of IAZA and FAZA treatment on target proteins and glutathione levels under hypoxia.

FaDu cells treated with IAZA (A) and FAZA (B) were processed for HIF1A, GAPDH and GST immunoblotting; no effects on protein levels were seen in response to drug treatment. Drug treatment significantly reduced GAPDH (C and D) and GST (E and F) enzymatic activities only under hypoxia. The cellular GSH pool remained unchanged in response to IAZA (G) and FAZA (H) treatment. Representative western blot images are shown. Mean \pm S.E.M. from three independent experiments are shown.

3.3.6 IAZA-treated mice showed an initial delay in tumour growth and a decrease in endpoint hypoxia levels.

Since IAZA showed a more robust response in *in vitro* experiments than FAZA, animal studies were carried out only with IAZA. To determine a safe dose for IAZA administration, a toxicity study in NOD/SCID/IL2R mice was performed with IAZA injected once intraperitoneally at 200 mg, 400 mg, or 600 mg per kg body weight. The drug was well tolerated, and no significant weight loss was observed in mice over 14 days post injection (**Fig. 3.6A**). Histopathological analysis showed no organ toxicity (**Fig. 3.6B**), and no significant differences were found in parameters analyzed for blood chemistry (**Suppl. Table 3.1**).

After establishing a toxicity profile, a tumour growth delay experiment was performed where NU/NU nude mice bearing subcutaneous FaDu tumours (~200-300 mm³) were injected with a single dose of 400 mg IAZA/kg b.w. Mice were monitored daily, tumour volume and body weight were recorded, and animals were sacrificed when the tumour volume reached ~1500 mm³. Although IAZA-treated mice showed an initial delay in tumour growth (**Fig. 3.6C**), the effects diminished over time and did not result in any significant increase in survival (**Fig. 3.6D**). Body weight and tumour volume of individual mice are shown in **Suppl. Fig. 3.5A-D**. Tumour sections were processed for endpoint hypoxia levels using N₃-AZA click chemistry, which was previously reported as a potent hypoxia marker comparable to pimodindazole immunostaining (Rashed, Stoica et al. 2021). A statistically significant decrease in hypoxia levels was seen in tumours from the IAZA-treated group compared to the vehicle-treated group (**Fig. 3.6E and F**).

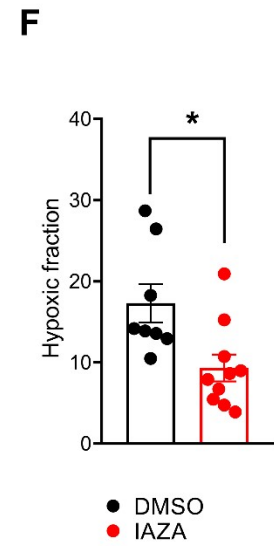
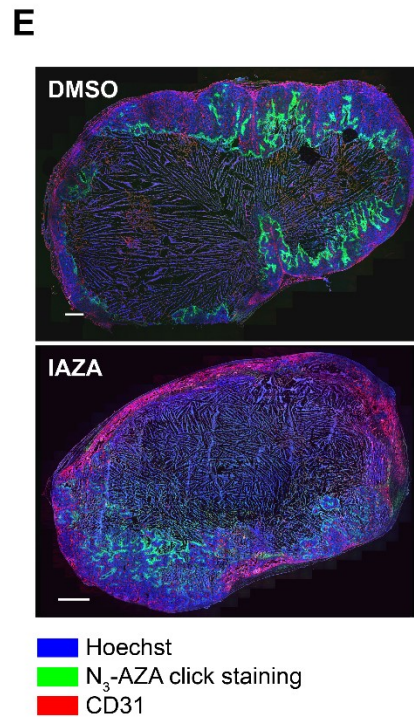
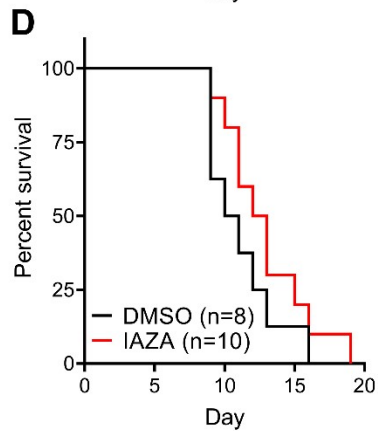
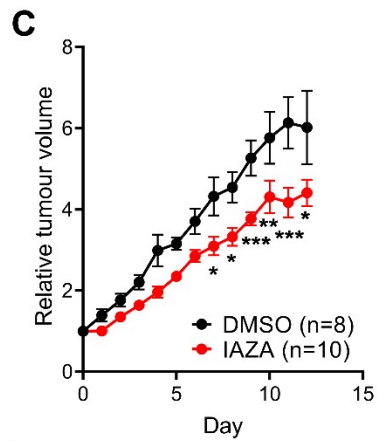
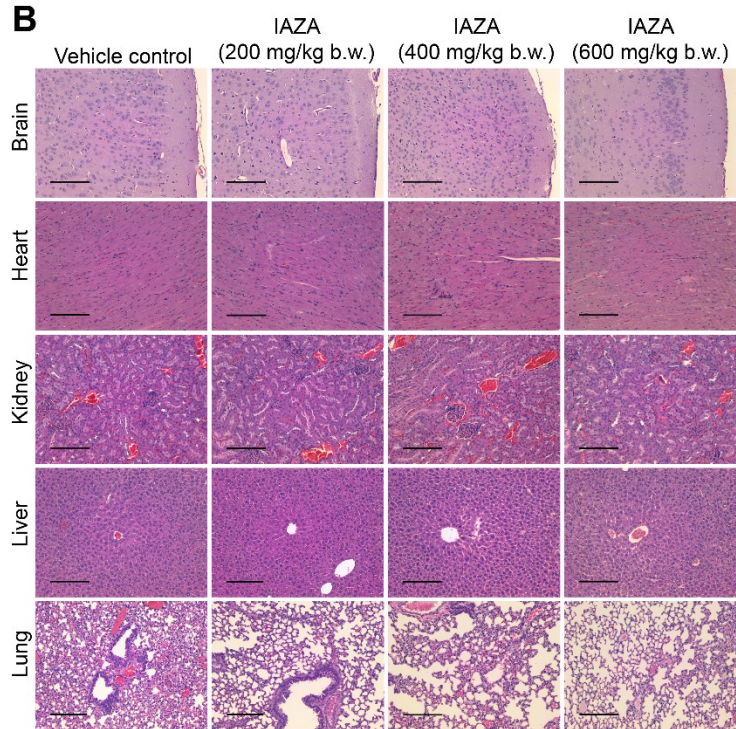
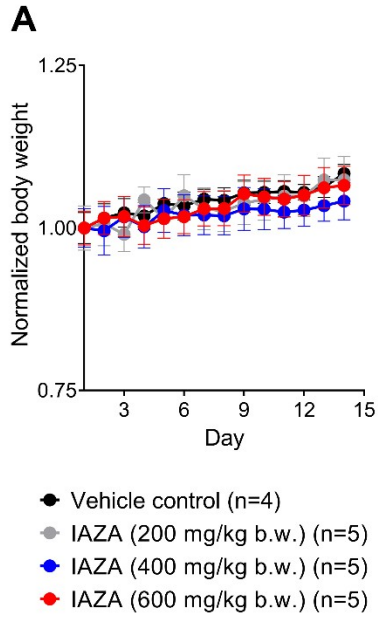


Figure 3.6 *In vivo* evaluation of IAZA toxicity and tumour growth delay properties.

IAZA was injected intraperitoneally in NOD/SCID/IL2R mice at 200, 400 or 600 mg/kg b.w. Changes in body weight were monitored for 14 days post injection (**A**), after which, mice were sacrificed, and histopathology analysis was performed on organ sections for possible signs of toxicity. Representative histopathology micrographs are shown (**B**). Tumour growth delay of a single IAZA (400 mg/kg b.w.) injection was monitored in NU/NU nude mice bearing subcutaneous FaDu tumours. IAZA-treated mice showed an initial delay in tumour growth (**C**), with a small increase in survival (**D**). Endpoint hypoxia levels were analyzed using N₃-AZA click staining; representative tumour sections are shown (**E**). Quantification of hypoxic fraction showed a significant reduction in hypoxia levels in tumours from IAZA-treated mice when compared to tumours from vehicle-treated mice (**F**). Data show mean± S.E.M.; scale bar = 1 mm (**B** and **E**).

3.4 Discussion

Tumour hypoxia is widely acknowledged as a formidable barrier for effective radio- and chemotherapy and more recently immunotherapy. Hypoxic tumour cells can escape the toxic effects of standard treatment modalities, and thus play a direct role in disease recurrence (Vaupel, Thews et al. 2001, Rockwell, Dobrucki et al. 2009). Consequently, eradication of hypoxic tumour fractions can significantly potentiate treatment outcome. Regardless, hypoxia-directed therapeutic interventions have yet to become a part of routine clinical practice, mainly because few drugs are able to reach and remain in the diffusion limited regions within the tumour. Hypoxic cells are also quiescent in nature, which protects them from conventional anti-cancer drugs that usually target rapidly proliferating cells (Li, Wu et al. 2017). One promising strategy to subvert this challenge is to use hypoxia activated prodrugs (HAPs), which are compounds with select chemical moieties that allow them to preferentially accumulate and become activated in hypoxic tissue (Wilson and Hay 2011). Nitroimidazoles (NIs), one of the most widely studied HAPs, garnered considerable attention as potential hypoxic anti-cancer drugs when the hypoxic radiosensitization properties of metronidazole (a 5-NI) was first reported in 1973 (Chapman, Reuvers et al. 1973). Despite showing encouraging results in pre-clinical models, several large-scale clinical trials with NIs failed to provide definitive therapeutic advantage. Nonetheless, there is merit to the idea that NIs can improve therapy outcome in a properly stratified patient population, as evident from the DAHANCA study with nimorazole (Overgaard, Eriksen et al. 2005, Toustrup, Sørensen et al. 2012). Considering that NI compounds have been under investigation for decades now, it is surprising that their molecular mechanism is still poorly understood, which has constrained further development of NI therapeutics. Indeed, most NI research nowadays focuses on their utility as hypoxic radiotracers; only a handful of mechanistic studies with NIs have been reported in recent times, mostly in anaerobic microbes (Leitsch, Kolarich et al. 2007, Leitsch, Kolarich et al. 2009, Leitsch, Schlosser et al. 2012). This warrants a methodological analysis of NIs in a human cancer model with a particular emphasis on elucidating the effects they have on hypoxic cancer cells.

Iodoazomycin arabinofuranoside (IAZA) and fluoroazomycin arabinofuranoside (FAZA) are 2-NI hypoxic radiotracers that have shown excellent tumour uptake in clinical studies,

demonstrating their abilities to overcome the diffusion barrier to reach hypoxic tumour niches. In addition, these compounds have also shown therapeutic potential in cell based assays: FAZA has been reported as a hypoxic radiosensitizer in human colorectal cancer cells (Kumar, Emami et al. 2009), while IAZA showed hypoxic cytotoxicity in murine breast cancer cells (Mannan, Somayaji et al. 1991) and sensitized hypoxic human hepatocellular carcinoma cells to ionizing radiation (IR) (Quan, Wang et al. 2015). The iodine moiety of IAZA makes it particularly promising for therapy; iodine in NIs has been reported to increase their hypoxic cytotoxicity (Krause, Jordan et al. 2005). It also makes IAZA a versatile molecule that can be labelled with an iodine radioisotope of choice for imaging (^{123}I and ^{124}I) and molecular radiotherapy (^{131}I).

In this study, a human head and neck cancer (HNC) model was used to assess the therapeutic potentials of IAZA and FAZA because (a) HNC tumours harbor significant levels of hypoxia (Hoogsteen, Marres et al. 2007), (b) pre-treatment tumour oxygenation status in HNC patients dictates response to therapy (Nordsmark, Overgaard et al. 1996), and (c) an improvement in HNC patient outcome was seen in a meta analysis of 50 randomized NI clinical trials (Overgaard 1994). First, the sensitivity of FaDu cells towards IAZA and FAZA treatment was tested under different O_2 levels. In general, the lower the O_2 levels, the higher the cells' sensitivity was towards the drugs (**Fig. 3.1D, E, G and H**). Depending on the assay, the IC_{50} values were $\sim 100\text{-}150\ \mu\text{M}$ for IAZA and $\sim 300\text{-}350\ \mu\text{M}$ for FAZA under $\leq 0.1\%$ O_2 levels. It is worth noting that cells in these O_2 levels (otherwise known as radiobiological hypoxia) represent the most challenging population to target therapeutically (Hammond, Asselin et al. 2014). Cells displayed higher sensitivity towards IAZA than FAZA, most likely due to the higher lipophilicity of IAZA, which might aid in its enhanced cellular retention (Kumar, Stypinski et al. 1999). This trend remained consistent across a panel of different human cancer cell lines (**Suppl. Fig. 3.1**). Since NIs, at high concentrations, are known to induce neurotoxicity (Agarwal, Kanekar et al. 2016), a conscious decision was made to limit the test concentrations in the micromolar range and close to $100\ \mu\text{M}$ when possible.

Interestingly, while morphological changes with IAZA and FAZA treatment were clearly evident under hypoxia (**Fig. 3.2A**), no significant increase in apoptotic (**Fig. 3.2B and C**), necrotic (**Fig. 3.2D**) or senescent (**Fig. 3.2F**) populations was recorded. Unlike doranidazole (another 2-NI) (Koike, Kota et al. 2020), IAZA and FAZA treatment (at the concentration

tested) did not induce ferroptosis under hypoxia (**Fig. 3.2G** and **H**). Instead, hypoxic treatment with 100 μ M IAZA or FAZA generated an inhibitory effect on cell proliferation (**Fig. 3.2I** and **J**). Cell cycle analysis showed a significant increase in S phase population in drug-treated hypoxic cells (**Fig. 3.3A**), which was further corroborated by staining for chromatin bound PCNA (**Fig. 3.3B** and **C**) and cyclin E1 protein levels (**Suppl. Fig. 3.2A** and **B**). The increase in S phase population arose not because more cells were actively dividing, rather hypoxic cells treated with the drugs appeared to progress through the S phase at a slower rate than the vehicle-treated cells. DNA replication was severely compromised in IAZA- and FAZA-treated hypoxic cells, which was analyzed by monitoring the uptake of a nucleoside analogue, EdU (**Fig. 3.3D** and **E**). The inhibitory effects with IAZA and FAZA on DNA synthesis are in agreement with previous reports using NIs in anaerobic bacteria (Plant and Edwards 1976, Sigeti, Guiney Jr et al. 1983). It is worth mentioning here that IAZA and FAZA are structural analogs of nucleosides, and previously FAZA has been reported to bind to human concentrative nucleoside transporters 1-3 (hCNT1-3) and has the potential to inhibit nucleoside transport (Maier, Schweifer et al. 2019). This could be one explanation for the slower proliferation rates observed in IAZA/FAZA-treated hypoxic cells. Of course, in that case, this phenomenon will be unique to only sugar coupled NIs, such as IAZA and FAZA, and not a general mechanism for all NIs.

Delay in DNA replication in drug-treated hypoxic cells induced replication stress, observed through nascent fork degradation in the DNA fibre assay (**Fig. 3.3G**), and further confirmed by analyzing retention of chromatin bound RPA in the nucleus. While intensity of RPA staining in IAZA-treated hypoxic cells was almost double (and statistically significant) than the vehicle-treated control cells, FAZA treatment (at 100 μ M) resulted in a non-significant increase in RPA staining (**Suppl. Fig. 3.2D** and **E**). Importantly, withdrawal of drugs and subsequent reoxygenation did not immediately reverse the phenotype; drug-treated hypoxic cells maintained a slower rate of DNA replication (**Fig. 3.3H** and **Suppl. Fig. 3.2C**), cell cycle progression (**Fig. 3.3A**) and proliferation (**Fig. 3.2I** and **J**).

Formation of DNA-NI adducts (Lafleur, Plijmackers-Westmijze et al. 1985) and/or subsequent DNA damage (Zahoor, Lafleur et al. 1987) has often been proposed as contributing factors for enhanced sensitivity of hypoxic cells towards NI treatment. Although direct binding of activated NIs to DNA has been reported earlier (Varghese and Whitmore 1980), the exact nature

and to what degree this binding happens require further investigation. To assess DNA-NI binding in hypoxic cells, a modified TARDIS assay (called TARDCS) was employed that utilizes N₃-AZA click chemistry. The TARDCS assay only captures covalent interactions of drug or macromolecules to DNA, while N₃-AZA allows for fluorescent labelling of NI-adducts formed under hypoxia through click chemistry. Analysis of N₃-AZA treated normoxic and hypoxic cells showed that covalent N₃-AZA-adducts were only formed under hypoxia (**Fig. 3.4A**). Addition of DNase I had a minimal effect on the N₃-AZA click signal, while proteinase K treatment completely removed all click staining (**Fig. 3.4A and B**). This implies that proteins, rather than DNA, are primary NI targets for covalent adduct formation. Since removal of proteins by proteinase K treatment removed all click staining, any DNA-NI interaction, if it occurs, would have to be non-covalent. While our observations are at odds with findings by Varghese et al. (Varghese and Whitmore 1983), recent evidence suggests that NI binding to DNA may potentially occur through hydrogen bonding and electrostatic interaction, instead of covalent association (Ahmadi, Shabrandi et al. 2019).

The capacity of activated NIs to directly induce DNA damage has been contested lately, with NI-induced DNA damages in earlier *in vitro* reports being attributed to the use of very high concentrations of drugs that are not achievable *in vivo* [reviewed in (Dingsdag and Hunter 2018)]. The effects of IAZA and FAZA treatment on DNA integrity in the present study were assessed using γ -H2AX immunofluorescent staining (**Fig. 3.4C**) and alkaline comet assay (**Fig. 3.4F**). While drug-treated hypoxic cells showed an increase in the percentage of γ -H2AX positive population (**Fig. 3.4D and E**), a relatively lower level of DNA damage was seen in the comet assay (**Fig. 3.4F**). It should be noted here that replication stress can also induce phosphorylation of H2AX in the absence of DNA damage (Ward and Chen 2001). Given the concentrations used in our assays and that IAZA and FAZA induce replication stress under hypoxia (**Fig. 3.3G, Suppl. Fig. 3.2D and E**), the γ -H2AX staining in this population is most likely to be a consequence of replication stress rather than DNA damage. We also analyzed generation of ROS in response to IAZA/FAZA treatment using two different approaches. Pre-incubating cells with a ROS scavenger (NAC) did not alter cell viability in response to IAZA/FAZA treatment under hypoxia, suggesting that they do not elevate ROS levels (**Suppl. Fig. 3.3A and B**). However, IAZA- and FAZA-treated hypoxic cells, when reoxygenated, showed significantly high levels of H₂O₂, indicating that 2-NI treatment generated a

compromised state in hypoxic cells that makes them susceptible to reoxygenation mediated stress (**Fig. 3.4G and H**). Considering that tumours often display dynamic oxygenation with fluctuating O₂ concentrations (termed cyclic hypoxia) [reviewed in (Bader, Dewhirst et al. 2021)], elevated ROS levels in reoxygenated cells treated with NIs might have significant biological implications.

Our data indicate that proteins are likely the primary targets of activated NIs for covalent adduct formation under hypoxia. To date, only a few studies have explored the proteins that NIs bind to. Consequently, the effects these interactions have on target protein stability, turnover, or function are poorly understood. Previously, we described a proteomic approach with N₃-AZA to identify NI target proteins, and reported a total of 62 candidate targets. Many of these proteins participate in critical biological functions involving cellular response to hypoxic stress (such as the glycolytic enzyme GAPDH and the detoxification enzyme GST) (Rashed, Stoica et al. 2021). As seen with N₃-AZA treatment, GAPDH and GST protein levels remained unaffected by IAZA and FAZA treatment, regardless of O₂ levels (**Fig. 3.5A and B, Suppl. Fig. 3.4**). Covalent attachment of the NIs appears to primarily affect the enzymatic function of these target proteins; both GAPDH and GST proteins significantly lost their catalytic activity in response to IAZA and FAZA treatment under hypoxia (**Fig. 3.5C-F**). GAPDH and GST play important roles in hypoxia adaptation, and there are direct consequences of GAPDH and GST inhibition on cell viability. For example, GAPDH depletion affects proliferation and induces cell cycle arrest in human lung and renal cell lines, and reduces growth of subcutaneously injected colorectal tumours in mice (Phadke, Krynetskaia et al. 2009, Liu, Tang et al. 2017). On the other hand, hypoxic cells elevate GST activity to counteract the effects of altered intracellular redox state (Millar, Phan et al. 2007). Previous knockdown studies of GSTP1 showed a profound effect on cell proliferation; siRNA-mediated knockdown of GSTP1 in HNC cells lines, HSC3 and SAS, suppressed cell growth by 50.5% and 35.2%, respectively (Mutallip, Nohata et al. 2011). In regenerating mouse livers, lack of GST reduced DNA replication, delayed or altered activation of signaling pathways (such as STAT3, JNK and ERK1/2) and postponed expression or activation of cell cycle regulators (Cyclin D1, CDK4, E2F1 and MCM7) (Pajaud, Ribault et al. 2015). Additionally, GSTP1 knockout mouse lung epithelial cells showed increased vulnerability towards hypoxia/reoxygenation stress, and had reduced viability (Fletcher, Boshier et al. 2015). Considering the inhibitory effects of IAZA and FAZA on

GAPDH and GST functions, it is thus tempting to speculate that drug-mediated deregulation of their catalytic activities may contribute to the sensitivity of hypoxic cells to these compounds. However, further studies would be required to conclusively identify the roles GAPDH and GST play in NI-mediated hypoxic sensitivity. Also worth noting is that in addition to GAPDH and GST, our proteomic analysis identified 60 more protein targets of IAZA and FAZA, and their contribution to the observed hypoxic cellular sensitivity cannot be ruled out (Rashed, Stoica et al. 2021). For example, several ribosomal proteins (RpL4, RpSA, RpS3), translation machinery proteins (eIF4AII, eEF1AI) and proteins involved in 3D protein folding (PPIB, PDI) formed covalent NI-adducts, which may affect protein synthesis and proper protein function. Cytoskeletal protein tubulin also appeared in our proteomic study as a target of NIs. Tubulin is an integral component of spindle fibres, and is necessary for chromosome movement and segregation during mitosis (Ferreira, Figueiredo et al. 2018). Moreover, our analysis identified chaperone proteins such as Hsp60, Hsp70 and Hsp90 as NI targets, which are known to be involved in hypoxia-responsive cellular proliferation (Xiong, Zhao et al. 2009), tolerance (Zhang, Zhao et al. 2009), apoptosis (Gupta and Knowlton 2002) and unfolded protein response (UPR) pathway (Davenport, Morgan et al. 2008). Finally, one should not rule out the possibility that the hypoxia selective sensitization phenomenon by IAZA and FAZA very likely be a combined effect of targeting many different pathways and cellular processes, and not a distinct isolated occurrence.

IAZA, administered intraperitoneally, was well tolerated in mice at levels up to 600 mg/kg b.w. (**Fig. 3.6A and B, Suppl. Table 3.1**). Although a single dose administration of IAZA (400 mg/kg b.w.) to tumour bearing mice had minimal effect on overall survival (**Fig. 3.6D**), a significant delay in initial tumour growth was observed (**Fig. 3.6C**). While these early effects gradually wore off, our results are still promising given that only a single dose of IAZA was administered to mice, while most anti-cancer drugs (including nimorazole) are given as multiple doses in a clinical setting. Indeed, multiple administrations of IAZA may prove useful at improving survival, which needs to be tested experimentally in future. Additionally, administration of encapsulated IAZA might be another approach to ensure maximum efficacy of IAZA delivery to target tumour sites. Nanoencapsulation of IAZA and its benefits have been characterized in a previous study (Quan, Wang et al. 2015). Encouragingly, even with a single dosage of IAZA, a significant decrease was seen in hypoxic fractions in the tumours (**Fig. 3.6E**

and F). This indicates that tumours in IAZA-treated mice may respond better to radiation and adjuvant chemotherapy.

In conclusion, we show that activated 2-NIs, IAZA and FAZA, negatively affect DNA synthesis and cell cycle progression under hypoxia, leading to slower proliferation of hypoxic NI-treated cells. Covalent binding of these NIs to proteins can inhibit catalytic functions of critical cellular enzymes. IAZA, even at a single i.p. injection, can significantly reduce tumour hypoxia burden, which further promises to enhance efficacy of radiation and chemotherapy when given in combination with NIs.

3.5 Acknowledgements

The authors would like to thank Dr. Lynne-Marie Postovit, Dr. Hans-Sonke Jans and Dr. Michael Hendzel for their guidance and advice, Dr. Gordon Chan and Dr. Armin Gamper for reagents, and Dr. Xuejun Sun, Geraldine Barron, Dr. Nirilanto Ramamonjisoa, Dan Mcginn, Dr. Aja Rieger and Cassandra Anne Ganje for technical assistance. This work was supported through grants 201201164 and 20131051 from Alberta Innovates through the CRIO program and CRIO Project-Cancer (P.K.; M.W.), RGPIN-2017-05752 from Natural Sciences and Engineering Research Council of Canada Discovery (I.H.I.), MOP-365197 from Canadian Institutes of Health Research Project Grant (I.H.I.) and RGPIN-2015-06339 from Natural Sciences and Engineering Research Council of Canada Discovery (R.N). F.B.R. received scholarships from the Terry Fox Foundation, Strategic Training in Transdisciplinary Radiation Science for the 21st Century (STARS21) program, the Yau Family Foundation, Alberta Cancer Foundation (Antoine Noujaim Scholarship), and the University of Alberta. D.D.D. received the Queen Elizabeth II Graduate Scholarship and DB Robinson Graduate Scholarship from University of Alberta. F.M. is a recipient of Marathon of Hope Graduate Studentships in Breast Cancer or Glioblastoma Research.

3.6 References

- Agarwal, A., S. Kanekar, S. Sabat and K. Thamburaj (2016). “Metronidazole-induced cerebellar toxicity.” *Neurology International* 8(1): 4-6.
- Ahmadi, F., N. Shabrandi, L. Hosseinzadeh and H. Azizian (2019). “Two DNA binding modes of a zinc-metronidazole and biological evaluation as a potent anti-cancer agent.” *Nucleosides, Nucleotides and Nucleic Acids* 38(7): 449-480.
- Ai, M., P. Budhani, J. Sheng, S. Balasubramanyam, T. Bartkowiak, A. R. Jaiswal, C. R. Ager, D. D. Haria and M. A. Curran (2015). “Tumor hypoxia drives immune suppression and immunotherapy resistance.” *Journal for ImmunoTherapy of Cancer* 3(2): 1-1.
- Bader, S. B., M. W. Dewhirst and E. M. Hammond (2021). “Cyclic hypoxia: An update on its characteristics, methods to measure it and biological implications in cancer.” *Cancers* 13(1): 23.
- Brown, J. M. (1999). “The Hypoxic Cell A Target for Selective Cancer Therapy—Eighteenth Bruce F. Cain Memorial Award Lecture.” *Cancer research* 59(23): 5863-5870.
- Chapman, J., A. Reuvers and J. Borsa (1973). “Effectiveness of nitrofurans in sensitizing hypoxic mammalian cells to X rays.” *The British Journal of Radiology* 46(548): 623-630.
- Cowell, I. G., M. J. Tilby and C. A. Austin (2011). “An overview of the visualisation and quantitation of low and high MW DNA adducts using the trapped in agarose DNA immunostaining (TARDIS) assay.” *Mutagenesis* 26(2): 253-260.
- Damiani, E., J. A. Solorio, A. P. Doyle and H. M. Wallace (2019). “How reliable are in vitro IC50 values? Values vary with cytotoxicity assays in human glioblastoma cells.” *Toxicology Letters* 302: 28-34.
- Davenport, E. L., G. J. Morgan and F. E. Davies (2008). “Untangling the unfolded protein response.” *Cell Cycle* 7(7): 865-869.
- Debacq-Chainiaux, F., J. D. Erusalimsky, J. Campisi and O. Toussaint (2009). “Protocols to detect senescence-associated beta-galactosidase (SA- β gal) activity, a biomarker of senescent cells in culture and in vivo.” *Nature Protocols* 4(12): 1798-1806.
- Dingsdag, S. A. and N. Hunter (2018). “Metronidazole: an update on metabolism, structure–cytotoxicity and resistance mechanisms.” *Journal of Antimicrobial Chemotherapy* 73(2): 265-279.
- Feoktistova, M., P. Geserick and M. Leverkus (2016). “Crystal violet assay for determining viability of cultured cells.” *Cold Spring Harbor Protocols* 2016(4): pdb. Prot087379.
- Ferreira, L. T., A. C. Figueiredo, B. Orr, D. Lopes and H. Maiato (2018). “Dissecting the role of the tubulin code in mitosis.” *Methods in Cell Biology* 144: 33-74.
- Fletcher, M. E., P. R. Boshier, K. Wakabayashi, H. C. Keun, R. T. Smolenski, P. A. Kirkham, I. M. Adcock, P. J. Barton, M. Takata and N. Marczin (2015). “Influence of glutathione-S-transferase (GST) inhibition on lung epithelial cell injury: role of oxidative stress and metabolism.” *American Journal of Physiology-Lung Cellular and Molecular Physiology* 308(12): L1274-L1285.
- Gupta, S. and A. A. Knowlton (2002). “Cytosolic heat shock protein 60, hypoxia, and apoptosis.” *Circulation* 106(21): 2727-2733.
- Halasi, M., M. Wang, T. S. Chavan, V. Gaponenko, N. Hay and A. L. Gartel (2013). “ROS inhibitor N-acetyl-L-cysteine antagonizes the activity of proteasome inhibitors.” *Biochemical Journal* 454(2): 201-208.

- Hammond, E., M.-C. Asselin, D. Forster, J. P. O'Connor, J. Senra and K. Williams (2014). "The meaning, measurement and modification of hypoxia in the laboratory and the clinic." *Clinical Oncology* 26(5): 277-288.
- Hoogsteen, I. J., H. A. Marres, J. Bussink, A. J. van der Kogel and J. H. Kaanders (2007). "Tumor microenvironment in head and neck squamous cell carcinomas: predictive value and clinical relevance of hypoxic markers. A review." *Head & Neck* 29(6): 591-604.
- Kizaka-Kondoh, S. and H. Konse-Nagasawa (2009). "Significance of nitroimidazole compounds and hypoxia-inducible factor-1 for imaging tumor hypoxia." *Cancer Science* 100(8): 1366-1373.
- Koch, C., R. Howell and J. Biaglow (1979). "Ascorbate anion potentiates cytotoxicity of nitroaromatic compounds under hypoxic and anoxic conditions." *British Journal of Cancer* 39(3): 321-329.
- Koike, N., R. Kota, Y. Naito, N. Hayakawa, T. Matsuura, T. Hishiki, N. Onishi, J. Fukada, M. Suematsu and N. Shigematsu (2020). "2-Nitroimidazoles induce mitochondrial stress and ferroptosis in glioma stem cells residing in a hypoxic niche." *Communications Biology* 3(1): 1-13.
- Krause, W., A. Jordan, R. Scholz and J.-L. M. Jimenez (2005). "Iodinated nitroimidazoles as radiosensitizers." *Anticancer Research* 25(3B): 2145-2151.
- Kumar, P., S. Emami, Z. Kresolek, J. Yang, A. McEwan and L. Wiebe (2009). "Synthesis and Hypoxia Selective Radiosensitization Potential of β -2-FAZA and β -3-FAZL: Fluorinated Azomycin β -Nucleosides." *Medicinal Chemistry* 5(2): 118-129.
- Kumar, P., D. Stypinski, H. Xia, A. McEwan, H. J. Machulla and L. Wiebe (1999). "Fluoroazomycin arabinoside (FAZA): synthesis, 2H and 3H-labelling and preliminary biological evaluation of a novel 2-nitroimidazole marker of tissue hypoxia." *Journal of Labelled Compounds and Radiopharmaceuticals: The Official Journal of the International Isotope Society* 42(1): 3-16.
- Lafleur, M., E. Plijmackers-Westmijze, A. Loman and H. Loman (1985). "Adduct Formation Is Involved in Radiosensitization, Mediated by Cytochrome c, of $\phi\phi$ X174 DNA by Misonidazole." *International Journal of Radiation Biology and Related Studies in Physics, Chemistry and Medicine* 47(4): 379-382.
- Lee, D.-J., D. Cosmatos, V. A. Marcial, K. K. Fu, M. Rotman, J. S. Cooper, H. G. Ortiz, J. J. Beitler, R. A. Abrams and W. J. Curran (1995). "Results of an RTOG phase III trial (RTOG 85-27) comparing radiotherapy plus etanidazole with radiotherapy alone for locally advanced head and neck carcinomas." *International Journal of Radiation Oncology* Biology* Physics* 32(3): 567-576.
- Leitsch, D., D. Kolarich, M. Binder, J. Stadlmann, F. Altmann and M. Duchêne (2009). "Trichomonas vaginalis: metronidazole and other nitroimidazole drugs are reduced by the flavin enzyme thioredoxin reductase and disrupt the cellular redox system. Implications for nitroimidazole toxicity and resistance." *Molecular Microbiology* 72(2): 518-536.
- Leitsch, D., D. Kolarich, I. B. Wilson, F. Altmann and M. Duchêne (2007). "Nitroimidazole action in Entamoeba histolytica: a central role for thioredoxin reductase." *PloS Biology* 5(8).

- Leitsch, D., S. Schlosser, A. Burgess and M. Duchêne (2012). “Nitroimidazole drugs vary in their mode of action in the human parasite *Giardia lamblia*.” *International Journal for Parasitology: Drugs and Drug Resistance* 2: 166-170.
- Li, J.-q., X. Wu, L. Gan, X.-l. Yang and Z.-h. Miao (2017). “Hypoxia induces universal but differential drug resistance and impairs anticancer mechanisms of 5-fluorouracil in hepatoma cells.” *Acta Pharmacologica Sinica* 38(12): 1642.
- Liu, K., Z. Tang, A. Huang, P. Chen, P. Liu, J. Yang, W. Lu, J. Liao, Y. Sun and S. Wen (2017). “Glyceraldehyde-3-phosphate dehydrogenase promotes cancer growth and metastasis through upregulation of SNAIL expression.” *International Journal of Oncology* 50(1): 252-262.
- Locke, A. J., L. Hossain, G. McCrostie, D. A. Ronato, A. Fitieh, T. A. Rafique, F. Mashayekhi, M. Motamedi, J.-Y. Masson and I. H. Ismail (2021). “SUMOylation mediates CtIP’s functions in DNA end resection and replication fork protection.” *Nucleic Acids Research* 49(2): 928-953.
- Maier, F. C., A. Schweifer, V. L. Damaraju, C. E. Cass, G. D. Bowden, W. Ehrlichmann, M. Kneilling, B. J. Pichler, F. Hammerschmidt and G. Reischl (2019). “2-Nitroimidazole-Furanoside Derivatives for Hypoxia Imaging—Investigation of Nucleoside Transporter Interaction, 18F-Labeling and Preclinical PET Imaging.” *Pharmaceuticals* 12(1): 31.
- Mannan, R. H., V. V. Somayaji, J. Lee, J. R. Mercer, J. D. Chapman and L. I. Wiebe (1991). “Radioiodinated 1-(5-iodo-5-deoxy-beta-D-arabinofuranosyl)-2-nitroimidazole (iodoazomycin arabinoside: IAZA): a novel marker of tissue hypoxia.” *Journal of Nuclear Medicine* 32: 1764-1770.
- Maréchal, A. and L. Zou (2015). “RPA-coated single-stranded DNA as a platform for post-translational modifications in the DNA damage response.” *Cell Research* 25(1): 9-23.
- Masaki, Y., Y. Shimizu, T. Yoshioka, Y. Tanaka, K.-i. Nishijima, S. Zhao, K. Higashino, S. Sakamoto, Y. Numata and Y. Yamaguchi (2015). “The accumulation mechanism of the hypoxia imaging probe “FMISO” by imaging mass spectrometry: possible involvement of low-molecular metabolites.” *Scientific Reports* 5(1): 1-9.
- McKeown, S. (2014). “Defining normoxia, physoxia and hypoxia in tumours—implications for treatment response.” *The British Journal of Radiology* 87(1035): 20130676.
- Millar, T. M., V. Phan and L. A. Tibbles (2007). “ROS generation in endothelial hypoxia and reoxygenation stimulates MAP kinase signaling and kinase-dependent neutrophil recruitment.” *Free Radical Biology and Medicine* 42(8): 1165-1177.
- Mirzayans, R., B. Andrais and D. Murray (2018). “Roles of polyploid/multinucleated giant cancer cells in metastasis and disease relapse following anticancer treatment.” *Cancers* 10(4): 118.
- Mutallip, M., N. Nohata, T. Hanazawa, N. Kikkawa, S. Horiguchi, L. Fujimura, K. Kawakami, T. Chiyomaru, H. Enokida and M. Nakagawa (2011). “Glutathione S-transferase P1 (GSTP1) suppresses cell apoptosis and its regulation by miR-133 α in head and neck squamous cell carcinoma (HNSCC).” *International Journal of Molecular Medicine* 27(3): 345-352.
- Nordsmark, M., M. Overgaard and J. Overgaard (1996). “Pretreatment oxygenation predicts radiation response in advanced squamous cell carcinoma of the head and neck.” *Radiotherapy and Oncology* 41(1): 31-39.

- Ohtsubo, M., A. M. Theodoras, J. Schumacher, J. M. Roberts and M. Pagano (1995). "Human cyclin E, a nuclear protein essential for the G1-to-S phase transition." *Molecular and Cellular Biology* 15(5): 2612-2624.
- Otsu, N. (1979). "A threshold selection method from gray-level histograms." *IEEE transactions on Systems, Man, and Cybernetics* 9(1): 62-66.
- Overgaard, J. (1994). "Clinical evaluation of nitroimidazoles as modifiers of hypoxia in solid tumors." *Oncology Research Featuring Preclinical and Clinical Cancer Therapeutics* 6(10-11): 509-518.
- Overgaard, J., J. G. Eriksen, M. Nordmark, J. Alsner and M. R. Horsman (2005). "Plasma osteopontin, hypoxia, and response to the hypoxia sensitiser nimorazole in radiotherapy of head and neck cancer: results from the DAHANCA 5 randomised double-blind placebo-controlled trial." *The Lancet Oncology* 6(10): 757-764.
- Overgaard, J., H. S. Hansen, A. Andersen, M. Hjelm-Hansen, K. Jørgensen, E. Sandberg, A. Berthelsen, R. Hammer and M. Pedersen (1989). "Misonidazole combined with split-course radiotherapy in the treatment of invasive carcinoma of larynx and pharynx: report from the DAHANCA 2 study." *International Journal of Radiation Oncology • Biology • Physics* 16(4): 1065-1068.
- Overgaard, J., H. S. Hansen, M. Overgaard, L. Bastholt, A. Berthelsen, L. Specht, B. Lindeløv and K. Jørgensen (1998). "A randomized double-blind phase III study of nimorazole as a hypoxic radiosensitizer of primary radiotherapy in supraglottic larynx and pharynx carcinoma. Results of the Danish Head and Neck Cancer Study (DAHANCA) Protocol 5-85." *Radiotherapy and Oncology* 46(2): 135-146.
- Pajaud, J., C. Ribault, I. B. Mosbah, C. Rauch, C. Henderson, P. Bellaud, C. Aninat, P. Loyer, F. Morel and A. Corlu (2015). "Glutathione transferases P1/P2 regulate the timing of signaling pathway activations and cell cycle progression during mouse liver regeneration." *Cell Death & Disease* 6(1): e1598-e1598.
- Phadke, M. S., N. F. Krynetskaia, A. K. Mishra and E. Krynetskiy (2009). "Glyceraldehyde 3-phosphate dehydrogenase depletion induces cell cycle arrest and resistance to antimetabolites in human carcinoma cell lines." *Journal of Pharmacology and Experimental Therapeutics* 331(1): 77-86.
- Plant, C. and D. Edwards (1976). "The effect of tinidazole, metronidazole and nitrofurazone on nucleic acid synthesis in *Clostridium bifermentans*." *Journal of Antimicrobial Chemotherapy* 2(2): 203-209.
- Postema, E. J., A. J. McEwan, T. A. Riauka, P. Kumar, D. A. Richmond, D. N. Abrams and L. I. Wiebe (2009). "Initial results of hypoxia imaging using 1- α -D-(5-deoxy-5-[18 F]-fluoroarabinofuranosyl)-2-nitroimidazole (18 F-FAZA)." *European Journal of Nuclear Medicine and Molecular Imaging* 36(10): 1565-1573.
- Qiu, S., G. Jiang, L. Cao and J. Huang (2021). "Replication fork reversal and protection." *Frontiers in Cell and Developmental Biology* 9: 1190.
- Quan, S., Y. Wang, A. Zhou, P. Kumar and R. Narain (2015). "Galactose-based thermosensitive nanogels for targeted drug delivery of iodoazomycin arabinofuranoside (IAZA) for theranostic management of hypoxic hepatocellular carcinoma." *Biomacromolecules* 16(7): 1978-1986.
- Rashed, F. B., A. C. Stoica, D. MacDonald, H. El-Saidi, C. Ricardo, B. Bhatt, J. Moore, D. Diaz-Dussan, N. Ramamonjisoa, Y. Mowery, S. Damaraju, R. Fahlman, L.I., P. Kumar

- and M. Weinfeld (2021). "Identification of proteins and cellular pathways targeted by 2-nitroimidazole hypoxic cytotoxins." *Redox Biology*: 101905.
- Rockwell, S., I. T. Dobrucki, E. Y. Kim, S. T. Marrison and V. T. Vu (2009). "Hypoxia and radiation therapy: past history, ongoing research, and future promise." *Current Molecular Medicine* 9(4): 442-458.
- Sasaki, K., A. Kurose and Y. Ishida (1993). "Flow cytometric analysis of the expression of PCNA during the cell cycle in HeLa cells and effects of the inhibition of DNA synthesis on it." *Cytometry: The Journal of the International Society for Analytical Cytology* 14(8): 876-882.
- Sigeti, J. S., D. G. Guiney Jr and C. E. Davis (1983). "Mechanism of action of metronidazole on *Bacteroides fragilis*." *Journal of Infectious Diseases* 148(6): 1083-1089.
- Silver, A. R., S. S. Mcneil, P. O'Neill, T. C. Jenkins and I. Ahmed (1986). "Induction of DNA strand breaks by reduced nitroimidazoles: Implications for DNA base damage." *Biochemical Pharmacology* 35(22): 3923-3928.
- Silver, A. R., P. O'Neill and T. C. Jenkins (1985). "Induction of DNA strand breaks by RSU-1069, A nitroimidazole-aziridine radiosensitizer: Role of binding of both unreduced and radiation-reduced forms to DNA, in vitro." *Biochemical Pharmacology* 34(19): 3537-3542.
- Souvatoglou, M., A. Grosu, B. Röper, B. Krause, R. Beck, G. Reischl, M. Picchio, H.-J. Machulla, H.-J. Wester and M. Piert (2007). "Tumour hypoxia imaging with [18F] FAZA PET in head and neck cancer patients: a pilot study." *European Journal of Nuclear Medicine and Molecular Imaging* 34(10): 1566-1575.
- Toustrup, K., B. S. Sørensen, P. Lassen, C. Wiuf, J. Alsner and J. Overgaard (2012). "Gene expression classifier predicts for hypoxic modification of radiotherapy with nimorazole in squamous cell carcinomas of the head and neck." *Radiotherapy and Oncology* 102(1): 122-129.
- Varghese, A. and G. Whitmore (1980). "Binding to cellular macromolecules as a possible mechanism for the cytotoxicity of misonidazole." *Cancer Research* 40(7): 2165-2169.
- Varghese, A. and G. Whitmore (1983). "Modification of guanine derivatives by reduced 2-nitroimidazoles." *Cancer Research* 43(1): 78-82.
- Vaupel, P., O. Thews and M. Hoekel (2001). "Treatment resistance of solid tumors." *Medical Oncology* 18(4): 243-259.
- Verwer, E. E., I. Bahce, F. H. van Velden, M. Yaqub, R. C. Schuit, A. D. Windhorst, P. Rajmakers, O. S. Hoekstra, A. A. Lammertsma and E. F. Smit (2014). "Parametric methods for quantification of 18F-FAZA kinetics in non-small cell lung cancer patients." *Journal of Nuclear Medicine* 55(11): 1772-1777.
- Vindigni, A. and M. Lopes (2017). "Combining electron microscopy with single molecule DNA fiber approaches to study DNA replication dynamics." *Biophysical Chemistry* 225: 3-9.
- Walsh, J. C., A. Lebedev, E. Aten, K. Madsen, L. Marciano and H. C. Kolb (2014). "The clinical importance of assessing tumor hypoxia: relationship of tumor hypoxia to prognosis and therapeutic opportunities." *Antioxidants & Redox Signaling* 21(10): 1516-1554.
- Ward, I. M. and J. Chen (2001). "Histone H2AX is phosphorylated in an ATR-dependent manner in response to replicational stress." *Journal of Biological Chemistry* 276(51): 47759-47762.

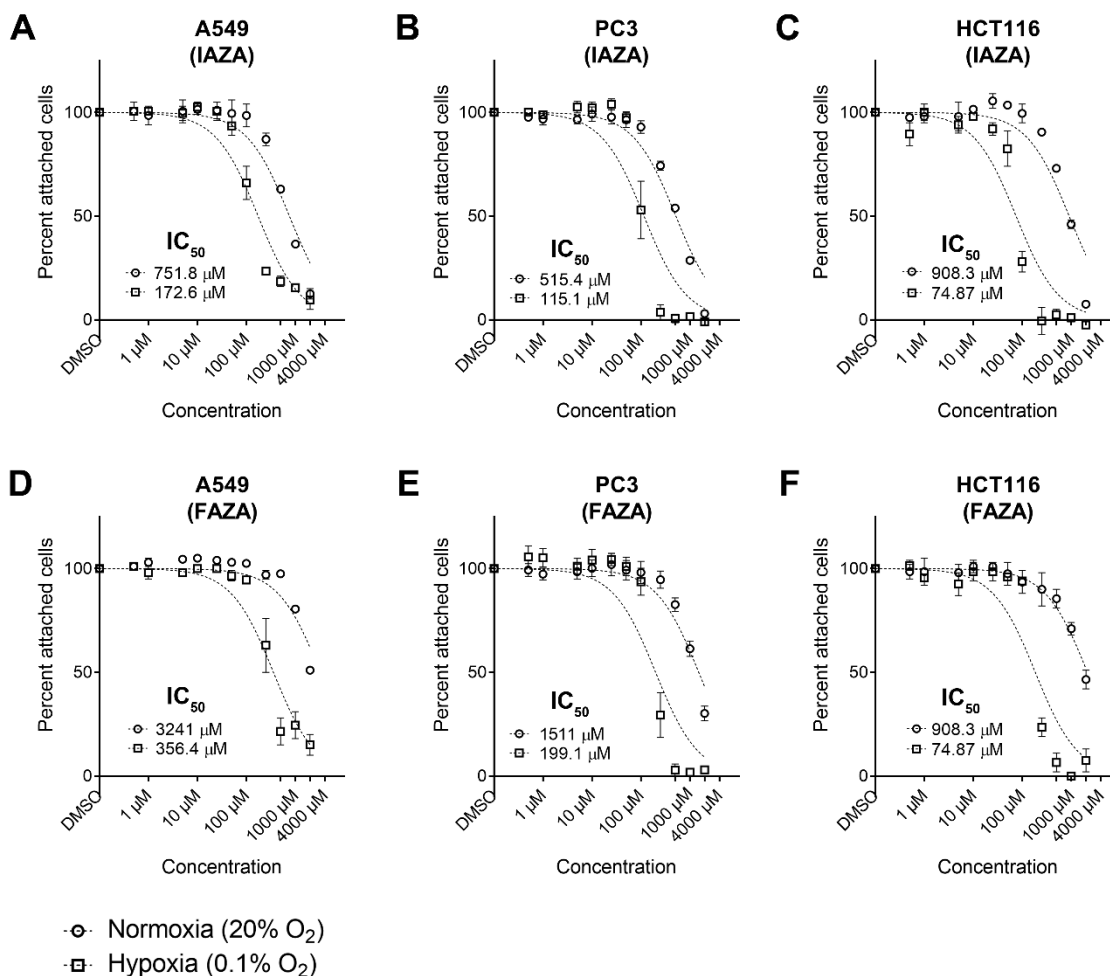
- Wilson, W. R. and M. P. Hay (2011). "Targeting hypoxia in cancer therapy." *Nature Reviews Cancer* 11(6): 393-410.
- Xiong, L., T. Zhao, X. Huang, Z.-h. Liu, H. Zhao, M.-m. Li, L.-y. Wu, H.-b. Shu, L.-l. Zhu and M. Fan (2009). "Heat shock protein 90 is involved in regulation of hypoxia-driven proliferation of embryonic neural stem/progenitor cells." *Cell Stress and Chaperones* 14(2): 183-192.
- Zahoor, A., M. Lafleur, R. Knight, H. Loman and D. Edwards (1987). "DNA damage induced by reduced nitroimidazole drugs." *Biochemical Pharmacology* 36(19): 3299-3304.
- Zeman, M. K. and K. A. Cimprich (2014). "Causes and consequences of replication stress." *Nature Cell Biology* 16(1): 2-9.
- Zhang, K., T. Zhao, X. Huang, Z.-h. Liu, L. Xiong, M.-m. Li, L.-y. Wu, Y.-q. Zhao, L.-l. Zhu and M. Fan (2009). "Preinduction of HSP70 promotes hypoxic tolerance and facilitates acclimatization to acute hypobaric hypoxia in mouse brain." *Cell Stress and Chaperones* 14(4): 407-415.

3.7 Supplementary information

Supplementary Table 3.1 Blood chemistry analysis of mice injected i.p. with IAZA (or vehicle control) showed no significant changes.

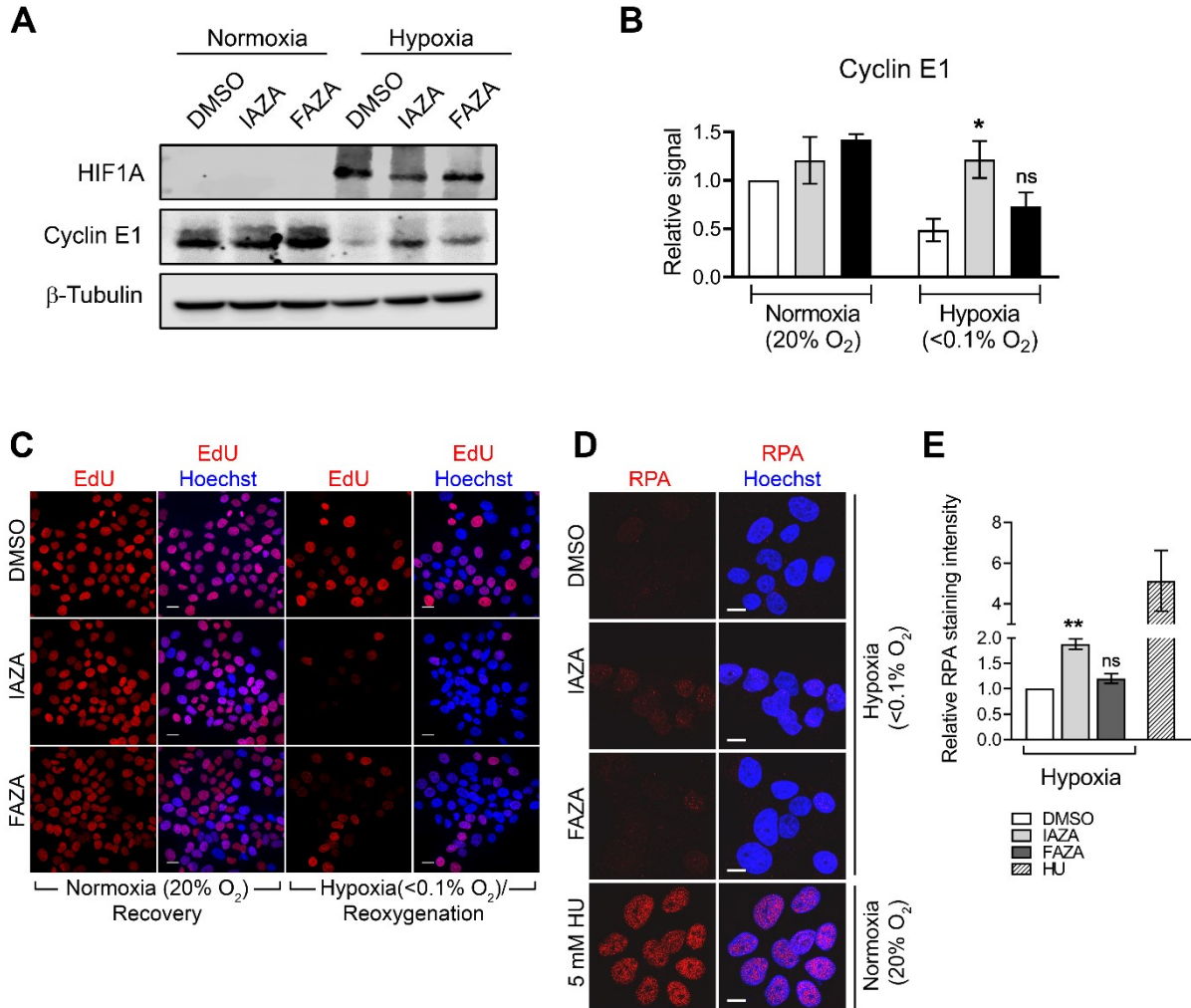
	Vehicle control	IAZA (200 mg/kg)	IAZA (400 mg/kg)	IAZA (600 mg/kg)
Glucose (mmol/L)	17.65±4.52	18.22±3.98	17.14±3.20	16.64±1.76
Urea (mmol/L)	8.975±0.64	7.72±0.56	7.38±1.19	7.06±0.48
Creatinine (µmol/L)	9±3.37	9.2±1.30	8.4±2.19	9±1.41
Phosphorus (mmol/L)	3.85±0.42	3.82±0.16	3.68±0.53	3.76±0.34
Calcium (mmol/L)	2.51±0.24	2.594±0.18	2.574±0.07	2.588±0.02
Sodium (mmol/L)	154.5±1.73	152.6±2.19	156.5±2.65	154.6±3.05
Potassium (mmol/L)	>9	>9	7.2 to >9	8.8 to >9
Chloride (mmol/L)	114.5±3.70	114.8±3.11	114±2.12	114.6±0.89
Bicarbonate (mmol/L)	22.75±1.71	21.8±1.30	23.8±2.17	21.2±3.42
Total Protein (g/L)	41.5±9.33	44.4±6.43	47.2±2.59	46.2±1.92
Albumin (g/L)	24.25±5.0	26.4±3.58	27.8±1.10	27.4±0.89
Globulin (g/L)	17.25±4.35	18±2.92	19.4±1.52	18.8±1.30
ALT ^[a] (IU/L)	78.5±82.33	48.6±36.32	114.8±206.98	26.8±13.94
AST ^[b] (IU/L)	373.5±334.34	219.2±211.69	230.4±375.32	107.4±112.30
ALP ^[c] (IU/L)	95.25±26.16	98.8±12.44	61.8±7.53	81±5.70
Total Bilirubin (µmol/L)	3.2±0.91	3.98±0.65	4.46±0.64	4.8±0.75
CK ^[d] (IU/L)	13505±15265.23	8194±10978.56	342±427.05	279.25±238.97

^[a] ALT: alanine aminotransferase; ^[b] AST: aspartate aminotransferase; ^[c] ALP: alkaline phosphatase; ^[d] CK: Creatine Kinase. Data represent mean± standard deviation.



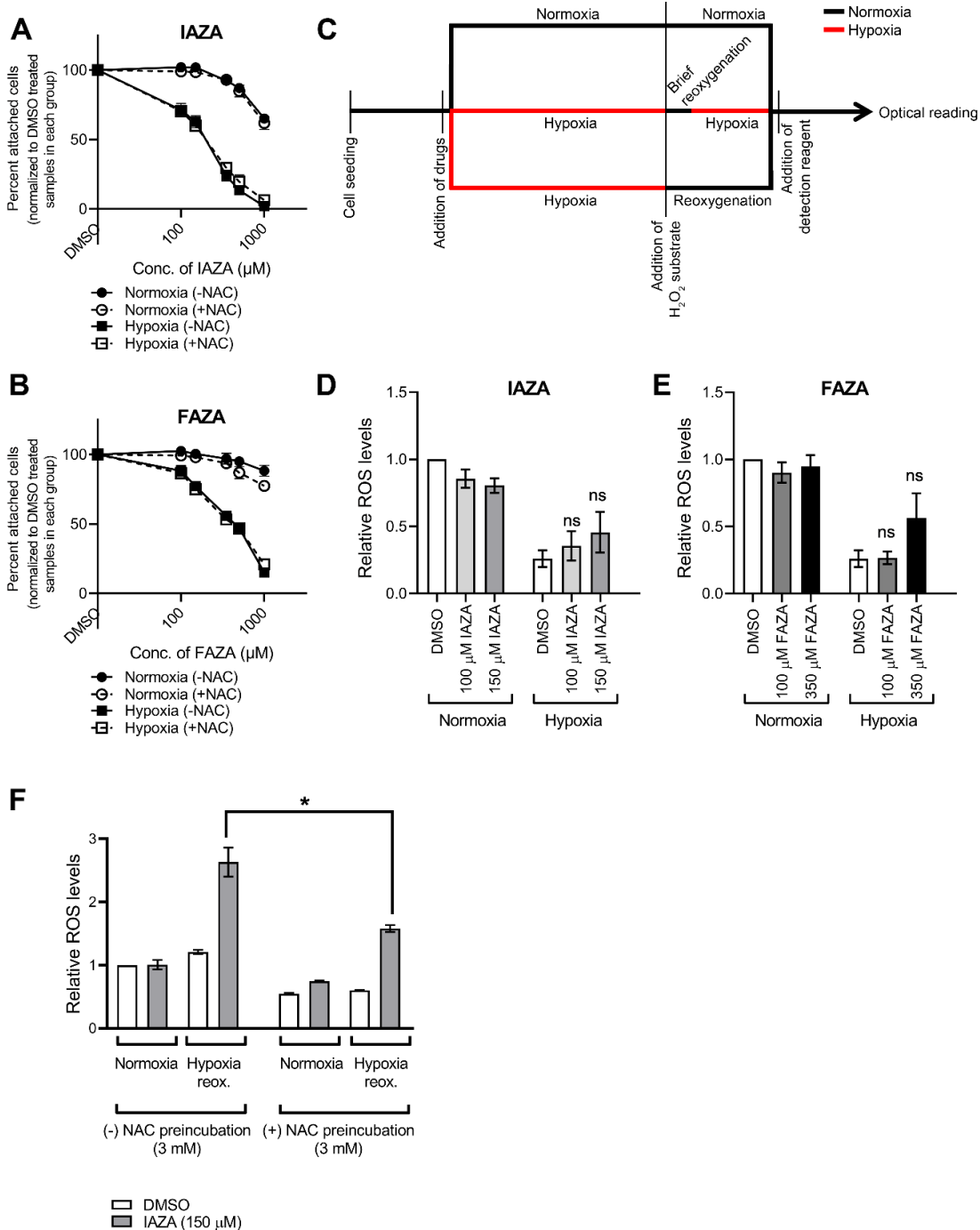
Supplementary Figure 3.1 Hypoxia selective sensitivity to IAZA and FAZA in additional human cancer cell lines.

Crystal violet staining assays were performed to assess sensitivity of human lung epithelial carcinoma A549 (A, D), prostate carcinoma PC3 (B, E) and colorectal carcinoma HCT116 (C, F) cells to IAZA (A-C) and FAZA (D-F) treatment under normoxia and hypoxia (0.1% O₂). Hypoxic cells showed higher sensitivity to drug treatment. Data show mean ± S.E.M. from three independent experiments.



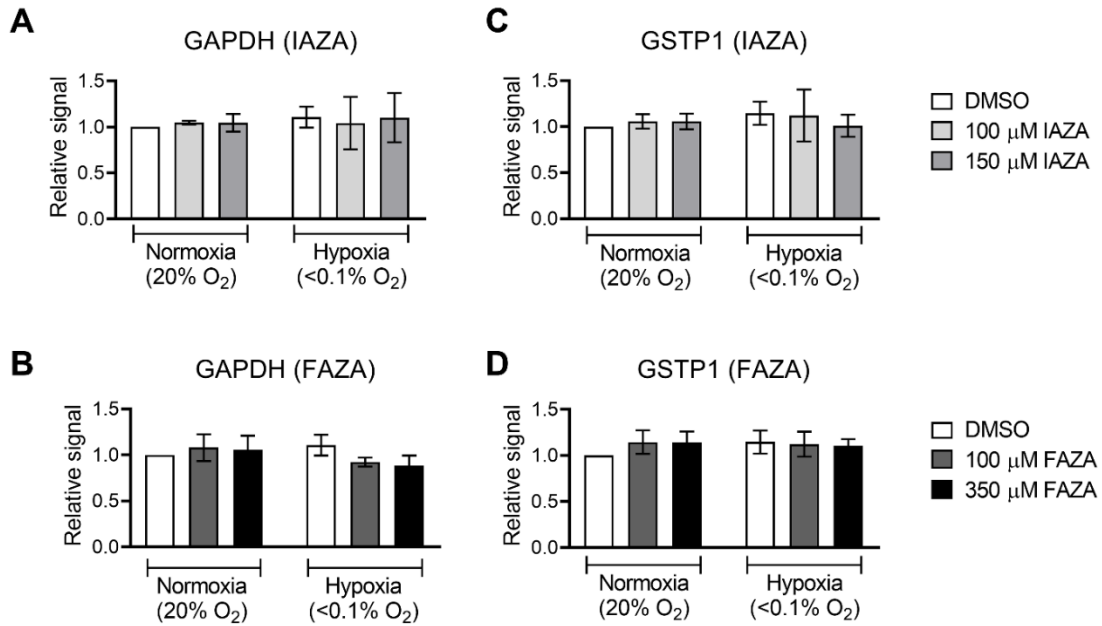
Supplementary Figure 3.2 IAZA- and FAZA-treated hypoxic cells have higher cyclin E1 levels, compromised DNA replication capacity even after reoxygenation, and show increased RPA retention.

Hypoxic cells treated with IAZA and FAZA had higher levels of cyclin E1, when compared to vehicle-treated hypoxic cells (A and B); a stronger signal in normoxic samples is probably reflective of more cells in late G1 phase (see Fig. 3A). Incorporation of EdU during reoxygenation and recovery was compromised in drug-treated cells (C). FaDu cells treated with IAZA (100 μ M), FAZA (100 μ M), hydroxyurea (5 mM) or vehicle control (0.02% DMSO) for 24 h under normoxia or hypoxia (<0.1% O₂) were processed for immunocytochemistry by probing for replication protein A2 (RPA). Salt-detergent extraction of cells prior to fixation ensures that only genomic DNA and any tightly bound proteins remain, while other cellular constituents are removed. Therefore, the resultant RPA staining represents chromatin bound RPA fraction (D). Quantification of nuclear RPA staining is shown in graph (E). Representative micrographs are shown; scale bar = 20 μ m (C and D); data represent mean \pm S.E.M. from three independent experiments.



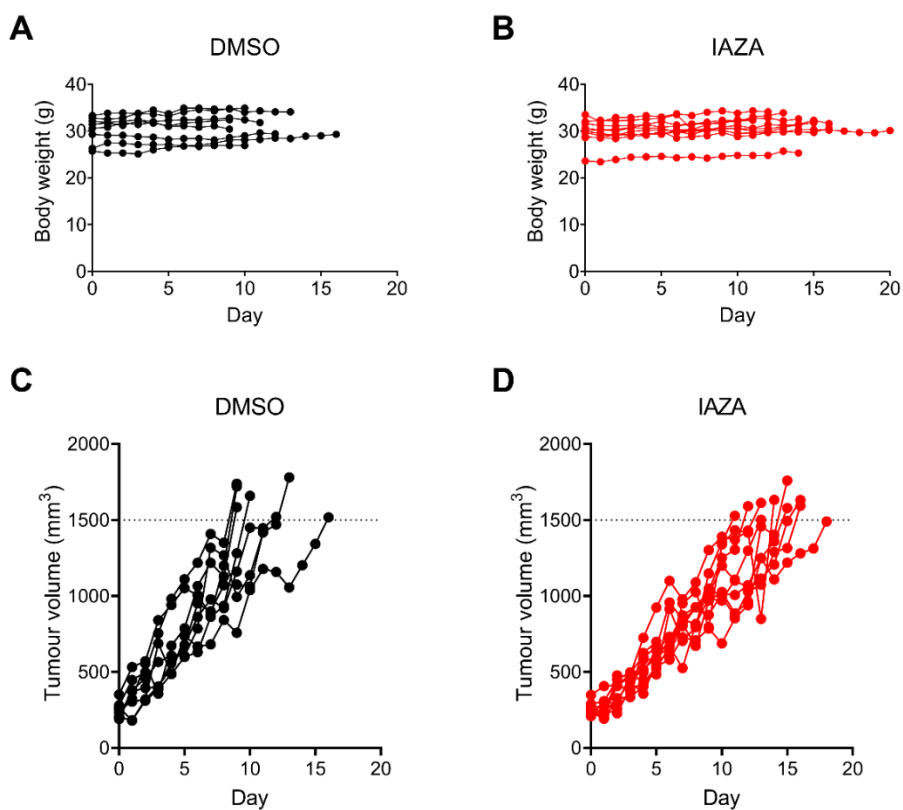
Supplementary Figure 3.3 Analysis of ROS generation in response to IAZA and FAZA treatment under hypoxia.

FaDu cells, preincubated with 3 mM NAC, were processed for the CVS staining assay with IAZA (A) and FAZA (B); cell viability did not change in response to NAC treatment. Experimental design for directly measuring cellular ROS levels (C); a full description of the experimental setup is provided in Materials and methods section. After addition of H_2O_2 substrate, if hypoxic drug-treated cells were placed back under hypoxia, a dose dependent non-significant increase in ROS levels were observed (D and E). Pre-incubation with 3 mM NAC decreased reoxygenation mediated ROS levels in IAZA-treated cells (F). Data show mean from three independent experiments; error bars represent S.E.M.



Supplementary Figure 3.4 Quantification of GAPDH and GST protein levels in IAZA and FAZA treated cells.

Extracts of FaDu cells treated with IAZA, FAZA or vehicle control (DMSO) were immunoblotted for GAPDH and GSTP1. Band intensities were measured using Image Studio lite and normalized to the vehicle-treated normoxic lane. No statistically significant differences were seen in GAPDH (A and B) and GSTP1 (C and D) protein levels in response to treatment. Data show mean from three independent experiments; error bars represent S.E.M.



Supplementary Figure 3.5 Monitoring individual mice for body weight, tumour growth and endpoint hypoxia.

NU/NU nude mice bearing subcutaneous FaDu tumours were injected i.p. with 400 mg/kg b.w. IAZA (or vehicle control, DMSO) once the tumours reached ~200-300 mm³. Body weight (A and B) and tumour volumes (C and D) were monitored daily, until the tumours reached a volume of ~1500 mm³, when mice were euthanized.

Chapter 4

Assessment of the Hypoxic Radiosensitization Potential of 2-Nitroimidazole Compounds, IAZA and FAZA, in a Head and Neck Tumour Model.

4.1 Introduction

Despite major advancements in the field of radiation biology and radiation delivery technologies in the last few decades, tumours often display resistance to radiotherapy (RT), leading to local disease recurrence (Kim, Hong et al. 2015). This is particularly challenging for managing malignancies (such as head and neck cancer, HNC) where RT, along with surgery (when possible), still remains the first line treatment (Yeh 2010). In advanced HNC cases, pre-treatment O₂ levels in tumours can alter the outcome of RT; HNC patients with poorly oxygenated (hypoxic) tumours fare poorly when treated with radiation or chemoradiation (Nordsmark, Overgaard et al. 1996, Stadler, Becker et al. 1999). Additionally, recurring HNC tumours are often more hypoxic, with partial O₂ pressure levels that are up to four-fold lower than that of non-recurring tumours (Brizel, Sibley et al. 1997). Taken together, these observations highlight the shortcomings present in current clinical management of HNC, which allow hypoxic cells to escape therapy.

Therapeutic targeting of hypoxic cancer cells requires special compounds capable of reaching and remaining in the diffusion limited tumour regions. Nitroimidazoles (NIs) are hypoxia selective agents that undergo bioreductive activation under low O₂, which allows them to preferentially accumulate in hypoxic cells (Kizaka-Kondoh and Konse-Nagasawa 2009). Long been in use for treating infections caused by anaerobic microbes, NIs caught renewed attention in 1970s with reports of their hypoxic radiosensitization potential (Chapman, Reuvers et al. 1973). However, despite showing promise in pre-clinical models, clinical trials with NIs were not particularly successful (Overgaard, Hansen et al. 1989, Lee, Cosmatos et al. 1995). Nonetheless, studies carried out by the Danish Head and Neck Cancer group reported an improved locoregional control and disease-free survival when advanced HNC patients were treated concurrently with nimorazole (a 5-NI) and RT (Overgaard, Hansen et al. 1998). Moreover, a meta analysis of 50 randomized NI clinical trials showed an overall improvement in patient outcome, particularly in HNC (Overgaard 1994). Collectively, these findings underscore the therapeutic value of NIs, at least in treating patients with HNC.

Iodoazomycin arabinofuranoside (IAZA) and fluoroazomycin arabinofuranoside (FAZA) are 2-NI compounds that, when radiolabelled, are capable of identifying hypoxic tumour regions

in clinical settings (**Fig. 3.1A and B**) (Souvatzoglou, Grosu et al. 2007, Postema, McEwan et al. 2009, Verwer, Bahce et al. 2014). Additionally, non-radiolabelled analogues of IAZA and FAZA have also shown promise as potential hypoxia directed therapeutics: they induced cytostasis in hypoxic HNC cells (discussed in **Chapter 3**), and sensitized hypoxic human hepatocellular carcinoma and colorectal cancer cells to IR, respectively (Kumar, Emami et al. 2009, Quan, Wang et al. 2015). However, radiosensitization potentials of these compounds in a HNC model have never been explored before. Therefore, this study aims to assess the therapeutic implications of combining IAZA or FAZA with RT, in HNC cell and animal models.

4.2 Materials and methods

4.2.1 Cell culture

A human head and neck squamous cell carcinoma cell line, FaDu, was purchased directly from American Type Culture Collection (Manassas, VA), expanded, and kept frozen in liquid nitrogen. Cells were cultured for a maximum of 2 months in DMEM/F-12 medium supplemented with 10% fetal bovine serum, 1% 2 mM L-glutamine and 1% penicillin streptomycin. Normoxic experiments were carried out in a humidified incubator at 37 °C with 5% CO₂. Hypoxia (<0.1% O₂) was induced using an in-house degassing/ regassing system equipped with metal canisters (Koch, Howell et al. 1979). Glass petri dishes were used to carry out hypoxic experiments in the canisters. Cells were routinely check for mycoplasma contamination.

4.2.2 Drug stock preparation

IAZA (Mannan, Somayaji et al. 1991) and FAZA (Kumar, Stypinski et al. 1999) were synthesized as described elsewhere. Stock solutions were prepared as 500 mM solutions in DMSO and stored at -20 °C.

4.2.3 Clonogenic survival assay

FaDu cells seeded in 60-mm glass petri dishes (at densities ranging from 300 to 10,000 cells per plate) were treated with vehicle control (0.02% DMSO) or drugs (100 µM) for 24 h under

normoxia or hypoxia (<0.1% O₂). Cells in radiation groups were irradiated (⁶⁰Co Gammacell, AECL, Chalk River, ON) 1 h prior to the end of the drug incubation. During radiation, cells were maintained in their respective O₂ conditions. Cells were then allowed to grow and form colonies in drug-free medium for 14 days under normoxia, after which colonies were stained with crystal violet, counted manually, and plotted as percentage of vehicle treated non-irradiated controls (under respective O₂ condition). For sensitizer enhancement ratio (SER) calculations, colony counts were plotted as percentage of respective non-irradiated vehicle or drug treated controls.

4.2.4 Immunofluorescence

FaDu cells grown on sterilized glass coverslips were treated with vehicle control or drug (100 μM) for 24 h under normoxia or hypoxia (<0.1% O₂); cells in the radiation group were irradiated with 5 Gy. Cells were fixed in 2% paraformaldehyde 1 h after irradiation. Fixed cells were blocked in 1% BSA for 20 min and probed with anti-phospho-histone H2A.X (Ser139) (γ-H2AX; 1:5000 dilution, 05-636, Millipore Sigma, Burlington, MA) followed by Alexa Fluor 488 conjugated anti-rabbit IgG (1:1000 dilution; Molecular Probes, Eugene, OR). Nuclei were counterstained with Hoechst 33342 (Life Technologies, Carlsbad, CA). Coverslips were mounted on glass slides, and imaged with a Plan-Apochromat 40X/1.3 Oil DIC lens on a Zeiss 710 confocal microscope using Zen 2011 software.

4.2.5 Alkaline comet assay

FaDu cells were treated as described above. Cells were harvested immediately after radiation in PBS by scraping, mixed with low melting point agarose, and spread on comet slides. Slides with solidified gels were put in lysis solution (4250-050-01, R&D systems, Minneapolis, MN) for 1 h followed by 1 h incubation in alkaline unwinding solution (200 mM NaOH, 2.5 mM EDTA) at 4 °C. To allow for DNA migration, slides were placed in an agarose gel apparatus containing alkaline electrophoresis buffer (200 mM NaOH, 1 mM EDTA), and current was applied at 21 V for 45 min. Slides were then rinsed twice in distilled H₂O, fixed with 70% ethanol for 5 min, and air dried before staining DNA with ethidium bromide (E7637, Sigma-Aldrich, Oakville, ON). Images were obtained with a digital upright 2 microscope (ZEISS

Axiolmager.Z1, Carl Zeiss, Jena, Germany), and comets were analyzed using CometScore™ software (TriTek Corp.).

4.2.6 Tumour growth delay assay

All animal experiments were carried out according to the protocols approved by the Cross Cancer Institute Animal Care Committee (protocol #AC18239) and following the Canadian Council on Animal Care guidelines. For tumour formation, 6×10^6 FaDu cells (in 0.1 ml serum-free medium) were injected in the upper right flank of male NU/NU mice. Tumours were measured with a Vernier caliper, and volume was determined by the formula: $(\pi/6)ab^2$, where a is the longest and b is the perpendicular shorter tumour axis. Once the tumours reached a volume between ~ 200 - 300 mm^3 , mice were injected intraperitoneally (i.p.) with either vehicle control (up to 15% DMSO v/v in 150 μl sterile water) or IAZA [400 mg/kg body weight (b.w.) in 150 μl DMSO: sterile water]. 2 h following injection, mice in the radiation group were anesthetized with isoflurane, placed lateral recumbent on the polystyrene bed with tumours facing upwards and Cone Beam Computed Tomography (CBCT) images were acquired. Using the MuriPlan software (Xstrahl), tumours were contoured, a three-beam treatment plan (equivalent to 10 Gy) was designed and delivered. Tumour volume and body weight were measured daily following treatment, and mice were sacrificed when tumours reached a volume of $\sim 1500 \text{ mm}^3$. 2 h prior to sacrifice, mice were injected i.p. with N_3 -AZA (60 mg/kg b.w.). After euthanization, tumours were excised and flash frozen in optimal cutting temperature compound (O.C.T., 4585, Fisher Scientific, Waltham, MA). Endpoint hypoxia levels were determined by N_3 -AZA click staining on central sagittal tumour sections, as described previously (Rashed, Stoica et al. 2021).

4.2.7 Data processing and statistics

Adobe Photoshop (Adobe Inc., San Jose, CA) was used to adjust for brightness and contrast, to add scale bars, and for rearrangement and labelling in microscopic images. γ -H2AX staining intensity within the nucleus was quantified with IMARIS software (Bitplane, Zürich, Switzerland) using Hoechst staining as a nuclear mask. Intensity values were divided into arbitrary intervals, plotted on the x axis and the percentage of cells with intensity levels that fall within that range were plotted on the y axis. On the resultant histogram, a maximum threshold was chosen so that the intensity of $\sim 95\%$ of cells in the vehicle treated non-irradiated normoxic

sample fall below this threshold. Percentage of cells above this threshold was considered positive for γ -H2AX. GraphPad Prism V7 (GraphPad Software, La Jolla, CA) was used to generate graphs and to perform statistical analysis. Graphs display the mean with standard error of the mean (S.E.M.). The 2-tailed unpaired t-test was used for statistical analysis, with $p < 0.05$ considered statistically significant. Asterisks depict statistically significant differences: ns (not significant), * ($P \leq 0.05$), ** ($P \leq 0.01$), *** ($P < 0.001$) and **** ($P < 0.0001$).

4.3 Results

4.3.1 IAZA and FAZA sensitize hypoxic cells to ionizing radiation.

Colony formation assays were performed to test cellular response to IAZA and FAZA (100 μ M), alone or in combination with ionizing radiation (IR, 5 Gy). As reported earlier in **Chapter 3**, hypoxic cells displayed preferential sensitivity towards 2-NIs treatment. Hypoxic incubation with IAZA or FAZA (100 μ M, 24 h) decreased colony counts by ~50% and ~25%, respectively; no effects were seen under normoxia (**Fig. 4.1C**). As expected, hypoxic cells were >2 times more resistant to IR than their normoxic counterparts. Combining IAZA or FAZA with radiation reversed this resistant phenotype. IAZA treated hypoxic irradiated cells showed a significant reduction in clonogenicity (~17%) when compared to vehicle treated hypoxic irradiated cells (~50%); colony counts in the former was similar to the normoxic irradiated group (~20%). Hypoxic cellular response to FAZA+ IR was relatively modest (~37%). These effects, however, appeared to be mostly additive. At higher radiation dosage, IAZA showed a respectable hypoxic radiosensitization with an SER value of 1.41 (**Fig. 4.1D**). FAZA treatment (100 μ M) under hypoxia generated an SER value of 1.09 (**Fig. 4.1E**).

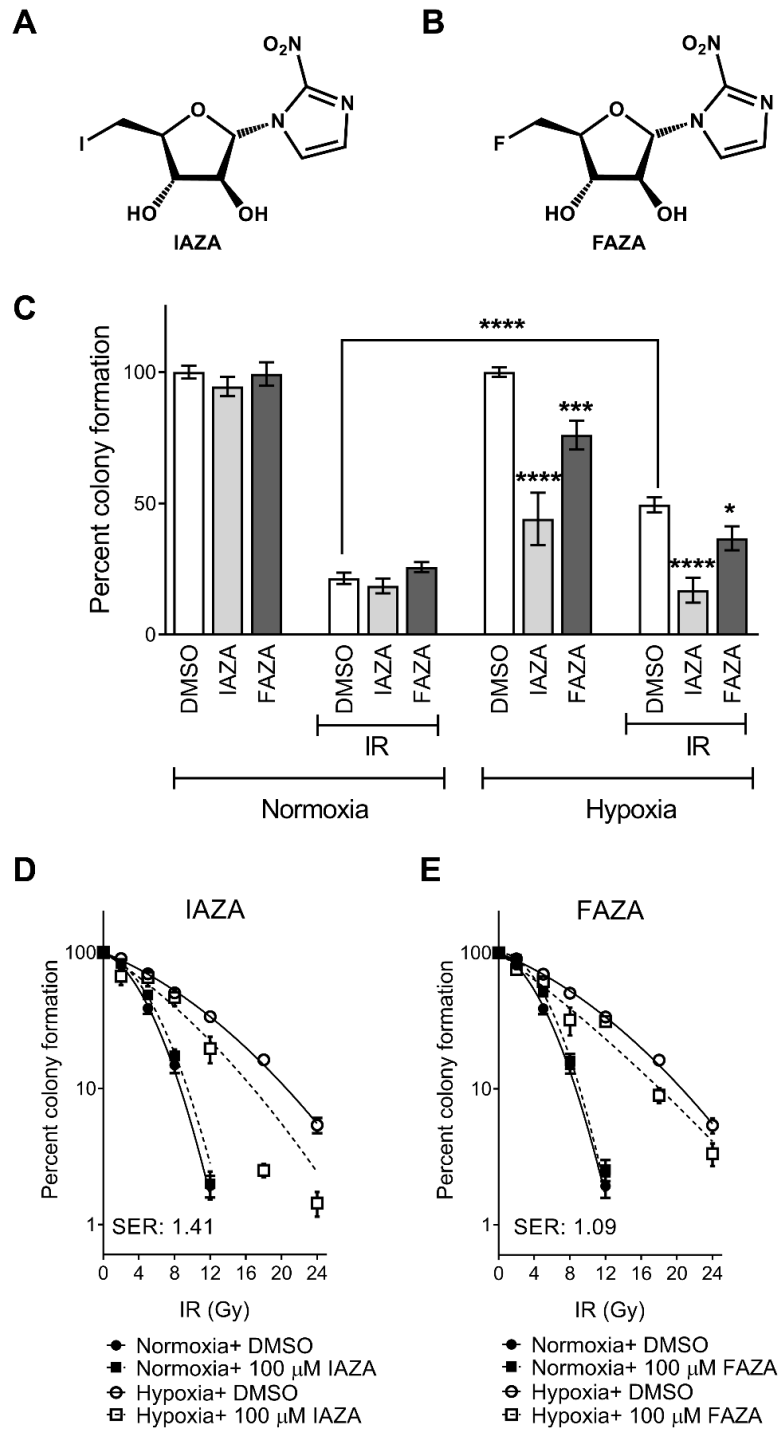


Figure 4.1 IAZA and FAZA sensitize hypoxic FaDu cells to IR.

Chemical formula for IAZA (**A**) and FAZA (**B**). IAZA and FAZA (at 100 μ M concentration) significantly reduced clonogenicity in hypoxic irradiated cells (**C**). Sensitization by IAZA and FAZA appear to be synergistic at higher radiation dosage; calculation of sensitizer enhancement ratios (SER) for IAZA (**D**) and FAZA are shown (**E**). Data show mean from at least three independent experiments; error bars represent standard error of the mean (S.E.M.).

4.3.2 IAZA and FAZA increase DNA damage in hypoxic irradiated cells.

To test if co-treating hypoxic cells with drugs and IR increases DNA damage, we performed immunofluorescent staining for phosphorylated histone 2A (γ -H2AX) as a readout of DNA double strand breaks. Hypoxic irradiated cells (5 Gy) showed a significant decrease in γ -H2AX positive population when compared to their normoxic counterparts, confirming the resistance of hypoxic cells to IR (**Fig. 4.2A** and **4.B**). Interestingly, IAZA treatment under hypoxia alone generated an increase in γ -H2AX positive population similar to that seen in the hypoxia radiation only group (~30%). Furthermore, combined treatment with IAZA and IR under hypoxia increased the γ -H2AX population to ~60%. Hypoxic cells treated with FAZA alone and in combination with IR consisted of ~17% and 56% γ -H2AX positive population, respectively (**Fig. 4.2C**). These observations were further validated by single cell gel electrophoresis (alkaline comet assay) that directly measures the structural integrity of cellular DNA. Radiation-induced DNA damage was significantly lower under hypoxia than normoxia, which was evident from a 50% reduction in comet tail moment seen in the hypoxic radiation group (**Fig. 4.2D**). In agreement with the γ -H2AX data, IAZA alone and in combination with IR showed a significant increase in comet tail moment, with the later generating DNA damage similar to the normoxic irradiated cells. While FAZA alone under hypoxia did not generate any observable DNA damage in comet assay, combination of FAZA with radiation under hypoxia significantly increased DNA damage when compared to hypoxic irradiated cells.

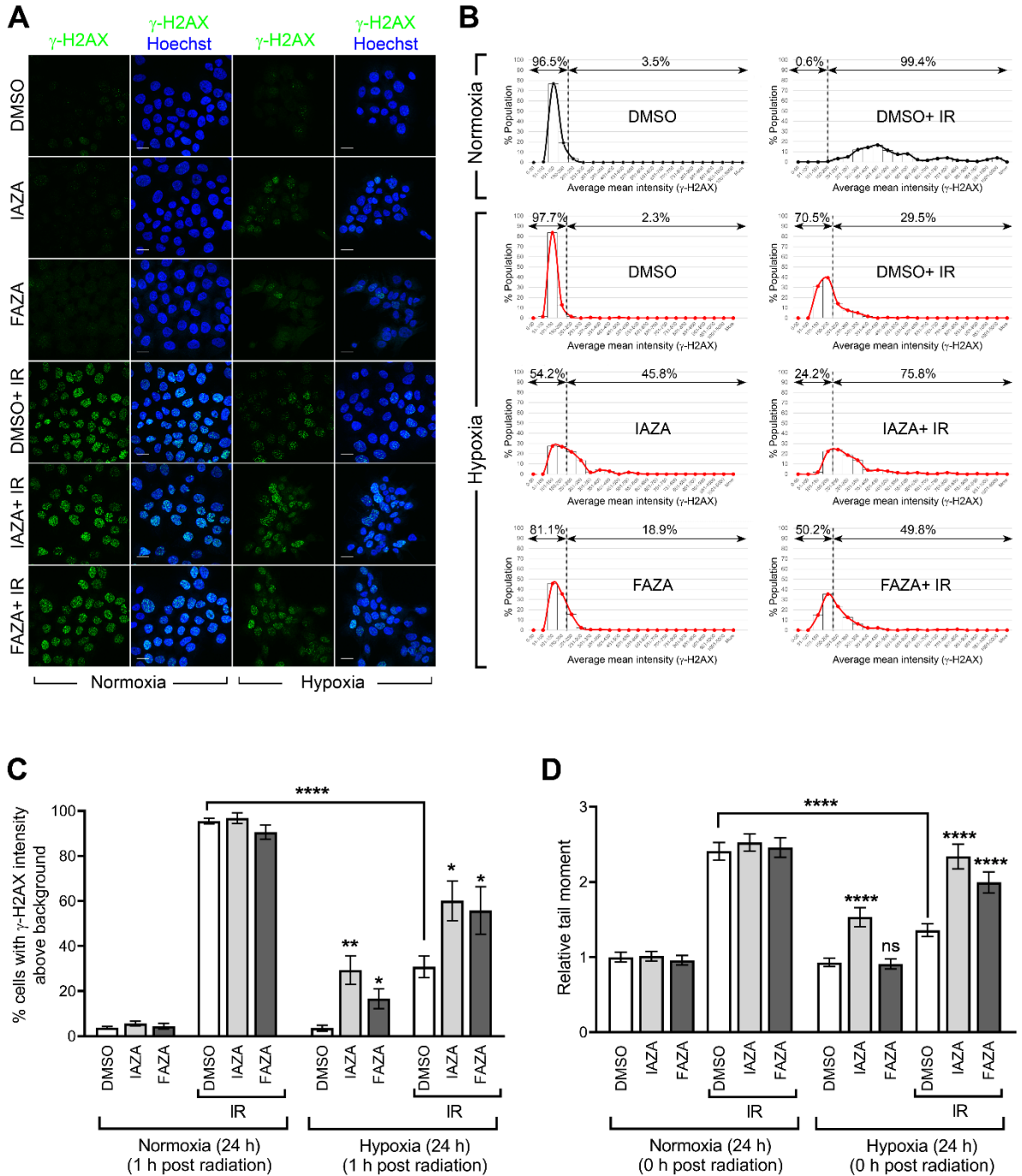


Figure 4.2 Co-treatment of IAZA or FAZA with 5 Gy IR increases DNA damage only under hypoxia.

(A) Representative micrographs showing immunofluorescent staining of γ -H2AX in FaDu cells treated with vehicle control (DMSO) or drugs (IAZA or FAZA; 100 μ M), with or without IR (5 Gy), under normoxia and hypoxia (<0.1% O_2). (B) Representative histograms showing quantification of γ -H2AX staining intensity. (C) IAZA and FAZA treatment increases percentage of γ -H2AX positive population in hypoxic irradiated samples. (D) Alkaline comet assay shows significant increase in DNA damage in hypoxic drug treated irradiated cells. Data show mean \pm S.E.M. (C and D); scale bar = 20 μ m.

4.3.3 A single i.p. administration of IAZA with a single irradiation of 10 Gy did not improve therapy outcome in FaDu tumour bearing mice.

Efficiency of IAZA as a hypoxic radiosensitizer was assessed in NU/NU nude mice bearing subcutaneous FaDu tumours. Mice were given a single intraperitoneal injection of IAZA (400 mg/ kg b.w.) or vehicle control, and tumours were irradiated with a single 10 Gy fraction (**Fig. 4.3A**). RT was performed with a Xstrahl-Small Animal Radiation Research Platform (SARRP), ensuring a realistic model of clinical RT plan (**Fig. 4.3B**). Growth of tumour, body weight and animal survival were monitored; data for individual animals are shown in **Fig. 4.4**. Effects of single i.p. administered IAZA on growth of subcutaneous FaDu tumours have been discussed elsewhere (**Chapter 3**). An excellent tumour growth control was seen with radiation, but no additional benefits were observed with combining IAZA with RT (**Fig. 4.3C**). Similarly, while radiation alone resulted in ~3 fold increase in survival (**Fig. 4.3E**), addition of IAZA to RT at the tested dose did not generate any additional therapeutic advantage (**Fig. 4.3D**). Ultimately, all tumours in the radiation group recurred, and grew to the terminal volume (1500 mm³). These tumours had somewhat lower levels of endpoint hypoxia (14.11±2.8% in DMSO+IR and 12.8±2.8% in IAZA+IR) than the vehicle treated group (17.31±2.4%) (**Fig. 4.3F**), although these differences were not statistically significant (**Fig. 4.3G**).

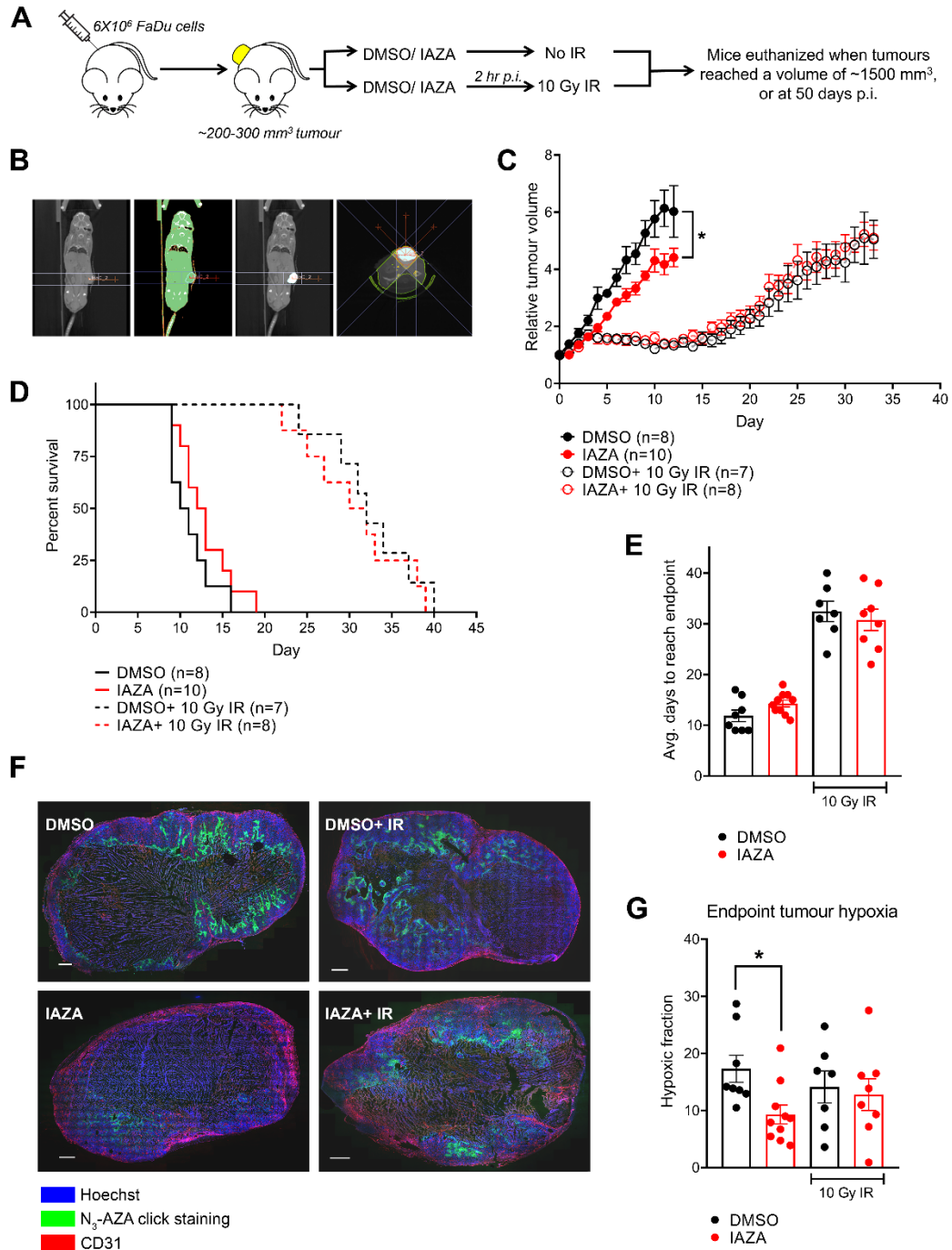


Figure 4.3 *In vivo* evaluation of IAZA as a hypoxic radiosensitizer.

(A) Study design for the *in vivo* experiment. NU/NU nude mice bearing subcutaneous FaDu tumours (~200-300 mm³) were injected i.p. with a single dose of IAZA (400 mg/kg b.w.) or vehicle control (DMSO); 2 h post injection, tumours were irradiated with 10 Gy IR using a SARRP. (B) Cone beam CT images were used to contour the tumours and design RT plan. (C) Relative tumour volumes are shown following treatment. Animals were sacrificed when tumours reached a volume of ~1500 mm³. (D) The Kaplan Meier curve shows survival trend of mice. (E) Average days it took for animals in each group to reach endpoint are shown. (F) N₃-AZA click staining on central sagittal tumour sections depicts endpoint hypoxia levels in different treatment groups. (G) Quantification of endpoint hypoxia levels in tumours. Data show mean ± S.E.M.

4.4 Discussion

IAZA and FAZA are 2-NI-based hypoxic radiotracers that have been clinically validated in different human malignancies, including cancers of head and neck (Urtasun, Parliament et al. 1996, Souvatzoglou, Grosu et al. 2007). Our group has previously shown that both compounds selectively prevent proliferation of hypoxic HNC cells (FaDu), and IAZA reduced tumour hypoxia levels in subcutaneous mouse tumours (**Chapter 3**). However, whether these compounds can also make hypoxic HNC cells and tumours sensitive to RT is not known. To address this question, clonogenic survival assays were performed with FaDu cells treated with drug and radiation, under normoxia and hypoxia (<0.1% O₂). A relatively low concentration of drugs (100 µM) was used for our assays because (a) we believe this would be reflective of clinically achievable dose, and (b) it would allow us to avoid concentration ranges that might induce clinical neurotoxicity as reported with other NIs (Overgaard, Hansen et al. 1989). Combining IAZA or FAZA with 5 Gy IR under hypoxia significantly reduced colony formation when compared to vehicle-treated hypoxic irradiated cells (**Fig. 4.1C**). In fact, hypoxic cells co-treated with IAZA and IR (5 Gy) showed similar clonogenicity as normoxic irradiated cells. Radiosensitization of hypoxic cells by IAZA and FAZA at 5 Gy IR generated mostly additive benefits, as the combined effects of drug and radiation was not greater than the cumulative effects of individual treatments. In fact, synergy only appeared when drug treated hypoxic cells were exposed to higher IR dosage: 12 Gy and up for IAZA, and 18 Gy and up for FAZA (**Fig. 4.1D and E**). The SER value for IAZA (1.41) indicates that it is a better radiosensitizer than FAZA (SER 1.09), at the concentration tested. Importantly, no effects were seen under normoxia with this treatment combination.

Induction of DNA damage is widely used as a readout for efficacy of RT treatment. IR is often ~2-3 times less efficient at inducing DNA damage under hypoxia than normoxia (Brown and Wilson 2004). Our data are in agreement with these observations and show that hypoxic FaDu cells responded poorly to IR (5 Gy) (**Fig. 4.2**). Using a surrogate marker for DNA double strand breaks (γ -H2AX), we found that the percentage of cells containing IR-induced DNA damage under hypoxia is almost one third of that seen under normoxia for the same radiation dose (**Fig. 4.2B and C**). Further validation comes from the direct assessment of DNA damage (using the alkaline comet assay) that showed almost 50% reduction in comet tail moment under hypoxia

when compared to its normoxic counterpart (**Fig. 4.2D**). In both assays, addition of IAZA or FAZA to IR under hypoxia significantly increased DNA damage, suggesting these compounds can potentiate the damaging effects of IR under hypoxia.

Given that the hypoxic radiosensitization effects of IAZA were more prominent than FAZA in cell-based studies, animal experiments were only performed with IAZA to test its effects on external beam RT in a subcutaneous tumour model of HNC. We previously identified 400 mg/kg b.w. i.p. dose of IAZA to be a well tolerated in NU/NU mice (**Chapter 3**). A radiation dose of 10 Gy was chosen based on radiation induced regression trend of subcutaneous FaDu tumours reported earlier (Zhu, Ruan et al. 2018). RT was delivered using a SARRP to best resemble the clinical delivery of radiation (**Fig. 4.3B**). RT treated tumours did not increase in volume for ~15 days post treatment, after which, tumours eventually recurred (**Fig. 4.3C**). No additional tumour regression was seen by combining IAZA with RT. Tumours in both groups took a similar time to grow up to the endpoint volume (**Fig. 4.3E**), resulting in no difference in survival (**Fig. 4.3D**). While these observations are not encouraging, several factors must be taken into account for a justified conclusion and interpretation of the data. Firstly, successful *in vivo* radiosensitization reports with 2-NIs often used a higher IR dosage, such as 15 Gy for doranidazole (Koike, Kota et al. 2020) and 30 Gy for glycididazole (Yasui, Kubota et al. 2018). *In vitro* hypoxic radiosensitization with IAZA also showed synergy only when cells were exposed to IR equivalent to 12 Gy and up (**Fig. 4.1D**). Thus, using a higher RT dose plan might prove to be more successful. More importantly, this study only explored the effects of a single dose of IAZA, while in clinical practice, chemical doses of the radiosensitizers are usually administered over multiple treatment sessions, both before and after RT. No significant differences in endpoint hypoxia levels were observed between the vehicle-treated and IAZA-treated recurring tumours (**Fig. 4.3G and F**). This suggests that the intracellular levels of IAZA had reduced below the therapeutically effective concentration by this time, most likely through metabolization and pharmacokinetic elimination. Considering the time frame when the irradiated tumours started growing back (~15 days post-RT), additional IAZA administrations would certainly be required to determine if curative effects are exerted on the hypoxic core of these recurring tumours. This is in line with a recent observation reporting significant residual hypoxia levels 2 week post-RT in HNC, which was predictive of patient outcome (Löck, Perrin et al. 2017).

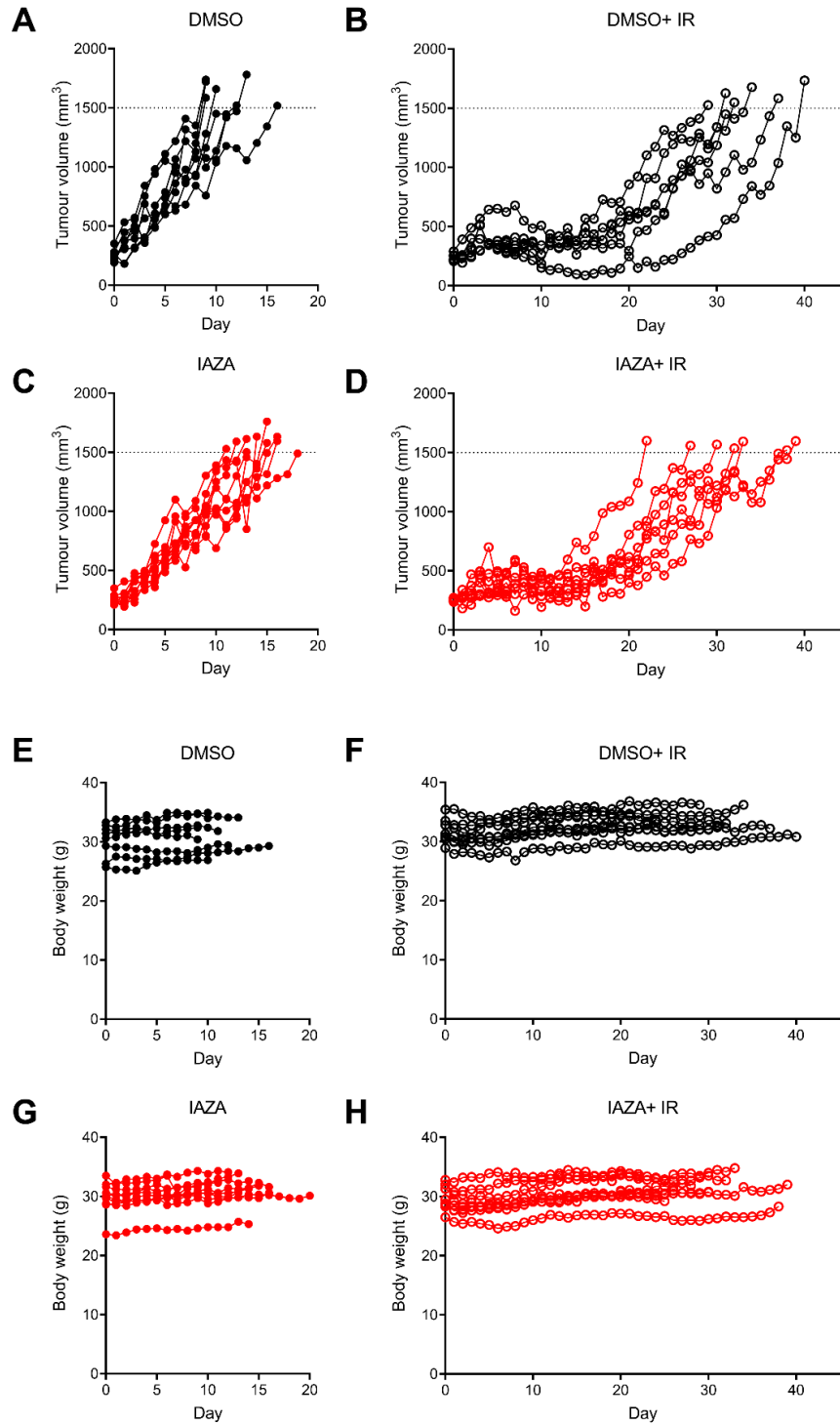


Figure 4.4 Monitoring individual mice for body weight, tumour growth and endpoint hypoxia.

NU/NU nude mice bearing subcutaneous FaDu tumours (~200-300 mm³) were injected i.p. with a single dose of IAZA (400 mg/kg b.w.) or vehicle control (DMSO); 2 h post injection, tumours were irradiated with 10 Gy IR using a SARRP. Animals were sacrificed when tumours reached a volume of ~1500 mm³. Tumour volumes (A-D) and body weights (E-H) of individual mice are shown.

In conclusion, a low dose of IAZA and FAZA can selectively sensitize hypoxic HNC cells to IR, although these effects are only additive if an insufficiently high radiation dose is used. At same concentrations, IAZA is a better hypoxic radiosensitizer than FAZA. Administration of a single i.p. dose of IAZA combined with a 10 Gy RT treatment plan did not improve therapy outcome in mice, suggesting multiple drug doses, as followed in clinical therapy practices, might be necessary to show therapeutic benefits.

Chapter 5

Discussion and future directions

Tumour hypoxia poses a significant challenge for effective radiotherapy, conventional chemotherapy and immunotherapy [reviewed in (Walsh, Lebedev et al. 2014)]. It is thus crucial to target and eliminate hypoxic tumours to improve patient outcome. Nitroimidazoles (NIs), such as nimorazole, can provide clinical benefit if given to patients who present with hypoxic tumours. However, a lack of mechanistic studies has made it difficult to further improve upon these compounds as potential hypoxia-targeted therapeutics. Furthermore, pre-clinical research with NIs often use unusually high chemical dosage (in the millimolar range), which consequently translates poorly in clinical settings. Given that (a) anti-cancer drugs are administered in multiple doses, and (b) multiple high doses of NIs induce neurotoxicity, it is necessary to study the biological implications of NI treatment at physiologically relevant dosage (micromolar ranges). Therefore, the current research explored the cellular fate induced by lower dose treatment with two 2-NI compounds, IAZA and FAZA. We aimed to identify the key cellular players that may mediate cellular sensitivity to NI treatment under hypoxia, and thereby offer insights into their potential mechanism(s) of action.

Hypoxic cells showed preferential sensitivity towards IAZA and FAZA treatment (**Fig. 3.1**), however, the cells did not die or become senescent in response to drug treatment at 100 μ M concentration (**Fig. 3.2**). This concentration was chosen so that the toxic effects of the drugs are only limited to hypoxic cells with no visible effects under normoxia, and was determined by cell viability and clonogenicity assays. Interestingly, treating cells with IAZA and FAZA under hypoxia affected DNA replication (**Fig. 3.3D** and **E**), which caused a delay in S phase progression (**Fig. 3.3A**). As a consequence, cell growth rates were significantly reduced (cytostasis) in drug-treated hypoxic cells, even after treatment had ended (**Fig. 3.2I** and **J**). The inhibitory effects seen on DNA synthesis in the present study are in agreement with earlier findings, where NIs (such as metronidazole and tinidazole) disrupted DNA synthesis in anaerobic bacteria *Bacteroides* and *Clostridium* (Plant and Edwards 1976, Sigeti, Guiney Jr et al. 1983). However, questions still remain as to how IAZA and FAZA can inhibit DNA replication. DNA polymerase activity is not known to be affected by NIs (Sigeti, Guiney Jr et al. 1983), and therefore, was not explored in this study. Instead, cell cycle analysis, PCNA and cyclin E1 immunostaining results suggest that IAZA- and FAZA-treated hypoxic cells most likely stall at early to mid S phase (**Fig. 3.3**, **Suppl. Fig. 3.2**). This points towards an impairment of DNA synthesis that may arise from a lack of available nucleotides. It is important to mention

here that IAZA and FAZA are structural nucleoside analogues, where the pentose sugar (like that of nucleosides) is attached to the NI moiety through ring nitrogen (**Fig. 1.5**). While NIs are largely considered to enter cells through passive diffusion, the close structural homology of IAZA and FAZA with nucleosides may additionally enable them to be transported via nucleoside transporters as well. While this has not been proven experimentally, Maier et al. reported that FAZA can bind to human concentrative nucleoside transporters (hCNT1-3), and thereby prevent cellular uptake of nucleosides (Maier, Schweifer et al. 2019). Similarly, we saw a significant reduction in EdU uptake (a nucleoside analogue) in IAZA- and FAZA-treated hypoxic cells (**Fig. 3.3D and E**), suggesting that the cellular capacity for efficient nucleoside uptake was disrupted by these compounds under hypoxia. Based on these reports and my data, we, therefore, predict that the binding of these 2-NI compounds to hCNT transporters may compete with or completely block nucleoside transport, which may lead to dampened DNA synthesis rates observed in these cells. Such interactions will probably only be limited to sugar coupled NIs that structurally resemble nucleosides. A point to be noted here is that it is yet to be established if NIs need to be bioreductively activated to bind to nucleoside transporters, or the binding can occur with the parent molecule. While we observed reduced EdU uptake only in hypoxic cells, Maier et al. reported the binding under normal O₂ conditions (using *Saccharomyces cerevisiae* with recombinant human nucleoside transporters) (Maier, Schweifer et al. 2019). Nevertheless, data from the present study suggest that binding to hCNT transporters is likely increased when the compound is bioreduced, further exacerbating their inhibitory effects on nucleoside transport. Functional studies, for example cell-free nucleoside transport assays with hCNT proteoliposomes (Huang, Zeng et al. 2017), can be used to provide additional insights into this mechanism. The cryo-EM structure for hCNT3 has recently been described (Zhou, Liao et al. 2020), which will allow to perform molecular docking studies to calculate their binding potentials with IAZA and FAZA. Additionally, the impacts of hypoxia selective entrapment of NIs on cellular nucleotide biosynthesis pathway needs to be explored as well since any irregularities in this pathway in response to IAZA/FAZA treatment might offer an alternative explanation for the observed phenotype. Overall, we found that impairment of DNA synthesis in IAZA- and FAZA-treated hypoxic cells generated replication stress, as is evident from increased chromatin bound RPA staining (**Suppl. Fig. 3.2D and E**), and nascent fork degradation in DNA fibre assay (**Fig. 3.3G and H**).

While activated NIs are known to form adducts with cellular components (DNA, proteins and glutathione) under hypoxia, the biological implications of this phenomenon with regard to NI mechanism of action is poorly understood. Hence, to study the cellular macromolecules targeted by NIs for adduct formation in hypoxic cells, a novel “click chemistry” compatible 2-NI compound, azidoazomycin arabinofuranoside (N_3 -AZA), was synthesized (**Fig. 2.1A**). This compound is a structural homolog of IAZA and FAZA with a 2-NI moiety that enables its selective accumulation in hypoxic cells, while its azido (N_3) group can react with an alkyne molecule in a copper (I) catalyzed click chemistry reaction. N_3 -AZA click chemistry allows for direct labelling of NI-adducts formed in hypoxic cells without using conventional antibody-based methods, and thereby supports versatile applications by using different kinds of alkyne molecules, such as biotinylated alkynes for adduct isolation and fluorescent alkynes for adduct visualization. Three different applications of this technique are outlined in this thesis and discussed briefly throughout this chapter.

Firstly, N_3 -AZA click chemistry was utilized to characterize the nature of NI-DNA adduction. For this, we modified a trapped in agarose DNA immunostaining (TARDIS) assay to incorporate N_3 -AZA click staining instead of immunological detection. The original TARDIS assay was developed to quantify melphalan- and cisplatin-DNA adducts, and was later adapted for identification of topoisomerase-DNA complexes (Cowell, Tilby et al. 2011). In the TARDIS assay, cells immobilized in low melting point agarose gel are subjected to detergent lysis and high-salt extraction that only leaves behind DNA and covalent adducts, which are then detected using antibodies specifically developed to recognize the adducts. In the modified assay (termed trapped in agarose DNA click staining, or TARDICS), the N_3 -AZA adducts can be directly visualized with a fluorescently tagged alkyne by using the click chemistry principle. Fluorescent covalent adducts of N_3 -AZA were only detected in hypoxic cells, proving the precision of our technique (**Fig. 3.4A and B**). In addition to the standard lysis and salt treatment, DNase I and proteinase K treatments were incorporated into the assay to determine if NI-DNA and NI-protein adducts are covalent in nature. Interestingly, covalent N_3 -AZA-adducts were still present after DNase I treatment but disappeared when immobilized cells were subjected to proteinase K. This suggests that under hypoxia, N_3 -AZA (and in extension, IAZA and FAZA) forms covalent adducts only with proteins, and not with DNA. While our findings contradict prior data suggesting that NIs form covalent adducts with DNA (Varghese and Whitmore 1983),

it does not rule out binding of NIs to DNA through other, weaker types of chemical bonds, such as through hydrogen bonding and electrostatic interaction as shown by Ahmadi et al. (Ahmadi, Shabrandi et al. 2019).

Since NI treatment, at high doses, has often been reported to directly induce DNA damage, the effects of IAZA and FAZA treatment, at 100 μ M concentration, on DNA integrity was tested. Fluorescent staining for γ -H2AX, a surrogate marker for DNA double strand breaks, was significantly increased in IAZA and FAZA treated hypoxic cells (**Fig. 3.4C-E**). However, when DNA damage was directly measured by the alkaline comet assay, a more modest increase was seen only with IAZA under hypoxia; FAZA-treated cells did not show any increase in comet tail moment (**Fig. 3.4F**). Therefore, we conclude that the effects of low dose treatment of NIs on DNA damage is minimal, and the increase in γ -H2AX staining observed in our experiments was most likely generated from the induction of replication stress. Further confirmation came from the observation that IAZA and FAZA treatment did not result in any significant increase in ROS levels under hypoxia (**Suppl. Fig. 3.3 D and E**). However, when drug-treated hypoxic cells were allowed to reoxygenate, levels of ROS drastically increased (**Fig. 3.4G and H**). This points towards enhanced susceptibility of drug-treated hypoxic cells to reoxygenation, which may have implications for solid tumours that undergo cyclic hypoxia.

Given that NIs formed stable covalent adducts only with proteins under hypoxia, we sought to isolate and identify these protein targets to assess how covalent binding with NIs may affect target protein stability and functions. To do so, N₃-AZA click chemistry was applied with a biotin-tagged alkyne. The resultant biotinylated NI-adducts were then isolated using streptavidin-mutated beads, and the eluates were analyzed with liquid chromatography coupled mass spectrometry (**Fig. 2.1F and G**). Overall, 62 protein targets were identified to bind covalently with N₃-AZA (**Table 2.1**), which were then categorized based on cellular localization, function, and the biological processes they are involved in (**Suppl. Fig. 2.2C**). In general, the propensity of NI-binding to proteins appeared to be dictated by their cellular abundance, although certain exceptions to this trend were also present (**Fig. 2.2C**). Proteins involved in several important pathways (such as glycolysis, HIF1A signaling, unfolded protein response etc.) appeared to be targeted by NIs (**Table 2.2**), which may have direct consequences for hypoxic cell viability. The effects of NI-binding on the glycolytic enzyme GAPDH and

detoxification enzyme GSTP1 were analyzed in terms of total protein levels, cellular distribution patterns, and enzymatic function. Interestingly, NI treatment only affected their catalytic activities under hypoxia, and these effects were not due to proteolysis or altered cellular localization (**Fig. 2.3** and **3.5A-F**). The fractions of total cellular GAPDH and GST pool that bind to NIs were analyzed, and it was predicted that at 100 μ M concentration of N₃-AZA, at least ~40% of GAPDH and ~57% of GSTP1 protein formed NI-covalent adducts (**Suppl. Fig. 2.4** and **2.5**). Since inactivation of these proteins have previously been reported to affect cell viability, these observations offer a potential explanation for NI mediated sensitivity seen in hypoxic cells. It is important to note here that apart from GAPDH and GST, a rigorous investigation of the remaining 60 protein targets of NIs was not performed in this study. This leaves a caveat in the interpretation, and the effects of NI binding to target proteins are likely to be considerably more complex than what is presented here. While the case for studying the impact of NI binding on peroxiredoxin-1 (Prdx1) has been highlighted in **Chapter 2**, other target proteins that were identified, such as ribosomal proteins (RpL4, RpSA, RpS3), translation machinery proteins (eIF4AII, eEF1AI), chaperon proteins (PPIB, PDI, Hsp60, Hsp70, Hsp90), cytoskeletal proteins (actin, tubulin) etc., have the potential to directly or indirectly contribute to the observed hypoxic sensitization by NIs. Therefore, a thorough investigation of these targets is required to conclusively identify how NI binding to proteins may mediate cell sensitization under hypoxia. Moreover, it is possible that NIs function by simultaneously targeting proteins in different pathways as well as the DNA replication machinery, and thus the observed phenotype is likely a combination of global disruption in many different cellular processes. A proposed model for NI mechanism of action, derived from these results, is shown in **Figure 5.1**.

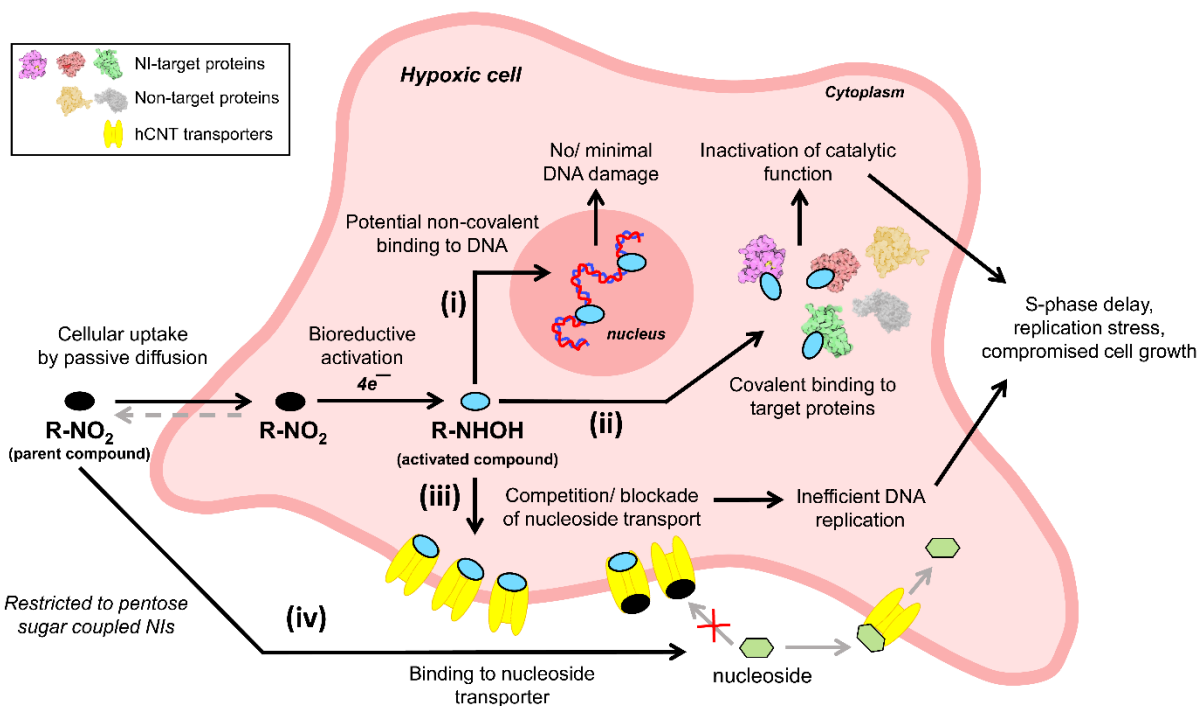


Figure 5.1 Potential mechanism of action for IAZA and FAZA (and by extension, for other 2-NIs in general)

(i) Bioreduced 2-NIs do not form covalent adducts with DNA, but there is indication that they may bind to DNA through non-covalent interactions; minimal to no DNA damage is observed as a consequence of such interactions. (ii) Activated NIs covalently bind to cellular proteins, and there is possibly some degree of specificity to these attachments. Covalent binding of NIs does not affect target protein stability or localization, but has the potential to limit their catalytic activities. (iii and iv) Pentose sugar coupled 2-NIs reduce intracellular nucleoside transport, most likely through binding to nucleoside transporters (hCNT1-3) and subsequently competing with or blocking nucleoside transport by them. Although it is not clear if such binding requires bioreduction, hypoxic activation of NIs strongly dampens nucleoside uptake (perhaps due to higher binding of drug to hCNT transporters). The observed hypoxia selective sensitization, evident through delay in S phase progression, induction of replication stress and reduced cell growth, is likely an outcome of all these events combined.

Many NIs have previously been reported to sensitize hypoxic cancer cells to ionizing radiation (IR). Therefore, the potential of IAZA and FAZA as hypoxia selective radiosensitizers in FaDu cells (a head and neck cancer model) was explored. Using the colony formation assay, it was found that both IAZA and FAZA reduced clonogenicity in hypoxic cells in response to 5 Gy IR, however the effect appeared to be additive (**Fig. 4.1C**). Synergy between drug and IR was only observed when hypoxic cells were irradiated with higher RT dosage (≥ 12 Gy for IAZA and ≥ 18 Gy for FAZA) (**Fig. 4.1D and E**). While this may limit the utility of IAZA or FAZA in conventional fractionated radiation treatment plans, it alternatively offers the possibility of using these compounds with high dose radiation treatment plans, such as stereotactic body radiotherapy (SBRT) or with dose painting strategies. Effects of combining IAZA/FAZA with IR on DNA damage was also explored in this project. When analyzed for IR induced DNA damage using γ -H2AX and alkaline comet assay, a statistically significant increase in DNA damage was observed in both IAZA and FAZA treated hypoxic irradiated cells (**Fig. 4.2**).

Our analysis identified IAZA to be a better hypoxic radiosensitizer than FAZA, and therefore, studies to explore the feasibility of using IAZA as a therapeutic agent were pursued in mouse models. Firstly, a safe dose for IAZA was identified with a dose escalation study with NOD/SCID/IL2R mice injected intraperitoneally (i.p.) with 3 different chemical doses of IAZA [200, 400 or 600 mg/kg body weight (b.w.)]. All the doses were relatively well-tolerated, and no adverse effects were observed on body weight, blood chemistry and tissue sections (**Fig. 3.6A and B, Suppl. Table 3.1**). Mice injected with the highest IAZA dose (600 mg/kg) showed only a temporary lethargic reaction but recovered within 30 min of injection. Therefore, for subsequent *in vivo* studies exploring radiation response, IAZA was used at a chemical dose of 400 mg/kg b.w. For radiation response analysis, NU/NU nude mice bearing subcutaneous FaDu tumours were injected i.p. with a single chemical dose of IAZA (or vehicle control) when the tumour volumes reached between 200-300 mm³, followed by a single dose of 10 Gy radiation 2 h post injection. To more closely mimic clinical radiation therapy (RT), external beam radiation was delivered using the small animal radiation research platform (SARRP) that allows for precise delivery of RT to the tumour while minimizing off target effects. Unirradiated mice injected with vehicle control or IAZA served as the no radiation control arm. A terminal tumour volume of ~ 1500 mm³ was chosen as the endpoint of this study. Interestingly, using a single chemical dose of IAZA by itself significantly delayed initial tumour growth, however these

effects were transient, and did not translate to improved outcome. RT-treated mice showed a regression in tumour volume that lasted up to 15 days, after which the tumours recurred and grew to the terminal volume by the 6-7th week post injection. Unfortunately, no additional regression in tumour volume nor a delay in tumour recurrence in the IAZA+RT group was observed when compared to RT alone group (**Fig. 4.3C and D**).

In addition to tumour volume and body weight, the endpoint hypoxia levels in our test animals were also monitored. Instead of using the standard pimonidazole immunostaining as a marker for hypoxia, a novel hypoxia staining method was developed that exploited N₃-AZA click chemistry. N₃-AZA-protein adducts formed in hypoxic cells were labelled with a fluorescent alkyne, which served as a surrogate marker for hypoxia. The technique was validated in cells and mouse tumour models, and turned out to be highly robust, reproducible, faster, and simpler than pimonidazole immunostaining (**Fig. 2.4 and 2.5**). One interesting observation from the cell imaging studies was that N₃-AZA click staining was predominantly nuclear (**Suppl. Fig. 2.6C**), which contrasted with our bioinformatic analysis with NI-protein targets that found most of the target proteins to be cytoplasmic (**Supple. Fig. 2.2C**). When taking into account the TARDCS data (**Fig. 3.4A and B**), this suggests the possibility for non-covalent binding of NIs to DNA/RNA. To perform endpoint hypoxia analysis, mice were injected i.p. with N₃-AZA (60 mg/kg b.w.) 2 h prior to sacrifice and the hypoxic fraction was determined from staining central sagittal sections of the tumours with N₃-AZA click chemistry. Tumours harvested from mice injected with IAZA (but subjected to no RT) had significantly lower levels of hypoxia, suggesting that even at a single dose, IAZA could target the hypoxic core of the tumour (**Fig. 3.6E and F**). However, no difference in endpoint hypoxia levels were seen in RT alone and IAZA+RT treated tumours (**Fig. 4.3F and G**). We predict that by the time these tumours relapsed (around the end of the 2nd week post injection), the amounts and effects of a single IAZA dose very likely wore off and this might have resulted in no additional reduction in hypoxia levels in tumours from the IAZA+RT group.

Although *in vivo* radiosensitization studies did not show any significant improvement in survival, these data still provide a few important insights. For example, an important observation from our *in vitro* radiosensitization data is that IAZA showed synergy only when sufficiently high radiation (≥ 12 Gy) was applied to cells (**Fig. 4.1D**). This needs to be

considered when planning future *in vivo* radiation response experiments. Indeed, 2-NIs (such as glycididazole and doranidazole) showed tumour control properties in animals that were subjected to 30 Gy of x-irradiation (Yasui, Kubota et al. 2018). Hence, a RT dose escalation study might prove to be helpful in determining if IAZA indeed has *in vivo* radiosensitization properties. Mice were also not stratified in our study based on their tumour hypoxia levels, which can potentially mask any gains obtained by hypoxia directed therapies, such as with IAZA. When we performed hypoxia fraction analysis on tumours with different volumes, no correlation was observed between tumour size and hypoxia levels, indicating that tumour size is a poor predictor for tumour oxygenation status (**Suppl. Fig. 2.10A**). Ideally, tumours should first be analyzed by functional hypoxia imaging before allocating mice to a certain treatment group, and PET imaging with ¹⁸F-FAZA can be an excellent approach to perform this kind of stratification. Another important factor that must be considered is that only a single dose of IAZA was administered to these animals while most chemotherapeutic agents are usually given in multiple doses in the clinic. Therefore, in future it will be worthwhile to further analyze the impact of multiple IAZA administration on tumour growth. Encouragingly, we have already performed a detailed multiple dose toxicity analysis with IAZA where both male and female Swiss albino mice were administered with daily oral dosage of IAZA (at 100, 200 and 400 mg/kg b.w.) or vehicle control for 4 weeks. Mice in the recovery arm were treated with IAZA (400 mg/kg b.w.) daily for 4 weeks followed by a 2-week recovery period (**Fig. 5.2A**). Mice were monitored for changes in body weight (**Fig. 5.2B-E**), and after sacrifice, were analyzed for blood chemistry (**Table 5.1 and 5.2**) and organ histopathology (data not shown). No adverse effects were observed that could be attributed to IAZA administration for the chemical doses tested. We did observe a decrease in the body weight of IAZA (400 mg/kg) treated male mice in the recovery group. Although the difference was statistically significant, it was minimal (**Fig. 5.2D**). Given that oral route is the most preferable route of drug administration for clinical use, these data thus lay the groundwork for future radiation response experiments with multi-dose IAZA treatment.

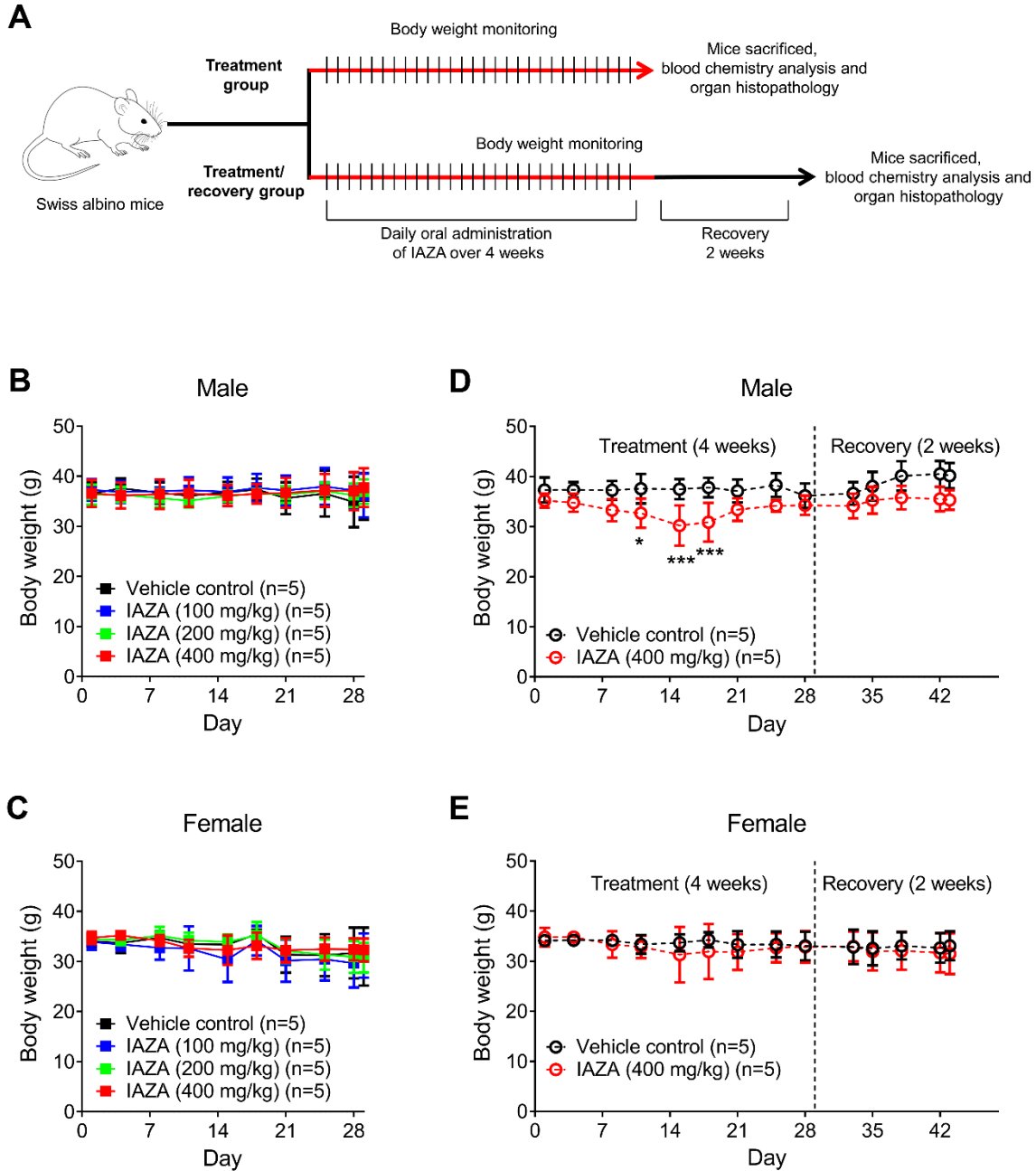


Figure 5.2 Oral administration of IAZA is relatively non-toxic in a mouse model.

Systemic toxicity profile of daily oral administration of IAZA was analyzed in a Swiss albino mouse model (A). IAZA was administered daily through oral gavage over a period of 28 days at 100 mg/kg, 200 mg/kg, or 400 mg/Kg body weight. Animals in recovery group received IAZA (400 mg/kg) for 4 weeks and were monitored for 2 additional weeks. Each group consisted of 10 mice (5 male and 5 female). No change in body weight in male (B) and female (C) mice in the treatment groups was observed. A statistically significant (albeit minimal) change in body weight was observed in male mice in the recovery group (D) but not in female (E) mice. Data represent mean \pm S.D; the differences in mean body weight among groups were analyzed using 2-way ANOVA.

Table 5.5.1 Blood chemistry analysis of male mice receiving IAZA (or vehicle control) via oral administration for 4 weeks, and after 2 weeks of recovery. Data represent mean \pm standard deviation.

	Vehicle control	IAZA (100 mg/kg)	IAZA (200 mg/kg)	IAZA (400 mg/kg)	Vehicle control recovery	IAZA (400 mg/kg) recovery
Glucose (mg/dL)	152.91 \pm 76.95	103.24 \pm 70.06	157.89 \pm 66.42	209.46 \pm 18.61	138.35 \pm 42.13	109.07 \pm 18.14
Urea (mg/dL)	42.71 \pm 15.60	48.59 \pm 12.22	39.32 \pm 3.87	41.68 \pm 1.63	47.93 \pm 1.85	50.39 \pm 4.79
Creatinine (mg/dL)	0.47 \pm 0.05	0.43 \pm 0.08	0.44 \pm 0.03	0.44 \pm 0.03	0.43 \pm 0.05	0.40 \pm 0.05
Sodium (mmol/L)	156.66	149.66 \pm 2.69	150.01 \pm 2.94	146.96 \pm 2.74	156.05 \pm 6.15	155.31 \pm 7.85
Potassium (mmol/L)	7.21	9.36 \pm 0.76	6.85 \pm 0.28	7.17 \pm 0.56	7.22 \pm 1.92	7.23 \pm 0.07
Total Protein (g/dL)	7.44 \pm 1.73	6.38 \pm 0.79	6.20 \pm 0.48	6.53 \pm 0.46	5.68 \pm 1.13	6.17 \pm 0.80
Albumin (g/dL)	3.79 \pm 1.13	3.15 \pm 0.14	2.96 \pm 0.14	3.09 \pm 0.07	2.82 \pm 0.35	2.98 \pm 0.31
ALT ^[a] (U/L)	113 \pm 45.59	120.8 \pm 105.54	87.40 \pm 40.35	76 \pm 14.65	66.5 \pm 8.58	102 \pm 43.55
AST ^[b] (U/L)	782 \pm 469.86	280 \pm 181.43	323 \pm 164.96	247.25 \pm 89.04	261.5 \pm 51.91	363 \pm 122.01
ALP ^[c] (U/L)	233.2 \pm 90	176.2 \pm 45.7	241.2 \pm 93.05	208 \pm 67.81	188 \pm 33.97	232.33 \pm 165.5
Total Bilirubin (mg/dL)	0.03	0.2 \pm 0.02	0.15	0.21 \pm 0.19	0.21 \pm 0.04	0.02
Cholesterol (mg/dL)	165.56 \pm 36.57	131.98 \pm 41.37	142.91 \pm 5.10	132.19 \pm 12.95	126.41 \pm 12.98	156.34 \pm 22.04
Triglycerides (mg/dL)	146.91 \pm 64.30	134.86 \pm 28.08	133.69 \pm 32.21	127.29 \pm 14.19	123.29 \pm 17.70	168.65 \pm 103.9

^[a] ALT: alanine aminotransferase; ^[b] AST: aspartate aminotransferase; ^[c] ALP: alkaline phosphatase. Data represent mean \pm standard deviation.

Table 5.2 Blood chemistry analysis of female mice receiving IAZA (or vehicle control) via oral administration for 4 weeks, and after 2 weeks of recovery. Data represent mean ± standard deviation.

	Vehicle control	IAZA (100 mg/kg)	IAZA (200 mg/kg)	IAZA (400 mg/kg)	Vehicle control recovery	IAZA (400 mg/kg) recovery
Glucose (mg/dL)	91.06±57.60	142.35±30.52	120.27±35.85	204.48±54.48	165.35±68.20	131.68±14.13
Urea (mg/dL)	30.94±11.98	36.70±9.20	39.22±7.64	21.23±3.19	29.54±11.54	30.79±7.30
Creatinine (mg/dL)	0.41±0.02	0.48±0.06	0.44±0.04	0.42±0.07	0.48±0.17	0.37±0.07
Sodium (mmol/L)	166.52±29.02	150.29±5.19	146.38±2.21	147.91±2.80	150.48±6.03	149.21±3.46
Potassium (mmol/L)	8.25±3.99	6.65±1.09	7.53±1.18	7.10±1.50	7.49±1.69	7.06±0.18
Total Protein (g/dL)	7.10±0.90	6.80±0.42	6.94±0.35	7.06±0.80	6.26±0.54	6.00±0.77
Albumin (g/dL)	3.11±0.25	3.20±0.23	3.60±0.95	3.38±0.26	3.53±0.79	3.07±0.27
ALT ^[a] (U/L)	55.80±8.20	89.75±37.04	90.00±52.09	72.60±43.78	151.6±113.31	114.8±132.08
AST ^[b] (U/L)	236.6±87.37	347±112.91	373.6±222.46	287.8±309.74	719.8±984.45	277.75±227.7
ALP ^[c] (U/L)	214±80.79	287±109.39	246.4±92.31	333±52.53	222.8±49.54	260.5±24.56
Total Bilirubin (mg/dL)	0.10±0.09	0.08±0.03	-	0.07±0.08	0.28	0.05
Cholesterol (mg/dL)	128.90±15.81	131.79±16.37	165.89±57.47	164.25±29.61	138.76±20.58	137.04±24.84
Triglycerides (mg/dL)	115.68±43.59	140.14±7.40	156.10±21.62	105.37±40.29	108.98±27.72	95.94±9.80

^[a] ALT: alanine aminotransferase; ^[b] AST: aspartate aminotransferase; ^[c] ALP: alkaline phosphatase. Data represent mean± standard deviation.

In addition to sensitization by external beam radiotherapy, hypoxia selective accumulation of radioactive IAZA (^{131}I -IAZA) can be used for delivering systemic radiotherapy to the otherwise resistant hypoxic tumour core. I-131 is a beta emitting radionuclide that has the potential to damage the cells it is retained in. The radioisotope also has diagnostic value and is compatible with single-photon emission computerized tomography (SPECT) imaging. These dual properties of I-131 isotope thus enable ^{131}I -IAZA to be simultaneously used as a diagnostic and therapeutic agent, i.e., making it suitable for “theranostic” applications. Therefore, hypoxic retention of ^{131}I -IAZA can be used to first identify hypoxic tumours by SPECT imaging, followed by targeted *in situ* radiotherapy to irradiate the tumour from within. Use of the same compound for both diagnosis and therapy offers simplified and cost-effective synthesis of the radioactive pharmaceutical (since only one drug needs to be synthesized), and also ensures that the same regions detected as hypoxic by imaging are targeted by the radiotherapy. To facilitate future *in situ* radiosensitization studies with ^{131}I -IAZA, a toxicity analysis of a single dose of non-radioactive IAZA, administered intravenously (i.v.), in NOD/SCID/IL2R mice was performed with doses ranging from 5 to 20 mg/kg b.w. Mice responded favorably to these dosing regimens and showed no adverse or toxic effects on body weight (**Fig. 5.3A**), blood chemistry (**Table 5.3**) and organ histology (**Fig. 5.3B**). These results support future molecular radiotherapy studies with ^{131}I -IAZA.

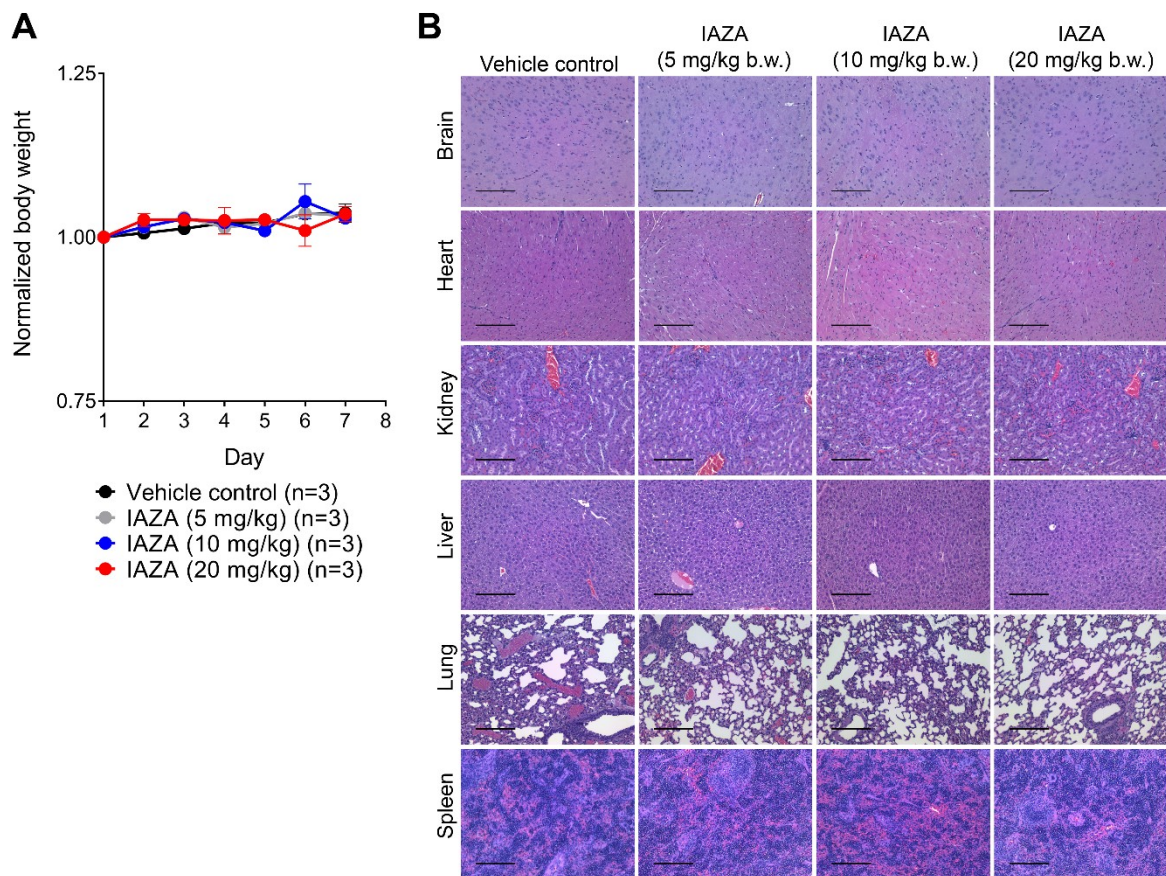


Figure 5.3: Intravenous administration of IAZA is non-toxic in mice.

IAZA was administered intravenously in NOD/SCID/IL2R mice at doses of 5, 10 or 20 mg/kg b.w. Changes in body weight were monitored for 14 days post-IAZA administration (A), after which, mice were sacrificed, and histopathology analysis was performed on organ sections. Representative histopathology micrographs are shown (B). Data represent mean \pm S.E.M.; scale bar=1mm.

Table 5.3 Blood chemistry analysis of mice administered i.v. with IAZA (or vehicle control) showed no significant changes. Data represent mean ± standard deviation.

	Vehicle control	IAZA (5 mg/kg)	IAZA (10 mg/kg)	IAZA (20 mg/kg)
Glucose (mmol/L)	14.97±2.29	15.70±0.50	14.67±1.21	14.60±0.62
Urea (mmol/L)	8.30±1.15	8.07±0.06	8.03±0.40	8.03±0.47
Creatinine (µmol/L)	12.33±1.53	11.33±0.58	13.00±1.73	11.33±2.08
Phosphorus (mmol/L)	3.73±0.25	3.97±0.64	3.90±0.26	3.90±0.30
Calcium (mmol/L)	2.73±0.05	2.70±0.11	2.73±0.03	2.68±0.04
Sodium (mmol/L)	156.67±1.15	155.00±1.73	156.33±0.58	154.67±2.08
Potassium (mmol/L)	>9	7.7 to 9	8.6 to 9	8.9 to 9
Chloride (mmol/L)	108.00±1.00	109.33±2.31	107.33±1.53	108.33±1.53
Bicarbonate (mmol/L)	24.00±2.65	25.00±2.00	25.33±2.52	23.33±2.89
Total Protein (g/L)	52.00±1.73	53.00±2.00	53.67±1.53	53.33±1.53
Albumin (g/L)	31.00	30.67±0.58	31.67±0.58	31.00±1.15
Globulin (g/L)	21.00±1.73	22.33±1.53	22.00±1.00	22.33±1.15
ALT ^[a] (IU/L)	30.00±9.85	19.67±5.51	19.67±2.08	18.67±2.52
AST ^[b] (IU/L)	80.00±26.21	72.00±22.11	65.57±16.74	54.33±8.39
ALP ^[c] (IU/L)	110.00±3.61	95.33±11.02	109.00±6.93	105.33±20.11
Total Bilirubin (µmol/L)	4.25±0.35	8.10±5.04	4.80±0.17	4.10±0.10
CK ^[d] (IU/L)	383.00±223.72	245.33±204.77	300.00±81.50	253.33±45.76

^[a] ALT: alanine aminotransferase; ^[b] AST: aspartate aminotransferase; ^[c] ALP: alkaline phosphatase; ^[d] CK: Creatine Kinase. Data represent mean± standard deviation.

In conclusion, this thesis demonstrated that 2-NI compounds, IAZA and FAZA, preferentially target hypoxic cells, and can induce cytostasis by disrupting DNA synthesis. This resulted in abnormal cell cycle profile and impacted cell growth. Using a novel click chemistry technique, it is shown that cellular DNA does not form covalent adducts with 2-NIs, however there is some indication that non-covalent binding does occur. The present study also, for the first time, described the protein targets of 2-NI compounds in a human head and neck cancer model, and demonstrated that binding of NIs to their target proteins negatively impacted their catalytic functions. Therefore, disruption of key cellular pathways such as glycolysis and detoxification processes may be responsible for the observed hypoxic sensitization by our compounds. Low dose 2-NI treatment did not induce DNA damage, rather cells showed signs of increased replication stress. However, when drug treated hypoxic cells were irradiated, the presence of the drugs potentiated DNA damage. IAZA happened to be a better radiosensitizer than FAZA, but still synergy was only seen in response to high radiation dose treatment. While single i.p. administration of IAZA is well-tolerated in mice (up to a chemical dose of 600 mg/kg b.w) and can reduce tumour hypoxia, combining a single dose IAZA treatment with a single 10 Gy RT did not improve tumour control or survival in tumour bearing mice. Regardless, the current study provides rationale for future exhaustive *in vivo* radiosensitization studies to assess the effects of multi-dose IAZA treatment. Also provided is supporting data to initiate systemic radiotherapy with radioactive ¹³¹I-IAZA. Overall, this study presents IAZA and FAZA, two 2-NI-based hypoxic diagnostic agents, as viable and important therapeutic agents, and provides a detailed mechanistic insight into the potential mechanism of action for 2-NI compounds.

Chapter 6

Bibliography

- Abou Khouzam, R., S. P. Rao, G. H. Venkatesh, N. A. Zeinelabdin, S. Buart, M. Meylan, M. Nimmakayalu, S. Terry and S. Chouaib (2021). "An eight-gene hypoxia signature predicts survival in pancreatic cancer and is associated with an immunosuppressed tumor microenvironment." Frontiers in Immunology **12**.
- Adams, G., I. Flockhart, C. Smithen, I. Stratford, P. Wardman and M. Watts (1976). "A correlation between structure, one electron reduction potential and efficiency of nitroimidazoles as hypoxic cell radiosensitizers." Radiation Research **67**: 9-20.
- Agarwal, A., S. Kanekar, S. Sabat and K. Thamburaj (2016). "Metronidazole-induced cerebellar toxicity." Neurology International **8**(1): 4-6.
- Ahmadi, F., N. Shabrandi, L. Hosseinzadeh and H. Azizian (2019). "Two DNA binding modes of a zinc-metronidazole and biological evaluation as a potent anti-cancer agent." Nucleosides, Nucleotides and Nucleic Acids **38**(7): 449-480.
- Ai, M., P. Budhani, J. Sheng, S. Balasubramanyam, T. Bartkowiak, A. R. Jaiswal, C. R. Ager, D. D. Haria and M. A. Curran (2015). "Tumor hypoxia drives immune suppression and immunotherapy resistance." Journal for ImmunoTherapy of Cancer **3**(2): 1-1.
- Ai, M., P. Budhani, J. Sheng, S. Balasubramanyam, T. Bartkowiak, A. R. Jaiswal, C. R. Ager, D. D. Haria and M. A. Curran (2015). "Tumor hypoxia drives immune suppression and immunotherapy resistance." Journal for ImmunoTherapy of Cancer **3**(S2): P392.
- Akel, G., P. Canal, E. Mockey, E. Vandevoorde, F. Laurent and G. Soula (1983). "Comparison of the fate of misonidazole (RO 07-0582) and its metabolite desmethylmisonidazole (RO 05-9963), two hypoxic cell radiosensitizers: penetration properties in tumor bearing rats." Journal de Pharmacologie **14**(1): 67-77.
- Anand, P., A. B. Kunnumakara, C. Sundaram, K. B. Harikumar, S. T. Tharakan, O. S. Lai, B. Sung and B. B. Aggarwal (2008). "Cancer is a preventable disease that requires major lifestyle changes." Pharmaceutical Research **25**(9): 2097-2116.
- Annunziato, A. (2008). "DNA packaging: nucleosomes and chromatin." Nature Education **1**(1): 26.
- Arsham, A. M., J. J. Howell and M. C. Simon (2003). "A novel hypoxia-inducible factor-independent hypoxic response regulating mammalian target of rapamycin and its targets." Journal of Biological Chemistry **278**(32): 29655-29660.
- Asquith, J., M. Watts, K. Patel, C. Smithen and G. Adams (1974). "Electron affinic sensitization: V. Radiosensitization of hypoxic bacteria and mammalian cells in vitro by some nitroimidazoles and nitropyrazoles." Radiation Research **60**(1): 108-118.
- Azuma, C., J. A. Raleigh and D. E. Thrall (1997). "Longevity of pimonidazole adducts in spontaneous canine tumors as an estimate of hypoxic cell lifetime." Radiation Research **148**(1): 35-42.
- Bader, S. B., M. W. Dewhirst and E. M. Hammond (2021). "Cyclic hypoxia: An update on its characteristics, methods to measure it and biological implications in cancer." Cancers **13**(1): 23.
- Bai, Y., W. Qi, L. Liu, J. Zhang, L. Pang, T. Gan, P. Wang, C. Wang and H. Chen (2021). "Identification of seven-gene hypoxia signature for predicting overall survival of hepatocellular carcinoma." Frontiers in Genetics **12**.
- Baird, N. A., D. W. Turnbull and E. A. Johnson (2006). "Induction of the Heat Shock Pathway during Hypoxia Requires Regulation of Heat Shock Factor by Hypoxia-inducible Factor-1." Journal of Biological Chemistry **281**(50): 38675-38681.

- Baluk, P., S. Morikawa, A. Haskell, M. Mancuso and D. M. McDonald (2003). "Abnormalities of basement membrane on blood vessels and endothelial sprouts in tumors." The American Journal of Pathology **163**(5): 1801-1815.
- Barnett, G. C., C. M. West, A. M. Dunning, R. M. Elliott, C. E. Coles, P. D. Pharoah and N. G. Burnet (2009). "Normal tissue reactions to radiotherapy: towards tailoring treatment dose by genotype." Nature Reviews Cancer **9**(2): 134-142.
- Baskar, R., K. A. Lee, R. Yeo and K.-W. Yeoh (2012). "Cancer and radiation therapy: current advances and future directions." International Journal of Medical Sciences **9**(3): 193.
- Batchelder, R., W. Wilson, M. Hay and W. Denny (1996). "Oxygen dependence of the cytotoxicity of the enediyne anti-tumour antibiotic esperamicin A1." The British Journal of Cancer. Supplement **27**: S52.
- Batie, M. and S. Rocha (2020). "Gene transcription and chromatin regulation in hypoxia." Biochemical Society Transactions **48**(3): 1121-1128.
- Bäumer, C., E. Fisch, H. Wedler, F. Reinecke and C. Korfhage (2018). "Exploring DNA quality of single cells for genome analysis with simultaneous whole-genome amplification." Scientific Reports **8**(1): 1-10.
- Beck, R., B. Röper, J. M. Carlsen, M. C. Huisman, J. A. Lebschi, N. Andratschke, M. Picchio, M. Souvatzoglou, H.-J. Machulla and M. Piert (2007). "Pretreatment 18F-FAZA PET predicts success of hypoxia-directed radiochemotherapy using tirapazamine." Journal of Nuclear Medicine **48**(6): 973-980.
- Bentzen, J., K. Toustrup, J. G. Eriksen, H. Primdahl, L. J. Andersen and J. Overgaard (2015). "Locally advanced head and neck cancer treated with accelerated radiotherapy, the hypoxic modifier nimorazole and weekly cisplatin. Results from the DAHANCA 18 phase II study." Acta Oncologica **54**(7): 1001-1007.
- Bentzen, S. M. and V. Gregoire (2011). Molecular imaging-based dose painting: A novel paradigm for radiation therapy prescription. Seminars in Radiation Oncology, Elsevier.
- Bernardi, R., I. Guernah, D. Jin, S. Grisendi, A. Alimonti, J. Teruya-Feldstein, C. Cordon-Cardo, M. C. Simon, S. Rafii and P. P. Pandolfi (2006). "PML inhibits HIF-1 α translation and neoangiogenesis through repression of mTOR." Nature **442**(7104): 779-785.
- Bertout, J. A., S. A. Patel and M. C. Simon (2008). "The impact of O₂ availability on human cancer." Nature Reviews Cancer **8**(12): 967.
- Bindra, R. S., S. L. Gibson, A. Meng, U. Westermark, M. Jasin, A. J. Pierce, R. G. Bristow, M. K. Classon and P. M. Glazer (2005). "Hypoxia-induced down-regulation of BRCA1 expression by E2Fs." Cancer Research **65**(24): 11597-11604.
- Bindra, R. S., P. J. Schaffer, A. Meng, J. Woo, K. r. Måseide, M. E. Roth, P. Lizardi, D. W. Hedley, R. G. Bristow and P. M. Glazer (2004). "Down-regulation of Rad51 and decreased homologous recombination in hypoxic cancer cells." Molecular and Cellular Biology **24**(19): 8504-8518.
- Bol, A., D. Labar, T.-T. Cao-Pham, B. Jordan, V. Grégoire and B. Gallez (2015). "Predictive value of 18F-FAZA PET imaging for guiding the association of radiotherapy with nimorazole: A preclinical study." Radiotherapy and Oncology **114**(2): 189-194.
- Bone and Cooper (2000). "In vitro inhibition of rat cauda epididymal sperm glycolytic enzymes by ornidazole, α -chlorohydrin and 1-chloro-3-hydroxypropanone." International Journal of Andrology **23**(5): 284-293.

- Brizel, D., S. Lin, J. Johnson, J. Brooks, M. Dewhirst and C. Piantadosi (1995). "The mechanisms by which hyperbaric oxygen and carbogen improve tumour oxygenation." British Journal of Cancer **72**(5): 1120-1124.
- Brizel, D. M., R. K. Dodge, R. W. Clough and M. W. Dewhirst (1999). "Oxygenation of head and neck cancer: changes during radiotherapy and impact on treatment outcome." Radiotherapy and Oncology **53**(2): 113-117.
- Brizel, D. M., S. P. Scully, J. M. Harrelson, L. J. Layfield, J. M. Bean, L. R. Prosnitz and M. W. Dewhirst (1996). "Tumor oxygenation predicts for the likelihood of distant metastases in human soft tissue sarcoma." Cancer Research **56**(5): 941-943.
- Brizel, D. M., G. S. Sibley, L. R. Prosnitz, R. L. Scher and M. W. Dewhirst (1997). "Tumor hypoxia adversely affects the prognosis of carcinoma of the head and neck." International Journal of Radiation Oncology• Biology• Physics **38**(2): 285-289.
- Brotzel, F. and H. Mayr (2007). "Nucleophilicities of amino acids and peptides." Organic & Biomolecular Chemistry **5**(23): 3814-3820.
- Brown, J. (1979). "Evidence for acutely hypoxic cells in mouse tumours, and a possible mechanism of reoxygenation." The British Journal of Radiology **52**(620): 650-656.
- Brown, J. M. (1999). "The Hypoxic Cell A Target for Selective Cancer Therapy—Eighteenth Bruce F. Cain Memorial Award Lecture." Cancer Research **59**(23): 5863-5870.
- Brown, J. M. (2007). "Tumor hypoxia in cancer therapy." Methods in Enzymology **435**: 295-321.
- Brown, J. M. and W. R. Wilson (2004). "Exploiting tumour hypoxia in cancer treatment." Nature Reviews Cancer **4**(6): 437-447.
- Carles, M., T. Fechter, A. L. Grosu, A. Sörensen, B. Thomann, R. G. Stoian, N. Wiedenmann, A. Rühle, C. Zamboglou and J. Ruf (2021). "18F-FMISO-PET Hypoxia Monitoring for Head-and-Neck Cancer Patients: Radiomics Analyses Predict the Outcome of Chemo-Radiotherapy." Cancers **13**(14): 3449.
- Chaplin, D. J., C. E. Peters, M. R. Horsman and M. J. Trotter (1991). "Drug induced perturbations in tumor blood flow: therapeutic potential and possible limitations." Radiotherapy and Oncology **20**: 93-101.
- Chapman, D. W., H.-S. Jans, I. Ma, J. R. Mercer, L. I. Wiebe, M. Wuest and R. B. Moore (2014). "Detecting functional changes with [18 F] FAZA in a renal cell carcinoma mouse model following sunitinib therapy." EJNMMI Research **4**(1): 27.
- Chapman, J., A. Reuvers and J. Borsa (1973). "Effectiveness of nitrofurantoin derivatives in sensitizing hypoxic mammalian cells to X rays." The British Journal of Radiology **46**(548): 623-630.
- Chatterjee, A. and S. Gupta (2018). "The multifaceted role of glutathione S-transferases in cancer." Cancer Letters **433**: 33-42.
- Chen, C., N. Pore, A. Behrooz, F. Ismail-Beigi and A. Maity (2001). "Regulation of glut1 mRNA by hypoxia-inducible factor-1: interaction between H-ras and hypoxia." Journal of Biological Chemistry **276**(12): 9519-9525.
- Chen, Y. L., Y. Zhang, J. Wang, N. Chen, W. Fang, J. Zhong, Y. Liu, R. Qin, X. Yu and Z. Sun (2019). "A 17 gene panel for non-small-cell lung cancer prognosis identified through integrative epigenomic-transcriptomic analyses of hypoxia-induced epithelial-mesenchymal transition." Molecular Oncology **13**(7): 1490-1502.

- Chouaib, S., Y. Messai, S. Couve, B. Escudier, M. Hasmim and M. Z. Noman (2012). "Hypoxia promotes tumor growth in linking angiogenesis to immune escape." Frontiers in Immunology **3**: 21.
- Clambey, E. T., E. N. McNamee, J. A. Westrich, L. E. Glover, E. L. Campbell, P. Jedlicka, E. F. De Zoeten, J. C. Cambier, K. R. Stenmark and S. P. Colgan (2012). "Hypoxia-inducible factor-1 alpha-dependent induction of FoxP3 drives regulatory T-cell abundance and function during inflammatory hypoxia of the mucosa." Proceedings of the National Academy of Sciences **109**(41): E2784-E2793.
- Collingridge, D., W. Young, B. Vojnovic, P. Wardman, E. Lynch, S. Hill and D. Chaplin (1997). "Measurement of tumor oxygenation: a comparison between polarographic needle electrodes and a time-resolved luminescence-based optical sensor." Radiation Research **147**(3): 329-334.
- Comerford, K. M., T. J. Wallace, J. Karhausen, N. A. Louis, M. C. Montalto and S. P. Colgan (2002). "Hypoxia-inducible factor-1-dependent regulation of the multidrug resistance (MDR1) gene." Cancer Research **62**(12): 3387-3394.
- Cowell, I. G., M. J. Tilby and C. A. Austin (2011). "An overview of the visualisation and quantitation of low and high MW DNA adducts using the trapped in agarose DNA immunostaining (TARDIS) assay." Mutagenesis **26**(2): 253-260.
- Curry, J. M., J. Sprandio, D. Cognetti, A. Luginbuhl, V. Bar-ad, E. Pribitkin and M. Tuluc (2014). Tumor microenvironment in head and neck squamous cell carcinoma. Seminars in Oncology, Elsevier.
- Damiani, E., J. A. Solorio, A. P. Doyle and H. M. Wallace (2019). "How reliable are in vitro IC50 values? Values vary with cytotoxicity assays in human glioblastoma cells." Toxicology Letters **302**: 28-34.
- Davenport, E. L., G. J. Morgan and F. E. Davies (2008). "Untangling the unfolded protein response." Cell Cycle **7**(7): 865-869.
- Debacq-Chainiaux, F., J. D. Erusalimsky, J. Campisi and O. Toussaint (2009). "Protocols to detect senescence-associated beta-galactosidase (SA-βgal) activity, a biomarker of senescent cells in culture and in vivo." Nature Protocols **4**(12): 1798-1806.
- Denekamp, J., B. Michael and S. Harris (1974). "Hypoxic cell radiosensitizers: Comparative tests of some electron affinic compounds using epidermal cell survival in vivo." Radiation Research **60**(1): 119-132.
- Deng, J., J. Li, A. Sarde, J. L. Lines, Y.-C. Lee, D. C. Qian, D. A. Pechenick, R. Manivanh, I. Le Mercier and C. H. Lowrey (2019). "Hypoxia-induced VISTA promotes the suppressive function of myeloid-derived suppressor cells in the tumor microenvironment." Cancer Immunology Research **7**(7): 1079-1090.
- Dewhirst, M. W. (2009). "Relationships between cycling hypoxia, HIF-1, angiogenesis and oxidative stress." Radiation Research **172**(6): 653-665.
- Dietrich, A., L. Koi, K. Zöphel, W. Sihver, J. Kotzerke, M. Baumann and M. Krause (2015). "Improving external beam radiotherapy by combination with internal irradiation." The British Journal of Radiology **88**(1051): 20150042.
- Ding, C., X. Fan and G. Wu (2017). "Peroxiredoxin 1—an antioxidant enzyme in cancer." Journal of Cellular and Molecular Medicine **21**(1): 193-202.
- Dingsdag, S. A. and N. Hunter (2018). "Metronidazole: an update on metabolism, structure–cytotoxicity and resistance mechanisms." Journal of Antimicrobial Chemotherapy **73**(2): 265-279.

- Dische, S. (1978). "Hyperbaric oxygen: the Medical Research Council trials and their clinical significance." The British Journal of Radiology **51**(611): 888-894.
- Dische, S. (1985). "Chemical sensitizers for hypoxic cells: a decade of experience in clinical radiotherapy." Radiotherapy and Oncology **3**(2): 97-115.
- Dische, S., M. Saunders, M. E. Lee, G. Adams and I. Flockhart (1977). "Clinical testing of the radiosensitizer Ro 07-0582: experience with multiple doses." British Journal of Cancer **35**(5): 567-579.
- Dubois, L. J., N. G. Lieuwes, M. H. Janssen, W. J. Peeters, A. D. Windhorst, J. C. Walsh, H. C. Kolb, M. C. Öllers, J. Bussink and G. A. van Dongen (2011). "Preclinical evaluation and validation of [18F] HX4, a promising hypoxia marker for PET imaging." Proceedings of the National Academy of Sciences **108**(35): 14620-14625.
- Dudás, J., V. H. Schartinger, A. Romani, G. Schweigl, K. Kordsmeyer, P. I. Marta, C. Url, F. Kral and H. Riechelmann (2014). "Cell cycle association and hypoxia regulation of excision repair cross complementation group 1 protein (ERCC1) in tumor cells of head and neck cancer." Tumor Biology **35**(8): 7807-7819.
- Duffy, J. P., G. Eibl, H. A. Reber and O. J. Hines (2003). "Influence of hypoxia and neoangiogenesis on the growth of pancreatic cancer." Molecular Cancer **2**(1): 12.
- Dutta, B., R. Yan, S. K. Lim, J. P. Tam and S. K. Sze (2014). "Quantitative profiling of chromatome dynamics reveals a novel role for HP1BP3 in hypoxia-induced oncogenesis." Molecular & Cellular Proteomics **13**(12): 3236-3249.
- Edwards, D. I. (1986). "Reduction of nitroimidazoles in vitro and DNA damage." Biochemical Pharmacology **35**(1): 53-58.
- Edwards, D. I. (2013). "Reduction of nitroimidazoles in vitro and DNA damage." Bioreduction in the Activation of Drugs; Alexander, P., Gielen, J., Sartorelli, AC, Eds: 53.
- Edwards, M. S., D. G. Gordon and V. A. Levin (1984). "Evaluation of desmethylmisonidazole-induced neurotoxicity in the rat using brainstem auditory evoked potentials." International Journal of Radiation Oncology* Biology* Physics **10**(8): 1377-1379.
- Eriksen, J. G. and J. Overgaard (2007). "Lack of prognostic and predictive value of CA IX in radiotherapy of squamous cell carcinoma of the head and neck with known modifiable hypoxia: an evaluation of the DAHANCA 5 study." Radiotherapy and Oncology **83**(3): 383-388.
- Eustace, A., N. Mani, P. N. Span, J. J. Irlam, J. Taylor, G. N. Betts, H. Denley, C. J. Miller, J. J. Homer and A. M. Rojas (2013). "A 26-gene hypoxia signature predicts benefit from hypoxia-modifying therapy in laryngeal cancer but not bladder cancer." Clinical Cancer Research **19**(17): 4879-4888.
- Evans, S. M., D. Fraker, S. M. Hahn, K. Gleason, W. T. Jenkins, K. Jenkins, W.-T. Hwang, P. Zhang, R. Mick and C. J. Koch (2006). "EF5 binding and clinical outcome in human soft tissue sarcomas." International Journal of Radiation Oncology* Biology* Physics **64**(3): 922-927.
- Evans, S. M., S. Hahn, D. R. Pook, W. T. Jenkins, A. A. Chalian, P. Zhang, C. Stevens, R. Weber, G. Weinstein, I. Benjamin, N. Mirza, M. Morgan, S. Rubin, W. G. McKenna, E. M. Lord and C. J. Koch (2000). "Detection of hypoxia in human squamous cell carcinoma by EF5 binding." Cancer Research **60**(7): 2018-2024.
- Fallone, F., S. Britton, L. Nieto, B. Salles and C. Muller (2013). "ATR controls cellular adaptation to hypoxia through positive regulation of hypoxia-inducible factor 1 (HIF-1) expression." Oncogene **32**(37): 4387-4396.

- Feitelson, M. A., A. Arzumanyan, R. J. Kulathinal, S. W. Blain, R. F. Holcombe, J. Mahajna, M. Marino, M. L. Martinez-Chantar, R. Nawroth and I. Sanchez-Garcia (2015). Sustained proliferation in cancer: Mechanisms and novel therapeutic targets. Seminars in Cancer Biology, Elsevier.
- Fels, D. R. and C. Koumenis (2006). "The PERK/eIF2 α /ATF4 module of the UPR in hypoxia resistance and tumor growth." Cancer Biology & Therapy **5**(7): 723-728.
- Feoktistova, M., P. Geserick and M. Leverkus (2016). "Crystal violet assay for determining viability of cultured cells." Cold Spring Harbor Protocols **2016**(4): pdb. prot087379.
- Fernald, K. and M. Kurokawa (2013). "Evading apoptosis in cancer." Trends in Cell Biology **23**(12): 620-633.
- Ferreira, L. T., A. C. Figueiredo, B. Orr, D. Lopes and H. Maiato (2018). "Dissecting the role of the tubulin code in mitosis." Methods in Cell Biology **144**: 33-74.
- Fletcher, M. E., P. R. Boshier, K. Wakabayashi, H. C. Keun, R. T. Smolenski, P. A. Kirkham, I. M. Adcock, P. J. Barton, M. Takata and N. Marczin (2015). "Influence of glutathione-S-transferase (GST) inhibition on lung epithelial cell injury: role of oxidative stress and metabolism." American Journal of Physiology-Lung Cellular and Molecular Physiology **308**(12): L1274-L1285.
- Fulda, S. and K.-M. Debatin (2007). "HIF-1-regulated glucose metabolism: a key to apoptosis resistance?" Cell Cycle **6**(7): 790-792.
- Ganapathy-Kanniappan, S. and J.-F. H. Geschwind (2013). "Tumor glycolysis as a target for cancer therapy: progress and prospects." Molecular Cancer **12**(1): 152.
- Gardner, T. B. and D. R. Hill (2001). "Treatment of giardiasis." Clinical Microbiology Reviews **14**(1): 114-128.
- Gillooly, J. F., A. Hein and R. Damiani (2015). "Nuclear DNA content varies with cell size across human cell types." Cold Spring Harbor Perspectives in Biology **7**(7): a019091.
- Goda, N., H. E. Ryan, B. Khadivi, W. McNulty, R. C. Rickert and R. S. Johnson (2003). "Hypoxia-inducible factor 1 α is essential for cell cycle arrest during hypoxia." Molecular and Cellular Biology **23**(1): 359-369.
- Graham, K. and E. Unger (2018). "Overcoming tumor hypoxia as a barrier to radiotherapy, chemotherapy and immunotherapy in cancer treatment." International Journal of Nanomedicine **13**: 6049.
- Gray, A., S. Dische, G. Adams, I. Flockhart and J. L. Foster (1976). "Clinical testing of the radiosensitiser Ro-07-0582. I. Dose tolerance, serum and tumour concentrations." Clinical Radiology **27**(2): 151-157.
- Grégoire, V., M. Guckenberger, K. Haustermans, J. J. Lagendijk, C. Ménard, R. Pötter, B. J. Slotman, K. Tanderup, D. Thorwarth and M. Van Herk (2020). "Image guidance in radiation therapy for better cure of cancer." Molecular Oncology **14**(7): 1470-1491.
- Guo, P. and B. M. Fu (2012). "Effect of wall compliance and permeability on blood-flow rate in counter-current microvessels formed from anastomosis during tumor-induced angiogenesis."
- Gupta, S. and A. A. Knowlton (2002). "Cytosolic heat shock protein 60, hypoxia, and apoptosis." Circulation **106**(21): 2727-2733.
- Gwak, G.-Y., J.-H. Yoon, K. M. Kim, H.-S. Lee, J. W. Chung and G. J. Gores (2005). "Hypoxia stimulates proliferation of human hepatoma cells through the induction of hexokinase II expression." Journal of Hepatology **42**(3): 358-364.

- Halasi, M., M. Wang, T. S. Chavan, V. Gaponenko, N. Hay and A. L. Gartel (2013). "ROS inhibitor N-acetyl-L-cysteine antagonizes the activity of proteasome inhibitors." Biochemical Journal **454**(2): 201-208.
- Hammond, E., M.-C. Asselin, D. Forster, J. P. O'Connor, J. Senra and K. Williams (2014). "The meaning, measurement and modification of hypoxia in the laboratory and the clinic." Clinical Oncology **26**(5): 277-288.
- Hammond, E. M., N. C. Denko, M. J. Dorie, R. T. Abraham and A. J. Giaccia (2002). "Hypoxia links ATR and p53 through replication arrest." Molecular and Cellular Biology **22**(6): 1834-1843.
- Hammond, E. M., M. J. Dorie and A. J. Giaccia (2003). "ATR/ATM targets are phosphorylated by ATR in response to hypoxia and ATM in response to reoxygenation." Journal of Biological Chemistry **278**(14): 12207-12213.
- Hammond, E. M., M. J. Dorie and A. J. Giaccia (2004). "Inhibition of ATR leads to increased sensitivity to hypoxia/reoxygenation." Cancer Research **64**(18): 6556-6562.
- Hammond, E. M., S. L. Green and A. J. Giaccia (2003). "Comparison of hypoxia-induced replication arrest with hydroxyurea and aphidicolin-induced arrest." Mutation Research/Fundamental and Molecular Mechanisms of Mutagenesis **532**(1-2): 205-213.
- Hanschmann, E.-M., J. R. Godoy, C. Berndt, C. Hudemann and C. H. Lillig (2013). "Thioredoxins, glutaredoxins, and peroxiredoxins—molecular mechanisms and health significance: from cofactors to antioxidants to redox signaling." Antioxidants & Redox Signaling **19**(13): 1539-1605.
- Harris, A. L. (2002). "Hypoxia—a key regulatory factor in tumour growth." Nature Reviews Cancer **2**(1): 38-47.
- Hartmann, A., M. Kunz, S. Köstlin, R. Gillitzer, A. Toksoy, E.-B. Bröcker and C. E. Klein (1999). "Hypoxia-induced up-regulation of angiogenin in human malignant melanoma." Cancer Research **59**(7): 1578-1583.
- Haustermans, v. d. K., A. Van der Kogel, B. Vanacker and E. Van der Schueren (1994). "Influence of combined use of nicotinamide and carbogen on rat spinal cord radiation tolerance." Radiotherapy and Oncology **31**(2): 123-128.
- Hay, M., L. Liew, W. Wong, B. Dickson, G. Cheng, C. Hong, W. Wilson and S. Jamieson (2020). "Hypoxia-activated prodrugs of DNA-dependent protein kinase as radiosensitisers." European Journal of Cancer **138**: S13-S14.
- Hendrickson, K., M. Phillips, W. Smith, L. Peterson, K. Krohn and J. Rajendran (2011). "Hypoxia imaging with [F-18] FMISO-PET in head and neck cancer: potential for guiding intensity modulated radiation therapy in overcoming hypoxia-induced treatment resistance." Radiotherapy and Oncology **101**(3): 369-375.
- Henk, J. (1986). "Late results of a trial of hyperbaric oxygen and radiotherapy in head and neck cancer: a rationale for hypoxic cell sensitizers?" International Journal of Radiation Oncology* Biology* Physics **12**(8): 1339-1341.
- Higashimura, Y., Y. Nakajima, R. Yamaji, N. Harada, F. Shibasaki, Y. Nakano and H. Inui (2011). "Up-regulation of glyceraldehyde-3-phosphate dehydrogenase gene expression by HIF-1 activity depending on Sp1 in hypoxic breast cancer cells." Archives of Biochemistry and Biophysics **509**(1): 1-8.
- Hildebrandt, T., J. Knuesting, C. Berndt, B. Morgan and R. Scheibe (2015). "Cytosolic thiol switches regulating basic cellular functions: GAPDH as an information hub?" Biological Chemistry **396**(5): 523-537.

- Hirata, E. and E. Sahai (2017). "Tumor microenvironment and differential responses to therapy." Cold Spring Harbor Perspectives in Medicine 7(7): a026781.
- Hirst, D., V. Hirst, B. Joiner, V. Prise and K. Shaffi (1991). "Changes in tumour morphology with alterations in oxygen availability: further evidence for oxygen as a limiting substrate." British Journal of Cancer 64(1): 54-58.
- Höckel, M., K. Schlenger, B. Aral, M. Mitze, U. Schäffer and P. Vaupel (1996). "Association between tumor hypoxia and malignant progression in advanced cancer of the uterine cervix." Cancer Research 56(19): 4509-4515.
- Höckel, M., K. Schlenger, S. Höckel, B. Aral, U. Schäffer and P. Vaupel (1998). "Tumor hypoxia in pelvic recurrences of cervical cancer." International Journal of Cancer 79(4): 365-369.
- Höckel, M., K. Schlenger, C. Knoop and P. Vaupel (1991). "Oxygenation of carcinomas of the uterine cervix: evaluation by computerized O₂ tension measurements." Cancer Research 51(22): 6098-6102.
- Hompland, T., C. S. Fjeldbo and H. Lyng (2021). "Tumor Hypoxia as a Barrier in Cancer Therapy: Why Levels Matter." Cancers 13(3): 499.
- Hoogsteen, I. J., H. A. Marres, J. Bussink, A. J. van der Kogel and J. H. Kaanders (2007). "Tumor microenvironment in head and neck squamous cell carcinomas: predictive value and clinical relevance of hypoxic markers. A review." Head & Neck 29(6): 591-604.
- Horsman, M. R., L. S. Mortensen, J. B. Petersen, M. Busk and J. Overgaard (2012). "Imaging hypoxia to improve radiotherapy outcome." Nature Reviews Clinical Oncology 9(12): 674-687.
- Hoskin, P., A. Sibtain, F. Daley and G. Wilson (2003). "GLUT1 and CAIX as intrinsic markers of hypoxia in bladder cancer: relationship with vascularity and proliferation as predictors of outcome of ARCON." British Journal of Cancer 89(7): 1290-1297.
- Hoskin, P. J., A. M. Rojas, S. M. Bentzen and M. I. Saunders (2010). "Radiotherapy with concurrent carbogen and nicotinamide in bladder carcinoma." Journal of Clinical Oncology 28(33): 4912-4918.
- Hou, A. L. (2016). A Novel Click Chemistry-Based Method to Detect Hypoxic Tumour Cells and Characterise Their Gene Expression, ResearchSpace@ Auckland.
- House, S. W., O. Warburg, D. Burk and A. L. Schade (1956). "On respiratory impairment in cancer cells." Science 124(3215): 267-272.
- Huang, S., J. E. Michalek, D. A. Reardon, P. Y. Wen, J. R. Floyd, P. T. Fox, G. D. Clarke, P. A. Jerabek, K. M. Schmainda and M. Muzi (2021). "Assessment of tumor hypoxia and perfusion in recurrent glioblastoma following bevacizumab failure using MRI and 18 F-FMISO PET." Scientific Reports 11(1): 1-12.
- Huang, W., X. Zeng, Y. Shi and M. Liu (2017). "Functional characterization of human equilibrative nucleoside transporter 1." Protein & Cell 8(4): 284.
- Hudson, C. C., M. Liu, G. G. Chiang, D. M. Otterness, D. C. Loomis, F. Kaper, A. J. Giaccia and R. T. Abraham (2002). "Regulation of hypoxia-inducible factor 1 α expression and function by the mammalian target of rapamycin." Molecular and Cellular Biology 22(20): 7004-7014.
- Hui, E. P., A. T. Chan, F. Pezzella, H. Turley, K.-F. To, T. C. Poon, B. Zee, F. Mo, P. M. Teo and D. P. Huang (2002). "Coexpression of hypoxia-inducible factors 1 α and 2 α ,

- carbonic anhydrase IX, and vascular endothelial growth factor in nasopharyngeal carcinoma and relationship to survival." Clinical Cancer Research **8**(8): 2595-2604.
- Hung, J.-J., M.-H. Yang, H.-S. Hsu, W.-H. Hsu, J. Liu and K. Wu (2009). "Prognostic significance of hypoxia-inducible factor-1 α , TWIST1 and Snail expression in resectable non-small cell lung cancer." Thorax **64**(12): 1082-1089.
- Hutchison, G. J., H. R. Valentine, J. A. Loncaster, S. E. Davidson, R. D. Hunter, S. A. Roberts, A. L. Harris, I. J. Stratford, P. M. Price and C. M. West (2004). "Hypoxia-inducible factor 1 α expression as an intrinsic marker of hypoxia: correlation with tumor oxygen, pimonidazole measurements, and outcome in locally advanced carcinoma of the cervix." Clinical Cancer Research **10**(24): 8405-8412.
- Ings, R. M., J. A. McFadzean and W. E. Ormerod (1974). "The mode of action of metronidazole in *Trichomonas vaginalis* and other micro-organisms." Biochemical pharmacology **23**(9): 1421-1429.
- Jain, K., G. Suryakumar, L. Ganju and S. B. Singh (2014). "Differential hypoxic tolerance is mediated by activation of heat shock response and nitric oxide pathway." Cell Stress and Chaperones **19**(6): 801-812.
- Jain, K. K. (2017). Physical, physiological, and biochemical aspects of hyperbaric oxygenation. Textbook of Hyperbaric Medicine, Springer: 11-22.
- Janssen, H., K. Haustermans, A. Balm and A. Begg (2005). "Hypoxia in head and neck cancer: how much, how important?" Head & Neck **27**(7): 622-638.
- Janssens, G. O., S. E. Rademakers, C. H. Terhaard, P. A. Doornaert, H. P. Bijl, P. van den Ende, A. Chin, H. A. Marres, R. de Bree and A. J. van der Kogel (2012). "Accelerated radiotherapy with carbogen and nicotinamide for laryngeal cancer: results of a phase III randomized trial." Journal of Clinical Oncology **30**(15): 1777-1783.
- Jenner, T. J., O. Sapor, P. O'Neill and E. M. Fielden (1988). "Enhancement of DNA damage in mammalian cells upon bioreduction of the nitroimidazole-aziridines RSU-1069 and RSU-1131." Biochemical Pharmacology **37**(20): 3837-3842.
- Kaanders, J. H., K. I. Wijffels, H. A. Marres, A. S. Ljungkvist, L. A. Pop, F. J. van den Hoogen, P. C. de Wilde, J. Bussink, J. A. Raleigh and A. J. van der Kogel (2002). "Pimonidazole binding and tumor vascularity predict for treatment outcome in head and neck cancer." Cancer Research **62**(23): 7066-7074.
- Kedderis, G. L., L. S. Argenbright and G. T. Miwa (1989). "Covalent interaction of 5-nitroimidazoles with DNA and protein in vitro: mechanism of reductive activation." Chemical Research in Toxicology **2**(3): 146-149.
- Keith, B. and M. C. Simon (2007). "Hypoxia-inducible factors, stem cells, and cancer." Cell **129**(3): 465-472.
- Kim, B. M., Y. Hong, S. Lee, P. Liu, J. H. Lim, Y. H. Lee, T. H. Lee, K. T. Chang and Y. Hong (2015). "Therapeutic implications for overcoming radiation resistance in cancer therapy." International Journal of Molecular Sciences **16**(11): 26880-26913.
- Kim, Y.-J., J.-Y. Ahn, P. Liang, C. Ip, Y. Zhang and Y.-M. Park (2007). "Human prx1 gene is a target of Nrf2 and is up-regulated by hypoxia/reoxygenation: implication to tumor biology." Cancer Research **67**(2): 546-554.
- Kizaka-Kondoh, S. and H. Konse-Nagasawa (2009). "Significance of nitroimidazole compounds and hypoxia-inducible factor-1 for imaging tumor hypoxia." Cancer Science **100**(8): 1366-1373.

- Knight, R. J., K. F. Kofoed, H. R. Schelbert and D. B. Buxton (1996). "Inhibition of glyceraldehyde-3-phosphate dehydrogenase in post-ischaemic myocardium." Cardiovascular Research **32**(6): 1016-1023.
- Koch, C., S. Evans and E. Lord (1995). "Oxygen dependence of cellular uptake of EF5 [2-(2-nitro-1H-imidazol-1-yl)-N-(2, 2, 3, 3, 3-pentafluoropropyl) a cet amide]: analysis of drug adducts by fluorescent antibodies vs bound radioactivity." British Journal of Cancer **72**(4): 869-874.
- Koch, C., R. Howell and J. Biaglow (1979). "Ascorbate anion potentiates cytotoxicity of nitroaromatic compounds under hypoxic and anoxic conditions." British Journal of Cancer **39**(3): 321-329.
- Koch, C. J. (2002). "[1] Measurement of absolute oxygen levels in cells and tissues using oxygen sensors and 2-nitroimidazole EF5."
- Kohshi, K., Y. Kinoshita, H. Terashima, N. Konda, A. Yokota and T. Soejima (1996). "Radiotherapy after hyperbaric oxygenation for malignant gliomas: a pilot study." Journal of Cancer Research and Clinical Oncology **122**(11): 676-678.
- Koike, N., R. Kota, Y. Naito, N. Hayakawa, T. Matsuura, T. Hishiki, N. Onishi, J. Fukada, M. Suematsu and N. Shigematsu (2020). "2-Nitroimidazoles induce mitochondrial stress and ferroptosis in glioma stem cells residing in a hypoxic niche." Communications Biology **3**(1): 1-13.
- Komar, G., K. Lehtiö, M. Seppänen, O. Eskola, H. Levola, P. Lindholm, H. Sipilä, J. Seppälä, R. Grénman and O. Solin (2014). "Prognostic value of tumour blood flow,[18 F] EF5 and [18 F] FDG PET/CT imaging in patients with head and neck cancer treated with radiochemotherapy." European Journal of Nuclear Medicine and Molecular Imaging **41**(11): 2042-2050.
- Koritzinsky, M., F. Levitin, T. van den Beucken, R. A. Rumantir, N. J. Harding, K. C. Chu, P. C. Boutros, I. Braakman and B. G. Wouters (2013). "Two phases of disulfide bond formation have differing requirements for oxygen." Journal of Cell Biology **203**(4): 615-627.
- Koshiji, M., K. K.-W. To, S. Hammer, K. Kumamoto, A. L. Harris, P. Modrich and L. E. Huang (2005). "HIF-1 α induces genetic instability by transcriptionally downregulating MutS α expression." Molecular Cell **17**(6): 793-803.
- Koumenis, C. and B. G. Wouters (2006). "'Translating' Tumor Hypoxia: Unfolded Protein Response (UPR)-Dependent and UPR-Independent Pathways." Molecular Cancer Research **4**(7): 423-436.
- Kramer, A., J. Green, J. Pollard, Jr. and S. Tugendreich (2014). "Causal analysis approaches in Ingenuity Pathway Analysis." Bioinformatics **30**(4): 523-530.
- Krause, W., A. Jordan, R. Scholz and J.-L. M. Jimenez (2005). "Iodinated nitroimidazoles as radiosensitizers." Anticancer Research **25**(3B): 2145-2151.
- Kubo, T., H. Nakajima, M. Nakatsuji, M. Itakura, A. Kaneshige, Y.-T. Azuma, T. Inui and T. Takeuchi (2016). "Active site cysteine-null glyceraldehyde-3-phosphate dehydrogenase (GAPDH) rescues nitric oxide-induced cell death." Nitric Oxide **53**: 13-21.
- Kumar, K. S. and J. F. Weiss (1986). "Inhibition of glutathione peroxidase and glutathione transferase in mouse liver by misonidazole." Biochemical Pharmacology **35**(18): 3143-3146.

- Kumar, P., S. Emami, Z. Kresolek, J. Yang, A. McEwan and L. Wiebe (2009). "Synthesis and Hypoxia Selective Radiosensitization Potential of β -2-FAZA and β -3-FAZL: Fluorinated Azomycin β -Nucleosides." Medicinal Chemistry **5**(2): 118-129.
- Kumar, P., S. A. McQuarrie, A. Zhou, A. J. McEwan and L. I. Wiebe (2005). "[¹³¹I] Iodoazomycin arabinoside for low-dose-rate isotope radiotherapy: radiolabeling, stability, long-term whole-body clearance and radiation dosimetry estimates in mice." Nuclear Medicine and Biology **32**(6): 647-653.
- Kumar, P., D. Stypinski, H. Xia, A. McEwan, H. J. Machulla and L. Wiebe (1999). "Fluoroazomycin arabinoside (FAZA): synthesis, 2H and 3H-labelling and preliminary biological evaluation of a novel 2-nitroimidazole marker of tissue hypoxia." Journal of Labelled Compounds and Radiopharmaceuticals: The Official Journal of the International Isotope Society **42**(1): 3-16.
- Kumar, P., L. Wiebe, M. Asikoglu, M. Tandon and A. McEwan (2002). "Microwave-assisted (radio) halogenation of nitroimidazole-based hypoxia markers." Applied Radiation and Isotopes **57**(5): 697-703.
- Kumareswaran, R., O. Ludkovski, A. Meng, J. Sykes, M. Pintilie and R. G. Bristow (2012). "Chronic hypoxia compromises repair of DNA double-strand breaks to drive genetic instability." Journal of Cell Science **125**(1): 189-199.
- Kuwai, T., Y. Kitadai, S. Tanaka, S. Onogawa, N. Matsutani, E. Kaio, M. Ito and K. Chayama (2003). "Expression of hypoxia-inducible factor-1 α is associated with tumor vascularization in human colorectal carcinoma." International Journal of Cancer **105**(2): 176-181.
- Lafleur, M., E. Plijmackers-Westmijze, A. Loman and H. Loman (1985). "Adduct Formation Is Involved in Radiosensitization, Mediated by Cytochrome c, of ϕ X174 DNA by Misonidazole." International Journal of Radiation Biology and Related Studies in Physics, Chemistry and Medicine **47**(4): 379-382.
- Lanzen, J., R. D. Braun, B. Klitzman, D. Brizel, T. W. Secomb and M. W. Dewhirst (2006). "Direct demonstration of instabilities in oxygen concentrations within the extravascular compartment of an experimental tumor." Cancer Research **66**(4): 2219-2223.
- LaRusso, N. F., M. Tomasz, M. Müller and R. Lipman (1977). "Interaction of metronidazole with nucleic acids in vitro." Molecular Pharmacology **13**(5): 872-882.
- Lauwaet, T., Y. Miyamoto, S. Ihara, C. Le, J. Kalisiak, K. A. Korthals, M. Ghassemian, D. K. Smith, K. B. Sharpless and V. V. Fokin (2020). "Click chemistry-facilitated comprehensive identification of proteins adducted by antimicrobial 5-nitroimidazoles for discovery of alternative drug targets against giardiasis." PLOS Neglected Tropical Diseases **14**(4): e0008224.
- Lawton, C. A., C. N. Coleman, J. W. Buzydlowski, J. D. Forman, V. A. Marcial, J. D. DelRowe and M. Rotman (1996). "Results of a phase II trial of external beam radiation with etanidazole (SR 2508) for the treatment of locally advanced prostate cancer (RTOG Protocol 90-20)." International Journal of Radiation Oncology* Biology* Physics **36**(3): 673-680.
- Le, Q.-T., E. Chen, A. Salim, H. Cao, C. S. Kong, R. Whyte, J. Donington, W. Cannon, H. Wakelee and R. Tibshirani (2006). "An evaluation of tumor oxygenation and gene expression in patients with early stage non-small cell lung cancers." Clinical Cancer Research **12**(5): 1507-1514.

- Le, Q.-T. and D. Courter (2008). "Clinical biomarkers for hypoxia targeting." Cancer and Metastasis Reviews **27**(3): 351-362.
- Le, Q.-T., C. Kong, P. W. Lavori, K. O'byrne, J. T. Erler, X. Huang, Y. Chen, H. Cao, R. Tibshirani and N. Denko (2007). "Expression and prognostic significance of a panel of tissue hypoxia markers in head-and-neck squamous cell carcinomas." International Journal of Radiation Oncology* Biology* Physics **69**(1): 167-175.
- Lee, D.-J., D. Cosmatos, V. A. Marcial, K. K. Fu, M. Rotman, J. S. Cooper, H. G. Ortiz, J. J. Beitler, R. A. Abrams and W. J. Curran (1995). "Results of an RTOG phase III trial (RTOG 85-27) comparing radiotherapy plus etanidazole with radiotherapy alone for locally advanced head and neck carcinomas." International Journal of Radiation Oncology* Biology* Physics **32**(3): 567-576.
- Lee, N. Y., J. G. Mechalakos, S. Nehmeh, Z. Lin, O. D. Squire, S. Cai, K. Chan, P. B. Zanzonico, C. Greco and C. C. Ling (2008). "Fluorine-18-labeled fluoromisonidazole positron emission and computed tomography-guided intensity-modulated radiotherapy for head and neck cancer: a feasibility study." International Journal of Radiation Oncology* Biology* Physics **70**(1): 2-13.
- Leitsch, D., D. Kolarich, M. Binder, J. Stadlmann, F. Altmann and M. Duchêne (2009). "Trichomonas vaginalis: metronidazole and other nitroimidazole drugs are reduced by the flavin enzyme thioredoxin reductase and disrupt the cellular redox system. Implications for nitroimidazole toxicity and resistance." Molecular Microbiology **72**(2): 518-536.
- Leitsch, D., D. Kolarich, I. B. Wilson, F. Altmann and M. Duchêne (2007). "Nitroimidazole action in Entamoeba histolytica: a central role for thioredoxin reductase." PLoS Biology **5**(8).
- Leitsch, D., D. Kolarich, I. B. H. Wilson, F. Altmann and M. Duchêne (2007). "Nitroimidazole action in Entamoeba histolytica: a central role for thioredoxin reductase." PLoS Biology **5**(8): e211.
- Leitsch, D., S. Schlosser, A. Burgess and M. Duchêne (2012). "Nitroimidazole drugs vary in their mode of action in the human parasite Giardia lamblia." International Journal for Parasitology: Drugs and Drug Resistance **2**: 166-170.
- Lequeux, A., M. Z. Noman, M. Xiao, D. Sauvage, K. Van Moer, E. Viry, I. Bocci, M. Hasmim, M. Bosseler and G. Berchem (2019). "Impact of hypoxic tumor microenvironment and tumor cell plasticity on the expression of immune checkpoints." Cancer Letters **458**: 13-20.
- Leu, A. J., D. A. Berk, A. Lymboussaki, K. Alitalo and R. K. Jain (2000). "Absence of functional lymphatics within a murine sarcoma: a molecular and functional evaluation." Cancer Research **60**(16): 4324-4327.
- Li, J.-q., X. Wu, L. Gan, X.-l. Yang and Z.-h. Miao (2017). "Hypoxia induces universal but differential drug resistance and impairs anticancer mechanisms of 5-fluorouracil in hepatoma cells." Acta Pharmacologica Sinica **38**(12): 1642.
- Li, Y., Y. Wang, E. Kim, P. Beemiller, C.-Y. Wang, J. Swanson, M. You and K.-L. Guan (2007). "Bnip3 mediates the hypoxia-induced inhibition on mammalian target of rapamycin by interacting with Rheb." Journal of Biological Chemistry **282**(49): 35803-35813.
- Liberti, M. V. and J. W. Locasale (2016). "The Warburg effect: how does it benefit cancer cells?" Trends in Biochemical Sciences **41**(3): 211-218.

- Lindquist, K. E. (2009). The development of hypoxia activated DNA repair inhibitors, University of British Columbia.
- Liu, K., Z. Tang, A. Huang, P. Chen, P. Liu, J. Yang, W. Lu, J. Liao, Y. Sun and S. Wen (2017). "Glyceraldehyde-3-phosphate dehydrogenase promotes cancer growth and metastasis through upregulation of SNAIL expression." International Journal of Oncology **50**(1): 252-262.
- Ljungkvist, A. S., J. Bussink, J. H. Kaanders, P. F. Rijken, A. C. Begg, J. A. Raleigh and A. J. Van Der Kogel (2005). "Hypoxic cell turnover in different solid tumor lines." International Journal of Radiation Oncology* Biology* Physics **62**(4): 1157-1168.
- Löck, S., R. Perrin, A. Seidlitz, A. Bandurska-Luque, S. Zschaecck, K. Zöphel, M. Krause, J. Steinbach, J. Kotzerke and D. Zips (2017). "Residual tumour hypoxia in head-and-neck cancer patients undergoing primary radiochemotherapy, final results of a prospective trial on repeat FMISO-PET imaging." Radiotherapy and Oncology **124**(3): 533-540.
- Locke, A. J., L. Hossain, G. McCrostie, D. A. Ronato, A. Fitieh, T. A. Rafique, F. Mashayekhi, M. Motamedi, J.-Y. Masson and I. H. Ismail (2021). "SUMOylation mediates CtIP's functions in DNA end resection and replication fork protection." Nucleic Acids Research **49**(2): 928-953.
- MacLauchlan, S. C., N. E. Calabro, Y. Huang, M. Krishna, T. Bancroft, T. Sharma, J. Yu, W. C. Sessa, F. Giordano and T. R. Kyriakides (2018). "HIF-1 α represses the expression of the angiogenesis inhibitor thrombospondin-2." Matrix Biology **65**: 45-58.
- Madan, E., R. Gogna and U. Pati (2012). "p53 Ser15 phosphorylation disrupts the p53-RPA70 complex and induces RPA70-mediated DNA repair in hypoxia." Biochemical Journal **443**(3): 811-820.
- Mahon, P. C., K. Hirota and G. L. Semenza (2001). "FIH-1: a novel protein that interacts with HIF-1 α and VHL to mediate repression of HIF-1 transcriptional activity." Genes & Development **15**(20): 2675-2686.
- Maier, F. C., A. Schweifer, V. L. Damaraju, C. E. Cass, G. D. Bowden, W. Ehrlichmann, M. Kneilling, B. J. Pichler, F. Hammerschmidt and G. Reischl (2019). "2-Nitroimidazole-Furanoside Derivatives for Hypoxia Imaging—Investigation of Nucleoside Transporter Interaction, 18F-Labeling and Preclinical PET Imaging." Pharmaceuticals **12**(1): 31.
- Manalo, D. J., A. Rowan, T. Lavoie, L. Natarajan, B. D. Kelly, S. Q. Ye, J. G. Garcia and G. L. Semenza (2005). "Transcriptional regulation of vascular endothelial cell responses to hypoxia by HIF-1." Blood **105**(2): 659-669.
- Manjunatha, U., H. I. Boshoff and C. E. Barry (2009). "The mechanism of action of PA-824: novel insights from transcriptional profiling." Communicative & Integrative Biology **2**(3): 215-218.
- Mannan, R. H., V. V. Somayaji, J. Lee, J. R. Mercer, J. D. Chapman and L. I. Wiebe (1991). "arabinofuranosyl)-2-thioimidazole." J Nucl Med **32**: 1764-1770.
- Mannan, R. H., V. V. Somayaji, J. Lee, J. R. Mercer, J. D. Chapman and L. I. Wiebe (1991). "Radioiodinated 1-(5-iodo-5-deoxy-beta-D-arabinofuranosyl)-2-nitroimidazole (iodoazomycin arabinoside: IAZA): a novel marker of tissue hypoxia." Journal of Nuclear Medicine **32**: 1764-1770.
- Marcus, Y., N. Tal, M. Ronen, R. Carmieli and M. Gurevitz (2016). "The drug ornidazole inhibits photosynthesis in a different mechanism described for protozoa and anaerobic bacteria." Biochemical Journal **473**(23): 4413-4426.

- Maréchal, A. and L. Zou (2015). "RPA-coated single-stranded DNA as a platform for post-translational modifications in the DNA damage response." *Cell Research* **25**(1): 9-23.
- Masaki, Y., Y. Shimizu, T. Yoshioka, F. Feng, S. Zhao, K. Higashino, Y. Numata and Y. Kuge (2016). "Imaging mass spectrometry revealed the accumulation characteristics of the 2-nitroimidazole-based agent "pimonidazole" in hypoxia." *PLoS One* **11**(8): e0161639.
- Masaki, Y., Y. Shimizu, T. Yoshioka, Y. Tanaka, K.-i. Nishijima, S. Zhao, K. Higashino, S. Sakamoto, Y. Numata and Y. Yamaguchi (2015). "The accumulation mechanism of the hypoxia imaging probe "FMISO" by imaging mass spectrometry: possible involvement of low-molecular metabolites." *Scientific Reports* **5**(1): 1-9.
- Mayer, A., M. Höckel and P. Vaupel (2005). "Carbonic anhydrase IX expression and tumor oxygenation status do not correlate at the microregional level in locally advanced cancers of the uterine cervix." *Clinical Cancer Research* **11**(20): 7220-7225.
- Mayer, A., A. Wree, M. Höckel, C. Leo, H. Pilch and P. Vaupel (2004). "Lack of correlation between expression of HIF-1 α protein and oxygenation status in identical tissue areas of squamous cell carcinomas of the uterine cervix." *Cancer Research* **64**(16): 5876-5881.
- McKenna, D. J., R. Errington and K. Pors (2018). "Current challenges and opportunities in treating hypoxic prostate tumors." *Journal of Cancer Metastasis and Treatment* **4**.
- McKeown, S. (2014). "Defining normoxia, physoxia and hypoxia in tumours—implications for treatment response." *The British Journal of Radiology* **87**(1035): 20130676.
- Meng, A. X., F. Jalali, A. Cuddihy, N. Chan, R. S. Bindra, P. M. Glazer and R. G. Bristow (2005). "Hypoxia down-regulates DNA double strand break repair gene expression in prostate cancer cells." *Radiotherapy and Oncology* **76**(2): 168-176.
- Mercer, J. R., A. J. McEwan and L. I. Wiebe (2013). "[131I] IAZA as a Molecular Radiotherapeutic (MRT) Drug: Wash-Out with Cold IAZA Accelerates Clearance in a Murine Tumor Model." *Current Radiopharmaceuticals* **6**(2): 87-91.
- Metwally, M. A. H., K. D. Frederiksen and J. Overgaard (2014). "Compliance and toxicity of the hypoxic radiosensitizer nimorazole in the treatment of patients with head and neck squamous cell carcinoma (HNSCC)." *Acta Oncologica* **53**(5): 654-661.
- Mi, H., A. Muruganujan, D. Ebert, X. Huang and P. D. Thomas (2019). "PANTHER version 14: more genomes, a new PANTHER GO-slim and improvements in enrichment analysis tools." *Nucleic Acids Research* **47**(D1): D419-D426.
- Michaels, H. B., E. C. Peterson, C. C. Ling and E. R. Epp (1981). "Combined effects of misonidazole radiosensitization and hypoxic cell toxicity in mammalian cells." *Radiation Research* **88**(2): 354-368.
- Millar, T. M., V. Phan and L. A. Tibbles (2007). "ROS generation in endothelial hypoxia and reoxygenation stimulates MAP kinase signaling and kinase-dependent neutrophil recruitment." *Free Radical Biology and Medicine* **42**(8): 1165-1177.
- Mirzayans, R., B. Andrais and D. Murray (2018). "Roles of polyploid/multinucleated giant cancer cells in metastasis and disease relapse following anticancer treatment." *Cancers* **10**(4): 118.
- Mortensen, L. S., J. Johansen, J. Kallehauge, H. Primdahl, M. Busk, P. Lassen, J. Alsner, B. S. Sørensen, K. Toustrup and S. Jakobsen (2012). "FAZA PET/CT hypoxia imaging in patients with squamous cell carcinoma of the head and neck treated with radiotherapy: results from the DAHANCA 24 trial." *Radiotherapy and Oncology* **105**(1): 14-20.

- Mowery, Y. M., D. J. Carpenter, A. J. Wisdom, C. T. Badea, L. Luo, Y. Ma, A. Pendse and D. G. Kirsch (2018). Characterization of novel primary mouse models of HPV-negative squamous cell carcinoma of the oral cavity. Radiation Research Society Annual Meeting. Chicago, Illinois
- Mumtaz, M., L. S. Lin, K. C. Hui and A. S. M. Khir (2009). "Radioiodine I-131 for the therapy of Graves' disease." The Malaysian Journal of Medical Sciences: MJMS **16**(1): 25.
- Mungai, P. T., G. B. Waypa, A. Jairaman, M. Prakriya, D. Dokic, M. K. Ball and P. T. Schumacker (2011). "Hypoxia triggers AMPK activation through reactive oxygen species-mediated activation of calcium release-activated calcium channels." Molecular and Cellular Biology **31**(17): 3531-3545.
- Murphy, B. J., K. R. Laderoute, R. J. Chin and R. M. Sutherland (1994). "Metallothionein IIA is up-regulated by hypoxia in human A431 squamous carcinoma cells." Cancer Research **54**(22): 5808-5810.
- Mutallip, M., N. Nohata, T. Hanazawa, N. Kikkawa, S. Horiguchi, L. Fujimura, K. Kawakami, T. Chiyomaru, H. Enokida and M. Nakagawa (2011). "Glutathione S-transferase P1 (GSTP1) suppresses cell apoptosis and its regulation by miR-133 α in head and neck squamous cell carcinoma (HNSCC)." International Journal of Molecular Medicine **27**(3): 345-352.
- Nagao, A., M. Kobayashi, S. Koyasu, C. C. Chow and H. Harada (2019). "HIF-1-dependent reprogramming of glucose metabolic pathway of cancer cells and its therapeutic significance." International Journal of Molecular Sciences **20**(2): 238.
- Nakajima, H., W. Amano, A. Fujita, A. Fukuhara, Y.-T. Azuma, F. Hata, T. Inui and T. Takeuchi (2007). "The active site cysteine of the proapoptotic protein glyceraldehyde-3-phosphate dehydrogenase is essential in oxidative stress-induced aggregation and cell death." Journal of Biological Chemistry **282**(36): 26562-26574.
- Nejad, A. E., S. Najafgholian, A. Rostami, A. Sistani, S. Shojaeifar, M. Esparvarinha, R. Nedaeinia, S. H. Javanmard, M. Taherian and M. Ahmadlou (2021). "The role of hypoxia in the tumor microenvironment and development of cancer stem cell: a novel approach to developing treatment." Cancer Cell International **21**(1): 1-26.
- Noman, M. Z., G. Desantis, B. Janji, M. Hasmmim, S. Karray, P. Dessen, V. Bronte and S. Chouaib (2014). "PD-L1 is a novel direct target of HIF-1 α , and its blockade under hypoxia enhanced MDSC-mediated T cell activation." Journal of Experimental Medicine **211**(5): 781-790.
- Noman, M. Z., M. Hasmmim, A. Lequeux, M. Xiao, C. Duhem, S. Chouaib, G. Berchem and B. Janji (2019). "Improving cancer immunotherapy by targeting the hypoxic tumor microenvironment: new opportunities and challenges." Cells **8**(9): 1083.
- Nordmark, M., J. Alsner, J. Keller, O. S. Nielsen, O. Jensen, M. Horsman and J. Overgaard (2001). "Hypoxia in human soft tissue sarcomas: adverse impact on survival and no association with p53 mutations." British Journal of Cancer **84**(8): 1070.
- Nordmark, M., S. M. Bentzen, V. Rudat, D. Brizel, E. Lartigau, P. Stadler, A. Becker, M. Adam, M. Molls and J. Dunst (2005). "Prognostic value of tumor oxygenation in 397 head and neck tumors after primary radiation therapy. An international multi-center study." Radiotherapy and Oncology **77**(1): 18-24.
- Nordmark, M., M. Overgaard and J. Overgaard (1996). "Pretreatment oxygenation predicts radiation response in advanced squamous cell carcinoma of the head and neck." Radiotherapy and Oncology **41**(1): 31-39.

- O'Dwyer, P., F. LaCreta, J. Walczak, T. Cox, S. Litwin, J. Hoffman, M. Zimny and R. Comis (1993). "Phase I/pharmacokinetic/biochemical study of the nitroimidazole hypoxic cell sensitiser SR2508 (etanidazole) in combination with cyclophosphamide." British Journal of Cancer **68**(4): 756-766.
- Ohtsubo, M., A. M. Theodoras, J. Schumacher, J. M. Roberts and M. Pagano (1995). "Human cyclin E, a nuclear protein essential for the G1-to-S phase transition." Molecular and Cellular Biology **15**(5): 2612-2624.
- Okkan, S., G. Atkovar, I. Sahinler, S. Turkan and R. Uzel (1996). "A randomised study of ornidazole as a radiosensitiser in carcinoma of the cervix: long term results." The British Journal of Cancer. Supplement **27**: S282.
- Okkan, S., Z. Yazici, R. Uzel, A. Akçasu, S. Turkan, M. Hacibekiroglu, P. Olgun and I. Egehan (1986). "Use of ornidazole in fractionated radiotherapy: dose tolerance, serum and tumour tissue concentration." Radiotherapy and Oncology **5**(4): 295-301.
- Olcina, M. M., I. P. Foskolou, S. Anbalagan, J. M. Senra, I. M. Pires, Y. Jiang, A. J. Ryan and E. M. Hammond (2013). "Replication stress and chromatin context link ATM activation to a role in DNA replication." Molecular Cell **52**(5): 758-766.
- Olive, P. L., C. Vikse and M. J. Trotter (1992). "Measurement of oxygen diffusion distance in tumor cubes using a fluorescent hypoxia probe." International Journal of Radiation Oncology* Biology* Physics **22**(3): 397-402.
- Otsu, N. (1979). "A threshold selection method from gray-level histograms." IEEE transactions on Systems, Man, and Cybernetics **9**(1): 62-66.
- Overgaard, J. (1994). "Clinical evaluation of nitroimidazoles as modifiers of hypoxia in solid tumors." Oncology Research Featuring Preclinical and Clinical Cancer Therapeutics **6**(10-11): 509-518.
- Overgaard, J., J. G. Eriksen, M. Nordmark, J. Alsner and M. R. Horsman (2005). "Plasma osteopontin, hypoxia, and response to the hypoxia sensitiser nimorazole in radiotherapy of head and neck cancer: results from the DAHANCA 5 randomised double-blind placebo-controlled trial." The Lancet Oncology **6**(10): 757-764.
- Overgaard, J., H. S. Hansen, A. Andersen, M. Hjelm-Hansen, K. Jørgensen, E. Sandberg, A. Berthelsen, R. Hammer and M. Pedersen (1989). "Misonidazole combined with split-course radiotherapy in the treatment of invasive carcinoma of larynx and pharynx: report from the DAHANCA 2 study." International Journal of Radiation Oncology* Biology* Physics **16**(4): 1065-1068.
- Overgaard, J., H. S. Hansen, M. Overgaard, L. Bastholt, A. Berthelsen, L. Specht, B. Lindeløv and K. Jørgensen (1998). "A randomized double-blind phase III study of nimorazole as a hypoxic radiosensitizer of primary radiotherapy in supraglottic larynx and pharynx carcinoma. Results of the Danish Head and Neck Cancer Study (DAHANCA) Protocol 5-85." Radiotherapy and Oncology **46**(2): 135-146.
- Padera, T. P., A. Kadambi, E. di Tomaso, C. M. Carreira, E. B. Brown, Y. Boucher, N. C. Choi, D. Mathisen, J. Wain and E. J. Mark (2002). "Lymphatic metastasis in the absence of functional intratumor lymphatics." Science **296**(5574): 1883-1886.
- Pajaud, J., C. Ribault, I. B. Mosbah, C. Rauch, C. Henderson, P. Bellaud, C. Aninat, P. Loyer, F. Morel and A. Corlu (2015). "Glutathione transferases P1/P2 regulate the timing of signaling pathway activations and cell cycle progression during mouse liver regeneration." Cell Death & Disease **6**(1): e1598-e1598.

- Palcic, B. and L. Skarsgard (1984). "Reduced oxygen enhancement ratio at low doses of ionizing radiation." Radiation Research **100**(2): 328-339.
- Pathan, M., S. Keerthikumar, C. S. Ang, L. Gangoda, C. Y. Quek, N. A. Williamson, D. Mouradov, O. M. Sieber, R. J. Simpson and A. Salim (2015). "FunRich: An open access standalone functional enrichment and interaction network analysis tool." Proteomics **15**(15): 2597-2601.
- Pelicano, H., D. Martin, R. Xu, and P. Huang (2006). "Glycolysis inhibition for anticancer treatment." Oncogene **25**(34): 4633-4646.
- Phadke, M. S., N. F. Krynetskaia, A. K. Mishra and E. Krynetskiy (2009). "Glyceraldehyde 3-phosphate dehydrogenase depletion induces cell cycle arrest and resistance to antimetabolites in human carcinoma cell lines." Journal of Pharmacology and Experimental Therapeutics **331**(1): 77-86.
- Phillips, T. L., T. H. Wasserman, R. J. Johnson, V. A. Levin and G. Vanraalte (1981). "Final report on the united states phase i clinical trial of the hypoxic cell radiosensitizer, misonidazole (RO-07-0582; NSC# 261037)." Cancer **48**(8): 1697-1704.
- Plant, C. and D. Edwards (1976). "The effect of tinidazole, metronidazole and nitrofurazone on nucleic acid synthesis in *Clostridium bifermentans*." Journal of Antimicrobial Chemotherapy **2**(2): 203-209.
- Postema, E. J., A. J. McEwan, T. A. Riauka, P. Kumar, D. A. Richmond, D. N. Abrams and L. I. Wiebe (2009). "Initial results of hypoxia imaging using 1- α -D-(5-deoxy-5-[18 F]-fluoroarabinofuranosyl)-2-nitroimidazole (18 F-FAZA)." European Journal of Nuclear Medicine and Molecular Imaging **36**(10): 1565-1573.
- Prabhakar, N. R. and G. L. Semenza (2015). "Oxygen sensing and homeostasis." Physiology **30**(5): 340-348.
- Qiu, S., G. Jiang, L. Cao and J. Huang (2021). "Replication fork reversal and protection." Frontiers in Cell and Developmental Biology **9**: 1190.
- Quan, S., Y. Wang, A. Zhou, P. Kumar and R. Narain (2015). "Galactose-based thermosensitive nanogels for targeted drug delivery of iodoazomycin arabinofuranoside (IAZA) for theranostic management of hypoxic hepatocellular carcinoma." Biomacromolecules **16**(7): 1978-1986.
- Raimondi, M. V., O. Randazzo, M. La Franca, G. Barone, E. Vignoni, D. Rossi and S. Collina (2019). "DHFR inhibitors: reading the past for discovering novel anticancer agents." Molecules **24**(6): 1140.
- Rajendran, J., D. Wilson, E. Conrad, L. Peterson, J. Bruckner, J. Rasey, L. Chin, P. Hofstrand, J. Grierson and J. Eary (2003). "[18 F] FMISO and [18 F] FDG PET imaging in soft tissue sarcomas: correlation of hypoxia, metabolism and VEGF expression." European Journal of Nuclear Medicine and Molecular Imaging **30**(5): 695-704.
- Rashed, F. B., A. C. Stoica, D. MacDonald, H. El-Saidi, C. Ricardo, B. Bhatt, J. Moore, D. Diaz-Dussan, N. Ramamonjisoa, Y. Mowery, S. Damaraju, R. Fahlman, L.I. Wiebe, P. Kumar and M. Weinfeld (2021). "Identification of proteins and cellular pathways targeted by 2-nitroimidazole hypoxic cytotoxins." Redox Biology: 101905.
- Raz, S., D. Sheban, N. Gonen, M. Stark, B. Berman and Y. Assaraf (2014). "Severe hypoxia induces complete antifolate resistance in carcinoma cells due to cell cycle arrest." Cell Death & Disease **5**(2): e1067-e1067.
- Reischl, G., D. S. Dorow, C. Cullinane, A. Katsifis, P. Roselt, D. Binns and R. J. Hicks (2007). "Imaging of tumor hypoxia with [124I] IAZA in comparison with [18F] FMISO and

- [18F] FAZA—first small animal PET results." Journal of Pharmacy and Pharmaceutical Sciences **10**(2): 203-211.
- Ren, Y., P. Hao, B. Dutta, E. S. H. Cheow, K. H. Sim, C. S. Gan, S. K. Lim and S. K. Sze (2013). "Hypoxia modulates A431 cellular pathways association to tumor radioresistance and enhanced migration revealed by comprehensive proteomic and functional studies." Molecular & Cellular Proteomics **12**(2): 485-498.
- Rey, S. and G. L. Semenza (2010). "Hypoxia-inducible factor-1-dependent mechanisms of vascularization and vascular remodelling." Cardiovascular Research **86**(2): 236-242.
- Reynolds, T. Y., S. Rockwell and P. M. Glazer (1996). "Genetic instability induced by the tumor microenvironment." Cancer Research **56**(24): 5754-5757.
- Rezvani, H. R., W. Mahfouf, N. Ali, C. Chemin, C. Ged, A. L. Kim, H. de Verneuil, A. Taïeb, D. R. Bickers and F. Mazurier (2010). "Hypoxia-inducible factor-1 α regulates the expression of nucleotide excision repair proteins in keratinocytes." Nucleic Acids research **38**(3): 797-809.
- Rice, G. C., V. Ling and R. T. Schimke (1987). "Frequencies of independent and simultaneous selection of Chinese hamster cells for methotrexate and doxorubicin (adriamycin) resistance." Proceedings of the National Academy of Sciences **84**(24): 9261-9264.
- Richter, J. D. and N. Sonenberg (2005). "Regulation of cap-dependent translation by eIF4E inhibitory proteins." Nature **433**(7025): 477-480.
- Ringborg, U., D. Bergqvist, B. Brorsson, E. Cavallin-Ståhl, J. Ceberg, N. Einhorn, J.-e. Frödin, J. Järhult, G. Lamnevik and C. Lindholm (2003). "The Swedish Council on Technology Assessment in Health Care (SBU) systematic overview of radiotherapy for cancer including a prospective survey of radiotherapy practice in Sweden 2001--summary and conclusions." Acta Oncologica **42**(5-6): 357-365.
- Rockwell, S., I. T. Dobrucki, E. Y. Kim, S. T. Marrison and V. T. Vu (2009). "Hypoxia and radiation therapy: past history, ongoing research, and future promise." Current Molecular Medicine **9**(4): 442-458.
- Rodríguez-Jiménez, F. J., V. Moreno-Manzano, R. Lucas-Dominguez and J. M. Sánchez-Puelles (2008). "Hypoxia causes downregulation of mismatch repair system and genomic instability in stem cells." Stem Cells **26**(8): 2052-2062.
- Rojas, A. M., V. K. Hirst, A. Calvert and H. Johns (1996). "Carbogen and nicotinamide as radiosensitisers in a murine mammary carcinoma using conventional and accelerated radiotherapy." International Journal of Radiation Oncology, Biology, Physics **34**(2): 357-365.
- Rowley, D. A., R. C. Knight, I. M. Skolimowski and D. I. Edwards (1979). "The effect of nitroheterocyclic drugs on DNA: an in vitro model of cytotoxicity." Biochemical Pharmacology **28**(19): 3009-3013.
- Rowley, D. A., R. C. Knight, I. M. Skolimowski and D. I. Edwards (1980). "The relationship between misonidazole cytotoxicity and base composition of DNA." Biochemical Pharmacology **29**(15): 2095-2098.
- Rudat, V., B. Vanselow, P. Wollensack, C. Bettscheider, S. Osman-Ahmet, M. J. Eble and A. Dietz (2000). "Repeatability and prognostic impact of the pretreatment pO₂ histography in patients with advanced head and neck cancer." Radiotherapy and Oncology **57**(1): 31-37.
- Ryan, H. E., J. Lo and R. S. Johnson (1998). "HIF-1 α is required for solid tumor formation and embryonic vascularization." The EMBO Journal **17**(11): 3005-3015.

- Said, H. M., C. Hagemann, J. Stojic, B. Schoemig, G. H. Vince, M. Flentje, K. Roosen and D. Vordermark (2007). "GAPDH is not regulated in human glioblastoma under hypoxic conditions." BMC Molecular Biology **8**(1): 55.
- Saksø, M., L. S. Mortensen, H. Primdahl, J. Johansen, J. Kallehauge, C. R. Hansen and J. Overgaard (2020). "Influence of FAZA PET hypoxia and HPV-status for the outcome of head and neck squamous cell carcinoma (HNSCC) treated with radiotherapy: Long-term results from the DAHANCA 24 trial (NCT01017224)." Radiotherapy and Oncology **151**: 126-133.
- Salminen, E., K. Clemens, M. Diwani, A. Flavin, N. Janjan, S. Kaasa, S. Kumar, R. Imai and T. Tamaki (2012). "Radiotherapy in palliative cancer care: Development and implementation."
- Sasaki, K., A. Kurose and Y. Ishida (1993). "Flow cytometric analysis of the expression of PCNA during the cell cycle in HeLa cells and effects of the inhibition of DNA synthesis on it." Cytometry: The Journal of the International Society for Analytical Cytology **14**(8): 876-882.
- Scanlon, S. E. and P. M. Glazer (2015). "Multifaceted control of DNA repair pathways by the hypoxic tumor microenvironment." DNA Repair **32**: 180-189.
- Semenza, G. L. (2011). "Hypoxia-inducible factor 1: regulator of mitochondrial metabolism and mediator of ischemic preconditioning." Biochimica et Biophysica Acta (BBA)-Molecular Cell Research **1813**(7): 1263-1268.
- Semenza, G. L., P. H. Roth, H.-M. Fang and G. L. Wang (1994). "Transcriptional regulation of genes encoding glycolytic enzymes by hypoxia-inducible factor 1." Journal of Biological Chemistry **269**(38): 23757-23763.
- Servagi-Vernat, S., S. Differding, F.-X. Hanin, D. Labar, A. Bol, J. A. Lee and V. Grégoire (2014). "A prospective clinical study of 18 F-FAZA PET-CT hypoxia imaging in head and neck squamous cell carcinoma before and during radiation therapy." European Journal of Nuclear Medicine and Molecular Imaging **41**(8): 1544-1552.
- Shannon, A. M., D. J. Bouchier-Hayes, C. M. Condron and D. Toomey (2003). "Tumour hypoxia, chemotherapeutic resistance and hypoxia-related therapies." Cancer Treatment Reviews **29**(4): 297-307.
- Sheldon, P.-W., J. Foster and J.-F. Fowler (1974). "Radiosensitization of C3H mouse mammary tumours by a 2-nitroimidazole drug." British Journal of Cancer **30**(6): 560-565.
- Sheldon, P. and J. Fowler (1978). "Radiosensitization by misonidazole (Ro-07-0582) of fractionated X-rays in a murine tumour." The British Journal of Cancer. Supplement **3**: 242.
- Siemann, D. W. (2011). "The unique characteristics of tumor vasculature and preclinical evidence for its selective disruption by tumor-vascular disrupting agents." Cancer Treatment Reviews **37**(1): 63-74.
- Siemens, D. R., N. Hu, A. K. Sheikhi, E. Chung, L. J. Frederiksen, H. Pross and C. H. Graham (2008). "Hypoxia increases tumor cell shedding of MHC class I chain-related molecule: role of nitric oxide." Cancer Research **68**(12): 4746-4753.
- Sigeti, J. S., D. G. Guiney Jr and C. E. Davis (1983). "Mechanism of action of metronidazole on *Bacteroides fragilis*." Journal of Infectious Diseases **148**(6): 1083-1089.
- Silver, A. R., S. S. Mcneil, P. O'Neill, T. C. Jenkins and I. Ahmed (1986). "Induction of DNA strand breaks by reduced nitroimidazoles: Implications for DNA base damage." Biochemical Pharmacology **35**(22): 3923-3928.

- Silver, A. R., P. O'Neill and T. C. Jenkins (1985). "Induction of DNA strand breaks by RSU-1069, A nitroimidazole-aziridine radiosensitizer: Role of binding of both unreduced and radiation-reduced forms to DNA, in vitro." Biochemical Pharmacology **34**(19): 3537-3542.
- Sim, J., A. S. Cowburn, A. Palazon, B. Madhu, P. A. Tyrakis, D. Macías, D. M. Bargiela, S. Pietsch, M. Gralla and C. E. Evans (2018). "The factor inhibiting HIF asparaginyl hydroxylase regulates oxidative metabolism and accelerates metabolic adaptation to hypoxia." Cell Metabolism **27**(4): 898-913. e897.
- Souvatzoglou, M., A. Grosu, B. Röper, B. Krause, R. Beck, G. Reischl, M. Picchio, H.-J. Machulla, H.-J. Wester and M. Piert (2007). "Tumour hypoxia imaging with [18F] FAZA PET in head and neck cancer patients: a pilot study." European Journal of Nuclear Medicine and Molecular Imaging **34**(10): 1566-1575.
- Sridhar, R., C. Koch and R. Sutherland (1976). "Cytotoxicity of two nitroimidazole radiosensitizers in an in vitro tumor model." International Journal of Radiation Oncology* Biology* Physics **1**(11-12): 1149-1157.
- Stadler, P., A. Becker, H. J. Feldmann, G. Hänsgen, J. Dunst, F. Würschmidt and M. Molls (1999). "Influence of the hypoxic subvolume on the survival of patients with head and neck cancer." International Journal of Radiation Oncology• Biology• Physics **44**(4): 749-754.
- Tang, M., E. Bolderson, K. J. O'Byrne and D. J. Richard (2021). "Tumor Hypoxia Drives Genomic Instability." Frontiers in Cell and Developmental Biology **9**: 430.
- Tausendschön, M., N. Dehne and B. Brüne (2011). "Hypoxia causes epigenetic gene regulation in macrophages by attenuating Jumonji histone demethylase activity." Cytokine **53**(2): 256-262.
- Teicher, B. A. (1995). "Angiogenesis and cancer metastases: therapeutic approaches." Critical Reviews in Oncology/hematology **20**(1): 9-39.
- Tercel, M. and F. B. Pruijn (2011). Agents and methods for detection and/or imaging of hypoxia, Google Patents.
- Tew, K. D. (1994). "Glutathione-associated enzymes in anticancer drug resistance." Cancer Research **54**(16): 4313-4320.
- Tharmalingham, H. and P. Hoskin (2018). "Clinical trials targeting hypoxia." The British Journal of Radiology **92**(1093): 20170966.
- Thomas, C. and C. D. Gwenin (2021). "The Role of Nitroreductases in Resistance to Nitroimidazoles." Biology **10**(5): 388.
- Thomlinson, R. H. and L. Gray (1955). "The histological structure of some human lung cancers and the possible implications for radiotherapy." British Journal of Cancer **9**(4): 539.
- Torres Filho, I. P., M. Leunig, F. Yuan, M. Intaglietta and R. K. Jain (1994). "Noninvasive measurement of microvascular and interstitial oxygen profiles in a human tumor in SCID mice." Proceedings of the National Academy of Sciences **91**(6): 2081-2085.
- Toustrup, K., B. S. Sørensen, P. Lassen, C. Wiuf, J. Alsner and J. Overgaard (2012). "Gene expression classifier predicts for hypoxic modification of radiotherapy with nimorazole in squamous cell carcinomas of the head and neck." Radiotherapy and Oncology **102**(1): 122-129.
- Townsend, D. M. and K. D. Tew (2003). "The role of glutathione-S-transferase in anti-cancer drug resistance." Oncogene **22**(47): 7369-7375.

- Traore, M. A. and S. C. George (2017). "Tissue engineering the vascular tree." Tissue Engineering Part B: Reviews **23**(6): 505-514.
- Trinkaus, M. E., R. Blum, D. Rischin, J. Callahan, M. Bressel, T. Segard, P. Roselt, P. Eu, D. Binns and M. P. MacManus (2013). "Imaging of hypoxia with 18F-FAZA PET in patients with locally advanced non-small cell lung cancer treated with definitive chemoradiotherapy." Journal of Medical Imaging and Radiation Oncology **57**(4): 475-481.
- Tristan, C., N. Shahani, T. W. Sedlak and A. Sawa (2011). "The diverse functions of GAPDH: views from different subcellular compartments." Cellular Signalling **23**(2): 317-323.
- Turaka, A., M. K. Buyyounouski, A. L. Hanlon, E. M. Horwitz, R. E. Greenberg and B. Movsas (2012). "Hypoxic prostate/muscle PO₂ ratio predicts for outcome in patients with localized prostate cancer: long-term results." International Journal of Radiation Oncology* Biology* Physics **82**(3): e433-e439.
- Urtasun, R., M. Parliament, A. McEwan, J. Mercer, R. Mannan, L. Wiebe, C. Morin and J. Chapman (1996). "Measurement of hypoxia in human tumours by non-invasive spect imaging of iodoazomycin arabinoside." The British Journal of Cancer. Supplement **27**: S209.
- Van Nostrand, D. (2009). "The benefits and risks of I-131 therapy in patients with well-differentiated thyroid cancer." Thyroid **19**(12): 1381-1391.
- Varghese, A. and G. Whitmore (1980). "Binding to cellular macromolecules as a possible mechanism for the cytotoxicity of misonidazole." Cancer Research **40**(7): 2165-2169.
- Varghese, A. and G. Whitmore (1983). "Modification of guanine derivatives by reduced 2-nitroimidazoles." Cancer Research **43**(1): 78-82.
- Varia, M. A., D. P. Calkins-Adams, L. H. Rinker, A. S. Kennedy, D. B. Novotny, W. C. Fowler Jr and J. A. Raleigh (1998). "Pimonidazole: a novel hypoxia marker for complementary study of tumor hypoxia and cell proliferation in cervical carcinoma." Gynecologic Oncology **71**(2): 270-277.
- Vaupel, P., M. Höckel and A. Mayer (2007). "Detection and characterization of tumor hypoxia using pO₂ histography." Antioxidants & Redox Signaling **9**(8): 1221-1236.
- Vaupel, P., O. Thews and M. Hoeckel (2001). "Treatment resistance of solid tumors." Medical Oncology **18**(4): 243-259.
- Verwer, E. E., I. Bahce, F. H. van Velden, M. Yaqub, R. C. Schuit, A. D. Windhorst, P. Rajmakers, O. S. Hoekstra, A. A. Lammertsma and E. F. Smit (2014). "Parametric methods for quantification of 18F-FAZA kinetics in non-small cell lung cancer patients." Journal of Nuclear Medicine **55**(11): 1772-1777.
- Vindigni, A. and M. Lopes (2017). "Combining electron microscopy with single molecule DNA fiber approaches to study DNA replication dynamics." Biophysical chemistry **225**: 3-9.
- Vordermark, D. and M. R. Horsman (2016). "Hypoxia as a biomarker and for personalized radiation oncology." Molecular Radio-Oncology: 123-142.
- Walsh, J. C., A. Lebedev, E. Aten, K. Madsen, L. Marciano and H. C. Kolb (2014). "The clinical importance of assessing tumor hypoxia: relationship of tumor hypoxia to prognosis and therapeutic opportunities." Antioxidants & Redox Signaling **21**(10): 1516-1554.
- Ward, I. M. and J. Chen (2001). "Histone H2AX is phosphorylated in an ATR-dependent manner in response to replicational stress." Journal of Biological Chemistry **276**(51): 47759-47762.

- Watson, E., K. Hainan, S. Dische, M. Saunders, I. Cade, J. McEwen, G. Wiernik, D. Perrins and I. Sutherland (1978). "Hyperbaric oxygen and radiotherapy: a Medical Research Council trial in carcinoma of the cervix." The British Journal of Radiology **51**(611): 879-887.
- Wei, J., A. Wu, L.-Y. Kong, Y. Wang, G. Fuller, I. Fokt, G. Melillo, W. Priebe and A. B. Heimberger (2011). "Hypoxia potentiates glioma-mediated immunosuppression." PLoS One **6**(1): e16195.
- Weidner, N. (1999). Tumour vascularity and proliferation: clear evidence of a close relationship, Wiley Online Library.
- Welz, S., D. Mönnich, C. Pfannenber, K. Nikolaou, M. Reimold, C. La Fougère, G. Reischl, P.-S. Mauz, F. Paulsen and M. Alber (2017). "Prognostic value of dynamic hypoxia PET in head and neck cancer: results from a planned interim analysis of a randomized phase II hypoxia-image guided dose escalation trial." Radiotherapy and Oncology **124**(3): 526-532.
- Wilson, W. R. and M. P. Hay (2011). "Targeting hypoxia in cancer therapy." Nature Reviews Cancer **11**(6): 393-410.
- Wishart, D. S. (2015). "Is cancer a genetic disease or a metabolic disease?" EBioMedicine **2**(6): 478-479.
- Wislocki, P. G., E. S. Bagan, W. J. Vandenheuvel, R. W. Walker, R. F. Alvaro, B. H. Arison, A. Y. Lu and F. J. Wolf (1984). "Drug residue formation from ronidazole, a 5-nitroimidazole. V. Cysteine adducts formed upon reduction of ronidazole by dithionite or rat liver enzymes in the presence of cysteine." Chemico-biological Interactions **49**(1-2): 13-25.
- Wiśniewski, J. R., M. Y. Hein, J. Cox and M. Mann (2014). "A "proteomic ruler" for protein copy number and concentration estimation without spike-in standards." Molecular & Cellular Proteomics **13**(12): 3497-3506.
- Wouters, B. G. and M. Koritzinsky (2008). "Hypoxia signalling through mTOR and the unfolded protein response in cancer." Nature Reviews Cancer **8**(11): 851-864.
- Xiong, L., T. Zhao, X. Huang, Z.-h. Liu, H. Zhao, M.-m. Li, L.-y. Wu, H.-b. Shu, L.-l. Zhu and M. Fan (2009). "Heat shock protein 90 is involved in regulation of hypoxia-driven proliferation of embryonic neural stem/progenitor cells." Cell Stress and Chaperones **14**(2): 183-192.
- Yamaji, R., K. Fujita, S. Takahashi, H. Yoneda, K. Nagao, W. Masuda, M. Naito, T. Tsuruo, K. Miyatake and H. Inui (2003). "Hypoxia up-regulates glyceraldehyde-3-phosphate dehydrogenase in mouse brain capillary endothelial cells: involvement of Na⁺/Ca²⁺ exchanger." Biochimica et Biophysica Acta (BBA)-Molecular Cell Research **1593**(2-3): 269-276.
- Yang, L., D. Roberts, M. Takhar, N. Erho, B. A. Bibby, N. Thiruthaneeswaran, V. Bhandari, W.-C. Cheng, S. Haider and A. M. McCorry (2018). "Development and validation of a 28-gene hypoxia-related prognostic signature for localized prostate cancer." EBioMedicine **31**: 182-189.
- Yaromina, A., D. Zips, H. D. Thames, W. Eicheler, M. Krause, A. Rosner, M. Haase, C. Petersen, J. A. Raleigh and V. Quennet (2006). "Pimonidazole labelling and response to fractionated irradiation of five human squamous cell carcinoma (hSCC) lines in nude mice: the need for a multivariate approach in biomarker studies." Radiotherapy and Oncology **81**(2): 122-129.

- Yasui, H., N. Kubota, J. Nishizumi, Y. Sakai, T. Yamamori and O. Inanami (2018). "Preclinical study on hypoxic radiosensitizing effects of glycididazole in comparison with those of doranidazole in vitro and in vivo." Oncology Letters **15**(2): 1993-1998.
- Yeh, S.-A. (2010). Radiotherapy for head and neck cancer. Seminars in plastic surgery, Thieme Medical Publishers.
- Yuan, J., L. Narayanan, S. Rockwell and P. M. Glazer (2000). "Diminished DNA repair and elevated mutagenesis in mammalian cells exposed to hypoxia and low pH." Cancer Research **60**(16): 4372-4376.
- Zahoor, A., M. Lafleur, R. Knight, H. Loman and D. Edwards (1987). "DNA damage induced by reduced nitroimidazole drugs." Biochemical Pharmacology **36**(19): 3299-3304.
- Zeman, M. K. and K. A. Cimprich (2014). "Causes and consequences of replication stress." Nature Cell Biology **16**(1): 2-9.
- Zeng, M., H. Kikuchi, M. S. Pino and D. C. Chung (2010). "Hypoxia activates the K-ras proto-oncogene to stimulate angiogenesis and inhibit apoptosis in colon cancer cells." PLoS One **5**(6): e10966.
- Zhang, H., H. Lu, L. Xiang, J. W. Bullen, C. Zhang, D. Samanta, D. M. Gilkes, J. He and G. L. Semenza (2015). "HIF-1 regulates CD47 expression in breast cancer cells to promote evasion of phagocytosis and maintenance of cancer stem cells." Proceedings of the National Academy of Sciences **112**(45): E6215-E6223.
- Zhang, K., T. Zhao, X. Huang, Z.-h. Liu, L. Xiong, M.-m. Li, L.-y. Wu, Y.-q. Zhao, L.-l. Zhu and M. Fan (2009). "Preinduction of HSP70 promotes hypoxic tolerance and facilitates acclimatization to acute hypobaric hypoxia in mouse brain." Cell Stress and Chaperones **14**(4): 407-415.
- Zhang, M., M. Hou, L. Ge, C. Miao, J. Zhang, X. Jing, N. Shi, T. Chen and X. Tang (2014). "Induction of peroxiredoxin 1 by hypoxia regulates heme oxygenase-1 via NF- κ B in oral cancer." PLoS One **9**(8).
- Zhong, H., K. Chiles, D. Feldser, E. Laughner, C. Hanrahan, M.-M. Georgescu, J. W. Simons and G. L. Semenza (2000). "Modulation of hypoxia-inducible factor 1 α expression by the epidermal growth factor/phosphatidylinositol 3-kinase/PTEN/AKT/FRAP pathway in human prostate cancer cells: implications for tumor angiogenesis and therapeutics." Cancer Research **60**(6): 1541-1545.
- Zhong, H., G. L. Semenza, J. W. Simons and A. M. De Marzo (2004). "Up-regulation of hypoxia-inducible factor 1 α is an early event in prostate carcinogenesis." Cancer Detection and Prevention **28**(2): 88-93.
- Zhou, X., H. Sun, H. Chen, J. Zavadil, T. Kluz, A. Arita and M. Costa (2010). "Hypoxia induces trimethylated H3 lysine 4 by inhibition of JARID1A demethylase." Cancer Research **70**(10): 4214-4221.
- Zhou, Y., L. Liao, C. Wang, J. Li, P. Chi, Q. Xiao, Q. Liu, L. Guo, L. Sun and D. Deng (2020). "Cryo-EM structure of the human concentrative nucleoside transporter CNT3." PLoS Biology **18**(8): e3000790.
- Zhu, H., S. Ruan, F. Jia, J. Chu, Y. Zhu, Y. Huang and G. Liu (2018). "In vitro and in vivo superior radiosensitizing effect of berbamine for head and neck squamous cell carcinoma." OncoTargets and Therapy **11**: 8117.